Biochemical analysis of the putative histidine protein kinases NME1 and NME2 and their therapeutic potential

Alice K. M. Clubbs Coldron

Thesis submitted in accordance with the requirements of the University of Liverpool for the degree of Doctor in Philosophy

March 31, 2022

THE UNIVERSITY OF LIVERPOOL

Acknowledgements

Undertaking a PhD project in Pat Eyers lab was a challenging but exciting journey that has shaped me not only as a scientist, but as a person. After going straight from undergraduate level to a PhD, it was a steep learning curve but the support received from Pat as my primary supervisor, and the lab, allowed me to develop as a researcher both independently and as part of a research group. The Eyers lab consists of inspiring and passionate scientists that encouraged me to achieve the best of my potential by creating a helpful and supportive network. In addition, I was also very lucky to receive a great deal of help and guidance from my secondary supervisor, Dave Fernig, who was always there to answer questions, no matter how big or small.

Dr Dom Byrne was a particularly crucial part of my PhD training and for that I am very grateful. He continuously put my work, and what's more, my wellbeing before anything else as he would always make himself available when I needed him. The comradery of the Eyers lab and other lab groups in Lab D and C has always helped me throughout my PhD, and with that, many of my colleagues went on to become my very good friends.

I began my PhD with Lauren Tomlinson, a member of Claire Eyers lab and she has since become one of my closest friends. We have always been there for one another through the ups and downs of the PhD and I want to thank her for that. In addition to this continuous moral support, she also supported me experimentally, as she carried out the NME mass spectrometry. Lauren allowed me to find enjoyment both within the PhD and outside of the PhD, and this was so important for us both and for that I am very appreciative.

I would also like to thank Claire Eyers lab, in particular Dr Chris Clarke, for the aid in protocols for histidine phosphorylation analysis and Jack Simpson from Neil Berry's lab in the School of Chemistry for the computational modelling of molecular docking.

Finally, I give thanks to my partner, who I met during the early stages of my PhD and has since provided me with unconditional support, as well as my family for always encouraging me to be resilient and having faith in me and my abilities.

Publications

Some of the work described in this thesis has been published.

1. Clubbs Coldron, A. K. M., et al. (2020). "Analysis of 1- and 3-Phosphohistidine (pHis) Protein Modification Using Model Enzymes Expressed in Bacteria." Methods Mol Biol 2077: 63-81.
2. Tomlinson, L. J., et al. (2020). "Determination of Phosphohistidine Stoichiometry in Histidine Kinases by Intact Mass Spectrometry." Methods Mol Biol 2077: 83-91.

Abstract

Canonical protein phosphorylation on Ser/Thr and Tyr residues is a central cellular regulatory mechanism. However, progress in studying the phosphorylation of non-canonical amino acids in eukaryotes, such as Histidine (His), has fallen behind, in large part because traditional experimental design is unsuitable for the analysis of non-canonical phosphorylation. However, pHis is a known enzyme intermediate in several enzymes, and recent work suggests that protein His phosphorylation is more common than previously thought, raising the question as to how His phosphorylation on proteins is regulated. However, the kinases and phosphatases that control these processes, both *in vitro* and in cells, have largely remained a mystery. Two phosphohistidine (pHis) isomers occur at positions N1 and N3 of histidine. Both are found in human proteins and evidence is accumulating that the N1 pHis-containing enzymes, NME1 and NME2, better known as nucleoside diphosphate kinases (NDPK), might also possess N1 pHis protein kinase activity on substrates other than themselves. In addition, the isomerase PGAM employs an N3 pHis enzyme intermediate, raising the possibility that it may act more broadly as a N3 pHis depositing enzyme for proteins.

The work described in this thesis uses different approaches to investigate the subunit stoichiometry and nucleotide-binding potential of NME1 and NME2. By exploiting mass spectrometry and immunoblot analysis with commercial pHis site specific monoclonal antibodies I discovered that NME1/2 and PGAM do not require Mg^{2+} ions for activity, in marked contrast to protein kinases. In addition, I develop a medium-throughput thermal shift assay, which I exploit to show that recombinant NME1/2 and PGAM interact with a variety of novel nucleotides *in vitro*. To build on these findings I evaluate the interaction of wild-type and mutant NME kinases with a variety of small molecule ligands, including a large panel of FDA-approved small molecules, leading to the discovery of compounds that modulate hexamer dissociation. This work is then expanded on to investigate the functions of conserved NME Cys residues in hexamer stability, and the response to a variety of redox-active compounds, suggesting a role that might be relevant to the management of cellular oxidative stress. By using an enzyme assay, the NDPK phosphotransfer was also shown to be sensitive to a variety of cellular nucleotides and acetyl donors, including the co-factor Coenzyme A, and its dephosphorylated-derivate, which was previously unknown. Given that NME1/ 2 have been reported to possess histidine protein kinase activity, using the tools generated, the potential activity towards a variety of peptide substrates was evaluated. Although no evidence for trans phosphorylation of these peptides was found, the work reported in this thesis suggests new potential approaches for studying His protein phosphorylation by these, and other, putative protein His kinases, whilst highlighting challenges and solutions for the future analysis of pHis.

Table of Contents

List of figures and tables

List of abbreviations

ADP	Adenosine diphosphate
ATP	Adenosine triphosphate
AGC	Protein kinase A, G and C families
ATP	Adenosine triphosphate
BME	β-mecaptoethanol
BSA	Bovine serum albumin
CRISPR	Clustered regularly interspaced short palindromic repeats
C-terminal	Carboxly-terminus
CDP	Cytidine disphosphate
CTP	Cytidine triphosphate
Da	Dalton
DMEM	Dulbecco's Modified Eagle medium
DMSO	Dimethyl sulphoxide
DNA	Deoxyribonucleaic acid
DSF	Differential scanning fluorimetry
DTT	Dithiothreitol
EGFR	Epidermal growth factor receptor
ERK	Extracellular signal regulated kinase
ERL	Erlotinib
FBS	Foetal bovine serum
FDA	Food and drug administration
GAPDH	Glyceraldehyde 3-phosphate dehydrogenase
GDP	Guanine disphosphate
GTP	Guanine triphosphate
GPCR	G-protein coupled receptor
GST	Glutathione-S-transferase
HPLC	High performance liquid chromatography
IMAC	Immobilised metal affinity chromatography
IM-MS	Ion-mobility Mass spectrometry
IP	Immunoprecipitation
IPTG	Isopropyl-1-thio-β-D-galactosidase
ITC	Isothermal titration calorimetry
kDa	Kilodalton

KSR	Kinase suppressor of Ras
L	Litre
LB	Luria-Bertani
LIC	Ligation independent cloning
MAPK	Mitogen activated protein kinases
MBP	Maltose binding protein
mg	micro gram
mL	Millilitre
Mr	Relative molecular mass
MS	Mass spectrometry
m/z	Mass to charge ratio
mTORC1	Mammalian target of rapamycin complex 1
mTORC2	Mammalian target of rapamycin complex 2
ng	nano gram
NDPK	Nucleoside diphosphate kinase
NME	Non-metastasis
NTP	Nucleoside triphosphate
NDP	Nucleoside diphosphate
N-terminal	Amino-terminus
OD	Optical density
PBS	Phosphate buffered saline
PCR	Polymerase chain reaction
PDB	Protein data bank
PDK1	3-phosphoinositide-dependent protein kinase 1
PH	Pleckstrin homology
PI3K	Phosphatidylinositol 3-kinase
PIF	PDK1-interacting fragment
PIP2	Phosphatidylinositol 4,5-bisphosphate
PIP3	phosphatidylinositol 3,4,5-triphosphate
PKA	Protein kinase A
PKB/AKT	RAC-alpha serine/threonine-protein kinase
PKC	Protein kinase C
PKIS1	Protein kinase inhibitor set 1
PLK	Polo like kinase
PRK2	Serine/threonine-protein kinase N

RNA	Ribonucleaic acid
SDS-PAGE	Sodium dodecyl sulphate-polyacrylamide electrophoresis
SEC	Size exclusion chromatography
SH	Src homology domain
TBS-T	Tris-buffered saline and 0.1% Tween 20
TDP	Thymine disphosphate
TTP	Thymine triphosphate
Tm	Melting temperature
TSA	Thermal shift assay
UDP	Uridine disphosphate
UTP	Uridine triphosphate
UPAX	Unbiased phosphopeptide enrichment by strong anion exchange
Ve	Volume of elution
Vo	Void volume
ΔTm	Relative difference in melting temperature
µL	Microlitre

List of amino acids

Amino acid	3 letter code	Single letter code
Alanine	ala	A
Arginine	arg	R
Asparagine	asn	N
Aspartic acid	asp	D
Cysteine	cys	C
Glutamine	gln	Q
Glutamic acid	glu	E
Glycine	gly	G
Histidine	his	H
Isoleucine	ile	I
Leucine	leu	L
Lysine	lys	K
Methionine	met	M
Phenylalanine	phe	F
Proline	pro	P
Serine	ser	S
Threonine	thr	T
Tryptophan	trp	W
Tyrosine	tyr	Y
Valine	val	V

Chapter 1: Introduction

Background

As little as 1.7% of the entire human genome encodes for proteins, however, these are responsible for carrying out diverse and specialised functions and are commonly referred to as the 'molecular powerhouses' of the cell (1, 2). Thousands of cellular chemical processes are controlled by combinations of enzymes and structural proteins, both spatially and temporally. Adenosine triphosphate (ATP) is universal metabolic source of energy in both unicellular and multicellular species (3). ATP drives all aspects of cellular life, including active transport, muscle contraction and cellular signalling (4). In addition, chemical reactions involving the post-translational transfer from ATP to biomolecules are catalysed by protein kinases and protein phosphatases. Canonical protein kinases catalyse the transfer of the negatively charged ATP gamma phosphate to a context-specific serine (Ser), threonine (Thr) or tyrosine (Tyr) amino acid residue on a target substrate. The localised negative charge resulting from the attached phosphate can alter the conformation of the target protein, which either activates or inhibits a particular function or interaction with broader sets of protein(s), sugars, lipids or nucleic acids. Canonical protein kinases are usually sub-divided into serine/threonine or protein tyrosine-kinase sub-classes depending on whether they phosphorylate amino acids with an alcohol (OH) group in the case of Ser/Thr, or a phenol group, in the case of tyrosine (5), or both, in which case they are termed dual-specificity kinases.

In terms of protein phosphorylation, phosphate esters predominate in eukaryotic cell signalling, however, growing evidence suggests that 'non-canonical' amino acid phosphorylation on aspartate (Asp), lysine (Lys), arginine (Arg), glutamate (Glu), cysteine (Cys) and histidine (His) may have a greater influence in phosphorylation-mediated signalling than originally thought (6-9). For example, recent studies on the non-canonical phosphorylated amino acid, phosphohistidine (pHis), have begun to expose the biological relevance of pHis and to suggest roles in a range of physiological processes including its use in eukaryotic signalling systems, as well as being connected to a multitude of human diseases (10). Phosphohistidine was first discovered in the 1960s (11), and has well-known functions in bacteria and plants in 'two-component' His and Asp-based signalling (12). However, a lack of suitable analytical techniques and reagents for pinpointing acid and heat-labile post translational modifications such as pHis has led to non-canonical phosphorylation studies lagging far behind those of Ser/Thr and Tyr phosphorylation. Unlike canonical phosphorylation substrates, non-canonical phosphorylation substrates do not have a well-characterised 'kinome'. To date, two mammalian histidine kinases (NME1 and NME2) which are known for

a variety of functions (13) have been proposed as His protein kinases. NME proteins were first discovered as non-metastatic (NME) suppressor genes and are found at higher levels in tumours with low metastatic potential (14). These proteins possess nucleoside diphosphate phosphotransferase (kinase) activity and mediate the transfer of a phosphate from a nucleoside triphosphate to a nucleoside diphosphate, contributing to nucleotide homeostasis in the cell (15). Although there is no doubt that phosphohistidine plays a more pivotal role in cellular signalling than originally believed, the idea that NME proteins are able to phosphorylate a target protein substrate on a histidine residue has come under some scrutiny and the mechanism of this process is not well understood (16). NME proteins are also capable of binding small molecule kinase inhibitors and so represent rational targets for drug discovery efforts (17). Repurposing biologically and/or clinically active compounds that target atypical-conformations of canonical kinases can help understand how ATP-competitive, allosteric, or covalent inhibitors might influence histidine kinase-based signalling mechanisms and global phosphohistidine levels that are relevant to both health and disease.

1.1 Cell communication, signalling and signal transduction

The ability of cells to interact and adapt to their environment is one of the fundamental concepts in signalling and cell biology. Within a multicellular organism, cells must constantly interpret a variety of extracellular signals and generate an appropriate response in order to correctly translate and communicate within and between cells. These signals can be soluble factors generated locally, for example for synaptic transmission, or those generated at a distant location, such as hormones and growth factors, which diffuse to their target cells. They can also be ligands on the surface of other cells, or can be formed in the extracellular matrix itself. A response stimulated through these signals is predominantly achieved through the cell surface expression of specific high-affinity receptors whose conformation transduces extracellular information across the plasma membrane and elicits the activation of an intracellular signalling pathway. Cells have developed sophisticated ‘second messenger’ systems to integrate inputs from multiple signals involving a series of protein modifications by specific enzymes (such as protein kinases); this subsequently triggers the recruitment and activation of linker and scaffolding proteins, the modification of second messengers, and increase in the concentrations of intracellular calcium, and ultimately, the mobilisation of transcription factors for gene activation in the nucleus. The specific proteins and accessory intermediates involved depends on the specific receptor and cell type, though much overlap is evident within and between eukaryotic species. This coordination between several different systems allows for complex signalling networks to form, and be regulated, within the cell.

1.1.1 Cellular metabolism

As glucose is the primary energy source for most eukaryotic cells, the maintenance of glucose homeostasis is an essential physiological process, which is regulated by hormones and is a key component of cellular metabolism and cell signalling. An elevation in blood glucose levels stimulates the release of insulin from pancreatic beta cells through a glucose-sensing pathway. Insulin binds to the insulin receptor (IR), which possesses an intracellular tyrosine kinase activity, and is expressed on skeletal muscle and adipose cells. This results in the phosphorylation of the insulin receptor substrate (IRS) protein and subsequent activation of the classical PI3K/Akt and Erk1/2 signalling pathways. Activation of AKT causes the translocation of Glut4 vesicles to the plasma membrane, driving glucose uptake, cell proliferation and survival. Aberrant insulin signalling can lead to a number of diseases, notably diabetes and obesity. At low cellular ATP levels and glucose deprivation, the serine/threonine kinase 5'-AMP activated protein kinase (AMPK) is activated in order to positively regulate signalling pathways that replenish ATP supplies. AMPK is an energy sensor kinase that is activated by elevated AMP/ATP ratios induced by cellular and environmental stress including heat shock and hypoxia, as well as low glucose. AMPK stimulates catabolic processes such as fatty acid oxidation and glycolysis via the inhibition of ACC and activation of PFK2. In addition to this, AMPK negatively regulates several proteins central to ATP-consuming processes such as mTORC2, glycogen synthase, SREBP-1 and TSC2 and as a result downregulates or inhibits gluconeogenesis and glycogen, lipid and protein synthesis. Cellular metabolism is also an important and well characterised feature in cancer cells (18, 19). In the 1920s, Otto Warburg observed that tumour cells undergo high rates of glycolysis and lactate production in the presence of oxygen, a condition usually found only in an oxygen deprived state (20, 21). This was later termed the Warburg effect and several signalling pathways such as Akt, Erk1/2 and AMPK converge on the key glycolytic enzymes PFK and PKM2 to regulate glycolytic flux and production of ATP. The transcription factors c-Myc and p53 also play important roles in this process by regulating glutamine and lipid metabolism thereby creating the cellular components necessary for supporting and sustaining rapid tumour cell growth (18, 20).

1.2 Protein kinases and the human kinome

The human kinome contains ~535 protein kinases (22), which comprise ~1.7% of human genes, making them the third largest gene family after GPCRs and transcription factors. In general, kinases are proteins that catalyse the transfer of a phosphate. This reaction can occur on the kinase itself, known as autophosphorylation, or to another target protein. Protein kinases catalyse a phosphotransferase reaction in which the gamma phosphate of ATP (or

GTP) is transferred to a target substrate. In this thesis, for the most part, I use 'kinases' as an abbreviation for 'protein kinases'. This reaction can be reversed, and this is catalysed by a large family of nearly 200 protein phosphatases, which transfer the phosphate from an appropriate phosphoprotein to a water molecule (Figure 1.1). Phosphorylation was first discovered in the 1950s by Krebs and Fischer in the context of glycogen metabolism, and among the >300 types of post translational modification, phosphorylation and dephosphorylation are viewed as one of the most prevalent and well understood mechanisms that permit cells to respond to extracellular stimuli and both amplify and diversify appropriate signals inside the subcellular environment (23). For example, in response to growth factors, epidermal growth factor receptors (EGFR) autophosphorylate, which then activates mitogen activated protein kinases (MAPK) and the phosphoinositde-3-kinase (PI3K) cascade to induce cellular proliferation (Figure 1.2). The protein kinases can be divided into eight 'sub-families' (Figure 1.3), based on the sequence similarity of their eukaryotic protein kinase (ePK) domain. These are usually termed the Tyrosine kinases (TK), tyrosine kinases-like (TLK), cyclin-dependent kinases (CDK), homologues of yeast Sterile 7, Sterile 11, and Sterile 20 kinases (STE), cyclin-dependent kinase, map kinase, glycogen synthase kinase 3 and CDK2-like kinases (CMGC), calcium/calmodulin-dependent protein kinase (CAMK), the AGC kinases (named after the protein kinase A, G and C families) and a broad family of 'Atypical' protein kinases. In order to regulate the structure and function of cellular proteins in a wide range of cellular processes, protein kinases have evolved a diverse range of substrates and mechanisms, but typically perform their tasks using common ancestral structural features found in the catalytic domain (Figure 1.4) (2, 24).

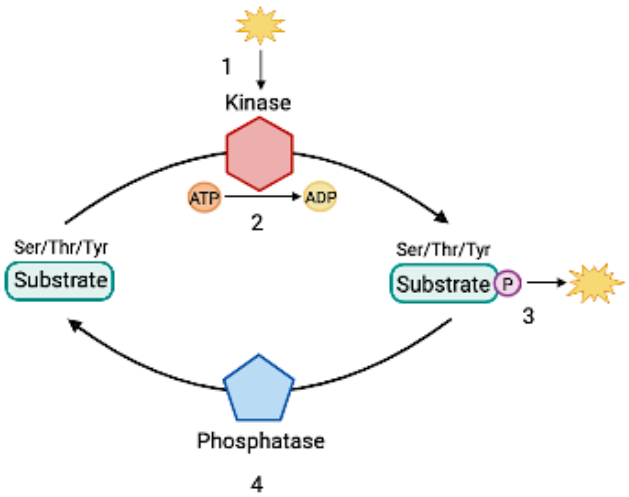

Figure 1.1. Schematic diagram of the mechanism of phosphate transfer by a canonical protein kinase. 1 A signal is detected, and the protein kinase is activated. **2** The protein kinase catalyses the transfer of the ATP γ-phosphate to Ser, Thr or Tyr on the substrate, yielding a covalently bound negatively charged phosphate group to the substrate **3** The phosphorylated substrate stimulates a signal cascade. **4** The removal of the phosphate group is catalysed by an enzyme known as a phosphatase.

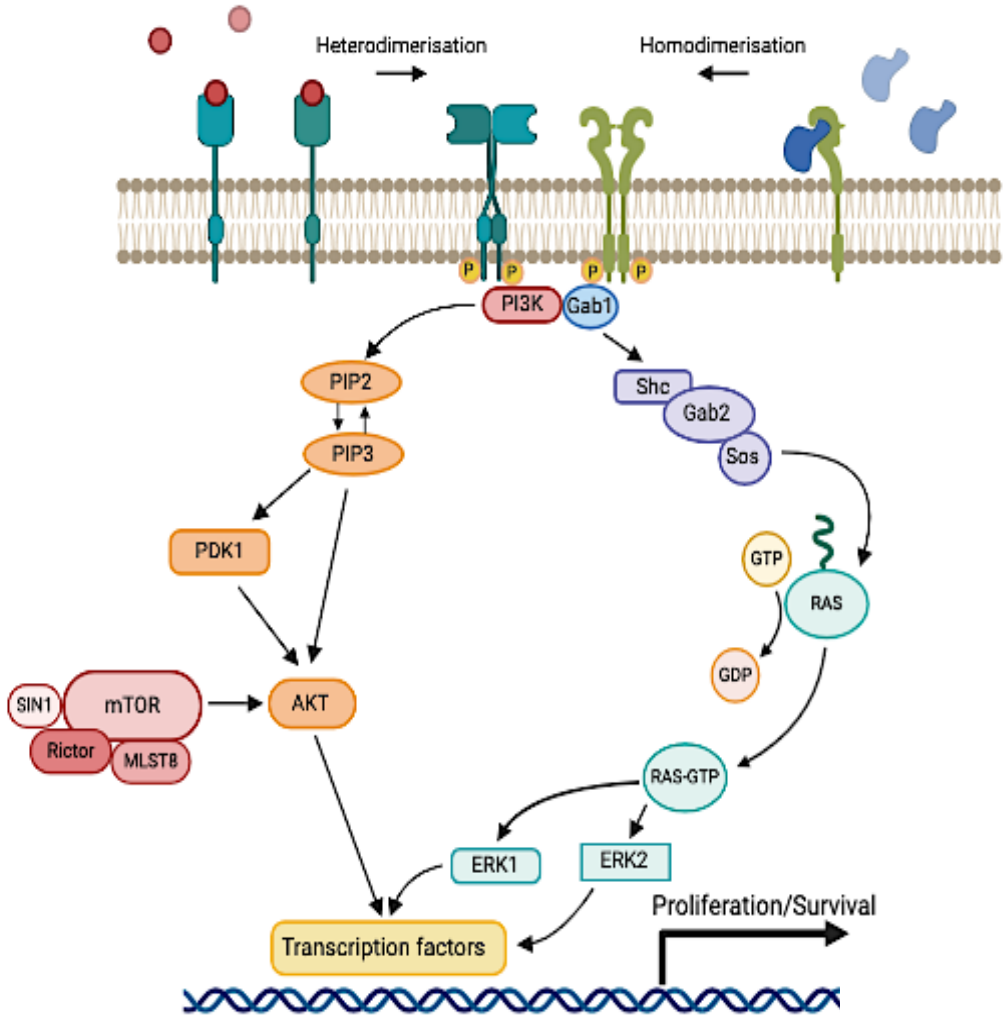

Figure 1.2. Example signal transduction pathway. Extracellular ligands bind to the receptor domains of EGFR kinases, including EGFR, HER3 and HER4, resulting in dimerization of the intracellular kinase domain. This activates the receptor kinases to *trans* autophosphorylate and activate the MAPK and PI3K/AKT signalling cascades. This schematic was created in BioRender.

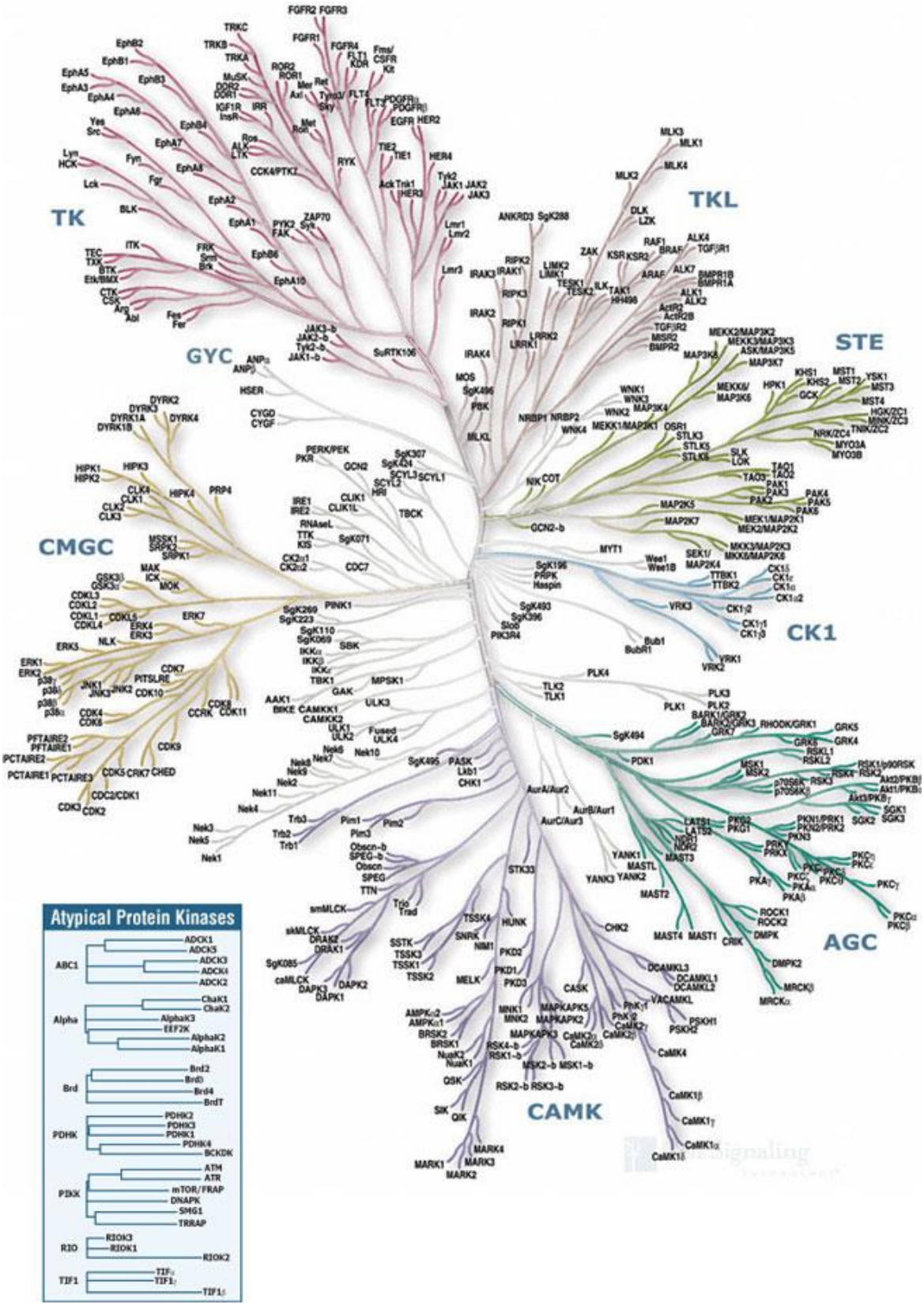

Figure 1.3. The human kinome. The eight major canonical protein kinase families and atypical protein kinases are named at the base of the branch. Illustration obtained from www.cellsignal.com.

1.2.1 Mechanism of ATP hydrolysis

The conserved motifs within the kinase domain (Figure 1.4) that are fundamental for ATP binding and hydrolysis were identified using amino acid sequence alignment from genomic data and local spatial pattern alignments obtained from structural data. In 1991, cAMP dependent protein kinase (PKA) was the first crystal structure of a kinase to be reported (25). The kinase domain consists of a small N-terminal lobe and a large C-terminal lobe. The N-terminal lobe is typically formed of five anti-parallel β-pleated sheets and an αC-helix. The C-terminal lobe on the other hand is mainly α-helical, containing the designated αF helix and catalytic loop, which are vital for aligning the 'regulatory' spine and for the hydrolysis of ATP. The interface of the αC-helix between the N-lobe and the C-lobe forms a cleft, which is the site of ATP and substrate binding, and the catalytic surface at which phosphate transfer occurs. Other structural aspects that play a pivotal role in the enzyme mechanism are the glycine-rich loop, a conserved lysine in the β3 sheet, the αC-helix, the catalytic motif, the activation segment and the hydrophobic αF helix (26). Interestingly, some 10% of kinomes throughout vertebrate species lack at least one of the canonical residues of the DFG motif and have been termed 'pseudokinases' (27), to reflect their loss of canonical nucleotide binding and/or catalysis.

1.2.1.1 The Glycine Rich Loop

The glycine rich loop refers to the consensus sequence GxGxxG in the β-turn-β motif between the β1 and β2 strands of the N-lobe. This motif is the most flexible part of the N-lobe due to reduced steric hindrance from the hydrogen R group of the glycine amino acids (28). The second Gly residue of this consensus sequence is considered the most important as it is the most highly conserved throughout the kinome. Upon ATP binding, this loop folds over the nucleotide and positions the γ-phosphate of ATP in a suitable orientation for transfer to the target substrate. The Gly-rich Loop connects the two β-strands that harbour the adenine ring (29).

1.2.1.2 The β3 lysine

Lysine is part of the VAxK motif that couples the α and β phosphates of ATP to the C-helix, stabilising the nucleotide as the glycine rich loop clamps down and exposes the γ-phosphate. The C-helix occupies an important position between both the N- and C-lobes (30). The C-terminus of the C-helix is tethered to the C-lobe by the αC-β4 Loop whereas its N-terminus interacts with the Activation Loop. The C-helix also contains another conserved residue, Glu, that bridges to Lys in the β-strand. This salt bridge is highly conserved through the entire protein kinase family and is often considered a hallmark of the active conformation state (31).

A reduction in protein kinase activity has been demonstrated in several biochemical studies as a result of a β3 lysine mutation to an uncharged alanine (Ala) or methionine (Met) (32).

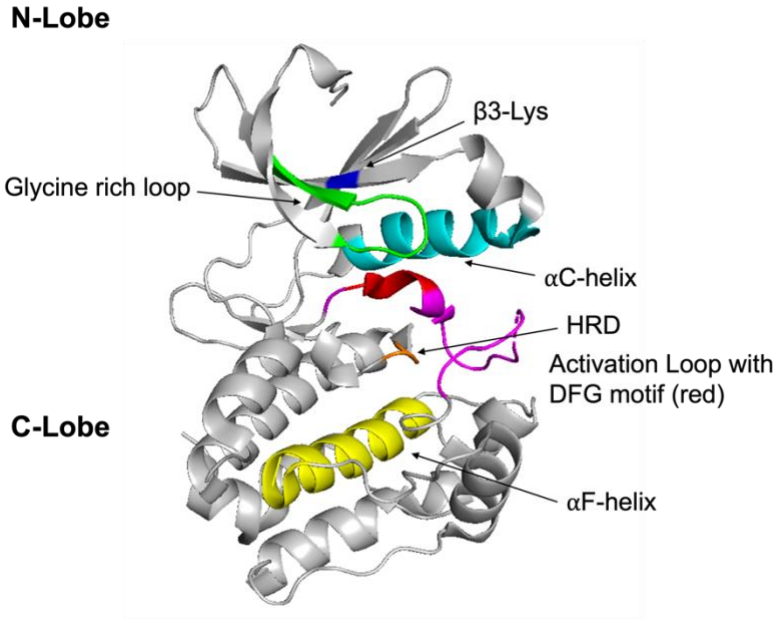

Kinase	Glycine Rich Loop	β3 Lysine	αC helix Glu	Asp and Asn	DFG Asp
EGFR	$_{719}$VLGSGAFG	$_{743}$VAIKE	$_{761}$DEA	$_{835}$HRDLAARN	$_{855}$DFG
HER3	$_{775}$VLGSGAFG	$_{750}$VAIKV	$_{769}$DEA	$_{843}$HRDLAARN	$_{863}$DFG
PKA	$_{49}$TLGTGSFG	$_{69}$YAMKI	$_{90}$NEK	$_{164}$YRDLKPEN	$_{184}$DFG
AKT1	$_{155}$LLGKGTFG	$_{176}$YAMKI	$_{197}$TEN	$_{272}$YRDLKLEN	$_{291}$DFG

Figure 1.4. Schematic representation of conserved protein kinase domain motifs and features important for catalysis. The key features of the protein kinase are the activation loop (magenta), containing the DFG motif (red), the glycine rich loop (green), the β3-Lys, Lys162 in AurA (blue) and the αC-helix. The crystal structure of Aurora A kinase was used here as an example. PDB ID: 1MQ4. Canonical residues involved in ATP binding are shown below and highlighted in red.

1.2.1.3 The αC-helix

The αC-helix is a distinct, very dynamic regulatory element in protein kinases and is the only conserved helix in the β-sheet-rich N-lobe. The C-helix functions as a 'Signal Integration Motif' as it connects to many different parts of the molecule and is responsible for mediating the conformational changes that take place within the catalytic centre (30). Positioning the αC-helix is one of the critical steps to prime the kinase for efficient catalysis and the distance between the N-terminus of the C-helix and the Activation Loop defines the open and closed conformations of the active or inactive enzyme (31).

The dynamic nature of the αC-helix can be modulated through activating or inhibitory regulatory mechanisms (33). In many AGC kinases, such as protein kinase A (PKA), protein kinase C (PKC), RAC-alpha serine/threonine-protein kinase (PKB/AKT1) and 3-phosphoinositide-dependent protein kinase 1 (PDK1) a hydrophobic motif is conserved. This C-terminal hydrophobic region has the general consensus sequence F/Y-X-X-F/Y-S/T/E/D-F/Y and consists of 50-60 amino acids after the conserved catalytic core (34, 35). Phosphorylation of this hydrophobic motif, such as Ser473 in AKT, can augment enzyme activity by acting as an allosteric effector. For example, phosphorylation of the hydrophobic motif causes it to dock on a hydrophobic surface created by the αC-helix, known as the PDK1-interacting fragment (PIF)-pocket (36). This interaction helps to stabilise the kinase in an active conformation, as the hydrophobic groove known as the PIF pocket only exists in the active state and simulates kinase catalytic activity through this intramolecular mechanism and is also thought to mediate protein-protein interactions (32, 37). Conversely, Src tyrosine kinase can be stabilised in an inactive conformation through a complex of Src-homology domains (SH2 and SH3) binding to the αC-helix and to an inhibitory phospho-tyrosine in the C-terminal tail (38, 39).

Another example of allosteric regulation of catalytic activity via the αC-helix are the cyclin-dependent kinases (CDKs). In the absence of cyclin, the CDK αC-helix (which serves as a cyclin docking site) is rotated to an outward state (40). In the structure of CDK2 without cyclin, the conserved Glu51 cannot form an ionic bond with the β3 Lys33. However, binding of cyclin directly to the αC-helix induces rotation to an inward state, thus restoring the Lys33-Glu51 salt bridge (41), which is integral for catalysis.

1.2.1.4 Magnesium binding DFG motif

The DFG motif forms a loop within the catalytic spine and is highly conserved throughout all protein kinase families. A Mg^{2+} ion stabilises the negative charges of the ATP phosphate groups and makes polar contacts with all three ATP phosphates (42). The Asp amino acid of the DFG motif is responsible for coordinating the positively charged Mg^{2+} ion. If the DFG motif is not correctly positioned within the catalytic domain, the active site is sterically blocking from binding ATP. For this reason, the Asp of the DFG motif is often mutated to an uncharged amino acid (Ala or Asn) in order to inactivate protein kinases.

Structural analysis of AKT shows that in the 'DFG-out' conformation of the kinase, the DFG phenylalanine (Phe) is flipped over and occupies the position in the C-spine that is filled by adenine ring of ATP in the active conformation (37, 43). This 'DFG-out' conformation is often

deemed a signature for the 'inactive' kinase state (44, 45). In the 'DFG-in' conformation, the hydrophobic Phe makes contacts with the catalytic motif and αC-helix when the kinase lobes close and the DFG loop faces inwards, which stimulates the formation of the β3 Lys-Glu ionic bond (46). Finally, the Gly stimulates correct positioning of the Asp residue through formation of a hydrogen bond. In the 'DFG-out' state, this hydrogen bond is disrupted, and the flexibility of movement offered with the DFG loop is a hindrance to Mg^{2+} ion binding (42).

1.2.1.5 The catalytic loop

The catalytic motif, often called the HRD motif, contains an Asp that becomes protonated by accepting a hydrogen from the hydroxyl group of the substrate amino acid, which in the case of canonical protein kinases is either Ser, Thr or Tyr (47). Many protein kinases require a divalent cation for efficient catalysis, and the Asn residue of the HRD motif also permits a second Mg^{2+} ions to bind as is orientates the catalytic Asp through coordinating Mg^{2+}, in addition to the Mg^{2+} ion coordinated by the DFG motif (42). The HRD motif (Figure 1.4) histidine is also very highly conserved and serves as a central scaffold for the catalytic spine, which binds to the carbonyl of the DFG Asp and makes a hydrophobic contact with the DFG Phe (48). The catalytic loop communicates with the activation segment, the major regulatory region of post-translational modification in kinases.

1.2.1.6 Activation loop phosphorylation

The catalytic motif is described as both the HRD motif or the HxD motif, due to the variability of the Arg residue. Protein kinases with the HRD catalytic motif ('RD kinases') require phosphorylation of the activation loop to drive the active conformation (Figure 1.4). The HRD Arg is prevalent in kinases that require phosphorylation because the positively charged Arg supports a link between the catalytic motif, activation loop and the DFG motif through interaction with the phosphorylated activation loop residue. For instance, phosphorylation of the Thr197 residue of PKA, which is adjacent to the catalytic HRD Asp, is required for full catalytic activity. The phosphate group from the phospho-Thr197 coordinates the αC-helix (His87), the catalytic motif (Arg165) and the β9 sheet (Lys189), allowing conformational movement from a DFG-out to a DFG-in catalytically active orientation (49).

Phosphorylation of the activation loop of EGF, fibroblast growth factor receptors (FGFRs) and insulin-like growth factor receptors (IGFRs) occurs upon dimerization and *trans*-autophosphorylation (50, 51). This autophosphorylation relieves the inhibition caused by the activation loop, which would otherwise occlude the active site and prevent substrate from binding (50).

1.2.1.7 The αF-helix

Recently, the hydrophobic αF-helix has been shown to serve as an organising element for the entire kinase core (Figure 1.4) (26). The αC-helix and the Activation Loop are very mobile, which allows the hydrophobic spine to be dynamically assembled and disassembled thereby regulating the protein kinase activity and thus designated as the regulatory Spine (R-spine). Both the C- and the R-spine are anchored to the F-helix, the C-spine directly to the hydrophobic C-terminus and the R-spine to the N-terminus (47). One of the regulatory spine residues is also part of the HRD motif of the Catalytic Loop (Figure 1.4, highlighted in orange). In most kinases this is a histidine whereas in some kinases such as PKA and the majority of the AGC superfamily the His is replaced by a Tyr (52). The backbone of the His/Tyr is anchored to the F-helix through a very highly conserved Asp (Asp 220 in PKA), which lies at the beginning of the F-helix. Asp is highly conserved even in ELKs and is the only electrostatic link that ties together the hydrophobic network (52). The second hydrophobic spine also encompasses residues from the N and C-lobes but is completed by the adenine ring of ATP and was thus termed the catalytic spine. The catalytic spine is formed from the Ala residue in the VAIK motif in the β3 sheet and this interacts with the adenine ring of ATP (52).

1.3 Mechanisms of canonical protein kinase domain activation

1.3.1 AGC kinase activation

The mechanism by which protein kinases perform ATP hydrolysis and phosphotransfer to regulate target proteins in cell signalling has been discussed. However, protein kinases are intracellular mediators of signals and have evolved multiple regulatory mechanisms to efficiently phosphorylate specific substrates. Some kinases are regulated by interactions with regulatory domains or inhibitory regions or subunits, which can modulate their localisation and ability to interact with substrates. Kinases from specific families, such as the AGC kinases, exploit *in cis* interactions of a C-terminal polypeptide tail with the catalytic domain in order to control substrate binding and catalytic activity. Allosteric interaction of the C-terminal tail with the regulatory site by the C-helix of the N-lobe known as the PDK1 interacting fragment-(PIF) pocket helps regulate AGC kinase activity. The PIF-pocket acts like an ON-OFF switch with different modes of regulation. Phenylalanine residues within the hydrophobic motif (HM) were shown to dock to a surface created by the C-helix and this interaction with the PIF-pocket allosterically affects the ATP binding site and peptide substrate binding site (37, 53, 54).

1.3.1.1 Regulation of AKT activity

AKT is a main effector downstream of PI3K stimulation and the formation of 3-phospholipids (Figure 1.2), and signals to key downstream elements such as glycogen synthase kinase 3 (GSK3), forkhead/winged helix class O (FOXO) transcription factors and the mammalian target of rapamycin complex 1 (mTORC1). The huge array of signalling networks responsive to AKT regulation appears ubiquitous in essentially every cell. Mouse and human genetic studies have also revealed specific physiological roles for the AKT networks in distinct organ systems. There are three isoforms of the Ser/Thr kinase (AKT1, AKT2 and AKT3) and comprehension of their regulatory functions is particularly important, as AKT dysfunction plays a role in various diseases, including cancer, cardiovascular disease, insulin resistance, inflammatory and autoimmune disorders, and neurological disorders (55-58).

AKT is phosphorylated in the activation loop (Thr308 in AKT1) by PDK1, but requires phosphorylation at a Ser473 residue, in the HM, by the mTORC2 complex for full activation (37, 56). *In vitro* AKT from HEK293T cells is inactive, but phosphorylation by PDK1 increases activity by ~ 100 fold (59). Subsequent phosphorylation of AKT at Ser473 by MAPKAP kinase-2 resulted in up to 1000-fold increased activity *in vitro* compared to the inactive form of AKT. When only the Ser473 residue is phosphorylated by MAPKAP kinase-2 (a non-specific 'upstream' kinase), total AKT activity increased ~ 6 fold (59). AKT has an N-terminal Pleckstrin homology (PH) domain which binds, *in cis*, to the kinase domain, stabilising an inactive conformation and sterically hindering binding of PDK1. On growth factor stimulation of receptor tyrosine kinases (RTKs) or G-protein-coupled receptors (GPCRs), PI3K is recruited to the plasma membrane, where it phosphorylates phosphatidylinositol 4,5-biphosphate (PIP_2), producing phosphatidylinositol (3,4,5)-triphosphate (PIP_3) (60). PIP_3 binds to the PH domain of AKT, thereby disrupting the inhibitory interaction between the N-terminal and catalytic domains. Binding of PIP_3 to the PH domain also serves to localise AKT to the plasma membrane with PDK1. PDK1 is then able to bind and phosphorylate AKT1 at Thr308. In contrast, the HM of ribosomal protein S6 kinase beta (S6K) is required to bind *in trans* to the PIF pocket of PDK1 to be phosphorylated. After phosphorylation of the activation loop by PDK1, S6K does not require phosphorylation of the HM to interact *in cis* to fully activate the kinase domain (61). The HM of AKT does not bind *in trans* to PDK1. Deleting the PH domain negates phosphorylation at Thr308 by PDK1. However, replacing the C-terminal tail of AKT with the C-terminal tail of PRK2 rescues AKT phosphorylation at Thr308 (37).

1.3.1.2 PRK2 regulation by the C-terminal tail

Serine/threonine-protein kinase N (PRK) kinases are closely related to PKCs and are described to mediate physiological effects downstream of Rho, such as Rho-dependent cell

migration (62). They are also implicated in aetiology of prostate cancer (63). PRK2 is auto-inhibited by dimerization of the kinase domain, mediated through the N-terminal pseudosubstrate PLK domains and not intramolecular interactions (64). This prevents the interaction with upstream kinase PDK1. Interaction of the N-terminal Rho-binding domains with GTP-Rho stimulates interaction with PDK1. The HM motif of PRK2, which has negatively charged Asp in place of a phosphorylation site, then binds *in trans* with the PIF pocket of PDK1 (65). Phosphorylation by PDK1 results in dissociation and supports the formation of an active PRK2 monomer with an *in cis* HM intramolecular interaction with the PIF-pocket.

1.3.2 Activation by intermolecular interaction

1.3.2.1 Activation of Aurora kinases

Aurora kinases lack N- or C-terminal extensions that bind *in cis* to the kinase domain. In contrast, a binding site adjacent to the Aurora A αC-helix interacts with regulatory partners such as *Xenopus* kinesin-like protein 2 (TPX2) and TACC3. The Aurora B and Aurora C specific activator inner centromere protein (INCENP) binds to Aurora B/C in a different orientation (66-68). Binding of TPX2 leads to activation of Aurora A *in vitro* (68), enhancing autophosphorylation of Thr288 (in the activation loop) many fold. When TPX2 is absent, the activation segment of Aurora A is orientated in an inactive conformation. However, binding of TPX2 induces a 10 Å shift of the phosphorylated Thr288 from an exposed to a buried position and leads protection from dephosphorylation by phosphatases. Thus, TPX2 synergises with Aurora A to increase phosphorylation and dephosphorylation is inhibited (66, 68).

1.3.2.2 Activation of Polo like kinases (PLKs)

Domains that flank the kinase domain are important for modulating, regulatory interactions, and activity. Polo-like kinases (PLKs) are cell cycle regulated kinases that are close relatives of the AGC superfamily of kinases. PLKs have two C-terminal polo-box domains (PBDs) that bind to specific target sequences when phosphorylated in order to regulate activity and the localisation of the kinase (69). The four human polo-like kinases control various aspects of the cell cycle.

1.3.2.3 Activation of EGFR family kinases

The epidermal growth factor receptor (EGFR) is a member of the ErbB receptor family, which in turn, is a member of the receptor tyrosine kinase superfamily. The ErbB receptor family consists of EGFR (also known as HER1), ErbB2 (HER2), ErbB3 (HER3) and ErbB4 (HER4). EGFR is involved in a variety of cellular processes including cell proliferation, motility, survival and differentiation (70-73). The receptor is activated by the binding of various ligands including

epidermal growth factor (EGF) and transforming growth factor α (TGFα) and it is well known that aberrant activation of EGFR is implicated in a variety of human cancers (74-76). EGFR is a transmembrane protein, consisting of an extracellular domain, a transmembrane domain, a juxtamembrane (JM) domain, a kinase domain, and a C-terminal regulatory tail (77, 78). Ligand binding induces translocation and homodimerization (with other EGFR proteins) and heterodimerisation (with different EGFR members, such as HER2 which cannot bind extracellular ligands) of the intracellular kinase domain. This leads to in trans autophosphorylation at specific tyrosine residues and these phosphotyrosine residues bind soluble or membrane-anchored effector proteins (50, 79, 80). The activated kinase domains stimulate downstream effectors such as Shc1 and Grb2 (10) and major signalling pathways including the Ras/Raf/mitogen-activated protein kinase pathway to activate extracellular signal regulated kinase (ERK1) and ERK2, or the PI3K/AKT pathways (Figure 1.2) (81, 82).

Allosteric intermolecular interactions drive the kinase domain of EGFR proteins into an active conformation following asymmetrical dimerization, whereby one kinase domain activates the other. The juxtamembrane (JM) domain is situated in the cytoplasmic domain at the N-terminal region and links the kinase domain to the transmembrane domain. The JM domain is formed of two segments; the JM-A segment which links to the transmembrane domain and the JM-B segment, which on dimerization binds to the C-lobe of the 'activator kinase', which allosterically stimulates the N-lobe of the 'receiver kinase' (83). Upon this allosteric activation, the JM domain forms what is referred to as a 'juxtamembrane-latch'. Dimerisation of the EGFR stabilises the helical JM-A dimer, which in turn stabilises the kinase domain dimer. In the absence of ligand, alternative dimer formation does not lead to activation as the C-terminal tails of the kinase domains inhibit the formation of the juxtamembrane latch (83, 84).

1.4 Small molecules and protein kinases

As protein kinases regulate nearly all aspects of cell life, and alterations in their expression or mutations in their genes have been implicated in multiple cancers, much research has focussed on the discovery and chemical modification of scaffolds to generate potent kinase inhibitors. The first kinase inhibitor to receive FDA approval, was the Abelson (ABL) tyrosine kinase inhibitor, imatinib (85) in 2001. ABL is deregulated in nearly all cases of chronic myeloid leukaemia (CML) (86). This was followed by the development of epidermal growth factor receptor (EGFR) inhibitors, demonstrated to be overexpressed in many cancer types, such as erlotinib and gefitinib (87, 88). Since then, the progress and development of potent and specific protein kinase inhibitors has been a major area of growth. Although much of the early research in kinase inhibitors focussed on oncology, kinase inhibitors are likely to be very useful in order

to treat a variety of diseases including Parkinson's disease, Alzheimer's disease and a variety of autoimmune and inflammatory diseases (89). To date, over 100 small molecule kinase inhibitors have been approved in the US by the FDA (https://www.ppu.mrc.ac.uk/list-clinically-approved-kinase-inhibitors). Target-validated kinase inhibitors are also powerful probes for the study of cell signalling. A lack of probe compounds to study His phosphorylation is one of the reasons this field has remained relatively stagnant.

1.4.1 ATP competitive inhibitors

Most protein kinase inhibitors are reversible competitive ATP mimicking compounds that can be broadly classified into two subgroups: type I inhibitors, such as imatinib, and type II inhibitors, such as staurosporine. Type I inhibitors bind to the kinase nucleotide-binding site and stabilise the 'DFG-in' (active) conformation, whilst type II inhibitors stabilise the DFG-out inactive conformation (85, 90) by targeting a new binding site. Type I inhibitors prevent the conformation of the protein kinase conducive of phosphotransfer and typically contain a heterocyclic ring structure reminiscent of the purine ring of ATP (85, 90, 91). Type II inhibitors achieve inhibition by occupying the hydrophobic groove adjacent to the ATP binding site that is accessible when the αC helix and DFG motif are in an outward orientation (91). Analysis of type II inhibitor binding found that many of these inhibitors share similar pharmacophore and exploit a conserved set of hydrogen bonds (85, 90). The ability to induce dramatic conformational changes in the enzyme is not unique to type II inhibitors however, for example the type I inhibitor alpelisib, a selective inhibitor of PI3Kα, has been approved for the treatment of breast cancer (92).

Due to the highly conserved nature of the kinase fold and specific mechanism of ATP binding and hydrolysis, finding selective ATP-competitive inhibitors for particular kinases has been extremely challenging. In addition, given the potential for kinome-rewiring and the generation of drug resistance, it is not uncommon to treat patients with combination therapy. For example, combining dabrafenib and trametinib to target the RAF-activated MAP kinase cascade for the treatment of aggressive melanoma improves relapse-free survival. Protein kinase inhibitors such as imatinib and sorafenib, which exhibit polypharmacology, can be repurposed to treat several distinct types of cancer. However, off-target engagement may also underlie serious side effects associated with therapy.

1.4.2 Allosteric inhibitors

Allosteric inhibitors, or also known as type III inhibitors exploit alternate binding pockets outside the canonical protein kinase active site. This has potential benefits, since these sites are sometimes specific to a particular kinase so that the binding of compounds distal to the

ATP-binding pocket induces a conformational change(s) elsewhere in the kinase. In this manner, it is possible for allosteric inhibitors to indirectly influence catalytic activity as well as non-catalytic regulatory functions such as scaffolding and regulatory mechanisms that are unique to a kinase (90). For instance, the PIF-pocket, by the αC-helix of PDK1 has been targeted. In AKT, the N-terminal PH domain binds intramolecularly with the kinase catalytic domain, stabilising the kinase in an inactive conformation. AKT inhibitors, including MK2206, exploit this and stabilise the inactive structure of the PIF-pocket by binding to the αC-helix, which locks the PH domain to the N-lobe of the kinase domain (93, 94). This direction of research has not only led to the discovery of allosteric inhibitors, but also allosteric activators of kinase activity (95) .

1.4.3 Covalent inhibitors

A number of kinase inhibitors are capable of forming a (usually reversible) covalent bond to a Cys residue in the kinase active site. Chemically, this occurs through the nucleophilic attack of a cysteine residue. Currently, there are six covalent inhibitors approved by the FDA (96), and afatanib, a second-generation EGFR inhibitor that targets Cys797 in the kinase domain, was the first (97). This was later followed by ibrutinib, a tyrosine kinase inhibitor (98), and Osimertinib, a third-generation T790M mutant selective EGFR inhibitor (99). Covalent inhibitors exploit the electron-rich nature of the sulfur present in a solvent exposed cysteine residue that is located before the conserved DFG motif of the kinase activation loop. This irreversible binding results in blocking of the ATP binding site to the kinase, thereby rendering the kinase inactive (100, 101). Irreversible kinase inhibitors have also been designed against vascular endothelial growth factor receptor 2 (VEGFR2) (102). Many kinases have a cysteine located in the vicinity of the ATP binding pocket and could therefore be a target for covalent inhibitors, however despite this, targeted inhibition by an irreversible approach raises concerns about the potential toxicity and modification of unanticipated targets.

1.4.4 Acquiring resistance to inhibitors

Protein kinase inhibitors have been beneficial for some cancer patients; however, these compounds are not curative. Before the introduction of imatinib, CML was a rare form of leukaemia. Ironically, the discovery of imatinib and subsequent treatment increased the incidence of this cancer because it manages, but does not cure the disease. Interestingly, the kinase-activating L858R mutation in EGFR is highly responsive to the FDA approved compounds erlotinib and gefitinib (87, 88, 100, 103). However, relapse due to a secondary, drug resistant mutation in EGFR whereby the gatekeeper threonine is converted to methionine can occur, which increases the affinity for ATP, rendering ATP competitive inhibitors ineffective (104). This highlights that most protein kinase inhibitors only delay disease and

tumour progression as particularly for advanced tumours, routes to circumvent target inhibition are taken and lead to drug-resistance (89).

Tumour resistance can occur via innate or acquired mechanisms. For example, when a tumour harbours oncogenic driver mutations associated with a protein kinase, not all tumour cells respond. This can be due to extrinsic factors such as the drug producing insufficient inhibition of the target kinase or in turn, disassociating from the kinase after an insufficient amount of time. Innate resistance is generally a result of co-existing genetic aberrations in multiple oncogenic pathways (89). The T790M mutation in EGFR described above is an example of this (105). Acquired resistance develops in patients with advanced metastatic disease. These mechanisms are caused by the ability of the tumour to maintain continued proliferative and survival signalling despite the presence of an inhibitor (106). One common mechanism is through the increased expression and activity of drug transporters, that actively export drugs from cells (89, 107). In order to treat any disease or tumour effectively, inhibitors that have improved selectivity, and subsequent reduction in side effects as well as the ability to combat resistance mechanisms need to be obtained. An example is osimertinib, which targets T790M EGFR, and is now the front-line therapy in NSCLC.

1.5 Protein pseudokinases and atypical protein kinases

Pseudokinases appear within all kinase superfamilies in humans and make up about 10% of the human kinome that possess mutations in positions that were thought to be crucially important for catalysis (108). Pseudokinases were initially thought to be inactive, but recent developments have demonstrated that they either act as scaffolds or possess atypical catalysis that is distinct from canonical kinases. This therefore led to the hypothesis that pseudokinase signalling could be propagated through either low levels of catalysis, made possible by an alternative active site geometry, via nucleotide binding-driven allosteric transitions, and/or through the direct modulation of binding surfaces (109). One example is a kinase family that lacks the universally conserved lysine in the β3 strand, known as WNK kinases: With No K (110). Instead of lysine the WNKS recruit another lysine from β2 to fill the same space and fulfil the same function. Another example is calcium/calmodulin-dependent serine protein kinase (CASK) which was shown as a Mg^{2+}-independent kinase that selectively phosphorylates neurexin 1 (111). It is thought that 'mimicking' an activated kinase conformation is a common feature of different pseudokinases (112-114). For instance, Vaccinia related kinase 3 (VRK3), has a series of hydrophobic mutant residues that fill the adenine binding pocket and complete the C-spine without ATP (115). Some two thirds of

pseudokinases have been implicated in a range of human diseases such as breast cancer and prostate cancer, glioblastoma and autoimmune diseases (109).

1.6 Non-canonical phosphorylation

As described previously, phosphorylation is an extensively studied and well-characterised post-translational modification of proteins in both eukaryotes and prokaryotes. Until recently, protein phosphorylation on Ser, Tyr and Thr was thought to be the primary mode of phosphorylation-mediated signalling in non-plant eukaryotes. In part, this was due to the high instability of phosphorylated non-canonical amino acids under standard methods of phosphoprotein characterisation. Phosphorylation on non Ser/Thr/Tyr amino acids, termed here 'non-canonical' phosphorylation, is relatively widespread in bacteria and plants. Non-canonical phosphorylation sites include histidine (His), aspartate (Asp), cysteine (Cys), lysine (Lys) and arginine (Arg) and there is growing evidence to suggest that these modifications are not only common (116), but they also play a role in regulating protein signalling functions.

1.6.1 Cysteine phosphorylation

In various proteins, cysteine (Cys) can be subject to multiple post-translational modifications (PTM), although phosphorylation on Cys was not considered a common PTM that had any regulatory role in both prokaryotes and eukaryotes (117). However, in *E. coli* and bacteria, phosphocysteine has been shown to be a catalytic intermediate in phosphotransferase systems. For example, the glucose transporter of the bacterial phosphotransferase system couples vesicle translocation to phosphorylation of the transport sugar and this phosphate is transferred to the glucose sugar from a cysteine amino acid and involves an extended phosphotransfer relay with several subunits of the phosphotransferase system (118).

In eukaryotes, a similar mechanism of cysteine phosphorylation is observed in protein-tyrosine phosphatases (PTPases) (119). PTPases govern the level and duration of tyrosine phosphorylation within the cell. Unlike alkaline and acid phosphatases, which hydrolyse the phosphate ester bond through a phosphoserine enzyme intermediate or a phosphohistidine intermediate, PTPases possess a catalytically essential cysteine residue which forms a covalent thiol-phosphate bond during the hydrolysis of tyrosine phosphate-containing substrates. The generation of the phosphocysteine protein is specific, as substitution of the catalytic Cys residue to a Ser abolishes the formation of an enzyme intermediate and as a consequence catalytic activity. The formation of a pCys enzyme intermediate is a conserved mechanism amongst all 100 tyrosine phosphatases in the human genome, and the catalytic Cys, and residues surrounding it in the $C(X)_5R$ motif are highly conserved from pathogenic bacteria to humans (120, 121).

1.6.2 Lysine and arginine phosphorylation

Phosphorylation of the nitrogens in lysine (Lys) and arginine (Arg) has been reported in both prokaryotes and eukaryotes (122), however, phosphorylated Lys and Arg are labile and are therefore difficult to analyse. In the Gram-positive model bacterium *Bacillus subtilis*, a 'specific' arginine kinase has been reported (123). The heat shock response in this organism is mediated by a complex regulatory network (124) that is governed by four major transcriptional regulators, including the alternative sigma factor σB (125), the two-component response regulator CssR (126), and the repressors HrcA (127) and the CtsR (128, 129). The CtsR represses transcription of the *clp*C heat shock operon and the *clp*E and *clp*P genes by specifically binding to a seven-nucleotide direct repeat consensus sequence (129) and stress induced transcription of the *clp* genes depends on the inactivation of CtsR by McsB (130). McsB has been reported to exhibit tyrosine kinase activity and shows homology to phosphagen kinases (PhKs) (130, 131) but was later found to be an arginine kinase, phosphorylating an arginine residue of CtsR (123). The selective introduction of a negatively charged phosphate moiety functions as a molecular switch to regulate DNA binding. The unphosphorylated CtsR binds with high affinity to its DNA consensus site, whereas the McsB-phosphorylated CtsR repressor is not able to bind to DNA, thus allowing heat-shock gene expression (123). The mammalian kinases involved in Lys and Arg modifications have not been identified and purified, making it difficult to determine the biological relevance of pLys and pArg in eukaryotes.

1.6.3 Histidine phosphorylation

His phosphorylation (pHis) was originally identified from a bovine preparation by Boyer and colleagues in the early 1960s as part of an oxidation reaction on an enzyme intermediate (11). Over the years however, characterisation of histidine phosphorylation and our understanding of its role within cellular signalling has remained largely limited to prokaryotes (described in Section 1.7). Phospho-histidine (and phospho-arginine) contains a phosphoaramidate bonds (P-N) and compared to the canonical phospho-esters, it is highly unstable under acidic conditions and at elevated temperature (8). This acid-lability and thermosensitivity of these particular modifications is not compatible with most standard phosphoproteomic methods used for pSer, pTyr and pThr and has therefore contributed to difficulties and slow progression when it comes to studying this modification (132, 133).

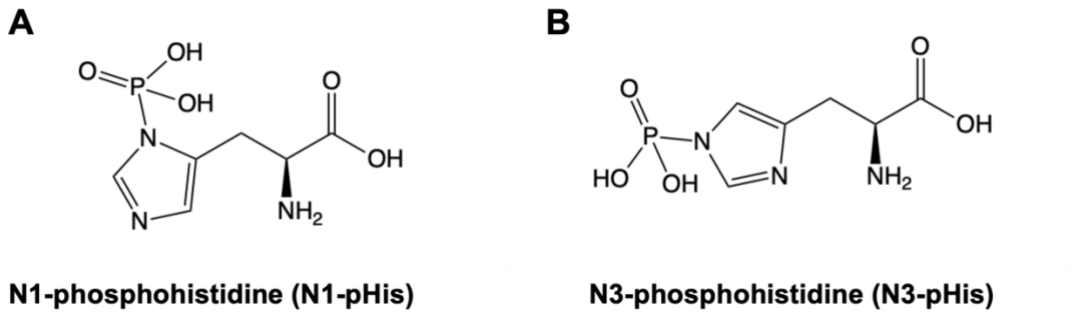

Figure 1.5 Structures of the two pHis isomers found in physiological conditions N1 phosphohistidine (N1-pHis) and N3 phosphohistidine (N3-pHis). Structures were generated in ChemDraw 19.1.

The five-membered imidazole side chain of histidine has two phosphorylatable nitrogens, N1 and N3, giving rise to two phosphoisomers, N1 pHis and N3 pHis, respectively (133) (Figure 1.5). These isomers undergo rapid hydrolysis by virtue of near-neutral pKa values, at 7.3 in N1 pHis and 6.4 in N3 pHis. Because of this, they do not share the same physical properties, as the N1 pHis isomer is relatively unstable compared to N3 pHis. This is demonstrated in the isolated amino acids by the fact that the rate of hydrolysis at pH 5.0 for the N1 pHis isomer is ~ 10 times higher than that of the N3 pHis isomer and is attributed to N1 pHis being more electrophilic and a better leaving group due to its proximity to the α-amino group (8, 133).

1.6.4 Methods and techniques to detect pHis

The pace at which studies into histidine phosphorylation fell behind that of serine, threonine and tyrosine phosphorylation and their respective kinases is accounted for by the technical difficulties associated with detecting pHis in proteins. Classical techniques widely employed in detecting protein phosphorylation utilise acidic treatments, which is not compatible with the acid-labile pHis modification, as well as other non-canonical phosphoamino acids such as those described above (134). Early methods designed to detect pHis involved phenol extraction (135) and gel-based assays (136), however these proved difficult to reproduce and apply quantitatively. Early studies have focused on the detection of phosphoramidate-containing proteins by thin layer electrophoresis, reverse-phase layer chromatography (137), high-performance liquid chromatography (138) and autoradiography (139, 140) which have all been instrumental in identifying and distinguishing biochemically derived phosphohistidine from phosphotyrosine and other phosphoamino acids.

Mass spectrometry is a useful tool for the identification of most phosphoamino acids, with phosphohistidine being no exception, as it has been utilised for the presence of both synthetically and enzymatically derived pHis (141, 142). Mass spectrometry has been used to

detect synthetic peptides containing pHis (116, 143). The development of N1 pHis and N3 pHis phosphospecific antibodies, which do not cross-react with either phosphotyrosine or other pHis isomers, has been crucial to increasing the depth of knowledge of phosphohistidine (9). Proteomic, immunological and biological analyses using these monoclonal antibodies has indicated that pHis has important functions in mammalian biology (8). Whilst a small number of analytical techniques have been developed to detect pHis, the purification and identification of mammalian histidine kinases has not been demonstrated unequivocally, and therefore histidine kinase activity and understanding the extent and regulation of pHis signalling in mammalian cells remains elusive.

1.7 pHis in prokaryotic cell signalling

1.7.1 Two component signalling system

Histidine phosphorylation is widely known for its role in the two-component system (TCS), or multi-component phosphorylation system used in bacteria for cell signal transduction. This system is reminiscent of mammalian tyrosine kinase receptors in both its structure and mode of action as it comprises a sensing domain on the outside of the plasma membrane, a transmembrane domain and a cytoplasmic domain containing the histidine that is targeted by kinase. The proteins involved in the bacterial TCS are the sensor histidine kinase (HK) and the response regulator (RR) (144), with these two factors being the some of the most abundant proteins across the bacterial and archaeal kingdom (145). In a prototypical TCS, the HK and RR serve to connect an environmental or cellular signal with an appropriate cellular response. The TCS components achieve this by communicating through phosphoryl-group transfer from a histidine (His) of the HK to an aspartate (Asp) of the RR (Figure 1.6). Some HK also function as a phosphatase for their respective RR under non-inducing conditions by catalysing the reverse reaction (146). A diverse range of signals can be detected by the HK. For example, Bacillus subtilis DesK kinase responds to temperature changes by detecting membrane fluidity (147). A wide variety of domains in the extracytoplasmic space such as PAS domains of CitA (citrate ligand) can detect small ligand nutrients such as amino acids and carboxylic acids are detected directly (148). Other kinases have been shown to recognise small antimicrobial peptides (149), oxygen concentration (150) and some can interact with proteins (151).

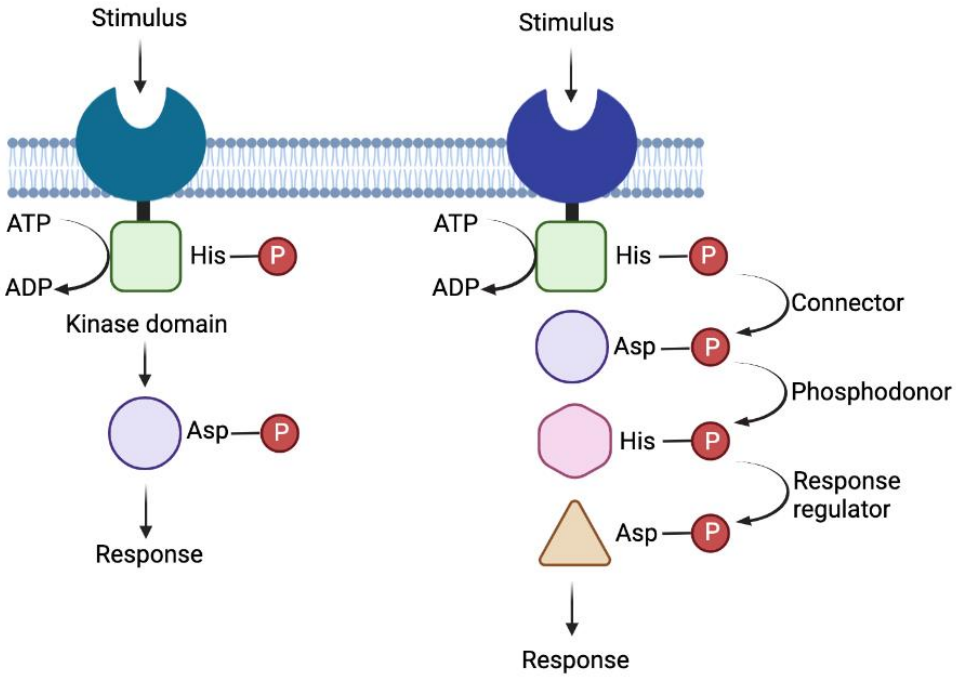

Figure 1.6. Schematic of the two-component signalling (TCS) system that utilises histidine protein kinases for cellular transduction. The flow diagrams on the left and right demonstrate a simple and a more complex overview of the phosphorelay system of in the TCS, respectively. Schematic was produced in Biorender.

1.7.2 Phosphoenolpyruvate:sugar phosphotransferase (PTS) system

In some bacterial and eukaryotic systems, such as the phosphoenolpyruvate;sugar phosphotransfer system, a cytosolic protein that possesses a phosphorylated histidine independent from the histidine kinase molecule can interact with another cellular protein to which it transfers a phosphoryl group (152). This type of phosphoryl group transfer in a phosphorelay system does not occur in phosphohydroxyamino acid-containing phosphoproteins, and therefore may be a reason for the occurrence of histidine kinases.

The PTS system is one of the most common biological systems that involves histidine phosphorylation (153). In this system, four successive phosphoryl transfers occur in a similar way to the TCS and lead to a final phosphorylation event of the sugar which is concomitant with the transport of the sugar across the bacterial cell membrane. Autophosphorylation of Enzyme I (EI) occurs through the phosphoenolpyruvate substrate and is followed by transfer of the phosphate group from EI to the histidine-containing protein (HPr). The enzymes that are involved in the third phosphorylation event, EIIA and EIIB can consist of multi-domain or separate proteins. EIIA phosphorylates EIIB and in turn this results in phosphorylation of the PEP and subsequent histidine residues of the proteins of the PTS, or in some cases, EIIB enzymes employ a cysteine residue in replace of histidine. During this process, the phosphoryl

groups alternate between being bound to the N3 atom of the histidine of one component and being bound to the N1 atom of the histidine side chain of the next component (153, 154).

1.8 pHis in mammalian cell signalling

1.8.1 Putative mammalian two-component histidine kinases

To date, there is no conclusive evidence that supports the presence of bacterial-like two-component histidine kinases in mammalian cells. However, a number of mammalian proteins have been shown to possess structural similarities to bacterial two-component histidine kinases, two of which are found in the mitochondria, and are known as branched chain α-ketoacid dehydrogenase kinase (BCKDHK) and pyruvate dehydrogenase kinase (PDHK) (155, 156). Both proteins contain prototypical two-component histidine kinase motifs and have been studied for histidine kinase activity. These proteins are known to be involved in the regulation of oxidative decarboxylation of pyruvate and although they have been shown to autophosphorylate on a serine residue in vitro, the ability of them to possess histidine kinase activity has been debated (156, 157). PDHK was observed to autophosphorylate on His and a phosphotransfer reaction for Glu243 and His239 of rat PDHK was proposed (158). However, reliable, and conclusive data was not revealed when His residues were mutated and therefore did not demonstrate the role of His residues in the kinase activity of the protein (159). Furthermore, no evidence was accumulated for the identification of a histidine kinase protein substrate for these proteins. Although these proteins may not determine the likelihood of two-component like histidine kinases in mammals, the structural similarities highlight the notion that histidine phosphorylation is a well-established form of cellular based signalling.

1.8.2 NME proteins

Whilst prokaryotes, lower eukaryotes and plants use pHis for signal transduction, as described previously, pHis as an enzyme intermediate is routinely used in all organisms (154). The side chain of His has a pKa close to physiological pH, which allows His to act as a nucleophile, a general acid or a general base in many enzymatic reactions (160). Unsurprisingly, therefore, His has been reported to be present in the active site of ~50 % of enzymes (154). The NME proteins, also known as nucleoside diphosphate kinases (NDPK), are an example of a protein that utilises pHis, at the N1 position, as an enzyme intermediate to carry out a catalytic reaction and this enzymatic activity was first discovered in pigeon breast muscle (161) and yeast (162) and the sequences encoding for proteins possessing this NDPK activity were subsequently identified (163-165).

The NME genes were first identified in mouse (14) and in the fruit fly Drosopholia (166). Several orthologs of these genes were identified from E. *coli* (167) to humans (168) and to date, ten genes displaying partial or complete NDPK domains have been identified in humans (15) (Figure 1.7). These ten NME genes have been separated based on their amino acid sequence into two distinct groups (15). These groups likely originate from a gene duplication of a single NDPK ancestor gene and have since been termed Group I and Group II (169). Group I comprises NME1, NME2 NME3 and NME4, whilst NME5, NME6, NME7, NME8 and NME9 belong to Group II. NME10, also named XRP-2, is the most recently described NME protein and possesses only a partial NDPK domain (170), and although it is lacking in NDPK enzymatic activity, it is widely expressed in a variety of tissues including the retina, but has not yet been fully characterised (170, 171).

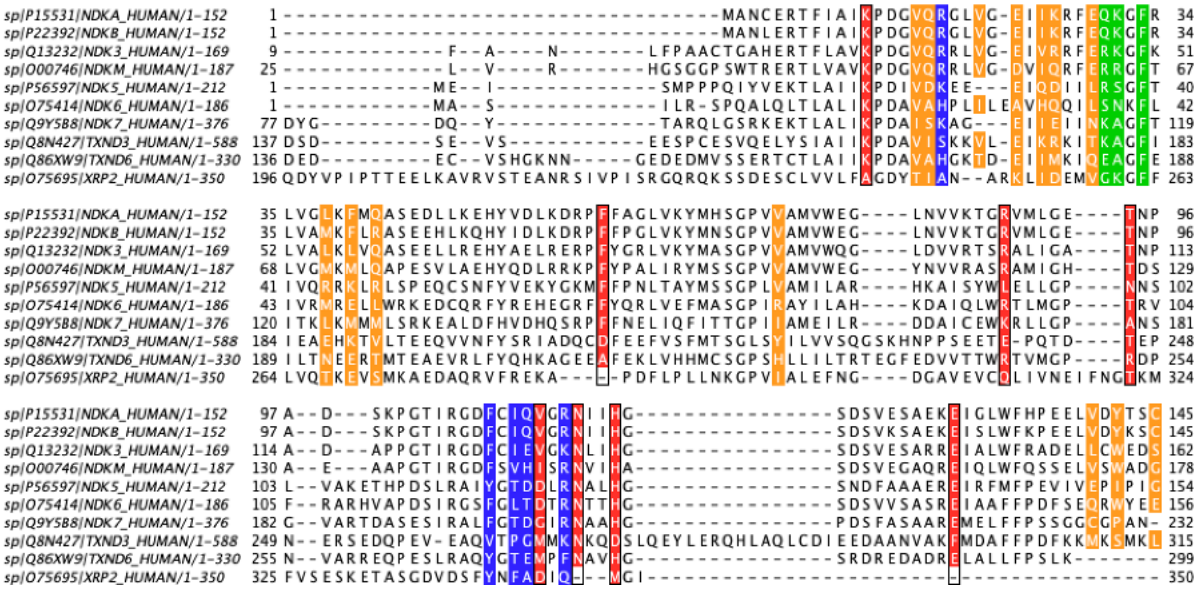

Figure 1.7. Amino acid sequence alignment of the NME protein family members. NME1-10 family members are shown as NDKA, NDKB, NDK3, NDKM, NDK5, NDK6, NDK7, TXND3, TXND6 and XRP2, respectively. The uniport ID for all proteins is listed to the left of the sequence. The residues involved in forming the large interface, small interface and small interface 2 are highlighted in orange, green and blue. Catalytic residues in the active site are highlighted in red. Alignment was carried out in Jalview.

Group I NME proteins share 58 to 88% identity with each other, whereas Group II proteins displayed more divergence with sequences sharing only 25 to 45% identity with Group I proteins (172). The subcellular location of Group I protein members vary, but NME1 and NME2, the most abundant proteins of Group I, are mainly found in the cytoplasm, but can also be found in the nuclei (173). Nuclear NME1 and NME2 interact with DNA in a non-sequence specific manner and this has been linked to local NTP synthesis relevant to DNA polymerase activity, as well as NME activities such as 3'-5'-exolnuclease activity demonstrated for NME1 and DNA repair and transcriptional regulation by both NME1 and NME2 (174, 175). Nuclear

NMEs were also found to interact with telomeres and postulated to play a role in telomere regulation (176). Furthermore, NME6, an inactive mitochondrial NME protein, was found to be localised with the regulator of chromatin condensation 1-like protein (RCC1L), which is part of a large GTP-binding protein family, but it is not known whether this protein can act as a GDP/GTP exchange factor. These nucleotide-related activities require more detailed analysis, for their structural bases and contributions in cancer and metastasis suppression.

NME3, which has been reported to be indicated in differentiation and apoptosis of myeloid neuroblastoma cells was also observed in the mitochondria (177). The mammalian NME4 protein is exclusively a mitochondrial isoform as it possesses a specific organelle targeting sequence. NME4 is bound to the mitochondrial inner membrane through an electrostatic interaction between a basic motif (Arg89-Arg90-Lys91) and a mitochondrial phospholipid, cardiolipin (178). Members of Group II present a high level of identity to the three tandemly repeated NDP kinase domains and as a result, are much larger proteins. Group II proteins are mainly found in ciliated structures, with the exception of NME6 which is ubiquitously expressed (172). Only the NME7 protein from group II was found to demonstrate catalytic NDP kinase activity (173).

1.8.2.1 Structure and multimerisation of NME

The first reported crystal structure of the human NME proteins was for NME2, which demonstrated that it adopts a hexameric architecture formed from a dimer of trimers or a trimer of dimers, with a D3 symmetry (179). Each monomer, with a molecular weight of ~ 17 kDa, folded into a compact α/β domain, which is built around an anti-parallel β sheet, followed by a C-terminal extension (Figure 1.8). As the human NME1-4 proteins are highly conserved and possess over 50% sequence identity, they all assume highly similar protein structures to NME2, with hexamer conformations and D3 symmetry. This is supported by structural similarity and RMSD values lower than 1.2Å, are observed for the Group I proteins (180). Despite the highly conserved sequences and structures, the cellular functions of NME1-4 appear to be distinct based on genetic analysis and are discussed below.

To form a hexamer with D3 symmetry, each monomer (Figure 1.8) forms three different interfaces with adjacent subunits. These interfaces are referred to as a large interface, a small interface close to the active site and another small interface opposite the active site (181) (Figure 1.7 and Figure 1.9). Dimer assembly occurs through the formation of a continuous β-strand between two subunits and the interaction of two antiparallel α-helixes. Within the helical structures, Glu29 forms hydrogen bonds with main chain amides of Val21 and Gly22 (182,

183). The association of the dimers involves Lys31 interacting with three main chain carbonyls of neighbouring subunits, such as Arg105, Gly106 and Glu107 (Figure 1.8). These interface residues are generally conserved across all NDP kinases, including human NME1-4, but not NME5-8 (183, 184). It is therefore suggested that the Group II human NME proteins may assemble in a different way to those in Group I, but the interactions and structure assembly is yet to be determined. Interestingly, the NDP kinase structure in *M. xanthus* was resolved as a tetrameric structure, and only the large interface is conserved in this protein with human NME2 (185). This suggested that the evolution of one or two multiple interfaces between the monomeric subunits may result in different assembly and therefore different functions in various species.

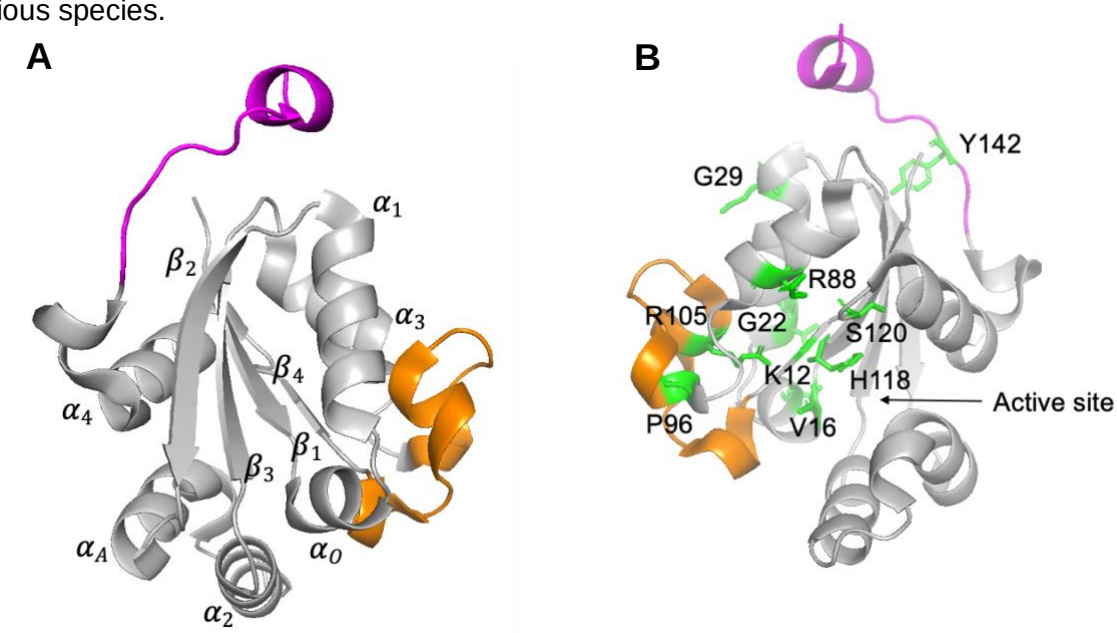

Figure 1.8. Structural elements and active site residues of the NME monomer. (A) Chain A of the NME1 hexamer, PDB Code: 1JXV, is shown and the helical and beta sheets that form the secondary structure are labelled and the C-terminus is highlighted in magenta and the Kpn loop is highlighted in orange (B) Conserved residues involved in nucleotide binding are highlighted in green.

The Kpn loop, formed from residues 96-116, is located between the α-3 helix and the β4 strand (179, 183). It is positioned at the active site of NMEs and also plays a role in surface contacts leading to protein oligomerisation (186). The loop is important for enzyme activity because of the conservation of His118 in the centre of the β4 strand, a very short strand which follows the Kpn loop (187). This results in an unfavourable conformation of the His residue but allows the maintenance of accessibility of the substrate to the active site. Furthermore, the Kpn loop and the C-terminal region has been proposed to be involved in hexamer formation, since a Pro96Ser substitution and a C-terminal truncation, destabilises the hexamer in favour of a dimer in *Leishmania* parasites (188). The C-terminal segment interacts with two neighbouring subunits and the Kpn loop to stabilise the hexamer via a trimer/large interface through

hydrophobic interactions. Hexamer assembly also involves Pro101 forming a network of hydrogen bonds with three water molecules and the interaction of Val16 with Trp142 of the C-terminus (182).

NME family members consist of six single subunits that are enzymatically active. In some cases, it has been reported that they exert a number of their activities as heteromeric complexes (189). For instance, NME2 and NME3 oligomers were proposed to be involved the complex formation of G-proteins in cardiomyocytes (190) but the exact mechanisms are unknown. Heterooligomerisation of NME proteins is therefore an area of research that needs to be studied in greater detail. As NME1 and NME2 share 88% identity, their individual ability to form heterohexameric isoenzymes has been investigated (182). Only 18 out of 152 amino acids in NME1 and NME2 differ, however NME1 is an overall acidic protein, compared to NME2 which is overall a basic protein, with predicted pI values of 5.83 and 8.52, respectively (15) due to some of these 18 amino acids possessing oppositely charged side chains (Figure 1.7). Irradiation-induced DNA damage in cells leads to NME1 and NME2 co-localisation and a change in NME1/NME2 homo- and hetero-hexamer ratios. In addition, mitochondrial elongation appears to be stimulated by NME3 oligomerisation, as opposed to catalytic NDPK activity. It was reported that the expression of both wild-type and catalytically dead H135Q NME3 restored mitochondrial fragmentation in glucose starved human cells, but a double mutant, E40/46D abolishing the salt-bridges between monomers, did not (177).

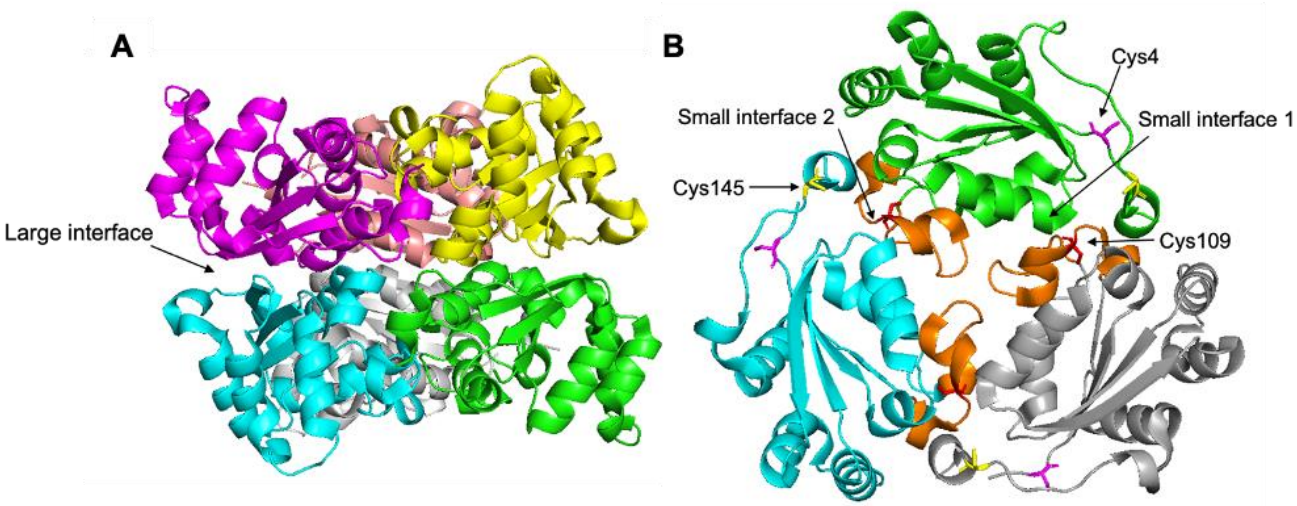

Figure 1.9. Schematic ribbon representation of the NME1 structure. (A) NME1 hexamer (dimer of trimers) showing the large interface between trimers, and for clarity, (B) showing a single NME1 trimer and the small interfaces, including the Kpn loop in orange, and conserved Cys residues involved in structure assembly at positions 109 and 145, as well as 4 are highlighted in red, yellow and magenta respectively. Ribbon diagram was produced in PyMol from the PDB file 1JXV.

NME proteins contain several conserved Cys residues (Figure 1.9). Indeed, NME oligomerisation has been reported to be regulated through redox-dependent mechanisms. For example, under oxidising conditions, a crystal structure of NME1 containing an intramolecular disulfide bond has been reported (191). This disulfide bond, between Cys4 and Cys145, disrupts the small interface of the protein involved in dimer assembly and is believed to induce a conformational change in the C-terminal region, of which Cys145 is a part of, thereby destabilising the hexamer and triggering dissociation. The population of NME1 dimer was increased and a concomitant reduction in the enzyme activity of NME1 has been reported (192). This apparent redox-sensitivity of NME1 was further supported by a study carried out in NME1 null mice, which exhibited lower tolerance to oxidative stress compared to wild-type mice (193). Together, the differences in quaternary structure between species, the assembly into homo/hetero isomers, and the oxidation-induced NME dimer formation all elucidated a potential mode of regulating the multitude of NME functions (189).

1.8.2.2 The NDP catalytic cycle

The NME proteins are strongly conserved throughout the phylogenetic kingdom and are present in a wide variety of organisms as nucleoside diphosphate (NDP) kinases. In humans, Group I protein members, NME1-NME4 all possess the NDP kinase active site motif (NXXHG/ASD) and are catalytically active as these nine residues are the most essential for catalysis and stability of the NDP kinase (180). The NDP kinase reaction (Figure 1.10) catalyses the transfer of the γ-phosphate from nucleoside triphosphates through a phosphohistidine (pHis) enzyme intermediate to nucleoside diphosphates vis a ping-pong reaction mechanism (172). Functional studies have shown that the phosphotransfer step essential for several biological roles occurs via His118 in the active site.

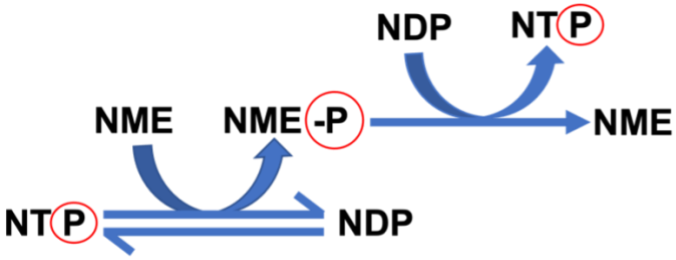

Figure 1.10. Schematic diagram describing the catalytic mechanism of the NDP kinase reaction of NME. Phosphate transfer is carried out via a ping-pong mechanism.

1.8.2.3 NME nucleotide substrate specificity

The NDP kinases are believed to be ubiquitous housekeeping enzymes that play an important role in the appropriate balance of intracellular NTP and dNTP pools to maintain essential cellular processes such as RNA synthesis, translation and high DNA replication fidelity (10).

They catalyse the transfer of the gamma phosphate group from nucleoside triphosphates such as GTP, TTP and ATP, to nucleoside diphosphates (NDPs) including ribo- and deoxyribo-GDP, ADP, UDP and CDP (Figure 1.11) (194). The second order rate constants for phosphorylation by natural NTPs are between 0.7 and 13 x 10 M^{-1} s^{-1}, equivalent to greater than 1000 s^{-1} (195, 196).

Crystal structures of the transient phosphorylated enzyme intermediate have not been solved, however substrate-complexed forms of the NDP kinase and structures in the inactive, nucleotide-free state are available (197-199). Each NME monomer possesses an active site that is located in a cleft formed by the two helices, termed α_A and α_2 (Figure 1.8). The nucleotide base is oriented near the surface of the protein and is stabilised by Phe60 of the α_2-helix and Val112 of the Kpn loop (see above) whereby a clamp like structure is formed. This clamp like structure in the substrate bound complex is assumed to be conserved across the catalytically active NME proteins, since NME1-3 all contain F60 and V112 residues, and in NME4 V112 is replaced with isoleucine, which is presumed to support this interaction. In contrast, Group II NME proteins are not able to form this clamp due to the absence of a residue equivalent to V112 (180).

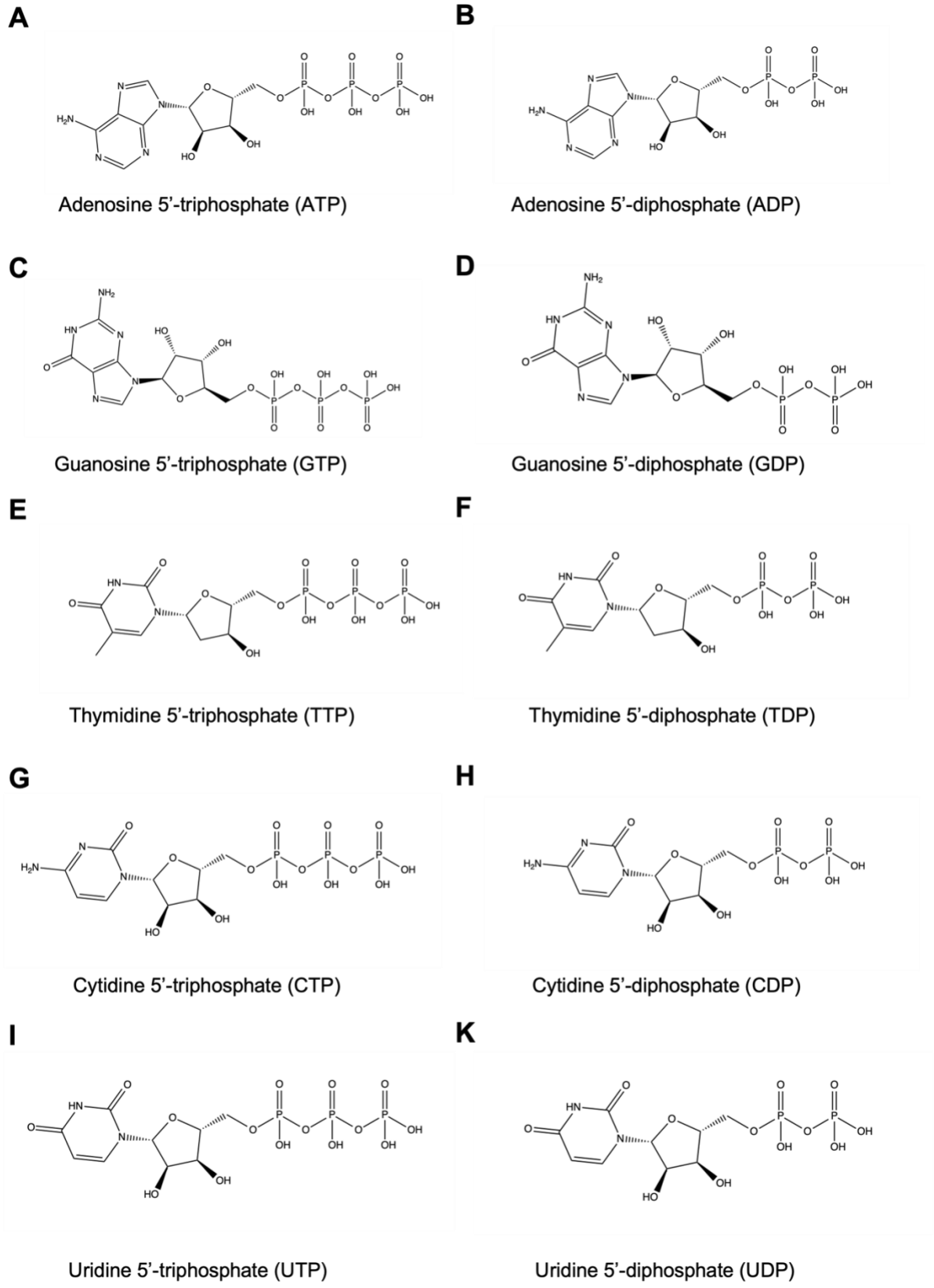

Figure 1.11. Chemical structures of diphosphate and triphosphate nucleosides. The nucleotides shown are substrates of the NDP kinases. Structures were generated with ChemDraw 19.1.

In contrast to the nucleotide base, the ribose sugar is buried in the nucleotide binding cleft of the protein. Side chains of K12 and N115 form hydrogen bonds to the 2' and 3' hydroxyl groups, with the phosphate moiety pointing towards His118 (Figure 1.8) (200). The active site His118 residue is stabilised by Glu129 and this interaction is reinforced through a hydrogen bond with N3 of the His118 imidazole group, leaving the N1 position available for phosphorylation and subsequent phosphate transfer to a nucleotide (201). Tyr94 and Arg88 are responsible for forming hydrogen bonds with the phosphogroups of the substrate and are conserved across the NDPK active NME proteins (Figure 1.8). Intriguingly, in the GDP-bound state, a Glu152 residue in an adjacent subunit of NME2 was found to form a salt bridge with the N2 amino group of GDP (197). Although this residue is conserved in NME1, no such interaction was reported for ADP in complex with NME1 (199).

1.8.2.4 NME is characterised as a 'metastasis suppressor'

The discovery of NME1 was linked early on to its role as a metastasis suppressor gene. Metastasis suppressor genes inhibit different biological processes during metastatic progression without globally influencing the development of the primary tumour. The number of human metastasis suppressor genes is now numbered at ~30 (202, 203), and NME1 was the first to be named, based on non-metastatic (NME) phenotypes linked to its expression (14). This initial study compared expression of NME1 in mouse metastatic melanoma cell lines with non-metastatic cells, and reported that NME1 expression was downregulated in metastatic cell lines (14). This was further investigated in melanoma and epithelial tumours, where NME1 expression was inversely correlated with metastasis potential (204-213).

Upregulated NME1 also correlates with poor prognosis in several cancer sub-types, including haematological cancers (214, 215) and work in neuroblastoma patients reported a positive correlation between NME1 expression and tumour progression (216, 217). In addition, a missense mutation (S120G) was identified in aggressive neuroblastomas. This appears to be specific to this tumour type as amino acid changes in NME1 (217, 218) are very rare in cancer databases, compared to other tumour suppressor genes such as p53. This data suggests potential dual roles of NME1 during tumour development, although further work is needed to confirm this. For example, it was proposed that overexpression of NME1 can be detected in the primary tumour during the early stages of tumorigenesis, followed by later downregulation of expression during metastasis (219).

Tumour cells must gain certain capabilities in order to execute the metastatic program. This includes the ability to acquire motility and invasion, which NME1 has been shown to suppress *in vitro* (220). Boissan *et al* demonstrated that mice expressing the SV 40 large T antigen in

the liver, which leads to hepatocellular carcinoma, exhibit a higher incidence of lung metastases when crossed with an NME1 knockout strain (221). Furthermore, the metastatic potential of cells is reduced in human and mouse invasive cell lines where NME1 was overexpressed, compared to the parental cell line where endogenous expression was low. In addition, in response to NME1 downregulation in previously non-invasive hepatocellular carcinoma cell lines (where NME1 levels are usually high), invasive and metastatic phenotypes are observed (222-224). This gives rise to a loss in intracellular adhesion, including increased expression of Rac1 signalling and MAPK/SAPK protein kinases, including ERK and JNK and activation of the P13K/Akt pathway activation.

NME1 is also thought to function in a late step of the metastatic cascade through the induction of tumour dormancy when apoptotic and proliferative signals are balanced. Tumour cell proliferation has been reported to be inhibited by the phosphorylation of Ser392 on the MAPK pathway scaffold KSR, which in turn reduces signalling to ERK (225). Phosphorylation of Ser392 has been proposed to be carried out by NME1 through a pHis enzyme intermediate (226). When studied in HepG2 cells in which NME1 was silenced, ERK, a protein that forms complexes with Raf/MEK in the RTK/Ras/ERK pathway (227, 228) was hyperactivated (219) consistent with high levels of ERK signalling in the proliferation of tumour cells (229-231). This implies that NME1 can negatively regulated the outcome of Ras/MAPK signalling, perhaps through KSR.

More recently, Wu *et al* showed that two non-phosphorylatable serine mutants of NME1 (S44A and S120G) were unable to suppress tyrosine phosphorylation of STAT3, which is involved in the upregulation of expression of metalloproteinase 9, an important metastatic factor. However, the H118F mutant of NME1 still maintained the ability to suppress STAT3 phosphorylation. In this instance at least, the autophosphorylation ability and protein kinase function of NME1 does not appear to be directly connected with the effect on STAT3 phosphorylation. Thus, much remains to be investigated concerning the relationship between the protein kinase activity of NME1 in general, and its protein histidine kinase activity in particular, and its anti-metastatic effect (232).

Thus, the NME gene family display pleiotropic functions and their effect on metastatic progression might actually be contradictory in distinct human cancers. These findings might be due to the presence of highly homologous NME isoforms in cells, especially NME1 and NME2, which are not discriminated by commercial antibodies. Conflicting data can also be explained by different cellular context, as NDPKs were proposed to act in opposing ways

depending on the cellular environment where cells attached to a surface show behaviour that differs markedly from cells proliferating in suspension.

1.8.2.5 Cellular NME binding partners and model organism studies

A model organism that has shed light on the functions of NME proteins is the fruit fly, *Drosophila melanogaster*. The mutation termed Killer of prune (Kpn), was shown to lead to lethality in individuals homozygous for the non-lethal mutation prune, which causes a 'prune' colour in the eye (233). It was later found that the gene responsible is abnormal wing disc (awd), which is a homolog of NME sharing 78% amino acid identity (168). The loss of function mutants lack NDPK activity, and furthermore, the phenotype can be rescued by human NME2, the most ancient NDPK, but not NME1 (234). This 'Killer of prune' notation has since been used to identify the Kpn loop structure in human NME proteins, described above, where Pro96 is located, described aboce.

It was also shown that in flies, the awd protein partners with Shibire, the homolog of human dynamin (235). Dynamin, plays a key role in the initiation of endocytosis as it is essential for the generation of vesicles (236) (Figure 1.12). The interaction of human NME1 with dynamin has been further studied in primate cell lines and in particular, human NME1 was shown to interact with dynamin in human breast carcinoma cells. GTP is believed to be supplied to dynamin by NME1 and NME2 NDPK activity, and thus increasing its GTPase activity, which in turn promotes dynamin oligomerisation and vesicle fission (237, 238). In breast carcinoma cells, this process contributes to suppression of tumour cell motility by promoting endocytosis of chemotactic receptors by facilitating dynamin (237).

Further insights into NME protein functions have been gained through studies on mice, where murine NME1 and NME2 share 94% and 98% with their human homologs, respectively (239). Several NME1 and NME2, as well as NME1/NME2 double knockout mice have been generated. Single mutant mice were found to be viable but did possess developmental defects for developing into adulthood. For example, NME1 knockout mice developed mild hypotrophy and females displayed defective mammary gland growth and maturation, and as a result those females were incapable of feeding their offspring (240, 241). A lack of NME2 affected the immune system in mice as T helper 1 and 2 cell types demonstrated an insufficient cytokine production (242). In addition to this, NME2 has been shown to be crucial for the activation of the KCa3.1 channel in these murine $CD4^+$ T cells (243) (Figure 1.12). The absence of both NME1 and NME2 is lethal and the double knockout mice died perinatally (244). Haematological defects such as anaemia with damaged maturation of erythrocytes were displayed, suggesting NME1 and NME2 functions are necessary for erythroid lineage

development (10, 244). The role of NME in phagocytosis is evolutionary conserved. NME1 was found to interact with Dynamin-2 in human macrophages, which is essential for the formation of macrophage phagosomes (245) and the depletion of NME1 led to decreased phagocytic capacity (246).

NME1 has also been shown to bind to Dbl-1, an exchange factor for the Rho-type GTPase CDC42, leading to inactivation and inhibition of cell migration (247). Several other mechanisms have been proposed through which NME1 exerts its effects on cell migration. In order to suppress tumour cell motility, NME1 has also been reported to bind to gelsolin and inactivate its actin-severing capacity (248). Furthermore, the awd/prune interaction established in flies has been further investigated in breast cancer models (249). This revealed that h-Prune (a phosphodiesterase), directly interact with human NME1, which results in increased cell motility (250). In addition, human NME1 and its homologs in C. *elegans* were shown to promote apoptotic cell death of several cell types (251). For example, human NME1 was observed to act in caspase independent apoptosis as a granzyme A-activated DNase (252, 253). However more work is are required to further investigate this.

Group I NMEs possess an affinity for membrane phospholipids. NME3 is recruited to the mitochondrial membrane via its hydrophobic anchor and phosphatidic acid (173), while NME4 binds to cardiolipin, a mitochondria specific phospholipid (178). This can facilitate cardiolipin externalisation and trigger mitophagy or apoptosis (254, 255), or the formation of the Nlpr3 inflammasome, a multiprotein complex that generates proinflammatory signals (256). Interestingly NME4, as well as NME3 and NME6 have been reported to be important for different signalling pathways such as inflammasome pathways, but the mechanisms are hereby unknown (257). Limited progress has been made establishing the function of Group II NMEs. Mutations in NME5 were repeatedly observed as a cause for primary ciliary dyskinesia in animals and humans (258-260). What's more, semi-lethal primary ciliary dyskinesia in rats was also reported for NME7 knockdowns (261), suggesting similar functions for NME5 and NME7 in ciliogenesis and control of ciliary transport in mammals (10, 173). Knockdown of NME7 in rat models was also linked to glucose intolerance or adiposity (262, 263). In all cases studied, NME function is related to NDPK activity, and is relevant to its cellular location and interaction partners (10, 173).

1.8.3 Additional functions of the NME family that require a pHis enzyme intermediate

NME1 and NME2 are best known to exploit a pHis enzyme intermediate for their nucleoside diphosphate kinase reaction. But most relevant to this thesis, they have also been reported to use a pHis modification for a number of distinct cellular processes (Figure 1.12). For example,

mutational analysis has been shown that NME utilises a pHis 118 enzyme intermediate in a protein kinase role involving NME1 Ser120 (Figure 1.8) (264). Aldolase C is a key enzyme in glycolysis and gluconeogenesis (265) and was suggested to be phosphorylated (at low levels) on an aspartic acid residue by NME1 (266). The amino acid identified as the phosphorylation site was Asp319 of aldolase C and this phosphorylation was greatly reduced in the presence of NME1 mutants P96S and S120G. Phosphoaspartic residues are reduced by $NaBH_4$, whereas phosphohistidine residues are not, and when incubated with $NaBH_4$, ^{32}P was no longer detected on aldolase C (266). More work is required to establish the relevance of this finding.

Gene	Function	pHis site	N1 or N3
NME1	NDPK, His kinase	H118	N1 pHis
NME2	NDPK, His kinase	H118	N1 pHis
NME3	NDPK, mitochondrial	H135	N1 pHis
NME4	NDPK, mitochondrial	H151	N1 pHis
NME7	NDPK, centrosomal	H206	N1 pHis
PGAM1	Glycolysis	H11	N3 pHis
PGAM5	Ser/Thr & His phosphatase	H105	N3 pHis
SUCGL	Succinyl-CoA ligase	H299	N3 pHis
ACLY	ATP-citrate synthase	H760	N3 pHis
PHPT1	pHis phosphatase	-	-
LHPP	pLys, pHis and pyrophosphatase	-	-
GNB1	GPCR signal transdction	H266	N3 pHis
KCa3.1/KCNN4	Calcium activated potassium channel	H358	N3 pHis
TRPV5	Calcium channel	H711	-
HISTH4	Nucleosome, chromatin regulation	H18	N1 pHis/N3 pHis
PLD	Phospholipid metabolism, signalling	H94	?
NAMPT	NAD+ biosynthesis	H247	N1 pHis

Table 1.1. pHis containing proteins, a brief description of function and the site of histidine phosphorylation are also shown.

The biological role pHis in proteins, particularly as a product of histidine kinase activity is still relatively poorly understood. In this context, the dimeric glycolytic enzyme PGAM (phosphoglycerate mutase) has been demonstrated to employ an N3 pHis (as opposed to a N1 pHis) covalent enzyme intermediate during the interconversion of 2 and 3 phosphoglycerate, and so is useful as a positive control for immunoblotting with 3 pHis-specific

antibodies (9). The structural basis for the differential binding of N1 and N3 pHis-specific antibodies to peptides with chemical pHis analogues has recently been disclosed (267). In addition to the NDPK catalytically active NME family members, a number of other proteins have been reported to possess or utilise phosphohistidine to carry out cellular processes (Table 1.1) and these are discussed further below.

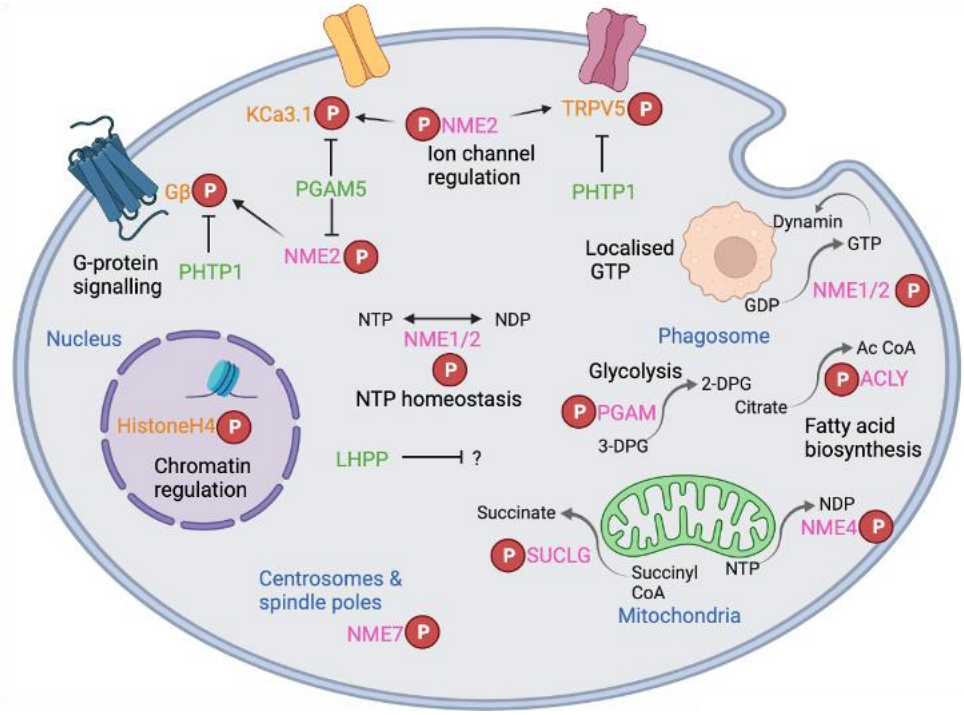

Figure 1.12. Schematic diagram of cellular functions of pHis signalling and the proposed histidine kinase activities of NME1 and NME2. Proteins that utilise pHis as an enzyme intermediate or in histidine protein kinase (HPK) reactions are shown in pink, and putative substrates of the HPK reaction are in orange. Histidine phosphatases are shown in green.

1.8.3.1 Putative NME protein kinase substrates in vertebrate cells

1.8.3.1.1 KCa3.1

The calcium activated potassium (K^+) channel KCa3.1, also known as KCNN4, plays a critical role in stimulating Ca^{2+} influx in a number of cells, including $CD4^+$ T and B lymphocytes and vascular smooth muscle cells (268-270). Through mediation of K^+ efflux from these cells, KCa3.1 is key to maintaining a negative cell membrane potential to electrochemically drive Ca^{2+} influx into these cells. The importance of KCa3.1 channels in a number of biological processes highlights the importance of understanding the mechanisms whereby it is regulated. It was recently reported that the channel requires phosphatidylinositol 3 phosphate (PI3P) for activity and this indirect interaction was mediated by a 14 amino acid stretch at the carboxyl terminus (271). It was later reported that this stretch of amino acids was responsible for the recruitment of a protein, together with PI3P that leads to the activation of KCa3.1 (243).

NME2 was shown to co-IP and also reported to be responsible for the phosphorylation of KCa3.1 channel at His358, which lies within the C-terminal tail (243). Among the four calcium activated potassium channels, KCa2.1, KCa2.2 and KCa2.3, KCa3.1 is unique in that it possesses a His residue. Binding of KCa3.1 to NME2 was also demonstrated through a yeast two-hybrid library screen to the 14 amino acid peptide in the carboxyl terminus. This was further supported by co-immunoprecipitation experiments in which NME2 and KCa3.1 were shown to interact both *in vitro* and after overexpression in Chinese hamster ovary (CHO) cells. Increased activation of the channel was observed in CHO cells where NME2 was overexpressed alongside KCa3.1 based on whole cell patch clamp experiments. This contrasted with the unchanged amplitude of cells where catalytically inactive (H118A) NME2 (but not NME1) were expressed, suggesting a link (through not necessary direct) to NME2 (243) as a potential protein histidine kinase for KCa3.1.

In addition, in NME2 knockdown cells, Ca^{2+} and KCa3.1 channel activity was found to be reduced and the proliferation of human $CD4^+$ T cells was inhibited. The recent identification of the protein histidine phosphatase PHPT1 as a potential KCa3.1 His358 phosphatase, which leads to negative regulation of $CD4^+$ T cells, further supports the importance of His phosphorylation for regulation of KCa3.1. PHPT1 appears to be specific for this site, because other putative histidine phosphatases, such as PGAM5, were unable to dephosphorylate His358 on the channel (243) when they were overexpressed.

1.8.3.1.2 TRPV5

The epithelial Ca^{2+} channel termed transient receptor potential-vanilloid-5 (TRPV5) plays an important role in the control of Ca^{2+} homeostasis and it is partly responsible for the reabsorption of Ca^{2+} in the kidney (272). NME2, but not NME1 was shown to regulate TRPV5 through phosphorylation on His711 in the intracellular channel C-terminus (273). Like KCa3.1, TRPV5 is a tetrameric channel that binds calmodulin and is regulated via Ca^{2+}/CaM signalling (274, 275). For both KCa3.1 and TRPV5, the histidine amino acid is thought to play an inhibitory role, which is released through phosphorylation. This was demonstrated through the mutation of His711 in TRPV5 to a phosphorylation-mimicking aspartic acid, which resulted in increased Ca^{2+} currents when analysed by patch clamp (276).

In a similar manner to KCa3.1, TRPV5 channel activity was increased when assessed by whole cell patch clamp experiments when co-transfected with wild-type NME2, as opposed to NDP ‘kinase dead’ H118A. Furthermore, this increase in activity was reversed upon incubation with the histidine phosphatase PHPT1 (273). Finally, cells in which NME2 levels were depleted

through siRNA showed a reduction in TRPV5 activity, however activity was not completely abolished. This data suggests that His phosphorylation on 711, distinguished through inactivity of the neutral TRPV5 H711N mutant in the presence and absence of NME2 (273), plays a role in the regulation of TRPV5 activation. Whether NME2 directly regulates His phosphorylation at this site in cells, or if it occurs through changes in nucleotide levels accompanied by mutations such as H118A, remain to be established biochemically.

1.8.3.1.3 Histone H4

Histidine phosphorylation on histone proteins was first characterised in yeast (277), but since then studies have shown that histone H4 (HH4) is phosphorylated on His in the nuclei of rat liver cells (278-281) and Walker-256 carcinosarcoma cells (135). The sites mapped were His18 and His75, which are conserved in HH4 across all species. The histone histidine kinase regenerating from rat liver cells was found to form N1 pHis, whereas from carcinosarcoma cells N3 pHis was formed, suggestive of a different His protein kinase activity. It has also been speculated that occurrence of pHis histone H4 is linked to different cellular conditions (7). For example, newly synthesised histone H4 lacks His phosphorylation and furthermore, nucleosome core particles containing appropriately packaged H4, is not a substrate for the unidentified histone histidine kinase (282). In addition to this, studies on foetal rat and human liver displayed 100-fold higher histone histidine kinase activity compared to adult liver (281). This has led to the idea that histidine phosphorylation of histone H4 occurred at the time histones are displaced from DNA during replication, perhaps in order to prevent premature formation of nucleosome complexes during DNA synthesis. In support of this theory, there is a large body of evidence of the control showing that covalent modification of histones, including phosphorylation, underlies fundamental cellular processes such as transcription, DNA repair and carcinogenesis (283-286). The putative phosphorylated His residues in H4 lie in regions of the protein that form interactions with other histones in the core nucleosome (7, 287), and phosphorylation would likely destabilise nucleosome structure. To date, the specific histone histidine kinase(s) that transfer phosphate to histone H4 in yeast and liver have not been identified. It is worth nothing that Histones have also been reported to be phosphorylated on both Lys and Arg (288), though their biological roles are uncertain. The discovery of a specific histone histidine kinase would better equip researchers to answer some of these unanswered questions surrounding the role of histidine phosphorylation on histone H4.

Another histone histidine kinase activity described in the literature, which also remains unidentified, was reported in islet β cells by Kowluru and colleagues (289). This kinase was shown to employ ATP and GTP as a substrate and to phosphorylate both exogenous histone

H4 and Gβ. However, the interpretation of these results is complicated by only partial purification of the protein and the potential presence of NME, an NDPK, which may be linked to the use of both ATP and GTP as a substrate. It is also possible that the histone histidine kinase revealed in this study is membrane-associated, since the molecular mass of the activity does not correlate with an NME monomer, or hexamer, and might therefore represent a new protein histidine kinase.

1.8.3.1.4 Heterotrimeric G-proteins

Heterotrimeric G-proteins consist of a guanine nucleotide-binding α-subunit, and a complex of β and γ subunits. This regulated complex plays a pivotal role in many signal transduction pathways and is activated by GDP/GTP exchange catalysed by G-protein coupled receptors. Several studies have demonstrated the formation of a high energy phosphoramidate bond in a histidine residue of the Gβ subunits enables the local formation of GTP via transferring of the His-phosphate onto GDP (290-295). This phosphorylation event was speculated to require a co-factor that acts as a histidine kinase (289, 293, 294). In a study reported by Cuello *et al*, several experiments were performed that link NME2 with the G$\beta\gamma$ dimers. In particular, the two protein complexes co-immunoprecipitate, suggesting that NME2 histidine kinase activity could be required for the Gβ His-phosphorylation reaction. Consistently, Gβ phosphorylation was observably increased in membranes of H10 cells overexpressing wild-type NME2 but not catalytically inactive (H118N) NME2 (296). Further studies led to the proposed site of histidine phosphorylation being the imidazoyl side chain of His266. This was supported by a lack of phosphorylation being detected in a protein termed Gβ5, in which the His was replaced with a lysine (297-300). However, structural analysis of heterotrimeric G proteins indicates that His266 is distant from GDP, meaning that a direct transfer of a phosphate is unlikely if NME2 were to function as a His protein kinase (301).

1.8.3.1.5 ATP citrate lyase and succinate thiokinase

Studies in rat liver showed that ATP citrate lyase is histidine phosphorylated at the N3 position based on autoradiography (302). ATP-citrate lyase is the primary source of cytosolic acetyl-CoA, which is used in a number of biosynthetic pathways, including fatty acid, cholesterol and ganglioside biosynthesis. NME1 was reported to His phosphorylate ATP-citrate lyase when incubated with PC12 cell cytosol. Succinate thiokinase, also known as succinyl-CoA synthetase (SUCLG), is a bacterial enzyme that was also proposed (but could not be conclusively shown) to be a substrate for NME1 *via* phosphorylation on His299 (303, 304). In contrast, previous studies have shown that both SUCLG and ATP citrate lyase can autophosphorylate on His (305), and this may account for the increase in histidine

phosphorylation in the presence of NME1, with NME1 increasing the local amount of NTPs for a separate protein His autophosphorylation reaction. Again, it is unclear if NME1 acts as a protein His kinase, or is instead a source of nucleotides for a His phosphorylation event catalysed by a separate protein kinase.

1.8.4 Mammalian histidine phosphatases

The discovery of widespread pHis in mammalian cells (116, 143) and the proposal that mammalian His kinases must exist, raises the question as to whether this post-translational modification can also be reversed by His-specific phosphatases. To this end, several putative phosphohistidine phosphastases have been described (180). Phosphohistidine phosphatase I (PHPT1) was the first histidine phosphatase evaluated biochemically, as far back as 1962 (11). PHPT1 can dephosphorylate a His residue on several of the proteins described above and shown in Figure 1.12, including KCa3.1 (306), TRPV5 (273), ACLY and GNB1 (296).

Another putative histidine phosphatase, phospholysine phosphohistidine inorganic phosphatase (LHPP), has also been reported after purification from porcine brain tissue (307). As its name suggests, this enzyme appears to dephosphorylate both pHis and pLys. Interestingly, like NME1, LHPP has also been described as a tumour suppressor in liver cancer, where its expression is downregulated, alongside upregulation of NME1/NME2 (308). The downregulation of LHPP has also been observed in colorectal (309), bladder, pancreatic (310), thyroid (311) and cervical cancer (312) cells. ACLY has been suggested to be a substrate for LHPP, based on mass spectrometry analysis of pHis containing proteins from mouse hepatocellular carcinoma cells (313).

Histidine phosphorylated NME2 at His118 has recently been shown to be dephosphorylated by the phosphoglycerate mutase family member, PGAM5. PGAM5 attacks the phosphate linkage on His to form a pH105 intermediate at the N3 position, which is subsequently hydrolysed to release phosphate. However, PGAM5 has also been reported to be a pSer phosphatase (306), as has the broad spectrum phosphatase encoded by bacteriophage Lambda. Other members of the PGAM family that share sequences with histidine phosphatases include STS-1 and STS-2, which are potential candidates for pHis dephosphorylation, but they have not been extensively studied. The major cellular phosphatases such as PP1, PP2A and PP2C have also been reported to exhibit dephosphorylation of pHis *in vitro* (180). As described above, histone H4 is also subjected to regulated through His phosphorylation and dephosphorylation, but again the enzymes responsible are not yet known (306, 314).

1.8.5 A comparison of NDP kinases and Ser/Thr/Tyr kinases

Regulated Serine/Threonine and Tyrosine protein kinases are implicated in the regulation of all aspects of eukaryotic cell biology. Like Ser/Thr and Tyr kinases, NME proteins are found in all eukaryotic organisms, but unlike protein kinases, they do not possess a bilobal kinase fold, and can accept nucleotide substrates with all known natural nucleobases in the form of 2'deoxyribose and ribose. In contrast, canonical protein kinases maintain specificity for ATP or GTP (199), although recent work shows that pseudokinases can sometimes bind nucleotides in unusual orientations to catalyse atypical post-translational modifications (315, 316). Phosphohydroxy amino acids such as Ser, Thr and Tyr all possess a phosphoester bond, which has a $\Delta G°$ of hydrolysis of between -6.5 to -9.5 kcal mol^{-1}. In contrast, pHis contains a phosphoramidate bond with a $\Delta G°$ of hydrolysis of -12 to -14 kcal mol^{-1} demonstrating that the thermodynamic stability of the P-N bond differs from a P-O bond. Moreover, the instability of the P-N bond at 95°C and under acidic conditions is well known (133), making it challenging to analyse by conventional techniques (Section 1.6.4).

Protein kinases and the NME family of NDPKs belong to different evolutionary families and are also unrelated in both sequence and in three-dimensional structure. A key difference is that the phosphate transferred to a Ser/Thr/Tyr residue is located on either the same protein itself (autophosphorylation either *in cis* or *in trans*) or on a distinct substrate protein. However, NDP kinases transfer a phosphate between one nucleotide and another employing a N1 pHis intermediate, which has not been shown for any protein kinase, to my knowledge. Although the general chemical mechanism is similar, whereby a nucleophilic imidazole or hydroxyl group attacks the γ-phosphate, generating an intermediate from which the NDP moiety departs (199), NDPK follows a ping-pong reaction mechanism, in which a pHis enzyme intermediate is formed. This is supported by X-ray structures of NDP kinase from *dictyostelium* (200) and cAPK (317), and by comparison of both in complex with the transition-state mimic ADP-AlF_3.

Protein kinases and NDP kinases also employ distinct chemical groups encoded by amino acids for catalysis and for driving interacting with their substrates, which generates different molecular environments for bound nucleotides (and potentially small molecule inhibitors). The nucleotide monophosphate moiety of the substrate maintains the same conformation in both types of enzyme with the base in anti-orientation and the α-phosphate *in trans* to the sugar, however the β and γ-phosphates behave differently, since the 3'OH hydroxyl group plays a major role in NDP kinases, forming a hydrogen bond with the triphosphate moiety, whereas

this hydroxyl group plays no known role in catalysis amongst protein kinases (199). Furthermore, the phosphate groups in NDP kinases form interactions with conserved Arg residues as well as Lys12 one main-chain NH away from Gly119 in space, whereas Lys residues in kinases interact with the phosphates, creating a different environment surrounding the nucleotide (318). Both kinases bind divalent metal ions, which compensate the negative charge of the phosphate groups. It is thought that the Arg amino acids involved in nucleotide binding in NDP kinases, potentially negates the need for Mg^{2+} ions for phosphotransfer, as discussed below. Finally, in addition to these differences in nucleotide binding and therefore environment within the active site described, the two types of kinases possess opposite chiralities in their phosphate-metal binding mode (199, 319).

1.9 NME proteins as potential histidine protein kinases

Interest in His phosphorylation has increased due to the recent demonstration by unbiased phosphopeptide enrichment by strong anion exchange (UPAX) and MS that His phosphorylation is common in human cells, coupled with the generation and commercial availability of pHis-specific antibodies. However, questions around the ability of NME1 and NME2 to act as protein histidine kinases, some of which are described above, have developed as the research in this field increases (320). For example, an intriguing hypothesis has emerged in which NME supplies GTP to activate mono-or heterotrimeric G proteins (13, 297, 321, 322). Several studies proposed that NME2 was associated with G$\beta\gamma$ dimers and directly phosphorylated GDP when it was bound; however only of those associations was reproduced and validated by an independent group (323) and the original findings were later retracted (324). Cuello *et al* later proposed that direct His phosphorylation, as opposed to enzymatic GDP/GTP exchange, activates the G-protein (Section 1.8.3).

However, much of this reported work discussed has yet to be replicated independently, and the risk of contamination of activities attributed to NMEs remains at the forefront of the field. In addition, the relative roles of NME proteins as nucleotide-modifying enzymes (NDPKs) vs. additional roles as protein His kinases remains controversial as the active site of NME the small 17 kDa proteins is unlikely to accommodate large protein substrates in a capacity that phosphate transfer from the pHis118 enzyme intermediate can occur. This is one of the reasons that the work described in this thesis focuses on this area, by generating recombinant enzymes that can autophosphorylate on His residues as part of their NDPK activity, and investigating them in detail in the context of nucleotide and small molecule binding, subunit composition, enzyme activity and effectiveness as potential protein histidine kinases.

Aims and objectives of thesis:

1. Analyse the biochemical and biophysical properties of purified wild-type and mutant NME proteins
2. Investigate redox regulation of NME1 and the effects on oligomeric structure
3. Identify any small molecule compounds that interact with NME1
4. Explore the histidine kinase activity and interaction of NME with putative His-containing substrates.

Chapter 2: Materials and Methods

2.1 Chemicals, reagents and antibodies

The pOPIN bacterial expression vectors were from OPPF-UK. The Flp-In T-Rex system for mammalian cell expression, including cells and pcDNA3 were purchased from Invitrogen. Restriction enzymes were purchased from New England Biolabs (NEB). CloneAmp HiFi PCR premix was purchased from Takara. All primers (Table 2.2) were purchased from Integrated DNA Technologies (IDT). All buffers were made using Milli-Q water unless otherwise indicated.

Mouse anti-6His HRP-linked primary antibody, goat anti-rabbit HRP secondary antibody and monoclonal rabbit antibodies N1-pHis and N3-pHis were all obtained from Sigma Aldrich. Goat anti-mouse HRP secondary antibody was purchased from Cell Signalling Technology. Mouse monoclonal pTyr antibody (P-Tyr-100), rabbit pT288 Aurora A antibody, anti-FLAG and anti-Myc antibodies were also purchased from Cell Signalling Technology. The diphosphate and triphosphate nucleotides were all purchased from Sigma Aldrich. Unless otherwise stated, all other reagents were purchased from Sigma.

The clinically approved kinase inhibitors and RAF kinase inhibitors were purchased from Tocris and SelleckChem. The FDA approved drug screening library was also purchased from SelleckChem and comprises 976 compounds ranging from protein tyrosine kinase inhibitors, molecules involved in immunology and inflammation, proteases and hormones. Compounds were stored frozen in 10 mM stocks in dimethyl sulphoxide (DMSO) in 96-well plates.

2.2 Transformation of *E. coli* and plasmid purification

2.2.1 Generation of chemically competent *E. coli*

TOP10 and BL21(DE3)pLysS *E. coli* strains were streaked onto Luria-Bertani (LB) agar plates from a glycerol stock and grown for 18 hours in an incubator at 37 °C. Single colonies from these plates were grown in 50 mL of LB media for a further 18 hours in a shaker incubator (250 RPM) at 37 °C. From the 50 mL subcultures, 2 mL of bacteria in suspension were added to 200 mL of fresh LB media and grown to an OD_{600nm} of 0.6. The cells were then centrifuged at 5000 x g for 10 minutes to obtain a cell pellet. The LB media was decanted leaving the pelleted bacteria, which were re-suspended in ice-cold Buffer 1 (100 mM rubidium chloride, 50 mM manganese chloride, 30 mM potassium acetate, 10 mM calcium chloride and 15% (v/v) glycerol). The cell suspensions were incubated on ice for 5 minutes and subsequently centrifuged once again at 4 °C to pellet the bacteria. The supernatant was decanted, and the bacteria was re-suspended in ice-cold Buffer 2 (10 mM MOPS, 10 mM rubidium chloride, 75 mM calcium chloride and 15% (v/v) glycerol) and incubated for a further hour on ice. The chemically competent bacteria were then aliquoted on ice at a volume of 200 μL into sterile 1.5 mL eppendorf tubes, flash frozen in liquid nitrogen and stored at -80 °C. BL21(DE3)pLysS cells were grown in the presence of 35 μg/mL chloramphenicol throughout all of the growth steps described above.

2.2.2 Transformation protocol

Chemically competent Top10 *E. coli* cells were transformed in order to amplify plasmid stocks for purification. Chemically competent BL21(DE3) pLysS was used for protein expression. In a 1.5 mL sterile eppendorf tube, 50 ng of plasmid DNA was added to 50 μL of chemically competent *E. coli* cells and incubated on ice for 30 minutes. The mixture was subsequently transferred to a heated water bath at 42 °C for 30 seconds in order to initiate bacterial heat shock. The bacteria were then transferred back to ice for a further 2 minutes. 250 μL of SOC (Super Optimal broth with Catabolite repression) media (2% tryptone, 0.5% yeast extract, 10 mM NaCl, 2.5 mM KCl, 10 mM $MgCl_2$, 10 mM $MgSO_4$, 20 mM glucose) was added to the transformation mixture and incubated at 37 °C for 1 hour in a shaker incubator. Finally, the bacterial suspension in SOC media was spread on an agar plate with, depending on the plasmid, appropriate antibiotic selection marker (Table 2.1) and incubated for 18 hours at 37 °C to allow colonies to grow.

2.2.3 Plasmid purification

Single colonies freshly transformed TOP10 *E. coli* were cultured in 5 mL of LB liquid media for 18 hours 37 °C in a shaking incubator. Bacterial pellets were collected by centrifugation for

10 minutes at 5000 x g. The supernatant was removed and plasmid DNA was purified using a QIAprep Spin MiniPrep kit, as described by the Manufacturer's instructions and stored in nuclease free water (Qiagen).

The ratio of absorbance at 260 nm and 280 nm was used to assess the purity and quantify the purified plasmid DNA, employing a Nanodrop 2000c system (Thermo Fisher Scientific). Plasmid stocks were stored as aqueous solutions at -20 °C.

2.2.4 DNA sequencing

The DNA was sequenced using 800 ng of plasmid DNA with 10 pmol/μL of appropriate sequencing primer (Table 2.2) in a total volume of 10 μL, before sending the sample for Automated Sanger Sequencing (GATC biotech).

Plasmid	Insert	Tag	Selection Marker
pOPINJ	Human NME1 Full-length amino acids 1-152	3C-cleavable N-terminal 6His-GST	Ampicillin
pOPINJ	Human NME2 Full-length amino acids 1-152	3C-cleavable N-terminal 6His-GST	Ampicillin
pOPINJ	Human PGAM1 Full-length amino acids 1-254	3C-cleavable N-terminal 6His-GST	Ampicillin
pET30	Human Aurora A Amino acids 1-403	N-terminal 6His-tag	Kanamycin
pET28a	Human ABL Amino acids 46-515	N-terminal 6His-tag	Kanamycin
pOPINJ	Human EPHA3 Full length amino acids 1-983	N-terminal 6His-tag	Ampicillin
pcDNA3	Human NME1 Full-length amino acids 1-152	3C-cleavable N-terminal MYC-tag	Ampicillin
pcDNA3	Human NME2 Full-length amino acids 1-152	3C-cleavable N-terminal FLAG-tag	Ampicillin

Table 2.1. All plasmid vectors, including the insert, selection marker and specific tags utilised and employed for DNA cloning

Sequencing primers	Primer Sequence
NME1	Forward: 5′-AAGTTCTGTTTCAGGGCCCGATGGCCAACTGTGAGCGTACC-3′ Reverse: 5′-ATGGTCTAGAAAGCTTTATCATTCATAGATCCAGTTCTGAGC-3′
NME2	Forward: 5′-AAGTTCTGTTTCAGGGCCCGATGGCCAACCTGGAGCGC-3′ Reverse: 5′-ATGGTCTAGAAAGCTTTATTATTCATAGACCCAGTCATGAGC-3′
PGAM1	Forward: 5′-AAGTTCTGTTTCAGGGCCCGATGGCCGCCTACAAACTGG-3′ Reverse: 5′-ATGGTCTAGAAAGCTTTATCACTTCTTGGCCTTGCCC-3′
SDM primers	
NME1 H118A	Forward: 5′-GTTGGCAGGAACATTATAGCTGGCAGTGATTCTGTGGAG-3′ Reverse: 5′-CTCCACAGAATCACTGCCAGCTATAATGTTCCTGCCAAC-3′
NME1 R105A	Forward: 5′-GACTCCAAGCCTGGGACCATCGCTGGAGACTTCTGCATACAAGTTGG-3′ Reverse: 5′-GCCAACTTGTATGCAGAAGTCTCCAGCGATGGTCCCAGGCTTGGAGTC-3′
NME2 H118A	Forward 5′-GTTGGCAGGAACATCATTGCTGGCAGTGATTCAGTAAAAAGTG-3′ Reverse 5′-CACTTTTTACTGAATCACTGCCAGCAATGATGTTCCTGCCAAC-3′
NME2 R105A	Forward 5′-GATTCAAAGCCAGGCACCATTGCTGGGGACTTCTGCATTCAG-3′ Reverse: 5′-CTGAATGCAGAAGTCCCCAGCAATGGTGCCTGGCTTTGAATC-3′
PGAM H11A	Forward: 5′-CAAACTGGTGCTGATCCGGGCCGGCGAGAGCGCATGGAAC-3′ Reverse: 5′-GTTCCATGCGCTCTCGCCGGCCCGGATCAGCACCAGTTTG-3′
pCDNA3 primers	
MYC-NME1	Forward: KpnI restriction site 5′-CGGGGTACCGCCACCATGGAACAAAAACTCATCTCAGAAGAGGATCTG *AGCAGCGGT*CTTGAAGTTCTTTTTCAAGGTCCTATGGCCAACTGTGAGCGTACC-3′ Reverse: NotI restriction site 5′-CGCGCGGCCGCTTATTATTATCATTCATAGATCCAGTTCTGAGC-3′
FLAG-NME2	Forward: KpnI restriction site 5′-CGCGGTACCCCACCATGGGACTACAAAGACGATGACGACAAG *AGCAGCGGT*CTTGAAGTTCTTTTTCAAGGTCCTATGGCCAACCTGGAGCGC-3′ Reverse: NotI restriction site 5′ CGCGCGGCCGCTTATTATTATTATTCATAGACCCAGTCATGAGC 3′

Table 2.2. All primers, including tags and restriction sites. Sequencing primers used for DNA amplification and GATC sequencing show the pOPIN infusion forward and reverse primer extension in orange. PCR SDM primers are designed for mutagenesis and the mutated codon is highlighted in yellow. pcDNA3 primers were designed for amplification of full length NME1/2 and to enable ligation in to the mammalian expression vector pcDNA3. GC extension in green, the restriction site is underlined, the kozak sequence in red, the tag peptide sequence in blue, the linker region in *italics*, the 3C protease cleavage site is underlined in red, the stop codon is in bold and the protein specific sequence is at the 3' end.

2.3 Site directed mutagenesis (SDM)

To specifically mutate an amino acid residue in NME1, NME2, PGAM1 and KCa3.1, primers were used that introduce designated mutation(s) into the coding sequence using a standard PCR-based mutagenesis approach. Primer pairs were designed to incorporate codons for the

desired mutation(s), which were flanked either side by ~15 bp of coding DNA (Table 2.2). The reverse primer is the exact reverse complement of the forward primer.

SDM PCR reactions were performed using 25 ng template plasmid DNA, 0.5 µM of forward/reverse primer, and 6.25 µL Clone Amp reaction mix (containing enzyme, optimised buffer and dNTPs (Takara)) with the final volume adjusted to 12.5 µl using nuclease free water (NFW). The PCR amplification was performed using the following parameters: 98 ˚C for 10 s, annealing temperature (2-5 ˚C below the specified primer melting temperature) for 10 s and lastly 72 ˚C extension for 1-2 min (varied as required for the size of the final PCR product). These parameters were cycled 40 times before a final extension at 72˚C for 10 min. The concentration of template DNA and primers, as well as extension times and annealing temperatures were optimised case by case if DNA yield was low and/or mutagenesis was unsuccessful. The PCR amplified plasmid products were incubated with DpnI (20U) for 1 hour at 37 °C to digest and remove the purine methylated template DNA. The PCR products were subsequently transformed into the Top10 *E. coli* and expanded overnight in 5 mL of LB after single colony selection. After purification of plasmids by QIA miniprep QuickSpin Kit (Qiagen), successful mutagenesis was determined by Sanger Sequencing (GATC Biotech).

2.4 Directional cloning in a mammalian expression vector

In order to efficiently express proteins in a mammalian expression system, cDNA encoding the proteins of interest were cloned into the mammalian expression vector, pcDNA3. The pcDNA3 vector contains multiple cloning sites (MCS), allowing the use of two different restriction enzymes to generate sticky ends for downstream ligation and sub-cloning. Compatible restriction sites are then incorporated by PCR into the flanking ends of the gene of interest which can then anneal to the target vector in the correct orientation.

NME1, NME2, and KCa3.1, which had previously been cloned into pOPINJ vectors, were sub-cloned in to pcDNA3 using the same PCR procedure described previously (Section 2.3) using forward and reverse primers designed to incorporate specific compatible restriction sites (Table 2.2). Forward primers resulted in a PCR product containing N-terminal MYC-peptide (NME1) or FLAG-peptide (NME2) (see Table 2.1) followed by a short linker region and a region encoding a 3C protease site. A Kozak consensus sequence was included in all primers designed for mammalian protein expression which is a nucleic acid motif that functions as the protein translation initiation site for most eukaryotic mRNA transcripts. If necessary, additional nucleotides were added to the primer to ensure a correct reading frame. Reverse primers incorporated tandem stop codons immediately preceding the insert. After PCR, the gene

inserts were resolved on a 1 % (w/v) agarose gel, purified using a QIAquick gel extraction kit and the DNA concentration was quantified using a Nanodrop (as previously described). 1 μg of the DNA insert was digested with 10 U of each corresponding restriction enzymes in 1X CutSmart buffer (New England Biolabs) at 37 °C overnight and this restriction digest was terminated through heating at 70 °C for 20 minutes in a water bath to inactivate the restriction enzymes. The pcDNA3 vector was digested in the same way as the insert and in order to prevent re-ligation of the vector without any insert, the vector was dephosphorylated. Dephosphorylation of the vector was done in a reaction mixture of the digested pcDNA3 vector, 1X Antarctic phosphatase buffer (New England Biolabs) and 5 U of Antarctic phosphatase (New England Biolabs). This reaction mixture was incubated at 37 °C for 30 minutes and then a further 15 minutes at 70 °C for 15 minutes to inactivate the Antarctic phosphatase enzyme. 0.075 pmol of the digested insert and 0.015 pmol of dephosphorylated vector were mixed together at a ratio of insert to vector 5:1 in the presence of 1X T4 DNA ligase buffer (New England Biolabs). Ligation was then carried out through the addition of 400 U T4 DNA ligase (New England Biolabs) and the ligation reaction mixture was incubated at ambient temperature for 15 minutes before heat inactivating the T4 DNA ligase at 70 °C for 10 minutes. The ligation reaction was then transformed into TOP10 *E. coli* (Section 2.2.2), along with a negative control ligation reaction that was subjected to the same procedure but contained no DNA insert. Between 3 and 5 colonies were picked and DNA was purified using a QIAprep Spin MiniPrep kit (Section 2.2.3). To confirm whether ligation was successful, a small sample of the ligated DNA product was treated with the appropriate restriction enzyme and analysed by agarose gel electrophoresis (Section 2.4.1). If the DNA insert was successfully ligated into the vector, digesting the DNA with both restriction enzymes would mean that two DNA bands would be observed after agarose gel electrophoresis as one band would correspond to the vector size and the other would correspond to the DNA insert size. Plasmids were then Sanger Sequenced (GATC) to ensure the DNA insert had no mutations and to confirm insert is the DNA sequence of interest.

2.4.1 Agarose gel electrophoresis and purification of DNA

For ligation of a DNA product into a new vector, DNA was amplified using PCR and isolated using electrophoresis in 1% (w/v) agarose gels. 1 g of agarose (Sigma Aldrich) was added to 100 mL of 1X Tris-acetate EDTA (TAE) buffer (40 mM Tris, pH 8.0, 20 mM acetate, 1 mM EDTA) and heated in a microwave to dissolve. After slight cooling, the mixture was supplemented with the intercalating DNA stain Midori Green (Sigma Aldrich) and was added to a gel cast and left to solidify. 6X DNA purple loading dye (New England Biolabs) was added to the DNA sample at an appropriate volume to dilute it 1X. The gel was placed in a tank

containing 1% TAE buffer and the DNA was subsequently electrophoresed at 100 volts for ~45 minutes. A UV transilluminator was employed to visualise the migrated DNA with reference to a 1-10 kb DNA ladder (New England Biolabs). The DNA fragment was excised using a clean scalpel blade, transferred to a sterile 1.5 mL eppendorf tube and purified using the QIAquick gel extraction kit (Qiagen) according to the manufacturer's instructions and collected in nuclease free water (NFW). The DNA content was then quantified using a NanoDrop.

2.5 Recombinant protein expression and purification

Bacterial expression vectors were transformed into BL21(DE3) pLysS *E. coli* and streaked onto agar plates (with appropriate selection markers) and incubated for 18 hours at 37 °C. All NME1 and NME2 proteins and PGAM were cloned in to pOPINJ vectors, which infer resistance to Ampicillin (50 μg/mL) and encode recombinant proteins with 3C protease cleavable N-terminal His-GST tags (Table 2.1). BL21(DE3) pLysS possesses an additional plasmid, which expresses T7 lysozyme and carries a resistance to chloramphenicol (34 μg/mL) (325). For expression of each protein, a single colony from the agar plate was transferred to 100 mL of LB media containing the appropriate antibiotics and incubated for 18 hours at 37 °C in a shaker incubator at 240 RPM. The subcultures of *E. coli* were then transferred to larger volumes of LB media (5 mL of subculture per litre of LB media). For expression of each protein this was 8 litres of culture medium. The flasks were incubated at 37 °C in a shaker incubator until bacteria reached an OD_{600nm} of 0.6 - 0.8, at which point protein expression was induced by the addition of sterile isopropyl-1-thio-β-galactosidase (IPTG) at a final concentration of 0.4 mM. The cultures were incubated at 18 °C for 18 hours in a shaker incubator shaking at 240 RPM. Lastly, the cultures were centrifuged at 5000 xG for 10 minutes and the bacterial pellet was collected and either harvested immediately or stored as frozen pellets at -20 °C.

The bacterial pellets (section 2.4) containing the exogenously expressed protein were subsequently lysed. Proteins were then purified from the soluble fraction using a combination of affinity chromatography and size exclusion chromatography.

2.5.1 Cell lysis of *E. coli*

The lysis method for *E. coli* was the same for the purification of all proteins. *E. coli* was suspended and lysed in ice cold pH 7.4 lysis buffer (50 mM Tris-HCl pH 7.4, 300 mM NaCl, 1% Triton X-100, 1 mM DTT, 0.1 mM EGTA, 0.1 mM EDTA, 10 mM Imidazole, 10% Glycerol and a cOmplete protease inhibitor cocktail tablet (Roche)). The cell lysis suspension mixture was then sonicated on ice for 30 second intervals at an amplitude of 16 microns using a 3 mm exponential microprobe attached to a MSE Soniprep 150 plus motor unit, followed by incubation on ice for 1 minute. This was repeated 5-6 times, until the cell lysate was homogenous. After sonication, the samples were centrifuged at 4 °C for 1 hour at 43,000 x g to pellet cellular debris. The supernatant of the cell lysate contained the soluble expressed protein, which was subsequently purified by immobilised metal affinity chromatography (IMAC) as all proteins expressed possessed a N-terminal 6His-tag (Figure 2.1).

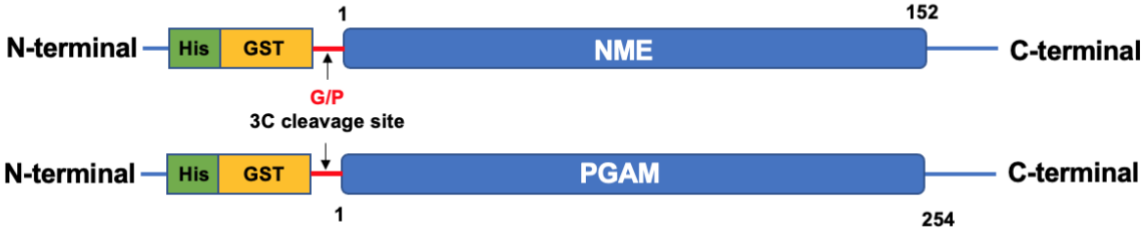

Figure 2.1. Schematic diagram of the protein design with the 3C cleavable His-GST tag. The His-GST tag is located at the N-terminus, followed by the 3C-cleavable site Leu-Glu-Val-Leu-Phe-Gln/Gly-Pro and the Gly/Pro site is contained within the linker between the affinity tag and the protein.

2.5.2 IMAC of recombinant His-GST tagged proteins

2.5.2.1 IMAC

After centrifugation, the lysate was filtered using a 0.45 μM syringe filter and incubated with 1 mL of Ni-NTA agarose beads (Sigma Aldrich), equilibrated in lysis buffer. Lysate/Ni-NTA mixtures were incubated at 4°C with gentle agitation using a magnetic stirrer for 1 hour. The beads were then collected in a reusable plastic filter column and the lysate was collected as it passed through (flow through fraction). The beads, with the His-tagged protein now bound, were washed incrementally with a high salt wash buffer (50 mM Tris-HCl, pH 7.4, 500 mM NaCl, 20 mM Imidazole) (~50 mL in total). Bound protein was then eluted from the affinity resin using either a competitive excess of imidazole or by proteolytic cleavage of the affinity tag as described below.

2.5.2.2 Imidazole dependent elution of His-GST tagged proteins

Bound recombinant His-tagged protein was eluted from the affinity resin using 10 mL of elution buffer (50 mM Tris, pH 7.4, 100 mM NaCl, 1 mM DTT, 500 mM Imidazole, 10% Glycerol) in

increments of 1 mL. Throughout the elution process 500 μL fractions were collected. All fractions were immediately transferred to ice and analysed by SDS-PAGE.

2.5.2.3 Cleavage of the His-GST tag by 3C protease

To proteolytically remove the N-terminal His-GST tag from Ni-NTA-bound protein, the affinity resin was first washed in ~10 mL of low salt wash buffer (50 mM Tris-HCl, pH 7.4, 100 mM NaCl, 1 mM DTT and 10 % v/v glycerol) as described above. The beads were then resuspended in 5 mL low salt wash buffer and transferred to a 5 mL eppendorf tube and centrifuged at 1000 xG for 5 minutes, removing all but 500 µL of the supernatant. 30 μM 3C protease was then added and incubated for 3 hours at 4°C with gentle agitation. The beads were collected by centrifugation for 5 minutes at 1000 x g and the supernatant, containing the His-GST cleaved protein was collected. The beads were washed with high salt wash buffer and centrifuged again at 1000 x g for 5 minutes. The supernatant was removed, and the beads were resuspended in 1 mL high imidazole elution buffer, centrifuged a further time and the supernatant, containing residual non-cleaved His-GST and His-3C protease was collected for SDS-PAGE analysis.

2.5.3 Size exclusion chromatography

After IMAC, proteins were further purified by size exclusion chromatography. A Superdex 200 (16/60) column set up with an Akta FLPC system and a Frac-920 (all GE Healthcare) was equilibrated with filtered, degassed gel filtration buffer (50 Mm Tris pH 7.4, 100 mM NaCl, 1 mM DTT, 10% (v/v) Glycerol). Before the protein was applied to the column, all samples were centrifuged for 20 minutes at 4°C at 16,000 x g to remove aggregated protein. The protein was then applied to the column at a flow rate of 0.5 mL/min and 1.5 mL fractions were collected. 10 μL samples of the fractions, deduced to contain protein by measuring absorbance at 595 nm, were analysed by SDS-PAGE (Section 2.6). The elution volume was used to estimate the molecular weight of the eluted proteins by comparing their elution volume with reference to Molecular Weight Standards (Chapter 3).

2.6 SDS-PAGE

SDS-PAGE was performed in order to visualise the purity and molecular weight of purified proteins, as well as prior to electrophoretic transfer to nitrocellulose during immunoblot analysis (Section 2.10). SDS-PAGE gels were made using a resolving buffer (1.5 M Tris-HCl, pH 8.8) and a stacking buffer (0.5 M Tris-HCl, pH 6.8). The resolving gel, in which the proteins were resolved, composed of 0.4 M resolving buffer, 10% or 12% Bis-Acrylamide (v/v), 0.01% (v/v) SDS, 0.01 % (v/v) ammonium persulfate (APS) and 0.1% (v/v) N,N,N′,N′-

Tetramethylethylenediamine (TEMED) (Sigma Aldrich). Proteins were loaded onto the gel through the stacking gel, which was composed of 0.1 M stacking buffer, 4% Bis-Acrylamide (v/v), 0.01% (v/v) SDS, 0.01 % (v/v) APS and 0.1% (v/v) TEMED.

2.6.1 SDS-PAGE

To verify the purity of protein purified from bacteria, proteins were denatured in 5x sample buffer (0.25 M Tris-HCl pH 6.8, 0.25% bromophenol blue, 500 mM DTT, 10% SDS and 50% glycerol) to a final concentration of 1% SDS and heated to 90 °C for 5 minutes before being subjected to electrophoresis. To detect proteins between 32 kDa and 80 kDa 10% polyacrylamide gels were used. To detect proteins below 32 kDa 12% polyacrylamide gels were used. Polyacrylamide gels resolved proteins ~1 hour (depending on the percentage) with an electric field strength of 20 Vcm^{-1} in running buffer (25 mM Tric-HCl, 190 mM Glycine and 0.1% SDS) and a prestained molecular mass standards (Biolabs) was also loaded onto the gel as a reference for the estimation of the molecular weight of the resolved proteins. Subsequently the gel containing the proteins was immersed and incubated in Coomassie stain (0.2% Brilliant blue R-250, 7.5% acetic acid, 50% methanol) for 1 hour with agitation. The stained gel was then washed for 16 hours using destain buffer (H_2O, methanol and acetic acid 50/40/10 v/v/v). For SDS-PAGE prior to western blot analysis to detect phosphohistidine (pHis), a modified 5x sample buffer (0.25 M Tris-HCl pH 8.8, 0.25% bromophenol blue, 500 mM DTT, 10% SDS and 50% glycerol) was used. Furthermore, the sample was not heated to denature the protein as this would hydrolyse the phosphoramidate (P-N) bond and electrophoresis was done at 4 °C using at 100 V instead of 200 V to avoid overheating.

2.7 Immunoblotting

Following SDS-PAGE, western blot analysis was employed to detect any protein(s) present in the resolving gel. The proteins within the resolving gel were blotted onto a nitrocellulose membrane (GE Healthcare) by electrophoretic transfer. To do this, the gel and nitrocellulose membrane were sandwiched together with blotted pads and 4 pieces of blotting paper either side of the gel and nitrocellulose membrane within a cassette and placed into a tank containing chilled transfer buffer (25 mM Tris, 190 mM Glycine, 0.1% SDS, 20% methanol). For transfer to occur, the tank was placed in a tray of ice and transfer was set to take place at 100 V for 1 hour. The membranes with bound protein(s) were incubated in 5% (w/v) non-fat milk (Marvel) in Tris-buffered saline and 0.1% Tween-20 (TBST) (20 mM Tris pH 7.6, 137 mM NaCl, 0.1% Tween-20 (v/v)) for 1 hour at room temperature with agitation on a seesaw rocker to block the membranes with milk proteins. Blocking the membrane with milk proteins prevents the antibodies applied to the nitrocellulose membrane from binding non-specifically. The blocked membranes were then incubated for 1 hour at room temperature or 12 hours at 4 °C with

primary antibody at indicated dilutions in 5% (w/v) milk TBST with agitation. The membranes were washed three times for 10 minutes each with 10 ml TBST before incubation with the secondary antibody at an indicated dilution in 5% (w/v) milk TBST for a further 1 hour at room temperature. The membranes were washed and Immunoblion Western Chemiluminescent HRP Substrate (Millipore) developing agent was added to the membranes in accordance with the manufacturer's instructions, placed into a plastic wallet to prevent the nitrocellulose membrane from drying and becoming brittle, and into an X-ray film cassette. The films were exposed to the membrane for indicated time periods and the film was developed using an ECOMAX X-ray film processor (Protec). In order to detect phosphohistidine (pHis) through western blot analysis, this western blot process was amended to prevent heating, and therefore hydrolysis of the P-N bond. This involved transfer of the proteins from the resolving gel to the nitrocellulose membrane taking place at 4 °C, using a current of 30 V, for 18 hours.

2.8 Bradford assay

Bovine serum albumin (BSA) (2 mg/mL) (Thermo Scientific) was used to generate a calibration curve of known protein concentrations. 0.5 mg/mL BSA in 1X Tris buffer, pH 7.4 was prepared to create a 2-fold dilution series and generate known BSA concentration standards (Figure 2.1). Bradford assays were performed as per the manufacturer's instructions. In brief, 200 μL of Coomassie Plus Protein Assay Reagent (Thermo Scientific) was mixed with 5 μL of protein sample and colorimetric detection of protein was determined by absorption measurements at 595 nm. Buffer containing blanks were subtracted from all measured data. Experiments were performed in a 96 well plate formatted and recorded using a spectrophotometer (what type, when back). A standard curve was generated to allow estimation of protein concentration for unknown samples, as well as to quantify the amount of protein in total cell lysates. The standards are related through a linear regression (R2) and the equation for the line is y=0.8033x + 0.0304. The absorbance (y) of the unknown protein is measured and used to calculate the concentration of the protein (x).

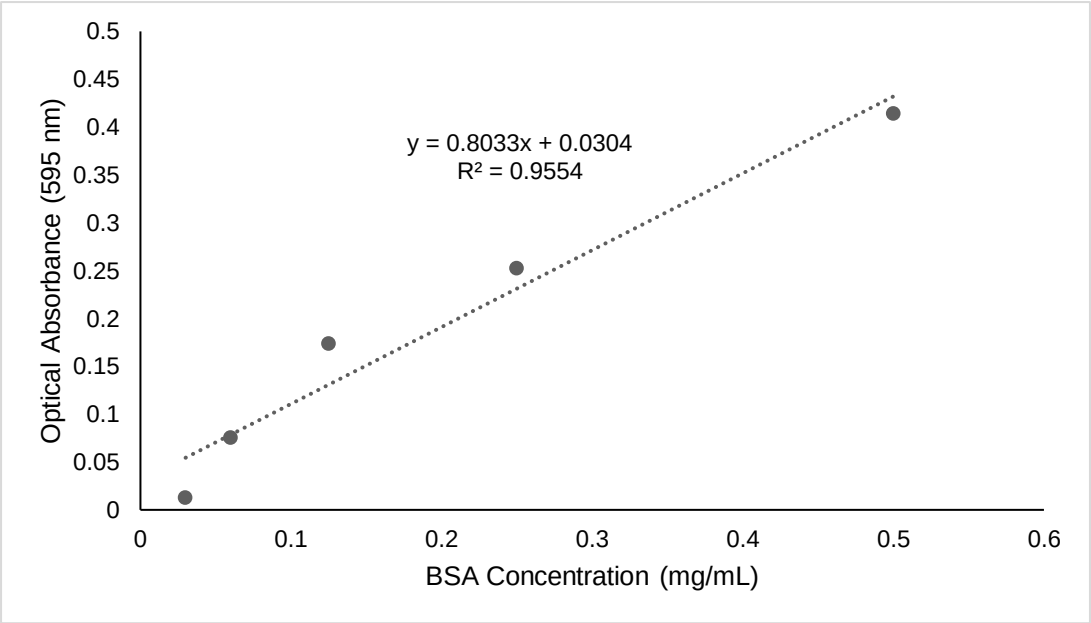

Figure 2.2. Bradford assay standard curve. Increasing concentrations of BSA incubate with Coomassie based reagent. The absorbance was measured at 595 nm using a spectrophotometer and a standard curve was plotted in Excel for determination of protein concentration.

2.9 Intact mass spectrometry

To identify phosphorylation-induced mass shifts and His protein kinase activity intact mass spectrometry was carried out. Autophosphorylation assays (Section 2.10.1) using the specified protein were set up, along with a control assay containing no phosphate donor. Reactions with ATP were vortexed and spun down in a microfuge for a few seconds and then analysed immediately. Protein mass was determined using a Waters Nano Acquity Ultra Performance Liquid Chromatography (UPLC) system coupled with a Waters Synapt G2Si. Instrument calibration was carried out with GluFib for a mass accuracy of 1 ppm or below. Proteins were eluted using a C4 trap column (Waters - MassPREP Micro Desalting Column) on the gradient shown in Table 2.3, with buffer A (0.1% (v/v) formic acid in HPLC grade water) and buffer B (0.1% (v/v) formic acid in HPLC grade acetonitrile). Data was processed using MassLynx (4.1) and deconvoluted using MaxEnt1. Deconvolution settings were as follows: 0.5 Da/channel resolution; Uniform Gaussian distribution with a width at half height of 0.500 Da; Minimum intensity ratios surrounding the peak for left and right at 33%. Figures were created using UniDec software.

Time (min)	Flow (µL/min)	Buffer A (%)	Buffer B (%)	Curve
Initial	25	95	5	6
0.10	40	95	5	6
5.10	40	95	5	6
5.20	25	95	5	6
6.00	25	95	5	6
6.10	25	95	5	6
7.60	25	10	90	6
7.90	25	95	5	6
8.60	25	10	90	6
8.90	25	95	5	6
9.60	25	10	90	6
11.60	25	10	90	6
11.70	25	95	5	6

Table 2.3. Details of the LC-MS gradient used for intact protein separation. Flow rate and buffer composition (% A and % B) are listed.

2.10 *In vitro* histidine phosphorylation assay

2.10.1 Autophosphorylation on N1-pHis or N3-pHis

To analyse the activity of histidine protein kinases, autocatalytic phosphate incorporation into histidine was detected by immunoblotting. 500 ng of recombinantly expressed NME1, NME2 or PGAM1 was incubated with indicated 100 µM phosphate donor or nucleotide of interest e.g. ATP/GTP for NME1 and NME2 or DPG for PGAM1 and/or 100 mM $MgCl_2$, buffered with 50 mM Tric-HCl, pH 8.0, 100 mM NaCl in a total volume of 40 µL for 20 minutes at ambient temperature. The reaction was terminated by adding 5x loading sample buffer (LSB) (0.25 M Tris-HCl pH 8.8, 0.25% bromophenol blue, 500 mM DTT, 10% SDS and 50% glycerol). In order to further investigate the conditions and reagents required for autophosphorylation to occur, nucleotide analogues such as PAP and PAPS at indicated concentrations were incorporated into the assay. Each assay was divided in two; one half of the reaction was heated to 95 °C for 30 minutes and/or acidified and the other half was left at ambient temperature. Acid treatment was done prior to adding the loading sample buffer and carried out by the addition of 0.01% acetic acid until the pH dropped to 4. The sample was incubated at ambient temperature for 1 minute before restoring the pH of the sample to pH 8.0. This served as a negative control, as any pHis formed would be eliminated when heated or acid treated. In order to detect any phosphorylation on histidine, the assay was followed by

immunoblot analysis (Section 2.7), using the monoclonal antibodies N1-phosphohistidine and N3-phosphohistidine.

2.11 Differential scanning fluorimetry (DSF) nucleotide screening and analysis of compound binding

DSF experiments were performed using an Applied Biosystems StepOnePlus Real-Time PCR instrument using a standard DSF procedure previously developed and validated for the analysis of kinases (326, 327). To assess the melting temperature of proteins (including WT NME proteins, PGAM1, their relative mutants and PKA) and generate a thermal melting profile, proteins were mixed with buffer (10 mM Tris, pH 7.4, 20 mM NaCl) and SYPRO Orange dye (Invitrogen), which was used as the fluorescence probe for detecting thermal unfolding as SYRPO Orange binds non-specifically to hydrophobic surfaces and has an excitation/emission wavelength profile that is compatible with qPCR machines (Figure 2.2). In each reaction mixture, the concentration of protein was 2-5 μM and the SYRPO Orange dye was diluted 1:1000 with a final reaction volume of 25 μL. The 25 μL reaction was transferred to individual wells of MicroAmp Fast Optical 96-well reaction plate (Applied Biosystems). The plates were sealed with optical adhesive covers and vortexed to mix the assays. The plate was then centrifuged for 30 seconds at 500 x g and transferred to the RT-PCR machine (Applied Biosystems StepOne Plus). The machine was set to measure fluorescence emitted from the sample as the temperature increased incrementally from 25 °C to 95 °C at a rate of 0.3 °C a minute. The data was collected by the StepOne Software v2.1. Using a combination of Microsoft Excel and GraphPad Prism, thermal denaturation profiles were generated. These were then normalised so that the lowest fluorescent reading was assigned as 0% and the highest as 100%. Data points at temperatures before and after the melting profile of the protein were removed and linear regression analysis was utilised by means of fitting the Boltzman sigmoidal equation to the denaturation curves, which allowed the T_m to be determined. Every assay condition was done in duplicate and the average T_m (temperature at which 50% of the protein is denatured) was taken. Mean T_m values were derived from three independent assays.

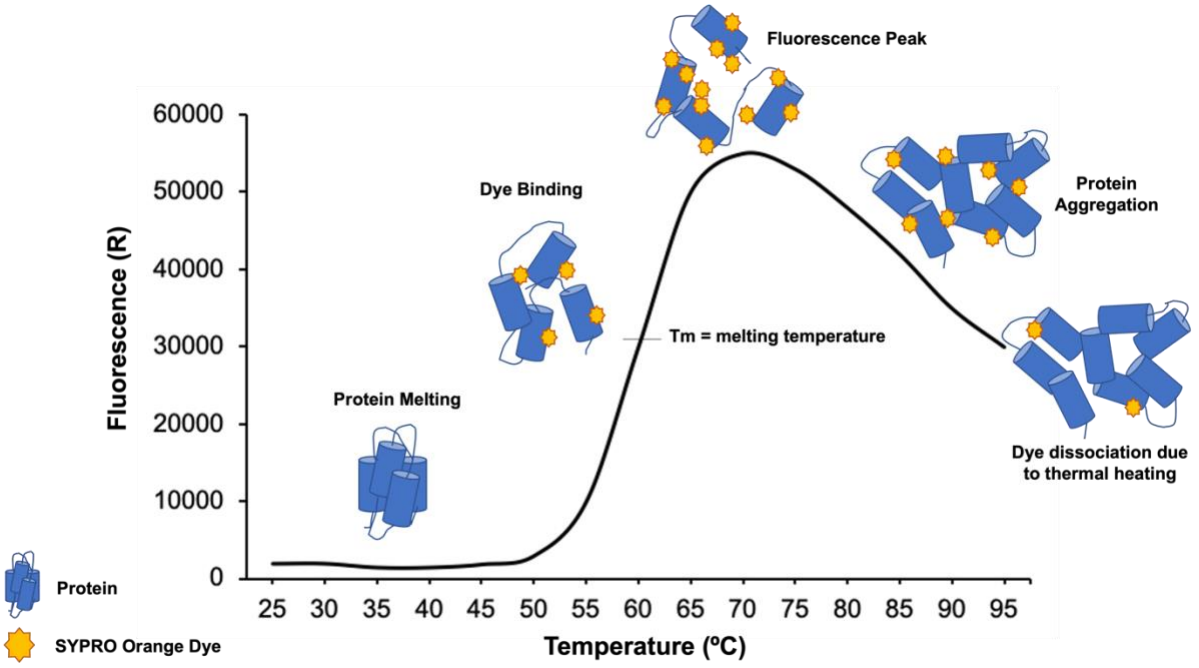

Figure 2.3. Differential Scanning Fluorimetry (DSF) schematic. An annotated example of a proteins thermal unfolding profile in a thermal shift assay. This typical melt curve shows a protein transitioning from a folded protein to a denatured protein, in which the fluorescent SYRPO orange dye can bind to the exposed hydrophobic regions. The dye dissociates as the protein progresses to an aggregate protein.

In order to analyse the effects of many different nucleotides, including ATP, nucleotide analogues and divalent cations on the stability of NME1, NME2 and PGAM1, the DSF assay was utilised to deduce the change in T_m values from the protein control (buffer) to the melting temperature of the protein in the presence of a nucleotide or divalent cation; this temperature change was referred to as the ΔT_m value. The reaction mixtures consisted of 2-5 μM protein, 1 mM of the indicated nucleotide and/or 100 mM $MgCl_2$ and 1:1000 SYPRO Orange dye in a total volume of 25 μL. These reaction mixtures were dispensed into individual wells of a MicroAmp Fast Optical 96-well plate and the experiment was conducted as described above.

For the FDA-approved drug library and FDA approved tyrosine kinase inhibitors (TKIs) compound screening and RAF inhibitors, 40 μM (final concentration) of each compound were pre-incubated with 2-5 μM of the indicated protein for 5 minutes and then subjected to DSF analysis. The final concentration of DMSO was no higher than 4% (v/v) in all conditions and therefore all control experiments contained 4% (v/v) DMSO.

2.12 Native-PAGE

Native-PAGE was carried out in the same way as described in Section 2.6.1 but under non-reducing conditions. The SDS was omitted from the acrylamide gel and the loading buffer, as well as DTT. Furthermore, the samples were not heat-treated before being subjected to gel electrophoresis.

2.13 Size exclusion chromatography-multi-angle laser light scattering (SEC-MALLS)

The molecular mass and heterogeneity of the protein in solution was analysed using SEC-MALLS. The protein was separated using a Superdex 75 column 10/300 (GE Healthcare) connected in series with a Wyatt Dawn8$^+$ and Wyatt Optilab T-rEX (Wyatt Technology) at 22 °C. The column and multi-angle light scattering system was washed with filter sterilised H_2O at a flow rate of 0.2 mL/min for a total of 4 column volumes and then equilibrated with buffer A (50 Mm Tris pH 7.4, 100 mM NaCl, 1 mM DTT, 10% (v/v) Glycerol) at the same flow rate overnight. To allow the baselines on the light scattering (LS) and retraction system (dRI) to settle, the buffer was pumped through the system at a flow rate of 0.6 mL/min. This flow rate was employed for the duration of the experiment as any changes in pressure would affect the results. The system was calibrated with 0.5 mg/mL BSA before applying and injecting the protein sample. Protein samples of 100 μL were filtered and then applied to the column at a flow rate of 0.6 mL/min. Data was analysed using Astra Software.

2.14 Native Ion Mobility Mass Spectrometry

Ion mobility-mass spectrometry experiments were acquired on a Waters Synapt G2-S*i* instrument operated in 'resolution' mode. Proteins were subjected to nano-electrospray ionization (nESI) in positive ion mode (at ~2 kV) with a pulled nanospray tip (World Precision Instruments 1B100-3). The pressure in the TWIMS cell was set at 2.78 mbar (nitrogen), with an IM wave height of 23 V, a wave velocity of 496 m/s and a trap bias of 33. NME was buffer exchanged into 150 mM ammonium acetate (IM-MS) using Amicon spin filter 10 kDa cut-off columns at 4°C. Spin columns were pre-washed with buffer prior to addition of protein and centrifuged 3x 10 minutes at 13,000 RPM. Following the final spin, the filter was inverted into a new collection tube and spun for 2 minutes at 3,000 RPM to collect the protein. Protein concentration was calculated using a NanoDrop spectrophotometer at a wavelength of 280 nm and adjusted to 5 μM for MS analysis. Inhibitor compounds and nucleotides were made up in 10 mM DMSO and then diluted to 200 μM in 150 mM ammonium acetate prior to use (stored at -20°C). 10:1 excess (compound/nucleotide:protein) was added following buffer

exchange and incubated for 10 minutes at ambient temperature. Data was processed using UniDec software to determine oligomeric state of proteins.

2.15 Nucleoside diphosphate kinase (NDPK) assay by western blot analysis

To assess the NDPK activity of NME1 and NME2 as opposed to the autophosphorylation activity, phosphorylated NME was required, and any excess ATP removed. A 50 µL reaction, containing 2 µg of NME in the presence of 2 mM ATP, buffered with Tris/HCl pH 8.0, was incubated at ambient temperature for 10 minutes before resuspending in 500 µL 1% Tris/HCl pH 8.0 wash buffer. To remove the excess ATP, the reaction mixture was transferred to a 1.5 mL Nanoset 50 kDa spin column and centrifuged at 4 °C until the volume was 50 µL. This dilution and subsequent concentration process was repeated 5 times to wash away ATP and phosphorylated NME (NME-P) was obtained. To determine if the NME proteins possessed NDPK activity, NME-P was incubated in the presence of ADP and subjected to western blot analysis utilising a monoclonal antibody that recognises N1 pHis (Section 2.10).

2.16 NDPK assay (ADP-Glo assay)

To evaluate the nucleoside diphosphate kinase (NDPK) activity of NME1 and NME2 proteins, the ADP-Glo kinase assay kit (Promega) was employed. This kinase assay kit measures kinase activity as a measure of ADP production during a kinase reaction, in which a phosphate is transferred from ATP to an amino acid in the kinase or to another protein, yielding ADP. The assay is performed in two steps; first, the ADP-Glo reagent is added to the kinase reaction in an equal volume to terminate the reaction and deplete any remaining ATP and second, the kinase detection reagent is added to convert the ADP produced to ATP (Figure 2.4). The ATP is then used by luciferase to generate light, which is measured using a lumonimeter. This signal therefore correlates with kinase activity or NDPK activity. In the case of a nucleoside diphosphate kinase, a substrate protein is not required as the ADP is produced from the transfer of a phosphate from one nucleotide to another through a phosphorylated enzyme intermediate. For example, an NDP kinase reaction for this assay requires a phosphate donor such as ATP and a phosphate acceptor, such as GDP and the NDPK activity is determined as a measure of ADP production and ATP depletion during the conversion of GDP to GTP. Other nucleoside triphosphates such as GTP are compatible with this assay as the luciferase reaction is specific for the conversion of ATP to ADP (328).

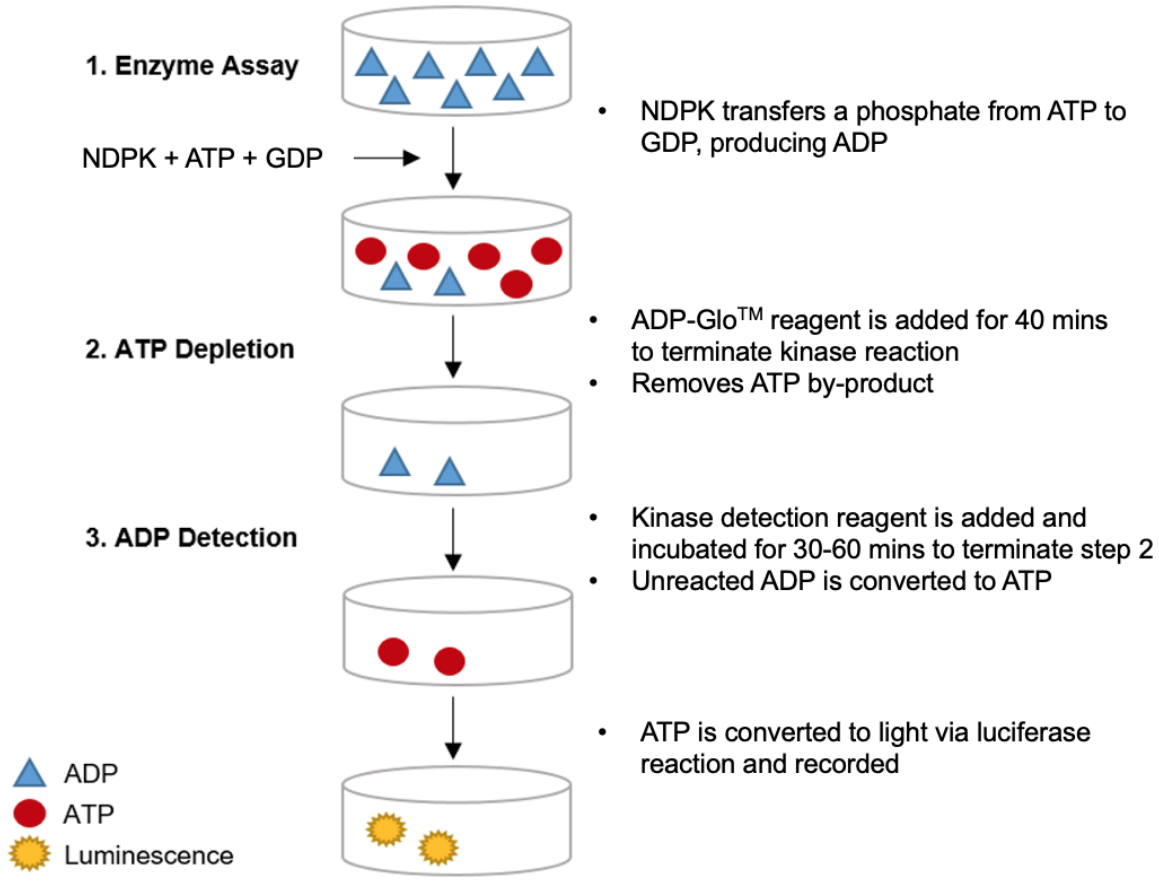

Figure 2.4 Simplified diagram of the ADP-Glo Kinase Assay. The assay is performed in three steps: 1) the NDP kinase reaction (NDPK + ATP and GDP) produces ADP 2) the kinase reaction is terminated, and ATP is depleted, and 2) the ADP is detected and converted to ATP to be measured using a luciferase/luciferin reaction to generate light. Image obtained from Promega.com and adapted for the NDPK reaction.

A kinase reaction containing 1 μM protein, the indicated amount of ATP (phosphate donor) and GDP (phosphate acceptor) and kinase reaction buffer (40 mM Tris, pH 7.4, 20 mM $MgCl_2$ and 0.1 mg/ml BSA) in a total reaction volume of 5 μL was incubated at 25 °C for 10 minutes. For nucleotide concentration dependent NDPK assays, a serial dilution of phosphate donor (ATP or GTP) was prepared in kinase reaction buffer. The kinase assay was then transferred to a 384 well plate and the ADP-Glo assay was carried out according to the manufacturer instructions (Promega). Each assay was done in triplicate and the kinase activity was determined as a percentage of ATP to ADP conversion control through processing using GraphPad Prism 6.0. This assay was also employed to screen for inhibitors from the FDA approved library that inhibited NDPK activity. Inhibitor assays were set up as using a kinase reaction as stated above with the addition of 40 μM of the indicated inhibitor compound being incubated with the NDPK for 10 minutes at ambient temperature prior to the addition of the ATP and GDP. The kinase reaction in the presence of inhibitor and ATP/GDP was then

incubated for a further 10 minutes at 25 °C and the experiment was completed as previously described.

2.17 Pyruvate kinase/Lactate dehydrogenase assay

Once optimised, the pyruvate kinase/lactate dehydrogenase (PK/LDH) assay was performed in a 200 µL reaction mixture in a 96-well plate containing 250 µM NADH, 2.5 U LDH, 2 U PK, 0.3 mM TDP, 0.3 mM ATP, 0.3 mM PEP, 100 nM $MgCl_2$ and 25 nM KCl buffered in 1% Tris-Acetate, pH 7.4. The enzymes utilised in this assay were all made up in 1% w/v BSA solution. The reaction was initiated by the addition of 25 nM purified recombinant 3C-cleaved NME1. The PK control reaction assay mixture omitted the TDP and ATP, and instead was initated by the addition of 0.3 mM ADP. The absorbance values were measured at 10 s intervals over a period of 20 minutes. The ΔOD_{340nm} was calculated measuring the change in absorbance of the linear portion of the reaction, which stopped at ~10 minutes. The absorbance at 10 minutes was subtracted from the absorbance at 10 s, yielding ΔOD_{340nm} in absorbance units (AU). When investigating any inhibitory effects of compounds through this assay, the process was carried out in the same way as described above however the reaction was initiated by the addition of the assay reaction mixture as NME1 was pre-incubated with the indicated concentration of the tested compound for 10 minutes prior to measuring the ΔOD_{340nm}.

2.18 Purification of GST-fusion peptides

Bacterial expression vectors were transformed into BL21(DE3) pLysS *E. coli* and streaked onto agar plates (with appropriate selection markers) and incubated for 18 hours at 37 °C. All the GST-fusion peptide sequences were cloned in to pOPINJ vectors, which infer resistance to Ampicillin (50 µg/mL) and encode recombinant proteins with 3C protease cleavable N-terminal His-GST tags. The purification process of the GST-peptides from *E. coli* was the same as described in Section 2.5.4 but each peptide was purified in 1 L of LB media, and subsequently lysed in 10 mL lysis buffer. The lysate was transferred to a 15 mL falcon tube for sonication and centrifuged as in Section 2.5.4. The supernatant was then collected and incubated with 200 µL of glutathione resin equilibrated in lysis buffer in a 50 mL falcon tube at 4 °C for 3 hrs.

The glutathione bead pellet was then separated from the supernatant by centrifugation at 14000 xG on a bench top centrifuge and collected. The supernatant (flow-through) was also collected for analysis by SDS-PAGE. The GST-peptide conjugated glutathione beads were then washed in 1 mL of wash buffer (50 mM Tris, 500 mM NaCl, pH 7.4) to remove any non-specific binding proteins. To elute the protein from the beads, the beads were suspended in

elution buffer (10 mM R-Glutathione, 5 mM DTT, 50 mM Tris pH 7.4, 100 mM NaCl, 10% v/v Glycerol) and centrifuged for 1 min and the eluate was collected. 10 µL of eluate was incubated for 15 mins at 37 °C in the presence of 2 µg 3C protease and was subjected to SDS-PAGE electrophoresis alongside the flow-through, eluate and eluate in the presence of 3C to identify the purified GST-fused peptides.

2.19 Maintenance of human cell lines

Adherent parental human Flp-In T-Rex-HeLa and parental Flp-In T-Rex-HEK293 cells (Invitrogen) were cultured in Dulbecco's Modified Eagle medium (DMEM) supplemented with sterilised 4 mM L-glutamine, 10% (v/v) Foetal Bovine Serum (FBS) and 100 I.U./mL Penicillin and 100 µg/mL Streptomycin (Gibco) to prevent bacterial contamination of cell cultures. The cells were cultured in 10 mL DMEM at 37 °C in a 5% CO_2 atmosphere and were passaged every 2 - 3 days in a lamina flow hood. To passage the cells, the media was removed and subsequently washed with 10 mL warm PBS. The PBS was then removed and 1 mL of trypsin/EDTA (Versene) (Gibco) was added to the cells and incubated at 37 °C in a 5% CO_2 atmosphere for 1 minute. Trypsin is a proteolytic enzyme that breaks down proteins to dissociate the adherent cells from the flask or vessel in which they are being cultured. The cells were then resuspended in 10 mL DMEM and 1 mL of these trypsinised cells were added to 9 mL of fresh media in a new sterile flask.

2.19.1 Generation of 'freeze down' mammalian cell stocks

Each cell line was grown in separate T-75 cell culture flasks in volume of 10 mL DMEM to ~90% confluency. Cells were harvested by trypsin/EDTA (Versene) treatment, washed in phosphate buffered saline (PBS) and centrifuged for 5 minutes at 220 x g. The cells were then re-suspended in Foetal Bovine Serum (FBS) with 10% DMSO (1 mL per flask). Cells were aliquoted at a volume of 1 mL into sterile cryogenic storage vials and transferred to an isopropanol-controlled rate freezing chamber (Mr. Frosty, Sigma Aldrich) for 24 hours, before being transferred to a -80 °C freezer for storage. To bring up cells post storage, the cell aliquot was thawed at 37 °C and mixed with 9 mL warm DMEM media in a T-75 flask and incubated overnight 37 °C in a 5% CO_2 atmosphere. The following day, the media was removed and 10 mL fresh media was added the cells.

2.20 Transient transfections

For transient transfections, human Flp-In T-Rex-HEK293 cells were cultured to 40% confluency. 20 µg of pcDNA3 plasmid, encoding the protein of interest was incubated in Opti-MEM reduced serum media containing polyethylenimine (PEI) at a PEI to plasmid ratio of 3:1.

For co-expression experiments, 20 μg of each plasmid was added in the same mixture with twice as much PEI. PEI is a stable cationic polymer used for transfecting DNA into a host cell as it condenses DNA into positively charged particles, forming a DNA:PEI complex, which bind to anionic cell surfaces and are consequently endocytosed into the cell cytoplasm. The DNA PEI mixture is incubated at ambient temperature for 20 minutes, vortexed and subsequently added to a dish of 40% HEK293 cells. The cells were then incubated at 37 °C in 5% CO_2 for 24 – 48 hours prior to lysis and immunoblot analysis (329).

2.21 Human cell lysis

2.21.1 Lysis in 2% SDS

For cells seeded into 10 cm^2 dishes, the medium was removed and the cells were washed with 10 mL warm PBS. Once the PBS was removed, 1 mL of warm trypsin/EDTA (Versene) was added to the cells and incubated at 37 °C in 5% CO_2 for 1 minute. The detached cells were resuspended in 10 mL DMEM media and transferred to a 15 mL falcon tube for centrifugation at 220 xG for 5 minutes. The pelleted cells were washed again with 10 mL ice cold PBS and centrifuged once again 220 xG for 5 minutes. Once the cells were pelleted, 100 μL of lysis sample buffer (50 mM Tris, pH 6.8, 2% SDS, 1% Triton X-100, 100 mM DTT, a protease inhibitor tablet and a phosphatase inhibitor tablet (Roche)) was added and incubated on ice for 10 minutes. When lysates were prepared for analysis of pHis, 50 mM Tris, pH 8.0 was used. The cells in sample buffer were sonicated for 10 seconds at an amplitude of 6, transferred to ice for 1 minute for cooling and sonicated once more. To quantify the protein concentrations, a sample of lysate was diluted 1:30 in PBS and subjected to Bradford assay and western blot analysis. This method of human cell lysis was used to analyse whole cell lysates, including nucleic proteins as SDS is a harsh detergent and denatures and releases all proteins present in the cell. This lysis method was therefore done to determine the presence of proteins and detect any phosphohistidine in whole cell lysates.

2.21.2 Lysis in 1% Triton X-100 prior to immunoprecipitation

This method of cell lysis was employed for immunoprecipitation experiments as Triton X-100 is a less harsh ionic detergent, releasing proteins from the cytoplasm and not the nucleus. This minimises protein denaturation and prevents the protein from detaching from the antibody conjugated beads. For cells seeded into 10 cm^2 dishes, the medium was removed and the cells were washed with 10 mL warm PBS. Once the PBS was removed, 1 mL of warm trypsin was added to the cells and incubated at 37 °C in 5% CO_2 for 1 minute. The detached cells were resuspended in 10 mL DMEM media and transferred to a 15 mL falcon tube for centrifugation at 220 x g for 5 minutes. The pelleted cells were washed again with 10 mL ice

cold PBS and centrifuged once again 220 x g for 5 minutes. Once the cells were pelleted, 100 μL of lysis buffer (50 mM Tris, pH 7.4, 150 mM NaCl, 1 mM EDTA/EGTA, 1% Triton X-100, a protease inhibitor and a phosphatase inhibitor (Roche)) and left on ice for 10 minutes before sonication as Section 2.21.1. When lysates were prepared for analysis of pHis, 50 mM Tris, pH 8.0 was used. Following this, the lysate was centrifuged at 16,000 xG for 20 minutes at 4 °C and the supernatant was collected and diluted 1 in 30 in PBS before being subjected to Bradford assay analysis to determine the protein concentration.

2.22 Protein immunoprecipitation

Immunoprecipitation experiments were set up initially by transfecting Flp-In T-Rex-HEK293 cells with the pcDNA3 plasmid encoding the protein of interest as described in Section 2.4, along with a GFP control, that served as a means for determining whether the transfection was successful and as a negative control for the immunoprecipitation experiment as GFP did not possess the appropriate peptide tag. Cells were harvested by trypsinisation as previously described in Section 2.15. For MYC-NME1 and FLAG-NME2 immunoprecipitations, the cleared lysates were incubated with 50 μL of either c-Myc conjugated agarose beads or FLAG M2 conjugated agarose beads (Sigma Aldrich) respectively. The lysate and agarose bead mixtures were placed in a rotating carousel, for gentle agitation, at 4 °C for 2 hours. The beads were then pelleted by centrifugation for 1 minute at 1000 x g and washed 3 times with wash buffer (50 mM Tris, pH 7.4, 500 mM NaCl). To elute the protein from the beads, 3C protease was added to the lysate agarose mixture and incubated for a further 3 hours at 4 °C, with gentle agitation. The beads were then pelleted by centrifugation as before, and the supernatant was collected, and the presence of protein was determined by immunoblot analysis.

2.23 GST-Pull down interaction assays

2.23.1 Pull down assay with recombinant NME1 and NME2

To determine if the GST-fused putative substrate peptides bound and interacted with purified recombinant 3C-cleaved NME1 or NME2, GST-pull downs were exploited. 1 μg of GST-peptide was added to glutathione agarose beads in the presence of 2 mM DTT. The peptide and glutathione bead mixtures were placed in a shaking incubator for gentle agitation at 1000 RPM, at 4 °C for 3 hours. The beads were then pelleted by centrifugation for 1 minute at 1000 x g and washed 3 times with wash buffer (50 mM Tris, pH 7.4, 500 mM NaCl). 2 μg of NME1 or NME2 bait was then added to the GST-peptide bound beads and incubated for a further hour at 4 °C, with gentle agitation. To elute the protein from the beads, an elution buffer containing 10 mM R-Glutathione (50 mM Tris, pH 8.0, 100 mM NaCl 10 mM R-Glutathione, 5

mM DTT, 10 % glycerol) was added to the mixture and the beads were then pelleted by centrifugation as before, and the supernatant was collected, and the presence of GST-peptide and protein was determined by immunoblot analysis.

2.23.2 Pull down assay with cell extract containing NME1 and NME2

GST-pull down assays were also carried out using HEK293T cell extract over-expressed with Myc-NME1 and Flag-NME2 (Section 2.18). In the same way as 2.11.1, 1 µg of GST-peptide was incubated for 3 hours at 4 °C with glutathione agarose beads in a shaking incubator at 1000 RPM. The peptide and agarose bead mixtures were then centrifuged for 1 minute at 1000 x g and washed 3 times with was buffer, before adding 50 µg cell extract overexpressed with Myc-NME1 and Flag-NME2. The lysate agarose mixture was then incubated for a further hour at 4 °C, with gentle agitation. To elute the protein from the beads, elution buffer (10 mM R-Glutathione, 5 mM DTT, 10 % glycerol, 50 mM Tris, 100 mM NaCl) was added to the mixture and the beads were then pelleted by centrifugation as before, and the supernatant was collected. The presence of GST-peptide and any bound protein was determined by immunoblot analysis utilising anti-GST and anti-NME antibodies.

2.24 Molecular modelling and docking of ligands to NME1

The work described here was carried out by Jack Simpson (PhD student of Dr Neil Berry, University of Liverpool). The human NME1 in the presence of ADP (PDB code: 2HVD) was downloaded and Chain B was chosen to carry out the docking process on. All molecules were downloaded from EBI, Drugbank or Chemspider as SDF files where possible, and where not possible were converted to SDF files using Spartan software. In Spartan, all molecules were optimised by calculating their equilibrium geometry using Molecular Mechanics forcefield (MMFF). The ADP ligand was then removed from the file and re-docked under in order to modify the ligand flexibility until docking poses (ideally 10) with a RMSD below 2.0 was achieved, meaning the docking procedure was suitable. The docking run with the highest number of poses with a RMSD of below 2.0 was determined to be the most ideal for docking new molecules in. Using this file and pose, the ADP ligand is replaced with the molecules of interest and docking runs were carried out in the software. Those docking poses that yielded the highest CHEMPLP score were saved and loaded into desertsci ViewContacts for further analysis. PyMol scripts were produced to calculate the interactions between the molecule and protein residues in ViewContacts and the structures were analysed in PyMol, where the models were visualised.

Chapter 3: Characterisation and biochemical analysis of the pHis containing proteins NME1, NME2 and PGAM

Introduction

The nucleoside diphosphate kinases (NDPKs) NME1 and NME2 are members of the mammalian non-metastasis (NME) family of proteins (15), which have been most extensively studied in the context of tumour suppression (14, 330). The NDPK proteins are found in all kingdoms of life, and ten members are recognised in higher vertebrates (Section 1.8.2), which share ~ 30% overall sequence homology when all ten are considered, although the most well-studied NDPKs, termed here NME1 and NME2, share 88% identity (172). The NDPK family are multifunctional proteins that are located in the cytosol, nucleus and mitochondria. They are involved in a variety of cellular functions including cell proliferation, membrane dynamics and remodelling (331) and 3'-5' exonuclease activity against single-stranded DNA (10, 266). The NME1 (also called NDPK-A) and NME2 (also called NDPK-B) proteins are responsible for maintaining the homeostasis of the nucleotide pool within the cell in which a phosphoryl group is transferred from a triphosphate nucleotide to diphosphate nucleotide such as adenosine triphosphate (ATP) to guanosine diphosphate (GDP) (332-335).

The NME proteins that possess NDPK activity catalyse this reaction through a N1-pHis enzyme intermediate, via transfer of the phosphate to an active site histidine through a bi-directional ping-pong mechanism (Figure 1.10) (335). N1-pHis was first discovered and reported by Boyer et al in the 1960s (11). However, as a non-canonical post-translational modification, histidine phosphorylation has not been studied as extensively as canonical phosphorylation on the hydroxyl groups Ser, Thr and Tyr which all form phosphoesters (336, 337). Phosphoesters bond formation is typical in canonical protein kinase reaction mechanisms, in which a phosphate group is transferred to a protein substrate and in turn alter the substrate's activity (338, 339). The majority of protein kinases possess a eukaryotic protein kinase catalytic domain (ePK), in which a catalytic DGF motif lies, and is optimised for protein substrate binding (340). In contrast to protein kinases, NME proteins possess an NDPK domain which is optimised for nucleotide binding and transfer a phosphate to a His amino acid in the active site, creating a heat and acid-labile phosphoramidate bond (133).

Studies on pSer, pThr and pTyr typically employ conditions (341) that were not compatible with studies for phosphohistidine (pHis) due to the lability of the phospharamidite bond on His at high temperatures and low pH (133, 342). Studies into pHis have progressed recently, and several reagents required to detect and identify pHis have been generated and shared commercially or collaboratively. This includes new monoclonal antibodies specific to N3-pHis

and N1-pHis (9), and have greatly advanced the analysis of pHis in intact proteins (7, 10, 13). Moreover, the heat and acid lability of the pHis moiety (133) is a useful indicator of the presence of phosphorylated histidine as opposed to the much more stable pSer, pThr and pTyr, which is evaluated further in this chapter. NME1 and NME2 have been increasingly exploited as a means to study and control for histidine phosphorylation due to the generation of an N1 pHis enzyme intermediate and the ability to maintain this activity after recombinant expression and purification of the enzymes from bacteria (343).

In order to catalyse the transfer of a phosphate group between nucleotides, recombinantly-expressed NME proteins need to be appropriately folded and stable in solution, thus, maintaining the correct environment to bind to the nucleotide. In this chapter, differential scanning fluorimetry (DSF) was utilised to assess the stability of the protein and its ability to bind to a variety of nucleotide, using thermal profiling as a proxy for binding. Each monomer possesses a nucleotide binding pocket in which the residues involved in nucleotide binding, including Arg105, Lys12 and Ser120 are situated (Figure 3.10) (344). In NDPK, two arginine residues Arg88, Arg105 and Lys12 donate hydrogen bonds to the nucleotide phosphate groups to help neutralise the negative charge, similar to the roles of the conserved β3-Lys of protein kinases. Upon nucleotide binding, Phe60 undergoes a conformational change and its side chain stacks onto the planar base of the nucleotide (199). This stacking buries the phosphate and orients it towards the catalytic residue His118. Arg88 also shifts locally to a position in which it interacts with the β-phosphate of ADP (199).

Under native conditions, the mammalian NDPK proteins NME1 and NME2 are reported to be homohexamers with a predicted molecular mass of 102 kDa, made up of six 17 kDa monomers of 152 amino acids each (198, 201). The structural elements of the protein that form the hexamer include both a dimer and trimer interface, with the trimer interface including the ‘Kpn loop’, which comprises residues 96-116 (Figure 1.8 and 1.9). Specific residues, including Arg105, are involved in catalysis in the active site, and also mediate surface contacts that support protein oligomerisation (187). The NME1 C-terminal tail segment is also important for bringing the dimers of the protein into contact, as Glu152 of the C-terminal tail interacts with Asp112 of a different subunit, helping drive assembly of the trimer (182, 345, 346). Finally, mutations of the highly conserved residue Pro96 in the Kpn loop, in conjunction with C-terminal deletions, resulted in dissociation of the NME hexamer into dimers (347).

In contrast to NME1 and NME2, phosphoglycerate mutase 1 (PGAM) employs N3 pHis as an enzyme intermediate. PGAM is a member of the ‘histidine acid phosphatase’ fold superfamily,

which also includes enzymes such as glucose-1-phosphatase and fructose-2,6-biphosphatase that are involved in glycolysis and gluconeogenesis pathways (348, 349). PGAM is responsible for isomerisation of the phosphate group from 3-phosphoglycerate to 2-phosphoglycerate for subsequent activation of the phosphate group and production of phosphoenolpyruvate (PEP). This proceeds via a N3 pHis enzyme intermediate in which a phosphate group is transferred from 2,3-biphosphoglycerate to His11 in the PGAM active site (350). PGAM is reported to exist as a homodimer in solution, with a predicted molecular mass of 58 kDa (351).

In the NDPK reaction, the enzyme catalyses a reversible reaction to transfer a phosphoryl group from a phosphate donor to a phosphate acceptor via autophosphorylation of a His residue. The NME1 and NME2 enzymes are therefore intermediary substrates in the nucleotide-kinase reaction mechanism (352). Due to the bi-directionality of the reaction, the pHis is not transferred to a protein substrate, therefore it is relatively hard to measure the NDPK activity (352). Therefore, in work described in this chapter, I explore multiple different techniques to purify and then assay NDPK activity of NME1 and NME2 in a reliable way

The experimental objectives of work described in this chapter are:

1. Cloning and purification of recombinant soluble human NME1/2 and PGAM
2. Biochemical and biophysical analysis of purified proteins.
3. Semi-quantitative analysis of nucleotide-binding and catalytic activity
4. Analysis of active-site mutants

3.1 Purification of His-GST tagged NME1

The expression plasmids described in this chapter were generated in house and the purification of recombinant His-GST tagged NME proteins was previously optimised as described (353), whereby proteins were purified by immobilised metal affinity chromatography (IMAC) in 50 mM Tris, pH 7.4, 100 mM NaCl, 1 mM DTT, 500 mM Imidazole, 10% glycerol (v/v) (Section 2.5.2), and then size-exclusion chromatography in 50 mM Tris pH 7.4, 100 mM NaCl, 1 mM DTT and 10% (v/v) glycerol (Section 2.5.3). This buffer composition often maintains protein kinase stability during the purification process, as is evaluated below for NME/PGAM. Full length human NME1 (1-152) encoded in a pOPINJ vector (OppF UK) was cloned with an N-terminal His-GST tag (Figure 2.1) and expressed in BL21(DE3)pLysS *E. coli*. After centrifugation and cell lysis, the protein was purified to near homogeneity by IMAC. Size-exclusion chromatography was then used to both further purify and evaluate the apparent multimerisation status in solution, using a Superdex 200 gel-filtration column (Figure 3.1A). Following size-exclusion chromatography, fractions eluting between 40 mL and 90 mL were

analysed by SDS-PAGE and Coomassie staining (Figure 3.1B), in addition to the insoluble bacterial cell pellet, the flow through containing unbound proteins and the pooled fractions of protein eluted from the Ni-NTA beads by 500 mM imidazole. Fractions 9-27 were resolved by electrophoresis in order to identify the fractions with the purest and highest yield of NME1 protein. Figure 3.1B shows that the two prominent absorbance peaks at 280 nm at ~47 mL and ~58 mL both contained a protein of the predicted molecular mass, ~43 kDa, equivalent to the NME1 protein fused to GST. Fractions 11-13 and 21-26 were pooled, aliquoted and flash frozen in liquid nitrogen for further analysis.

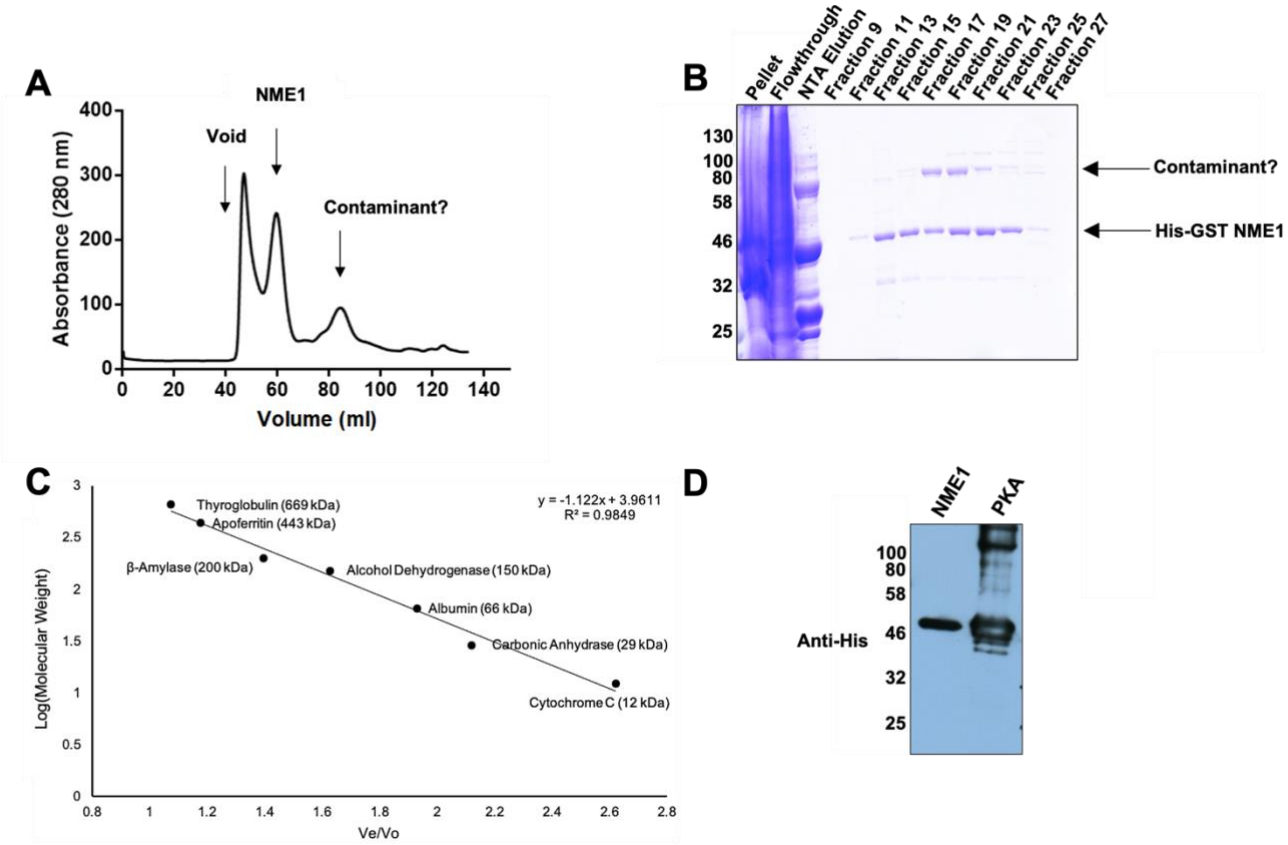

Figure 3.1. Purification of His-GST-tagged NME1 from BL21(DE3)pLysS. *E. coli* transformed with pOPINJ encoding full length His-GST-tagged NME1 were induced with IPTG for 16 hours at 18°C. Following cell lysis and centrifugation the protein was purified and analysed by SDS-PAGE. (A) UV profile of partially-purified His-tagged NME1. The cleared bacterial lysate was bound to a nickel affinity column and eluted (Section 2.5.2). Fractions (0.5 mL) were collected and the UV peak pooled and further resolved on a S200/60 size-exclusion chromatography (SEC) column (Section 2.5.3). (B) Fractions 7-29 from (A) were analysed further. 10 µL of the indicated fraction was boiled with 2 x SDS sample buffer and subjected to electrophoresis on a 10 % SDS poly acrylamide gel. The bacterial cell pellet, post IMAC lysate (non-bound flow through) and pooled IMAC eluate are also shown, as are the predicted His-GST NME1 and a potential high molecular-weight contaminant. (C) Calibration of S200/60 column with molecular weight standards, plotted against elution volume (Ve) over void volume (Vo) (D) Western blot of recombinant His-GST-NME1 and His-PKA. 200 ng of purified NME1 or PKA were resolved by electrophoresis on a 10 % polyacrylamide gel. The protein was transferred to a nitrocellulose membrane and probed with an anti-His antibody conjugated to HRP. Binding was detected by chemiluminscence, confirming the presence of His-NME1 at approximately 50kDa.

Molecular mass markers consisting of thyroglobulin dimer (~669 kDa) (354), apoferritin multimer (355), β-amylase tetramer (~200 kDa) (356), alcohol dehydrogenase tetramer (~150 kDa) (357), monomeric bovine serum albumin (~66 kDa) (358), carbonic anhydrase monomer (~29 kDa) (359) and cytochrome C dimer (~12 kDa) (360) were resolved on a S200 gel-filtration column (Figure 3.1C) in order to determine the relative molecular mass (M*r*) of NME1, which was calculated based upon the elution volume and by comparison with the standards. The molecular mass of a His-GST tagged NME1 monomer is predicted to be ~43 kDa. Native human NME1 and NME2 proteins, exist as homohexamers (183), with a predicted mass of ~258 kDa for the hexameric oligomeric state for His-GST tagged NME1. At the elution volume of 58.74 mL, the calculated M*r* of His-GST tagged NME1 was 275 kDa, which is close to the predicted molecular mass of an NME1 homohexamer. We can therefore conclude that NME1 is a near symmetrical hexamer, which is in accordance with the literature (182). At the elution volume of 46.58 mL, the calculated M*r* of His-GST tagged NME1 was 537 kDa, which suggests that the NME1 eluted at this volume was a multimer, potentially a dimer of hexamers. Utilising a 6xHis horse radish peroxidase (HRP)-conjugated antibody, 200 ng of His-GST NME1 was subjected to SDS-PAGE (Section 2.6) and immunoblot analysis (Section 2.7) (Figure 3.1D) to further help identify the purified protein. In Figure 3.1D a protein band that corresponds to the predicted molecular mass of His-GST tag NME1 at ~46 kDa is shown in Lane 1. The co-purified *E. coli* protein at ~80 kDa detected by SDS-PAGE analysis (Figure 3.1B) was not detected by the 6xHis antibody, suggesting that this contaminant is unlikely to be an oligomer of NME1.

3.2 Purification of His-GST tagged NME2 and His-GST tagged PGAM

Full-length His-GST tagged NME2 (1-152) was expressed and purified as described above for His-GST tagged NME1 (Figure 3.2) (Section 2.5). Size-exclusion chromatography was used to resolve NME2 using a S200 gel-filtration column (Figure 3.2A) and the peak that possessed the highest absorbance at 280 nm eluted at a volume of ~59 mL. Fractions were then analysed by SDS-PAGE (Figure 3.2B). In order to identify the fractions with the purest and highest yield of NME2 protein, fractions 11-31, corresponding to elution volumes of 48 mL to 90 mL were resolved by electrophoresis. In addition to these eluates, the fractions containing insoluble proteins, the flow through containing unbound proteins and the pooled fractions of protein eluted from the Ni-NTA beads by 500 mM imidazole were also analysed. Figure 3.2A shows a prominent absorbance peak at 280 nm at 59.45 mL. The calculated molecular mass of His-GST tagged NME2 hexamer from size-exclusion on Superdex 200 is 281 kDa. A His-GST tagged NME2 monomer has a molecular mass of ~43 kDa, therefore a hexamer has a molecular mass of ~260 kDa (182). This, therefore, suggests that the purified

recombinant His-GST tagged NME2 is a hexamer in fractions 23-28. At the elution volume of 46.98 mL, the calculated M*r* of His-GST tagged NME2 was 549 kDa, similarly to NME1, suggesting the potential presence of a dimer of two homohexamers. Fractions 12-16 and 21-28 were pooled, aliquoted and flash frozen in liquid nitrogen for further analysis. Utilising a 6xHis HRP-conjugated antibody, 200 ng of His-GST NME2 was subjected to electrophoresis under denaturing and reducing conditions prior to subsequent immunoblot analysis. This data (Figure 3.2D) supports the identification of the purified protein as a His-GST tagged NME2, which migrates at ~43 kDa. Therefore, the hexamer observed in solution is likely to be converted to a monomer under reducing conditions.

The same purification processes were used to express and purify full length His-GST tagged PGAM (1-254) (Figure 3.2). BL21(DE3)pLysS *E. coli* cell lysate with expressed PGAM was purified by IMAC in 50 mM Tris, pH 7.4, 100 mM NaCl, 1 mM DTT, 500 mM Imidazole, 10% (v/v) glycerol (Section 2.5.2) and size-exclusion chromatography in 50 mM Tris pH 7.4, 100 mM NaCl, 1 mM DTT and 10% (v/v) glycerol (Section 2.5.3). Full length His-GST PGAM was separated on a Superdex 200 gel-filtration column and fractions with the highest absorbance at 280 nm, as well as the pellet containing insoluble proteins, the flow-through containing unbound proteins during IMAC and pooled fractions eluted from Ni-NTA beads, were subjected to SDS-PAGE analysis (Figure 3.2C). Fractions 7-12 and 21-25 were pooled, omitting fractions containing a prominent ~80 kDa protein contaminant. As this contaminant was also found in His-GST tagged NME1, NME2 and PGAM protein samples purified from *E. coli*, it is likely to be a co-purifying bacterial *E. coli* protein and not an oligomer of NME1, NME2 and PGAM. Immunoblot analysis (Figure 3.2D) demonstrate that the ~56 kDa protein is indeed His-GST tagged PGAM.

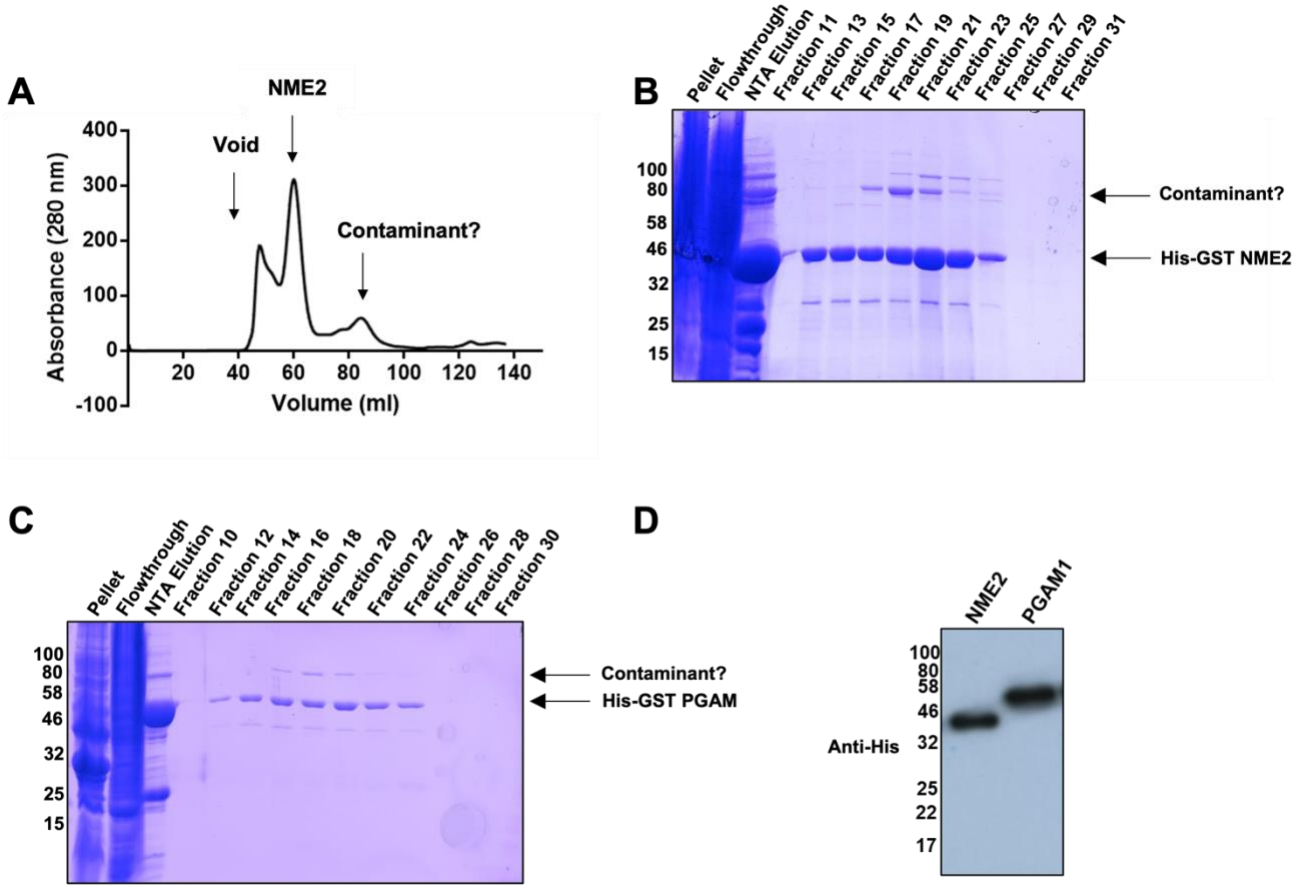

Figure 3.2. Purification of His-GST-tagged NME2 and His-GST tagged PGAM1 from BL21(DE3)pLysS. *E. coli* transformed with pOPINJ encoding full length His-GST-tagged NME2 or full length His-GST tagged PGAM1 were induced with IPTG for 16 hours at 18°C, and the bacteria were lysed after centrifugation. (A) UV profile of partially-purified His-tagged NME2 from cleared bacterial lysate after SEC. Fractions (0.5 mL) were collected, pooled and subjected to size-exclusion chromatography (SEC) on a S200/60 column as described in Figure 3.1 (B) 10 µL of each fraction was subjected to SDS-PAGE 9 (Section 2.6) on a 10 % (w/v) SDS poly acrylamide gel showing the predicted His-GST NME2 and a potential high molecular-weight contaminant, in addition to the bacterial cell pellet, the unbound fraction and the pooled eluate from the IMAC column. (C) GST-His-tagged PGAM1 was purified by IMAC and SEC and fractions (1.5 mL) 6-30 were resolved on a 10% acrylamide SDS-PAGE gel as in (B). (D) Western blot of recombinant His-GST-NME2 and His-PGAM1 (see below). 200 ng of purified NME2 or PGAM1, both of which contain a 6His tag, were resolved by electrophoresis on a 10 % (w/v) polyacrylamide gel. The protein was transferred to a nitrocellulose membrane and probed with an anti-His antibody conjugated to HRP and detected by chemiluminescence (Section 2.7).

3.3 3C proteolytic cleavage of the His-GST tag on NME1, NME2 and PGAM

Protein tags such as GST can both promote and interfere with target protein folding and oligomerisation (361, 362). The multimer previously observed when purifying NME1 and NME2 by SEC might therefore be a result of the affinity tag (362). To work with the highest quality protein possible corresponding to the native His-kinase, the linked His-GST tag was therefore removed proteolytically (Section 2.5.2.3). An initial experiment was performed to

determine the efficiency of proteolytic cleavage by human rhinovirus (HRV) 3C protease, a 25 kDa protein which recognises the N-terminal cleavage site Leu-Glu-Val-Leu-Phe-Gln/Gly-Pro encoded at the N-terminus before the NME1, NME2 and PGAM amino acid coding sequences (Figure 2.1). The proteins were incubated with Ni-NTA beads for 1 hour at 4 ºC to allow the His-GST tagged protein to bind to the resin. 3C protease was then added to the Ni-NTA bound protein and the sample was incubated at 4 ºC for 2 hours (Section 2.5.2.3). The Ni-NTA resin was then heated to 95 °C in SDS-PAGE sample buffer and collected for analysis (Figure 3.3A). Prior to proteolytic cleavage His-GST tagged NME1 resolved at ~43 kDa (Figure 3.3A, Lane 1). The sample collected after incubation with 3C protease (Lane 2) contained three polypeptide bands. The ~28 kDa band is likely to be the His-GST tag that has been removed from NME1 and eluted from the beads, as GST has a molecular mass of 25-28 kDa. The band that migrated at ~25 kDa corresponds to the molecular mass of the 3C protease, which is corroborated by the band in control Lane 7 containing only 3C protease. The predicted molecular masses of NME1 and NME2 are between 17-19 kDa, and the third band observed in Lane 2, at a molecular mass of ~19 kDa is therefore untagged NME1. His-GST tagged NME2 prior to proteolytic cleavage, was resolved at ~43 kDa in Lane 3. In Lane 4, the band pattern was similar to that of the cleaved NME1 fraction with band at ~27 kDa, ~ 25 kDa and a band at a molecular mass of ~17 kDa corresponding to monomeric untagged NME2 (Figure 3.4A).

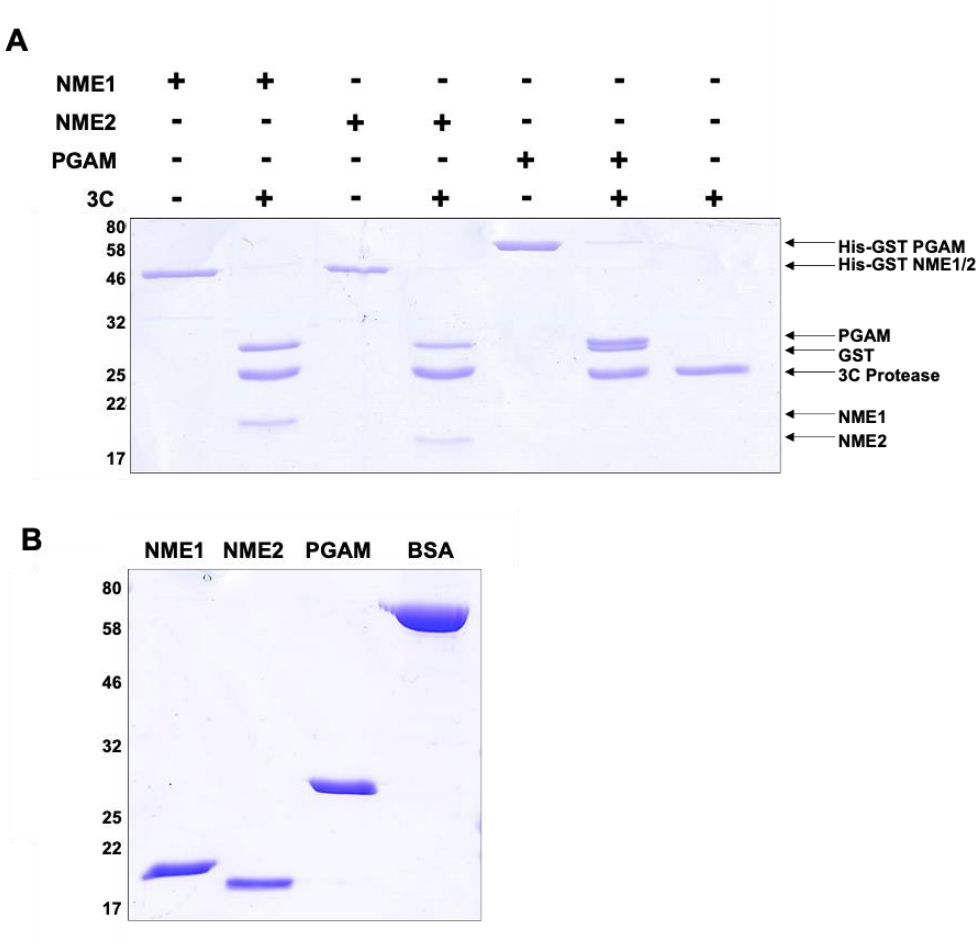

Figure 3.3. SDS-PAGE and Coomassie blue staining of purified recombinant NME1, NME2 and PGAM before and after proteolytic removal of the N-terminal His-GST tag. Ni-NTA-bound His-GST tagged protein was incubated with 3C protease (which cleaves between LEVLFQ/GP amino acids) for 3 h (Section 2.7) and unbound (eluted) proteins were collected. (A) SDS-PAGE of protein before and after 3C cleavage resolved on a 10 % (w/v) polyacrylamide gel. (B) Following 3C cleavage, recombinant proteins were subjected to size-exclusion chromatography and then 2 µg of each of the protein peaks was analysed by SDS-PAGE as in (A).

Purified His-GST tagged PGAM resolved at ~55 kDa. This is in accordance with the predicted molecular mass of His-GST of between 53-56 kDa (Figure 3.3A, lane 5). In addition to bands corresponding to the cleaved His-GST tag at ~27 kDa and the free 3C protease at ~25 kDa, a ~28 kDa band is clearly observed (Figure 3.4A, Lane 6). Cleaved PGAM has a predicted molecular mass of ~29 kDa which therefore suggests that the ~28 kDa protein band is purified untagged PGAM. These findings suggest that His-GST affinity tag cleavage by 3C protease was both accurate and efficient and was evaluated further by MS (see below). As the 3C protease and the His-GST tag both possessed an encoded His-tag, these contaminants were easily removed after proteolytic cleavage, by binding to the Ni-NTA resin. These were then separated from the purified cleaved protein by centrifugation, and the flow through containing the purified recombinant protein was collected and subjected to size-exclusion

chromatography. The purified proteins were then resolved by SDS-PAGE (Figure 3.3B) and their purity determined by comparison with BSA as a standard.

To further confirm the identity of each of the purified recombinant proteins, intact mass spectrometry (MS) (Section 2.12) was used to analyse the untagged purified proteins (Figure 3.4). The predicted mass of full-length NME1, including the 3C protease cleavage site residues Gly and Pro is 17,303 Da. The intact MS analysis for NME1 identified a peak with a m/z value of 17,304 Da (Figure 3.4A), confirming the identity of the intact purified protein. In Figure 3.4B, purified NME2 was analysed by intact MS and a peak with an m/z value of 17,453 Da was revealed. The predicted mass of full length NME2 is 17,452 Da. Both NME1 and NME2 show a mass difference of ~1 Da which might be due either to deamidation of a single Asparagine, or Glutamine residue to either Aspartate and Glutamate, but this cannot be confirmed through intact MS analysis (363). Purified PGAM, with a predicted molecular mass of 28,958 Da was also subjected to intact MS analysis and a peak was identified with the mass of 28,958 Da. Large differences detected in theoretical and observed mass by intact MS are generally a result of post translation modifications (364). For example, Aurora A kinase was discovered to have 14 sites of phosphorylation, eliciting a mass difference of ~ 1.12 kDa after MS (365). Thus, the collective data and the analysis using intact mass spectrometry of the purified recombinant proteins NME1, NME2 and PGAM not only confirms the identification of each protein but suggests that no proteolysis or major post translational modifications are present on any of the proteins.

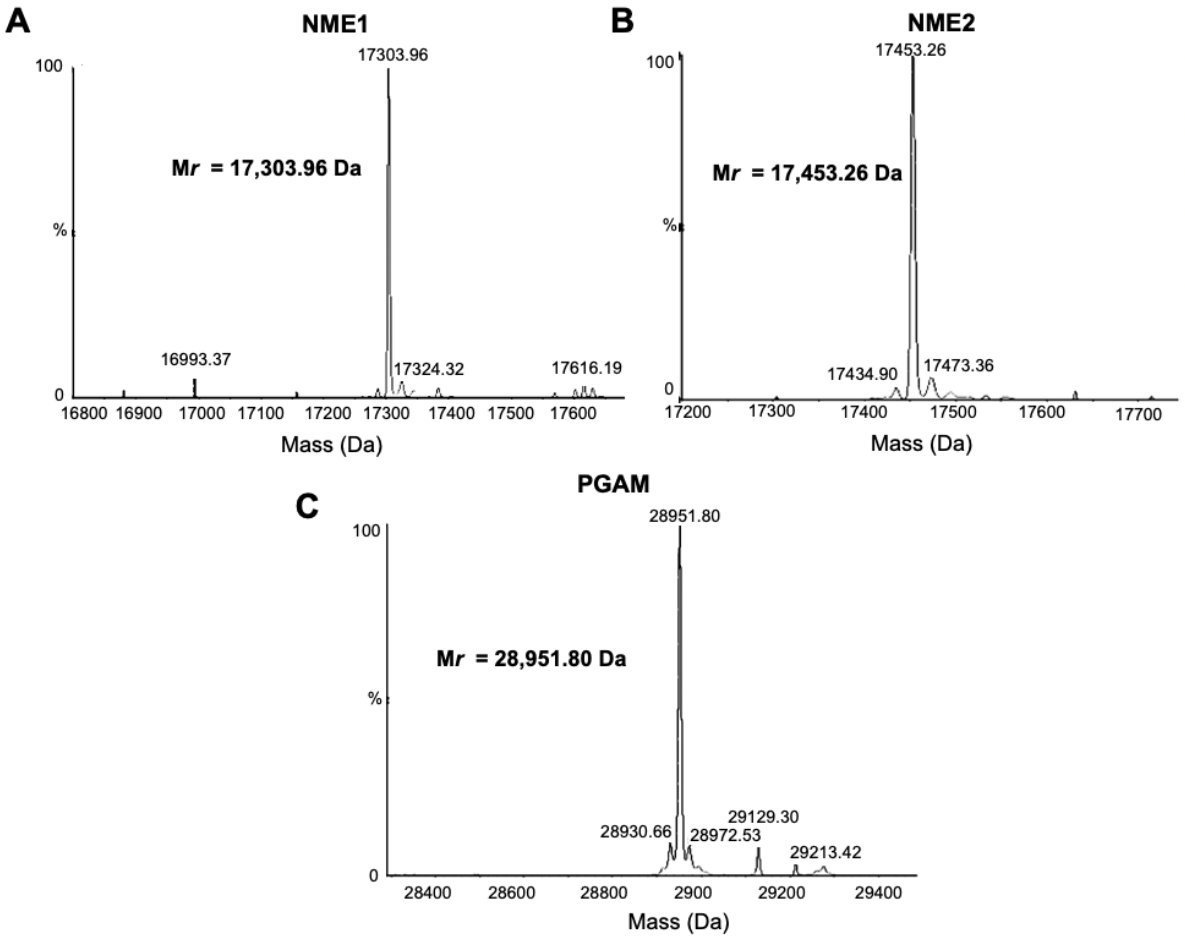

Figure 3.4. Intact mass spectra of purified (A) NME1, (B) NME2, or (C) PGAM1 after 3C cleavage. Samples were analysed by LC-MS using a Waters Synapt G2Si. Data were processed using MassLynx (4.1) and deconvoluted using MaxEnt1. Deconvolution settings were as follows: 0.5 Da/channel resolution; Uniform Gaussian distribution with a width at half height of 0.500 Da. The masses of each of the intact proteins are indicated.

3.4 Investigating NME1, NME2 and PGAM binding partners by Differential Scanning Fluorimetry (DSF)

3.4.1 DSF analysis of purified NME1

The use of differential scanning fluorimetry (DSF) as a tool to analyse protein kinase ligand interactions is relatively well-established and it has been shown that the stabilising effects of ligands and compounds upon binding is often quantitatively proportional to the affinity of the ligand, especially in the case of protein kinases (327, 366-368). Lower concentrations of ligand induce lower changes in melting temperature of the protein, and *vice versa* for higher concentrations of ligand. This was previously demonstrated by our group, where the melting temperature of purified His-tagged PKA (5 µM) in the presence of 100 µM staurosporine was ~12 °C compared to ~9 °C in the presence of 10 µM compound (369). To assess if nucleotides bind to NME1, NME2 and PGAM and induce a thermal shift, and can so be employed in order to analyse autophosphorylation on histidine, DSF was employed (Section 2.13). The buffer

used in the DSF assays shown is Tris-HCl buffer, made to a pH of 7.4. The pK_a of Tris can change depending on the temperature, for example, as temperature increases the buffer capacity of Tris decreases, as hydrogen bonds are broken and free H^+ is released into solution, making it more acidic (370). Although this may have an effect on the melt curves displayed by the proteins, this buffer was deemed appropriate for the analysis of ligand binding as the melt curves were compared in the absence and presence of ligand, therefore making any change in pH relative. However, experiments to assess the effect of pH on the T_m of these proteins and binding capacity to different nucleotides could be an interesting area of research.

Figure 3.5 shows the effects of prior incubation of a series of nucleotides from 30 µM ATP increasing in 2-fold increments to 1 mM ATP with NME1 (Figure 3.5A and B), NME2 (Figure 3.5C and D) or PGAM (Figure 3.5E and F). Figure 3.5A shows dose-responsiveness of the thermal unfolding profile of NME1 in the presence of increasing ATP concentrations. The unfolding profile of NME1 in the absence of nucleotides is shown in black. In the presence of 30 µM ATP (green), the thermal unfolding profile shifted to a higher melting temperature and increased incrementally up to + 6.4 ºC in the presence of 1 mM ATP. As the protein displayed a classical sigmoidal unfolding profile, this suggests that prior to denaturation, NME1 was folded, and that the thermal stability of this folded protein structure was increased by the presence of the known ligand ATP.

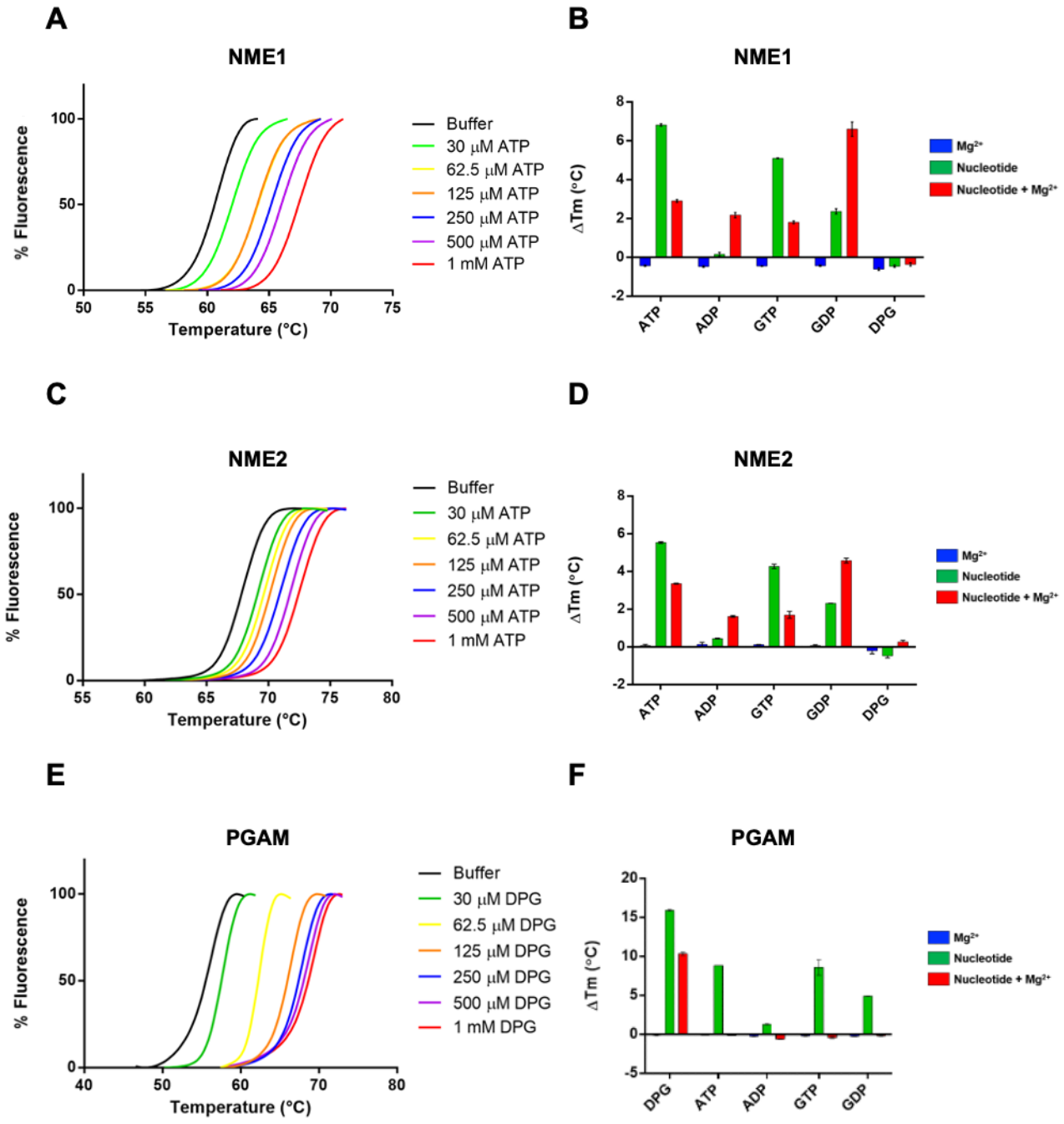

Figure 3.5. Thermal stability of NME1, NME2 or PGAM in the presence or absence of biochemicals. The purified recombinant proteins were incubated in the presence or absence of the indicated nucleotide (or 2,3 DPG in the case of PGAM) and/or subjected to differential scanning fluorimetry (DSF) to analyse the thermal stabilisation of nucleotide binding. Thermal unfolding profiles (Section 2.13) of a final concentration of 5 μM for each protein: (A) NME1, (C) NME2 and (E) PGAM and the average (N=2) change in melting temperature (ΔTm) of (B) NME1, (D) NME2 and (F) PGAM in the presence of the indicated addition (1mM). Thermal unfolding profiles were generated by normalising the data and assigning the lowest fluorescent reading as 0% and the highest as 100%. Linear regression analysis was utilised by means of fitting the Boltzman sigmoidal equation to the denaturation curves, which allowed the Tm to be determined. ΔTm values were calculated by subtracting the Tm value for the protein in Tris buffer, pH 7.4 from the Tm value in the presence of biochemical.

NME1 was also analysed in the absence and presence of ATP, ADP, GTP and GDP pre-incubated with $MgCl_2$ and the change in melting temperature (ΔT_m) of the protein was plotted (Figure 3.5B). ΔT_m was calculated by subtracting the melting temperature at which 50 % of the protein is unfolded in the presence of Tris-HCl buffer (pH 7.4) from the melting temperature at 50% in the presence of nucleotide (369) (Section 2.13). In the presence of $MgCl_2$ alone (blue), the melting temperature of NME1 was reduced by -0.38 ºC. This lies within the typical variability seen in this assay (368), and within the error envelope seen in the assays carried out here of ~ 0.5 ºC, as anything below this is unreliable. This suggests that $MgCl_2$ either fails to bind, or if it does, does not elicit sufficient change in protein stability. In the presence of the triphosphate nucleotide, ATP (green), the T_m of NME1 increased by +6.8 ºC, indicative of ATP binding. It was previously reported that NME1 has very high affinity for ATP, with a measured dissociation constant (Kd) of 0.5 µM (199). Together, these data support the use of DSF as a semi-quantitative technique to assess ligand binding through shifts in T_m (371). Interestingly, in the presence of both ATP and $MgCl_2$ (red), a much lower +2.8 ºC T_m shift was observed compared to ATP alone. In contrast, when NME1 was incubated with ADP and $MgCl_2$, the T_m was higher than in the presence of nucleotide alone, at +2.2 ºC. The presence of $MgCl_2$ may alter the local binding site of ATP/ADP due to additional bonds or bonds being broken between the substrate and the protein and this would therefore effect the stability of the protein in the presence and absence of $MgCl_2$. A similar pattern was demonstrated for guanosine nucleotides. NME1 incubated in the presence of GDP yielded a higher melting temperature than ADP alone at +2.4 ºC, and in the presence of GDP and $MgCl_2$ the melting temperature increased by +6.5 ºC. In the presence of GTP, NME1 exhibited a T_m shift of +5.0 ºC and in the presence of GTP and $MgCl_2$, the T_m shift was reduced to +1.8 ºC. This contrasts with protein kinases, where ATP requires Mg-binding in order to induce stabilisation measured by thermal assays such as DSF (326, 327).

3.4.2 DSF analysis of purified NME2

In a similar way, the purified recombinant protein NME2 was also incubated in the absence and presence of different nucleotides. A dose response of the thermal unfolding profile of NME2 in the presence of increasing ATP concentrations is shown in Figure 3.5C. Like NME1, the higher the ATP concentration, the greater the thermal stabilisation and therefore the higher the T_m shift measured. NME2 was also incubated with ADP, GTP and GDP, as well as $MgCl_2$ and analysed by DSF and the change in melting temperature (ΔT_m) was plotted in Figure 3.5D. In the presence of $MgCl_2$ alone (blue), NME2 T_m was increased by +0.14 ºC, which is within the error envelope of the assay as variability is seen below +0.3 °C and cannot be concluded as a true result (368). This suggested that the protein was either not binding to Mg^{2+} ions or

such binding had no effect on the protein's melting profile. However, in the presence of ATP (green), the T_m of NME2 increased by +5.5 ºC. The stability of the protein increased, and this indicated that the ATP was binding. In the presence of both ATP and $MgCl_2$ (red), the NME2 exhibits a similar effect to NME1, as the Mg^{2+} ions appeared to reduce the stabilising effect of the ATP, causing a T_m shift of +3.5 ºC. The T_m shift in the presence of ADP alone was +0.1 ºC but when incubated with ADP and $MgCl_2$, the T_m increased to +1.7 ºC. A similar result was observed for the guanosine nucleotides as in the presence of GTP alone the T_m shift was +4.4 ºC and in the presence of GTP and $MgCl_2$, the T_m shift was +1.9 ºC. NME2 incubated with GDP had a T_m shift of +2.3 ºC, and in the presence of GDP and $MgCl_2$ the T_m shift was +4.9 ºC. Thus, NME1 and NME2 demonstrate very similar thermal profiles in the presence of the adenosine and guanosine triphosphate and diphosphate nucleosides. Together, these data clearly show that the binding of NME1 and NME2 for nucleotides is readily detected by DSF, and also demonstrates differences between nucleoside diphosphate kinases and protein kinases, as in contrast to NME1 and NME2, $MgCl_2$ is necessary for ATP binding to monomeric Ser/Thr protein kinases including Aurora A (AurA) or PKA (shown in Section 4.5, Figure 4.15) (369).

3.4.3 DSF analysis of purified PGAM

Human PGAM autophosphorylates on position N3 of Histidine 11 by transferring a phosphate group from 2,3-diphosphoglycerate (DPG). PGAM is not known to autophosphorylate using any other nucleotides, however DSF analysis was employed as described for NME1 and NME2 in order to investigate this matter further (Figure 3.5F). Furthermore, to determine whether PGAM was folded into a native-like structure and was stabilized after binding to DPG, a dose-response assay was set up (Figure 3.5E). The thermal unfolding profile of PGAM in the presence of DPG demonstrates that the higher the DPG concentration, the greater the thermal stability and therefore the higher the calculated T_m of PGAM (Figure 3.5E). Figure 3.5F shows the ΔT_m of PGAM (calculated as above) in the presence of DPG, ATP, ADP, GTP and GDP. $MgCl_2$ had little, or no, effect on PGAM, with a T_m shift of -0.4 ºC. However, in the presence of the phosphate donor DPG, calculated T_m value increased by +16.0 ºC, which suggests that DPG binding has a very substantial effect on PGAM stability. Whether this is directly related to affinity cannot be determined directly by this assay, however, as PGAM has been shown to have a submicromolar K_m value of 0.33 µM for DPG in an enzyme assay, it is likely that the large shift in the T_m of PGAM is real (350). Intriguingly, PGAM behaved similarly to NME1 and NME2 in the presence $MgCl_2$, since the +16.0 ºC ΔT_m shift induced with DPG was reduced to a ΔT_m of +11.0 ºC after incubation with DPG and $MgCl_2$. When incubated with the nucleotides, ATP, ADP, GTP and GDP alone, a positive T_m shift was established, whereas, in the presence of nucleotide and $MgCl_2$ the T_m shifts were negligible. For example, in the

presence of ATP, the T_m of PGAM increased by +8.0 ºC and increased by +1.4 ºC with ADP. Incubation with GTP and GDP caused T_m shifts of +8.5 ºC and +5.0 ºC, respectively.

3.5. Measurement of NME1, NME2 and PGAM pHis autophosphorylation activity

3.5.1 Analysis of the pHis autophosphorylation activity of the putative histidine kinases NME1, NME2 and PGAM

In Section 3.4, purified NME1, NME2 and PGAM were determined to be folded, since they were stabilised by appropriate ligands during differential scanning fluorimetry (DSF). In all cases, the stability of NME1/2 and PGAM proteins increased in the presence of their respective phosphate donor, ATP for NME1 and NME2 or 2,3-diphosphoglycerate (DPG) with PGAM (Figure 3.5) as reported (367, 371). In order to evaluate whether NME1, NME2 and PGAM are enzymatically active, and require binding of distinct nucleotides in order to autophosphorylate on a specific His residue, N1 pHis and N3 pHis monoclonal antibodies were exploited for immunoblotting analysis (9). The His-GST tagged proteins were utilised in a number of immunoblot analysis experiments, such as the one described in Figure 3.5. As the protein tag does not contain a His that becomes phosphorylated, it is not likely to interfere with the analysis and presence of pHis in NME1/2 and PGAM.

NME1 was incubated with ATP, ADP, GTP and GDP and histidine phosphorylation was analysed (Figure 3.6A). In the presence of ATP, ATP/$MgCl_2$, GTP and GTP/$MgCl_2$, a band at ~43 kDa, corresponding to N1 histidine phosphorylated (N1 pHis) His-GST NME1 was detected. On the other hand, when incubated with the diphosphate nucleotides ADP and GDP, no N1 pHis NME1 was detected, demonstrating that ADP and GDP were not suitable phosphate donors and/or binding partners for histidine phosphorylation of NME1. An anti His-tag antibody was used to determine the total protein of NME1 in all samples analysed (Figure 3.6A, bottom panel). The same samples were also probed using a N3 phosphohistidine (N3 pHis) antibody, with PGAM as a positive control. This demonstrates that both ATP and GTP enabled phosphorylation of NME1 at the N1 position of histidine, but not at the N3 position.

Immunoblot analysis was also carried out on NME2 incubated with these diphosphate and triphosphate nucleotides (Figure 3.6B). This revealed that in the presence of ATP, ATP/$MgCl_2$, GTP and GTP/$MgCl_2$, a band at ~43 kDa corresponding to N1 pHis His-GST NME2 was detected. In contrast, when incubated with the diphosphate nucleotides ADP and GDP, no pHis NME2 was detected. The presence of His-tagged NME2 in these samples was confirmed (Figure 3.6B, bottom panel), demonstrating that ADP and GDP are not suitable phosphate donors for N1 histidine phosphorylation on NME2. It is apparent from both Figure 3.5 and Figure 3.6 that Mg^{2+} ions are not required for histidine autophosphorylation of NME1 and

NME2, and are potentially inhibitory (Figure 3.5). This is also notable in Figure 3.6 in the presence of GTP/$MgCl_2$ as the pHis signal for both NME1 and NME2, is reduced.

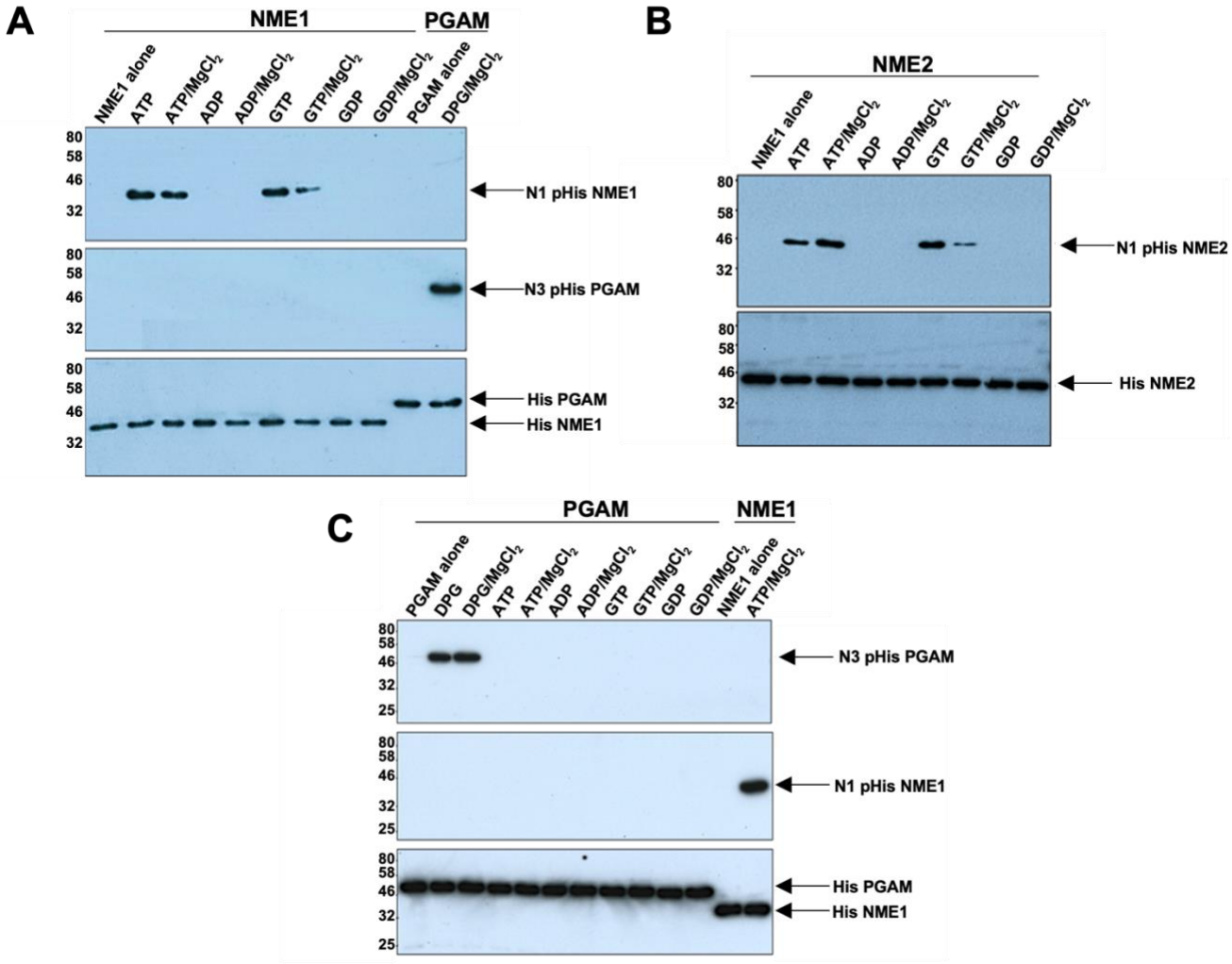

Figure 3.6. Immunoblot analysis of phosphate donor capability. GST-tagged enzymes (200 ng) were pre-incubated with 1 mM ATP or 1 mM ATP and 10 mM $MgCl_2$ (A) NME1 or (B) NME2, or (C) 1 mM DPG (PGAM1) were analysed after exposure to the indicated nucleotides or 2,3 DPG (DPG) by SDS-PAGE and immunoblotted with the monoclonal antibodies anti-N1 pHis (NME1/2) and anti-N3 pHis (PGAM1) (Section 2.10). Total protein was determined using an anti-His antibody. A representative immunoblot is shown from N=2.

Diphosphate and triphosphate nucleotides were next tested to determine if they were suitable phosphate donors for N3 pHis autophosphorylation activity by PGAM (Figure 3.6C). However, DPG alone and in the presence of $MgCl_2$ was the only nucleotide that elicited N3 pHis PGAM when analysed by immunoblotting. These samples were also probed using a commercial monoclonal N1 pHis antibody (Figure 3.6C, middle panel), and the absence of N1 pHis in PGAM supported the ability of these monoclonal antibodies to specifically distinguish between the N1 and N3 positions on histidine. Equal protein loading was confirmed using an anti-His

tag antibody, which was not removed to allow rapid comparison of loading (Figure 3.6C, bottom panel).

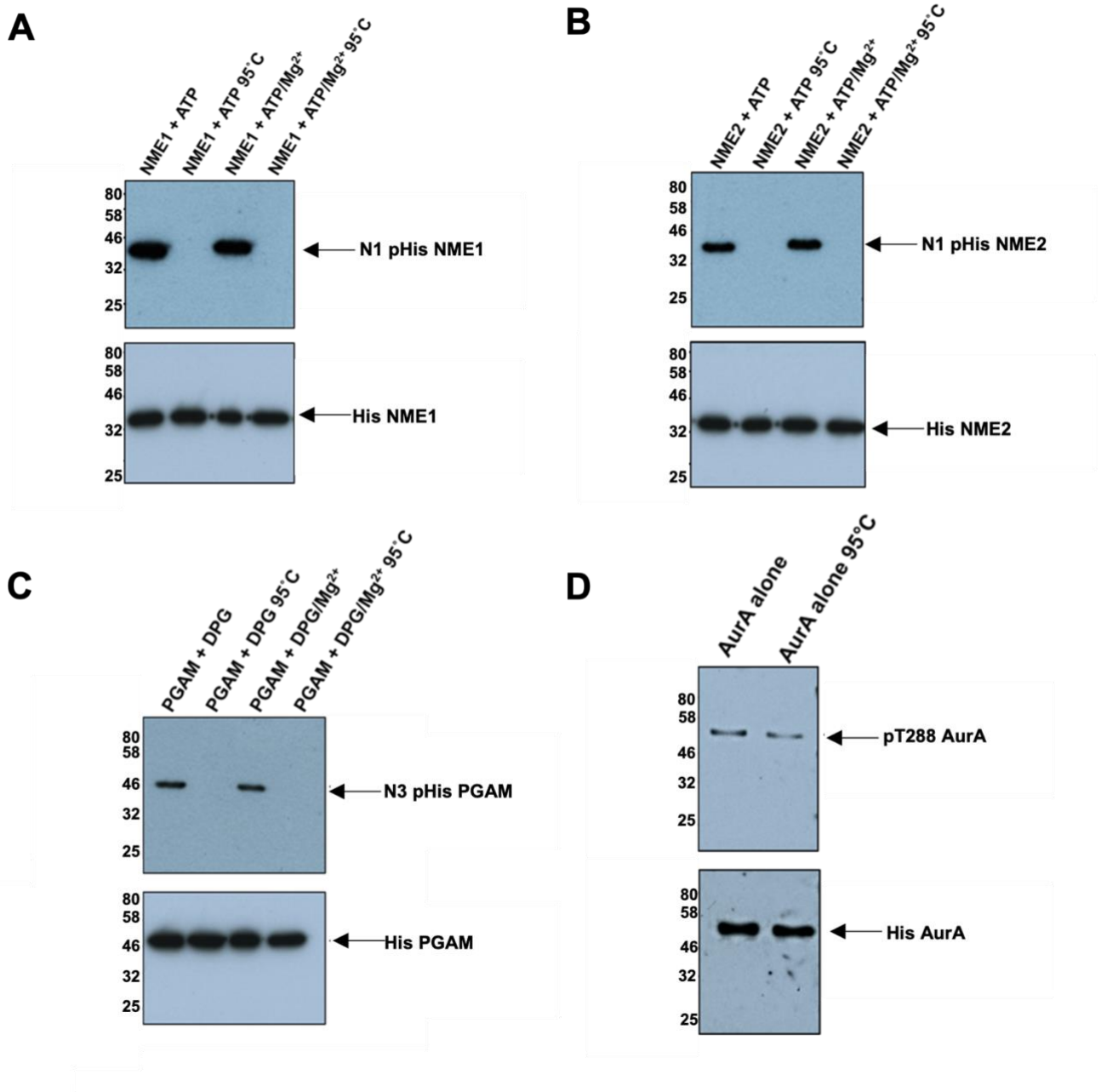

Figure 3.7. Analysis of heat lability of histidine phosphorylation on NME1, NME2 and PGAM. Each GST-tagged enzyme (200 ng) was preincubated with 1 mM ATP or ATP and 10 mM $MgCl_2$ (A) NME1 and (B) NME2, or (C) 1 mM DPG (PGAM1) were analysed after exposure to the indicated nucleotides by SDS-PAGE and immunoblotting using the monoclonal antibodies anti-N1 pHis (NME1/2) and anti-N3 pHis (PGAM1) (Section 2.10). One half of each enzyme reaction was heated to 95 °C for 5 minutes prior to analysis. (D) Heated or unheated recombinant Aurora A (200 ng) was immunoblotted with anti-pT288 Aurora A antibody. Total protein was determined by stripping and reprobing blots with anti-His antibody. A representative immunoblot is shown from N=3.

Phosphorylated histidine (pHis) is heat-labile due to the phosphoramidate bond possessing a high ΔG° value for hydrolysis, at ~ -12 kcal mol^{-1} compared to the more stable phosphoester

bond at ~ -6.5 kcal mol^{-1} (133). As the proteins were determined to be enzymatically active in the presence of appropriate phosphate donors (Figure 3.6), to further confirm that the signal detected is pHis, the heat lability of the unstable modification on the purified proteins was analysed by immunodetection (Section 2.10) using N1 pHis and N3 pHis monoclonal antibodies described above (Figure 3.7). NME1 (Figure 3.7A) and NME2 (Figure 3.7B) were incubated in the presence of ATP and ATP/$MgCl_2$ and duplicate samples heated to 95 ºC as controls. In the top panel of Figure 3.6A and B, in the presence of ATP and ATP/$MgCl_2$, a band is detected at the appropriate molecular mass for N1 phosphorylated NME1 and NME2. When the same samples were heated to 95 ºC, no detectable N1 phosphorylated polypeptide was observed, in accordance with the heat lability of pHis (133). The bottom panel of Figure 3.7A and B shows total NME protein loading detected by an anti-His tag antibody. When PGAM was incubated with the phosphate donor DPG, in the presence and absence of $MgCl_2$ and immunoblotted with the anti-N3 pHis antibody, bands corresponding to N3 phosphorylated PGAM were observed (Lanes 1 and 3). Due to the heat lability of N3 pHis, N3-phosphorylated PGAM was no longer detected after brief heating at 95 ºC. In contrast, human full-length Aurora A (purified as described in Section 2.5) remains autophosphorylated on Thr288 after heating to 95 ºC, based on immunoblotting with an antibody that specifically recognises phosphorylated T288 (Figure 3.7D). This is consistent with the chemical nature of the bonds involved; whereas phosphoester bonds are essentially stable to boiling, phosphoramidate bonds formed by phosphorylation on nitrogenous groups such as the imidazole ring of His, are not (8, 133).

The time-dependent analysis of NME1 and NME2 pHis incorporation was analysed by immunoblot, after establishing a time course assay with purified NME1 in the presence of ATP (Figure 3.8A). As shown in Figure 3.8A, it is clear that the reaction in which NME1 transfers a phosphate from ATP to His is essentially instantaneous, as at 10 seconds N1 pHis was detectable on NME1. The level of N1 pHis detected on NME1 increased up until 4 minutes, where the reaction began to plateau. The relative amount of ATP required to detect N1-pHis on NME1 or NME2 (Figure 3.8B) was also analysed. The limit of detection for N1 pHis on NME2 was at 1 µM ATP, since no N1 pHis NME2 was detected at concentrations below this. On the other hand, the limit of detection for N1-pHis in NME1 was below 0.1 µM ATP.

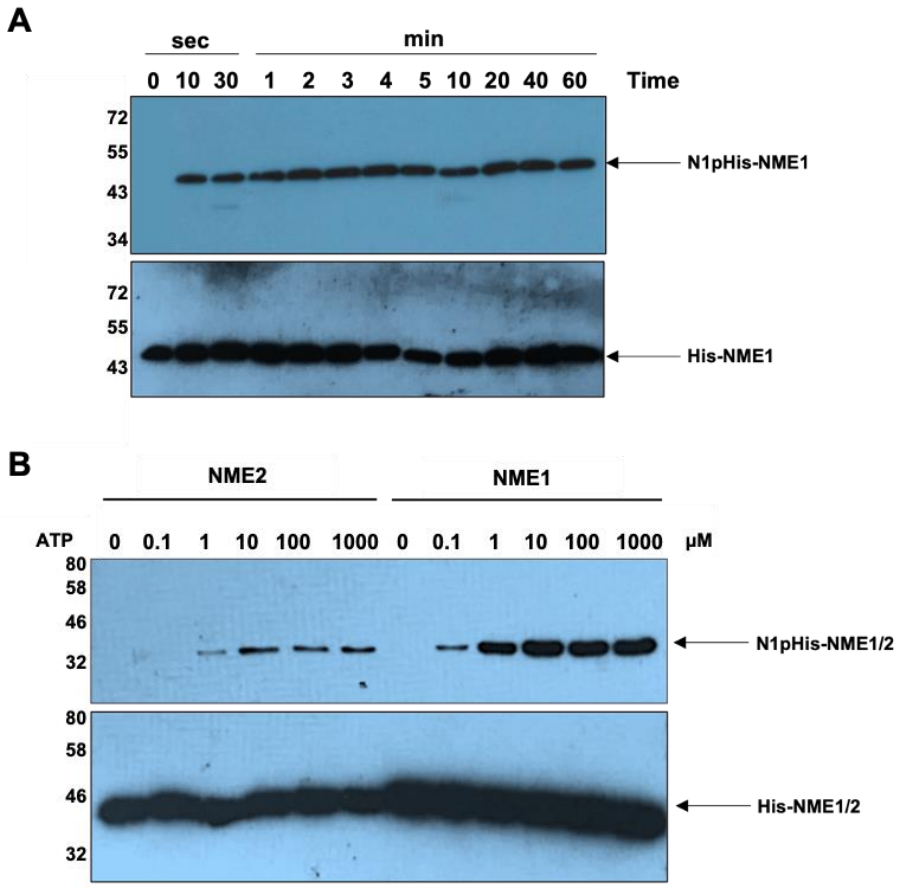

Figure 3.8. Western blot analysis of NME autophosphorylation activity: determining the limits of pHis detection *in vitro*. (A) 1 µg of NME1 was incubated with 50 µM ATP and the reaction was terminated by adding sample buffer (pH 8.8) at different time points after the assay was initiated. (B) Analysis of autophosphorylation of 1 µg of NME1 or NME2 after incubation with the indicated ATP concentration. Samples from both (A) and (B) were resolved on a 15% acrylamide gel and analysed by western blot using the anti-N1 phosphohistidine antibody. Total protein levels were revealed using anti-His antibody. A representative immunoblot is shown from N=2.

3.5.2 Do NME1 and NME2 have specificity towards different nucleotides?

NME1 and NME2 are important for controlling the levels of various nucleotide pools in cells (372), and this is supported by my finding that they bind (Figure 3.5) and utilise different nucleotides to drive histidine autophosphorylation (Figure 3.6). To evaluate this further, NME1 and NME2, were incubated with the nucleotides cytidine triphosphate (CTP), uridine triphosphate (UTP) and thymidine triphosphate (TTP) and analysed by DSF and immunoblotting (Figure 3.9). In the presence of CTP, the melting temperature of the NME1 increased by +5.8 ºC. This was greatly reduced in the presence of $MgCl_2$, when the T_m shift was only +0.9 ºC. CDP and CTP were reported to be the poorest nucleotide binders of NME1 by Chen *et al*, with a high dissociation constant (K_D) for CTP of >20 µM (199). This is supported by the data described here, as CDP appeared to have a very low ΔT_m indicative of poor binding and CTP yielded one of the lowest ΔT_m shifts. UTP resulted in a T_m shift of +6.2 ºC, and with

the addition of $MgCl_2$ the T_m shift reduced to +1.8 ºC. When incubated with TTP alone, the melting temperature of NME1 increased by +6.1 ºC compared to that of NME1 in buffer alone. The difference between the T_m of NME1 in the presence of TTP and TTP with $MgCl_2$ was the smallest of all the nucleotides analysed. In the presence of TTP and $MgCl_2$ the T_m shift was +5.9 ºC, suggesting that $MgCl_2$ had essentially no effect on NME1 binding to the TTP nucleotide.

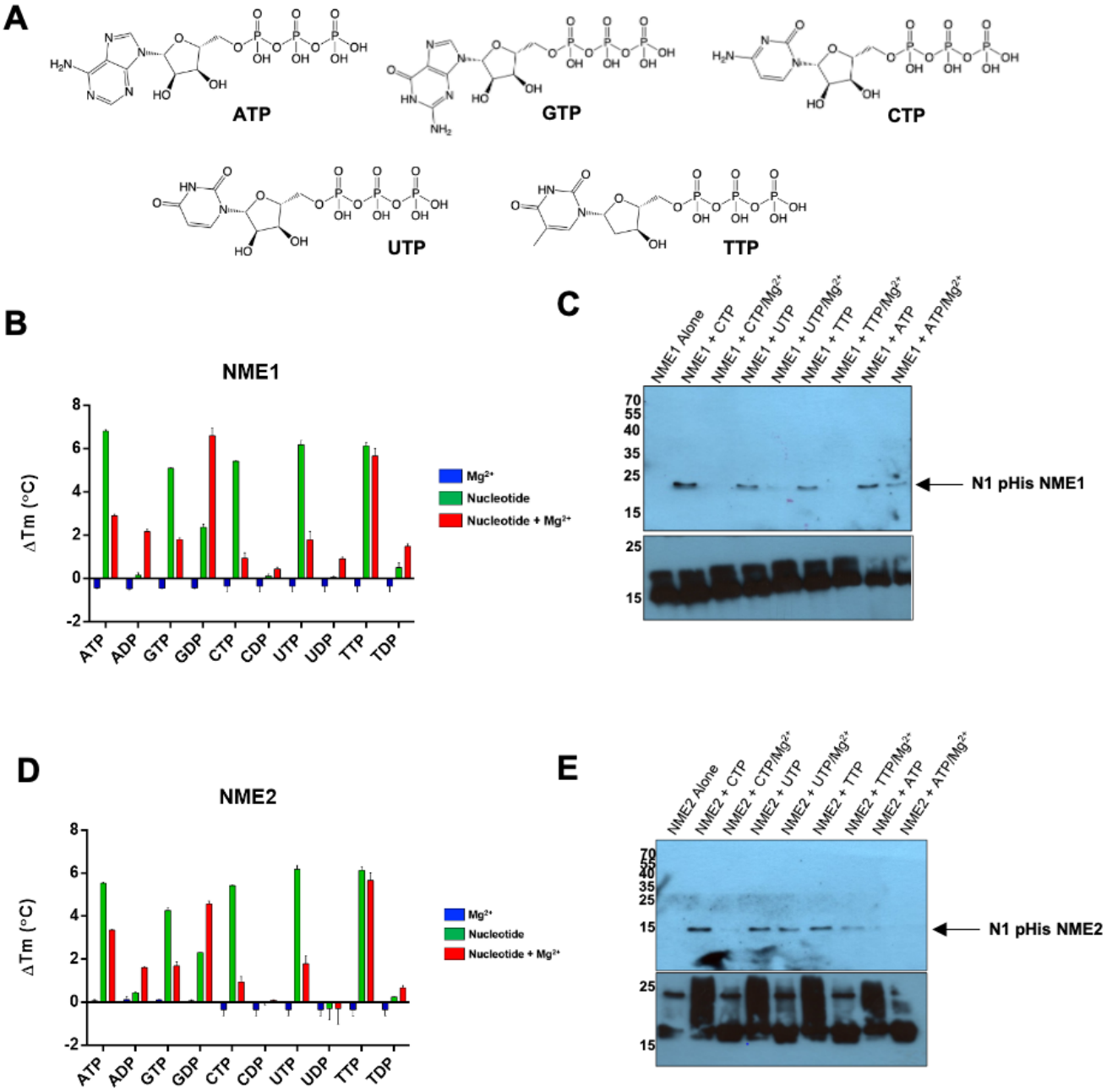

Figure 3.9. DSF and western blot analysis of nucleotide binding and the ability to donate a phosphate for histidine autophosphorylation. (A) Chemical structure of nucleotide tri-hosphates. Nucleoside diphosphates are omitted for clarity (B) The purified recombinant proteins were incubated for 5 minutes in the presence or absence of 1 mM of the indicated nucleotides and/or 10 mM $MgCl_2$ and then subjected to differential scanning fluorimetry (DSF) to analyse the thermal stability of each protein mixture relative to a solvent control. The average (N=2) change in melting temperature (ΔTm) of (5 μM) enzymes (B) NME1, (D) NME2 and histidine phosphorylation (Section 2.12) of 500 ng enzyme (C) NME1 or (E) NME2 are presented. Equal protein loading was confirmed by immunoblotting using anti-NME1 or NME2 antibodies. Thermal unfolding profiles and ΔTm values were calculated as described in Figure 3.5.

The data presented for NME1 DSF analysis (Figure 3.9B) correlate with the results obtained by immunoblot analysis (Figure 3.9C) in that the triphosphate nucleotides that displayed a

positive T_m shift by DSF also resulted in N1 pHis autophosphorylation. Furthermore, Mg^{2+} ions that reduced the T_m shift when incubated with nucleotide and protein, were not necessary for histidine autophosphorylation and reduced the levels of pHis NME1 detected (Figure 3.6A). In the absence of any nucleotide NME1 displays no pHis activity detectable by the N1 pHis antibody. In the presence of CTP, UTP, TTP and ATP, histidine phosphorylated NME1 migrated to the correct molecular mass of ~17 kDa. When incubated with both nucleotide and $MgCl_2$, N1 pHis NME1 is not detected other than with UTP and ATP, which is greatly reduced compared to incubation with nucleotide alone.

Similar results were observed for purified recombinant NME2. DSF analysis of NME2 (Figure 3.9D) showed that in the presence of CTP, the T_m of NME2 shifted +5.6 ºC and with the addition of $MgCl_2$, the T_m of NME2 increased by +1.0 ºC. In the presence of UTP, the T_m shift was +6.2 ºC, and this was reduced to +1.9 ºC with the addition of $MgCl_2$. Furthermore, the nucleotide TTP caused a T_m shift of +6.1 ºC and when NME2 was incubated with TTP and $MgCl_2$, the melting temperature of NME2 increased by +5.8 ºC. Immunoblot analysis showed that NME2 transferred a phosphate group from CTP, UTP and TTP to its active site His at position N1. Thus, the band at ~17 kDa corresponding to pHis NME2, was detected in the presence of CTP, and this was nearly undetectable in the presence of CTP and $MgCl_2$. In the presence of UTP and TTP, both with and without $MgCl_2$, a phosphorylated protein was observed in all samples, and the addition of $MgCl_2$ reduced phosphorylation, this being more significant with TTP and $MgCl_2$. In summary, Figure 3.9 demonstrates that although NME1 and NME2 have a higher affinity for some nucleotides more than others, this data suggests that both proteins bind all these nucleotides tested, and are able to use them as in a phosphotransfer reaction.

3.6 Analysis of NME1, NME2 and PGAM active site mutants and their effect on structure and enzyme activity

3.6.1 Purification and identification of NME and PGAM mutant proteins

NME1, NME2 and PGAM are believed to autophosphorylate on a single His residue as part of the NDPK reaction (9). Both NME1 and NME2 transfer the gamma phosphate residue from a nucleoside triphosphate, such as ATP, onto position N1 of His 118 (9). In contrast, PGAM is believed to transfer a single phosphate from 2,3-diphosphoglycerate (DPG) onto position N3 of His 11 (9). To assess the role of His in enzyme activity and verify the specific phosphosite in NME1, NME2 and PGAM, His to Ala mutants at His118 and His11 were purified, respectively. In addition to this, to explore the importance of the conserved cysteine residues in NME1, a single (C109A) and double cysteine mutant (C109A/C145A) were

produced. The NME and PGAM mutants (highlighted in Figure 3.10) were purified in the same way as the wild-type proteins, as described above, using immobilised metal affinity chromatography (IMAC) and size-exclusion chromatography (SEC) to purify proteins from the bacterial lysate (Section 2.5), expressed from an appropriately mutated plasmid in BL21(DE3)pLysS *E. coli* (Section 2.2). Once purified by IMAC, the His-GST tag was removed using 3C protease and the proteins were resolved on a Superdex 200 column (Figure 3.11). To determine the presence and purity of the eluted NME proteins and the PGAM proteins, they were resolved on a 12% (w/v) acrylamide gel (Figure 3.12). The NME1 polypeptides migrated at ~17 kDa and the NME2 polypeptides were evident at ~15 kDa. The PGAM polypeptides were resolved at ~26 kDa. This confirmed that the mutant proteins had been successfully expressed and purified.

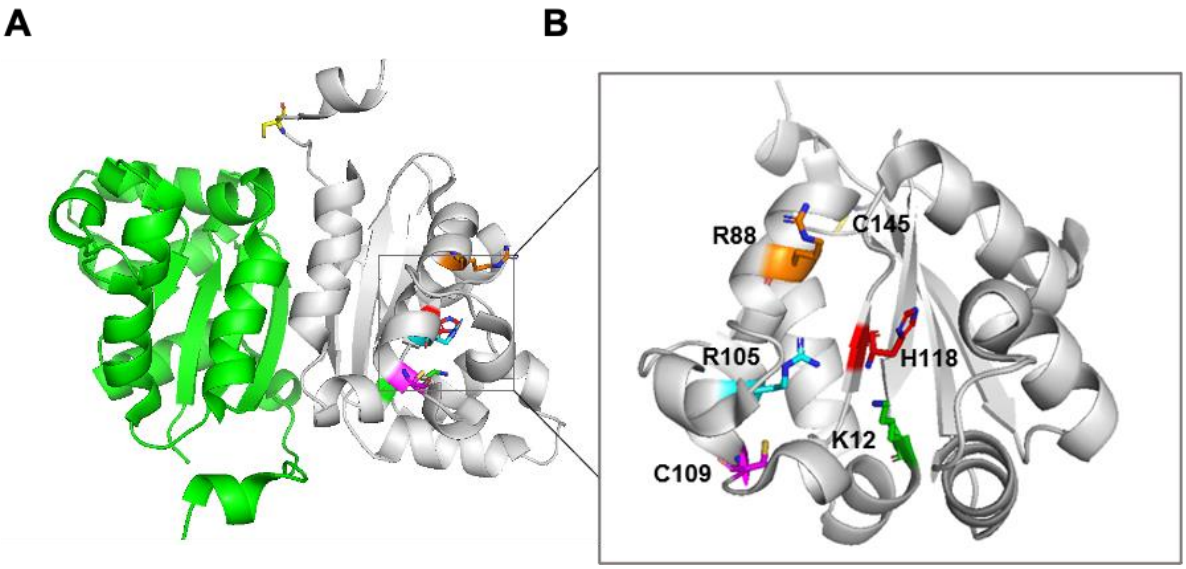

Figure 3.10. Cartoon of dimeric human NME1 (PDB Code: 1XJV). The position of conserved residues (Section 1.8.2 from Intro) in the crystallographic NME1 dimer in the active site of a single NME1 monomer are indicated. See Introduction for further information. (A) Crystal structure of NME1 dimer (monomers in green and grey) (B) Ribbon diagram of the monomer (grey) and side-chain of the conserved active site residues His118 (red), Lys12 (green), Arg88 (orange), Arg105 (cyan) and the conserved residues involved in protein stabilisation and folding, Cys109 (magenta) and Cys145 (yellow), are shown as sticks. Cartoons were generated using PyMoL.

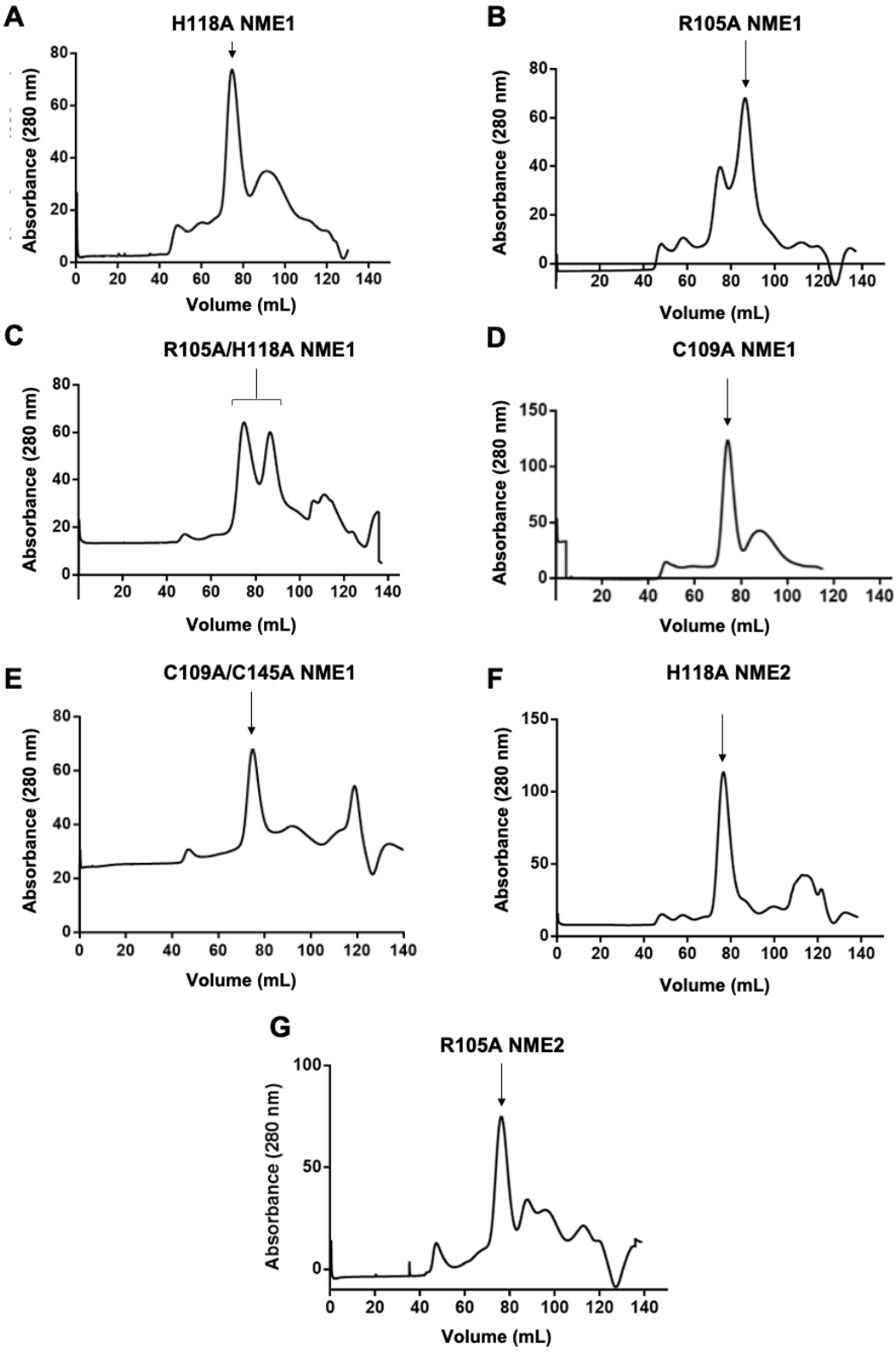

Figure 3.11. Size-exclusion chromatography of NME proteins. Elution volumes and the absorbance at 280 nm are shown for a series of NME1 and NME2 active site mutants. Arrows indicate the UV peak corresponding to the centred region of elution.

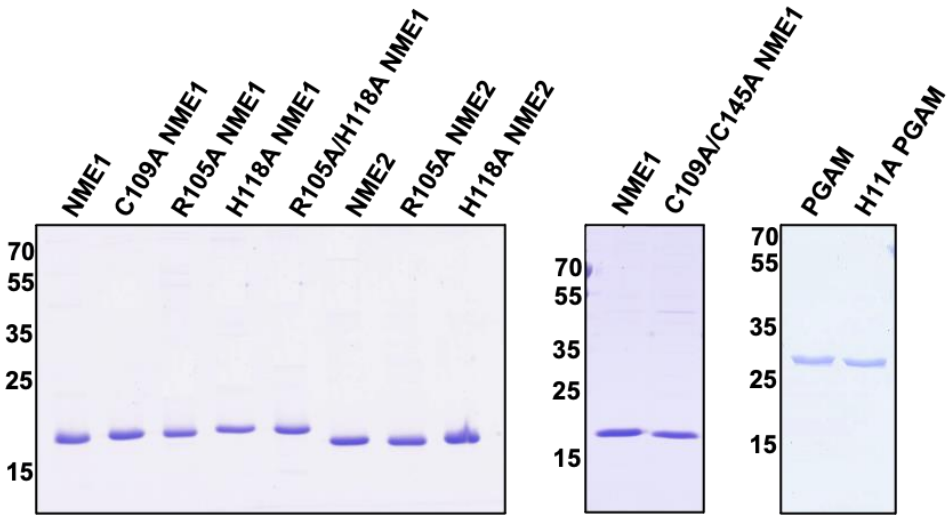

Figure 3.12. SDS-PAGE analysis and Coomassie blue staining of NME1, NME2 and PGAM proteins and active site mutant proteins after purification. After IMAC and SEC, 1 µg of the indicated protein was boiled with 2 x SDS sample buffer and subjected to electrophoresis on a 12 % (w/v) acrylamide gel (Section 2.6.1).

To further confirm and identify the purified mutant proteins, they were analysed by intact mass spectrometry (Figure 3.13). All the mutant proteins analysed possessed a mass difference of +1.0 Da from the predicted theoretical molecular mass. As described above, a mass difference of +1.0 Da could be a result of the deamidation of Asparagine or Glutamine to Aspartate or Glutamate. The intact mass spectrum displayed in Figure 3.13 confirmed that full-length NME mutant proteins had been isolated through IMAC and SEC.

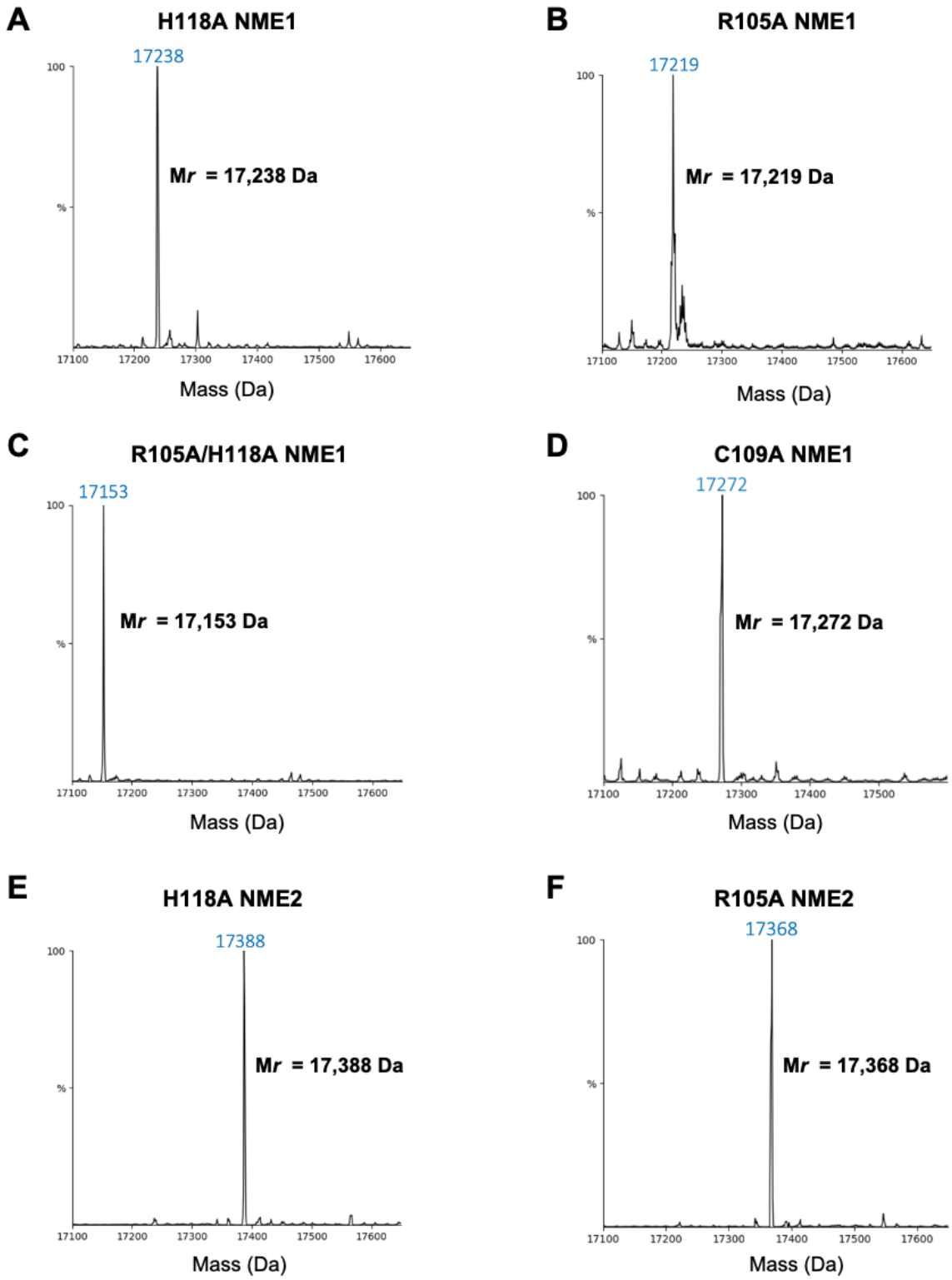

Figure 3.13. Intact molecular mass of purified NME proteins. The indicated proteins were purified by IMAC and pooled after SEC and then analysed by LC-MS using a Waters Synapt G2Si. Data were processed using MassLynx (4.1) and deconvoluted using MaxEnt1. Deconvolution settings were as follows: 0.5 Da/channel resolution; Uniform Gaussian distribution with a width at half height of 0.500 Da. (A) H118A NME1, (B) R105A NME1, (C) R105A/H118A NME1, (D), C109A NME1, (E) H118A NME2, and (F) R105A NME2. Representative spectra are shown from N=3.

3.6.2 Analysis of NME protein oligomeric state

The NME proteins are known to be oligomeric proteins, with a 3-dimensional structure of six functionally independent monomers that assemble into dimers and trimers, to form a hexamer (182, 183). The biological activity and function of NME1 and NME2 proteins is dependent on its oligomeric state (373). It was therefore important to confirm the oligomeric state of the proteins purified in *E. coli*. The techniques utilised to do this were size-exclusion chromatography with multi angle laser light scattering (SEC-MALLS) (Figure 3.14) and native mass spectrometry (MS) (Figure 3.15).

Size-exclusion chromatography linked to multi angle laser light scattering (SEC-MALLS) is used to determine the molecular mass of a protein in solution, which provides information as to oligomeric states (374). SEC-MALLS relies on the separation of macromolecules during flow through of a column and the differences in retention time due to different lengths of time spent diffusing in and out of the stationary phases before eluting from the column (375). More data can be obtained from this when combined with multi-angle light scattering and differential refractive index (dRI) detectors as the MALLS detector measures the proportion of light scattered by an analyte into multiple angles relative to the incident laser beam (Figure 3.14A). SEC-MALLS calculates the average molecular mass of molecules in an elution volume separated by the column, which assumes that the elution is homogenous and can therefore be affected by purity of the protein (375).

Compared to non-native MS (see Section 3.6.1 above), native MS is a form of electrospray ionisation in which conditions are optimised to sustain the protein in the folded native states, whereby proteins are separated based on their size and charge (376-378). To maintain the folded state, non-denaturing conditions are required, and the pH and ionic strength are carefully controlled. Native MS relies on the protein maintaining its native structure in the gas phase. A less structured/unfolded protein will pick up more charges during the electrospray ionisation phase than a more structured, folded protein (376). This differs to SEC-MALLS, as the SEC-MALLS has the advantage of determining the molecular mass of the protein in solution.

The SEC-MALLS system was calibrated with 50 µg bovine serum albumin (BSA) standard (Figure 3.14B) which eluted as a monomer and dimer, in accord with the literature (358). Afterwards, 50 µg of recombinant NME protein was analysed and the molecular mass was obtained using a differential index reading (Figure 3.14). Utilising SEC-MALLS analysis, WT NME1 was calculated to have a mass of 93 kDa (Figure 3.14A). The predicted molecular mass of monomeric NME1 is 17 kDa, and the hexameric form of NME1 is predicted to be 102 kDa.

Based on the calibration of the system, WT NME1 was indicated to be a hexamer in solution. The enzymatically inactive H118A NME1 protein was calculated to be 90 kDa (Figure 3.14B), and this indicated that this mutant was also present as a hexamer in solution. On the other hand, the R105A NME1 mutant had a calculated mass of 29 kDa (Figure 3.14C). The molecular mass of a NME1 dimer is predicted to be 34 kDa, therefore it is likely that this mutant is a dimer in solution. Analysis by SEC-MALLS revealed that WT NME2 had a molecular mass of 112 kDa (Figure 3.14D). Like NME1, the predicted molecular mass of a monomeric NME2 is 17 kDa (102 kDa for a hexamer) which indicated that the WT NME2 protein in solution is a hexamer, which correlates closely with the data shown in Figure 3.2.

Further SEC-MALLS analysis was performed using purified NME proteins, and the data is summarised in Table 3.1. This confirmed that H118A NME2, similarly to H118A NME1 and wild-type NME2 was likely to be a hexamer in solution as the calculated molecular mass was close to the predicted molecular mass of an NME2 hexamer, 103 kDa. When incubated with ATP or ADP, the molecular mass of the protein changes only by negligible amount, suggesting the oligomeric state of the protein did not change. This data also highlights the effect of the R105A and H118A mutations in combination as the R105A/H118A NME1 elutes in two separate volumes, one corresponding to a dimeric form and the other corresponding to a hexameric form of the protein (Figure 3.11C).

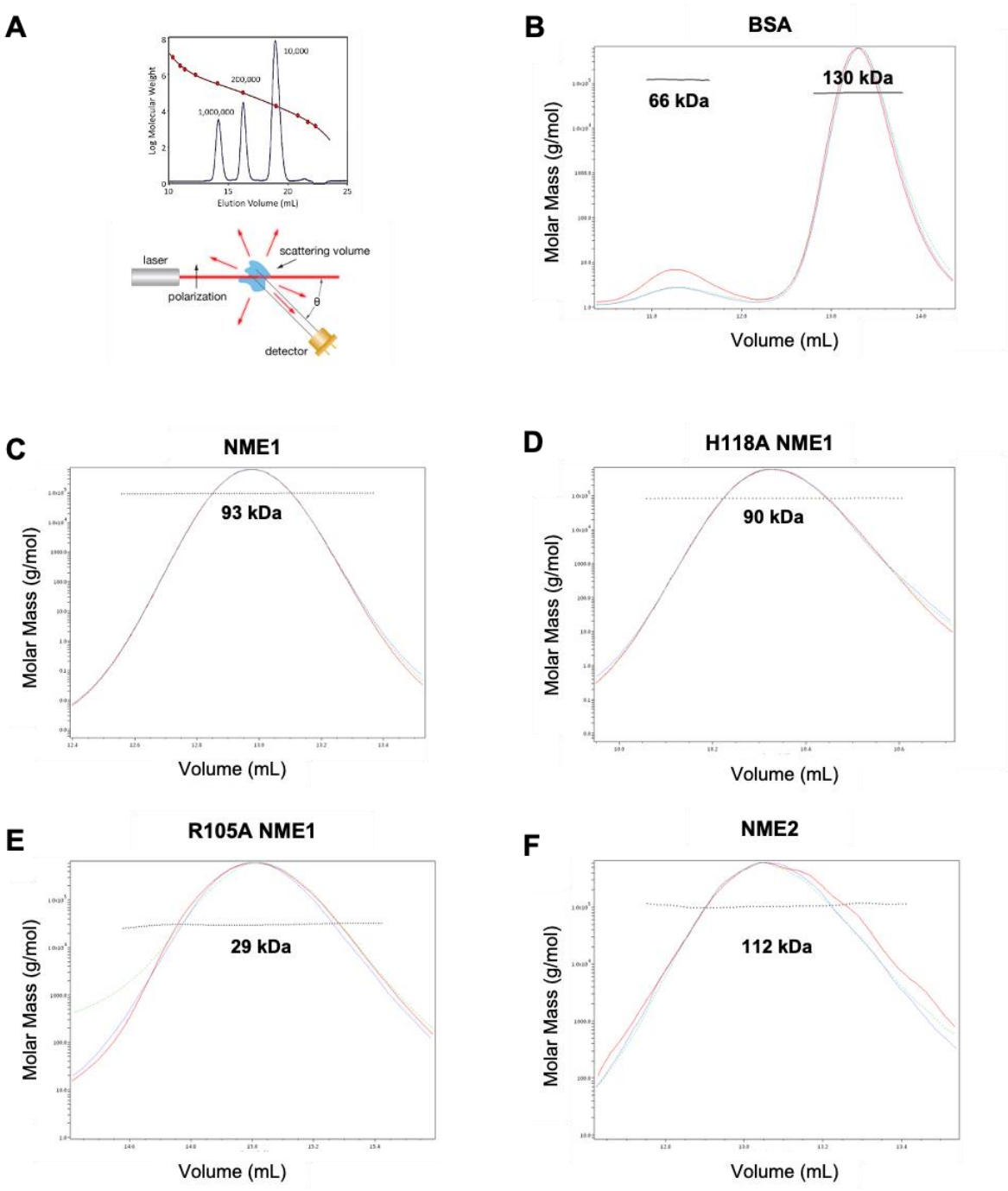

Figure 3.14. Average molecular mass per volume unit and Differential refractive index (dRI) of purified NME proteins. (A) Schematic of SEC-MALLS. SEC resolves the protein by size and MALLS permits molecular mass to be determined independently of retention time. The molecular weight of (B) BSA, (C) NME1, (D) H118A NME1, (E) R105A NME1 and (F) WT NME2 were estimated after processing SEC-MALLS data using Astra 6.1 software. The dRI is shown in red and the predicted molecular mass is indicated by the black dotted line.

Name of Protein/ligand	Approximate Molecular Mass	Predicted Oligomeric State
NME1	93 kDa	Hexamer
NME1 + ATP	93 kDa	Hexamer
NME1 + ADP	94 kDa	Hexamer
H118A NME1	90 kDa	Hexamer
H118A NME1 + ATP	87 kDa	Hexamer
H118A NME1 + ADP	86 kDa	Hexamer
R105A NME1	29 kDa	Dimer
R105A NME1 + ATP	29 kDa	Dimer
R105A NME1 + ADP	31 kDa	Dimer
R105A/H118A NME1	89 kDa;29 kDa	Hexamer;Dimer
NME2	112 kDa	Hexamer
NME2 + ATP	104 kDa	Hexamer
NME2 + ADP	104 kDa	Hexamer
H118A NME2	110 kDa	Hexamer
H118A NME2 + ATP	89 kDa	Hexamer
H118A NME2 + ADP	90 kDa	Hexamer
NME1 + NME2	85 kDa	Hexamer

Table 3.1. Apparent molecular mass and predicted oligomeric state of purified NME proteins inferred from SEC-MALLS analysis. The approximate molecular mass in the presence or absence of 1 mM ATP or 1 mM ADP is given to the nearest 1kDa.

Ion mobility mass spectrometry was also exploited to investigate the oligomeric state of the purified proteins. WT and mutant NME proteins were buffer-exchanged into 150 mM ammonium acetate, which maintains the protein in the folded state and allows the solution to become volatile in order for the protein to enter the gas phase (378). The MS spectra is deconvoluted in UniDec and the output spectra shows the mass of the native protein (Figure 3.15). As stated previously, the predicted molecular mass of an NME1 hexamer was 102 kDa and through MS analysis, the mass of WT NME1 was calculated to be 104 kDa (Figure 3.15A). The mass of H118A NME1 (Figure 3.15B) was calculated to be 100 kDa, suggestive of a hexamer. Similar to the results of SEC-MALLS analysis, the mass of both the R105A NME1 mutant (Figure 3.15C) and the R105A/H118A NME1 mutant (Figure 3.15D) was 35 kDa, indicative of a predicted 34 kDa NME1 dimer. C109A NME1 was calculated to have a mass of 105 kDa, demonstrating that the protein exists as a hexamer under native conditions.

The analysis of NME2 by native MS showed that WT NME2 (Figure 3.15F) was likely a hexamer, at 108 kDa, as well as H118A NME2 (Figure 3.15G), which displayed a molecular

mass of 101 kDa. Using native MS, the mass of R105A NME2 was revealed to be 43 kDa, suggesting that like R105A NME1, R105A NME2 was also a dimer in native conditions. This contradicts the data shown in in Figure 3.11, as R105A NME2 eluted at a similar volume to that of H118A NME2, which was found to be a hexamer. These differences may be a result of R105A NME2 forming multimers in solution, or due to the variation in techniques utilised. NME1 and NME2 are found as homohexamers in native conditions (183), and this is in agreement with the data shown in Figures 3.1 and 3.2, which showed that the purified recombinant proteins NME1 and NME2 were likely hexamers. Using a number of different techniques previously described, the collective data (Figure 3.1, 3.2, 3.14 and 3.15) show that WT NME1, WT NME2, H118A NME1, H118A NME2 and C109A NME1 are hexamers and R105A NME1, R105A NME2 and R105A/H118A NME1 are dimers in solution.

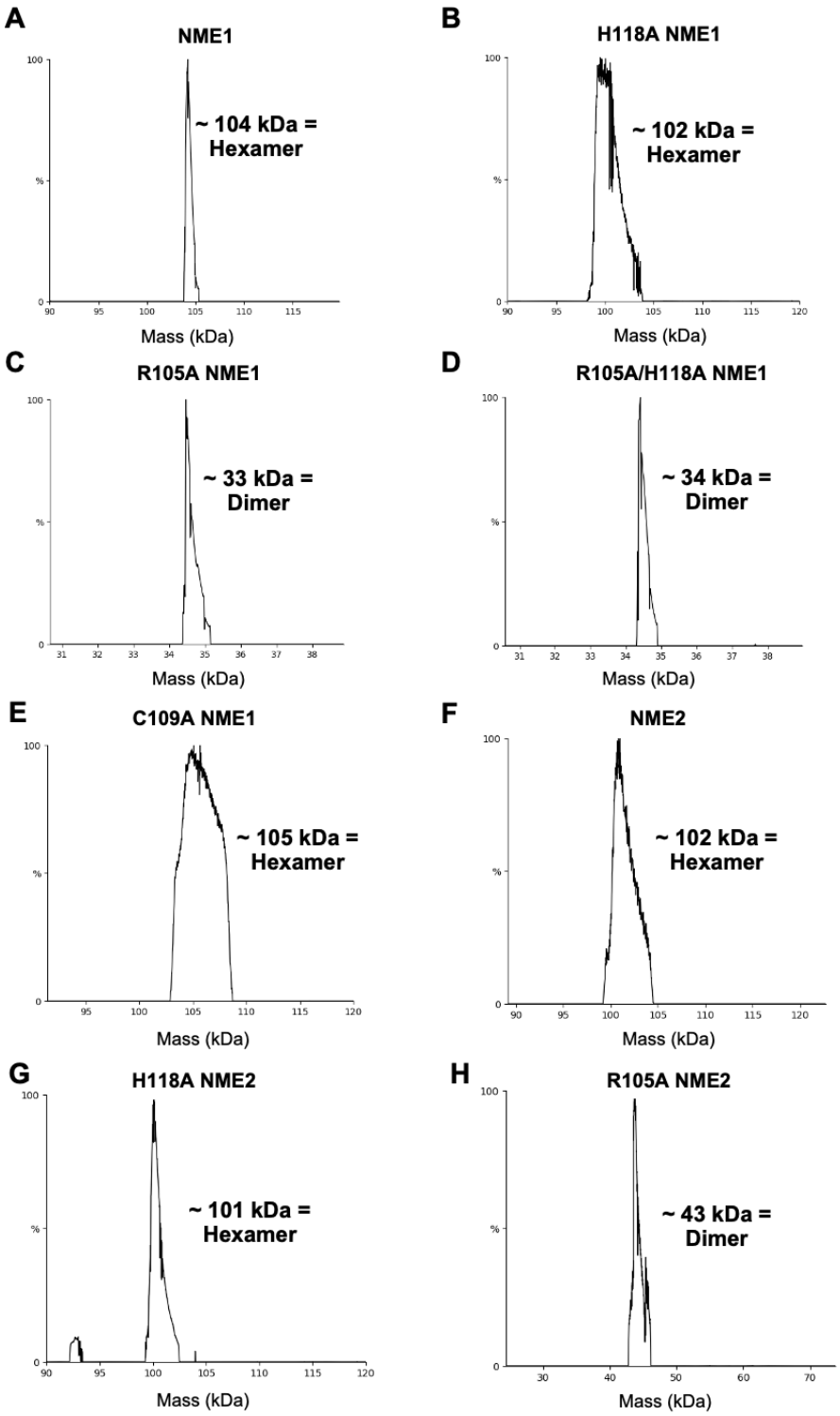

Figure 3.15. Native mass spectra of purified proteins. Purified recombinant NME proteins were buffer exchanged into 150 mM ammonium acetate using Amicon 10 kDa cut-off spin columns prior to MS analysis. Samples were analysed using a Waters Synapt G2Si. The oligomeric state of the protein was estimated by processing the native ESI spectrum using MassLynx 4.1 and UniDec. (A) WT NME1 (B) H118A NME1 (C) R105A NME1, (D) R105A/H118A NME1, (E) C109A NME1, (F) WT NME2 (G) H118A NME2 (G) and R105A NME2 (H). The respective mass of monomeric NME1 is 17.1 kDa and NME2 is 17.3 kDa. Representative spectra are shown from N=3.

3.6.4 Analysis of the His autophosphorylation activity of NME and PGAM active site mutants

The identity and native structure of the active site mutants have previously been verified. Differential scanning fluorimetry (DSF) was then employed to determine the folding and stability of the proteins under thermal stress and to report on the interaction of these proteins with ATP. As shown in Figure 3.16 and summarised in Table 3.2, thermostabilisation of the NME1 and NME2 recombinant mutants in the presence of ATP was observed for all purified mutants, with the exception of R105A/H118A NME1. Among the active site mutant H118A and R105A proteins, the extent of thermal stabilisation upon incubation with ATP was reduced, with the most significant reduction in the R105A mutants, compared to wild-type proteins. For example, in the presence of ATP, R105A NME1 was revealed to have a +2.3 °C T_m shift and R105A NME2 a +2.2 °C T_m shift, compared to +6.8 °C for wild-type (WT) NME1 and +5.6 °C for WT NME2. This reduction is likely to reflect the loss of or weaker nucleotide binding, through abolition of key charge:charge or hydrogen bond interactions between nucleotide and protein.

Name of Protein	T_m (°C)	ΔT_m + ATP (°C)
NME1	60.1 ± 0.33	+6.8 ± 0.09
H118A NME1	58.3 ± 0.09	+2.3 ± 0.16
R105A NME1	59.6 ± 0.62	+1.7 ± 0.37
R105A/H118A NME1	44.8 ± 0.10	-0.3 ± 0.29
C109A NME1	64.5 ± 0.04	+5.9 ± 0.07
C109A/C145A NME1	61.3 ± 0.01	+6.9 ± 0.53
NME2	67.8 ± 0.05	+5.6 ± 0.01
H118A NME2	65.2 ± 0.01	+4.8 ± 0.47
R105A NME2	64.7 ± 0.14	+2.2 ± 0.32

Table 3.2. Melting temperature (T_m) values for the purified recombinant proteins and the change in melting temperature (ΔT_m) in the presence of ATP. T_m values presented are of protein in Tris-HCl, pH 7.4 buffer alone, and the ΔTm values of protein in the presence of 1 mM ATP calculated according to Section 2.10. Mean ΔTm values ± SD (N=2) are shown.

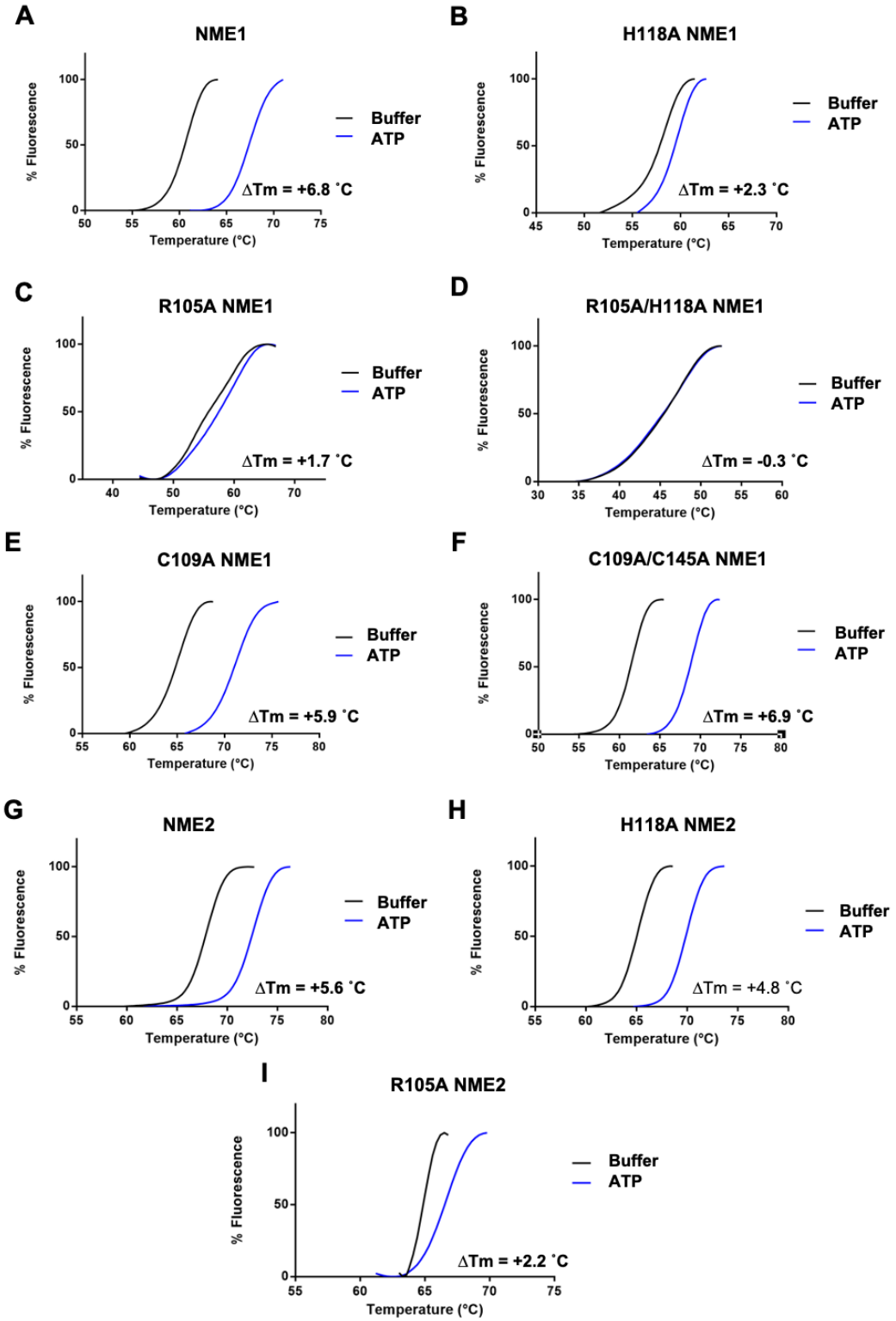

Figure 3.16. Thermal analysis of NME1 and NME2 active site mutants heated in the presence and absence of ATP. The purified recombinant protein was incubated in the presence or absence of the indicated nucleotide. Thermal unfolding profiles (Section 2.13) of (5 μM) enzymes (A) WT NME1, (B) H118A NME1, (C) R105A NME1, (D) R105A/H118A NME1, (E) C109A NME1, (F) C109A/C145A NME1, (G) WT NME2, (H) H118A NME2 and (I) R105A NME2 in the presence of 1 mM are presented. Thermal unfolding profiles and ΔTm values were calculated as described in Figure 3.5.

In order to further evaluate effects of NME/PGAM mutations, H118A NME1, H118A NME2 and H11A PGAM (Figure 3.17) proteins, along with R105A NME1 and R105A NME2 (Figure 3.18) were subjected to DSF in the presence of different nucleotides. The phosphate donor, 2,3-DPG was included for PGAM. The thermal stabilisation of wild-type proteins in the presence of indicated nucleotides are shown side-by-side for easy comparison (Figure 3.16-8). Notably, H118A NME1 and H118A NME2 active site mutants both displayed an increase in stability when incubated with nucleotides and $MgCl_2$. These data, as well as the findings shown in Figure 3.16, support a hypothesis that H118A mutants are still capable of binding to nucleotide substrates, and suggest that His118 plays a greater role in phosphate transfer than binding and orienting the substrate. Compared to wild-type NME1, H118A NME1 demonstrated a +13.3 °C increase in melting temperature (T_m) in the presence of ATP and $MgCl_2$, while wild-type NME1 demonstrated only a +2.5 °C increase in T_m. Figure 3.16 demonstrates that H118A NME1 and H118A NME2 proteins were less stable than the wild-type proteins, with an approximate -2 °C reduction in T_m for both proteins, therefore it could be possible that Mg^{2+} ions alone might help to increase the stability of the mutant proteins. However, when incubated with $MgCl_2$ alone, the stability of the protein was unaffected. This suggests that the greatest effect on the stability of the mutant proteins is a result of both the Mg^{2+} ions and nucleotide binding to the protein.

In contrast, a histidine to alanine mutation in PGAM appears to abolish binding to ATP, ADP, GTP and GDP. Similar to H118A NME1 and H118A NME2, in the presence of DPG and $MgCl_2$ the T_m of H11A PGAM is increased by ~4 °C compared to wild-type PGAM. In the presence of DPG alone, the T_m of H11A PGAM was determined to be +16 °C, the same as the shift established for wild-type PGAM. Due to the proximity of the histidine residue in the active site, the binding of DPG may be unaffected upon mutation, as the residues crucial for DPG binding, such as Tyr26, are still present (379). However as this cannot be determined by DSF analysis, to further explore this theory, active site mutants substituting Tyr 26, or other residues such as Arg116, Arg117, which are involved in DPG binding (380, 381) would be required for further analysis.

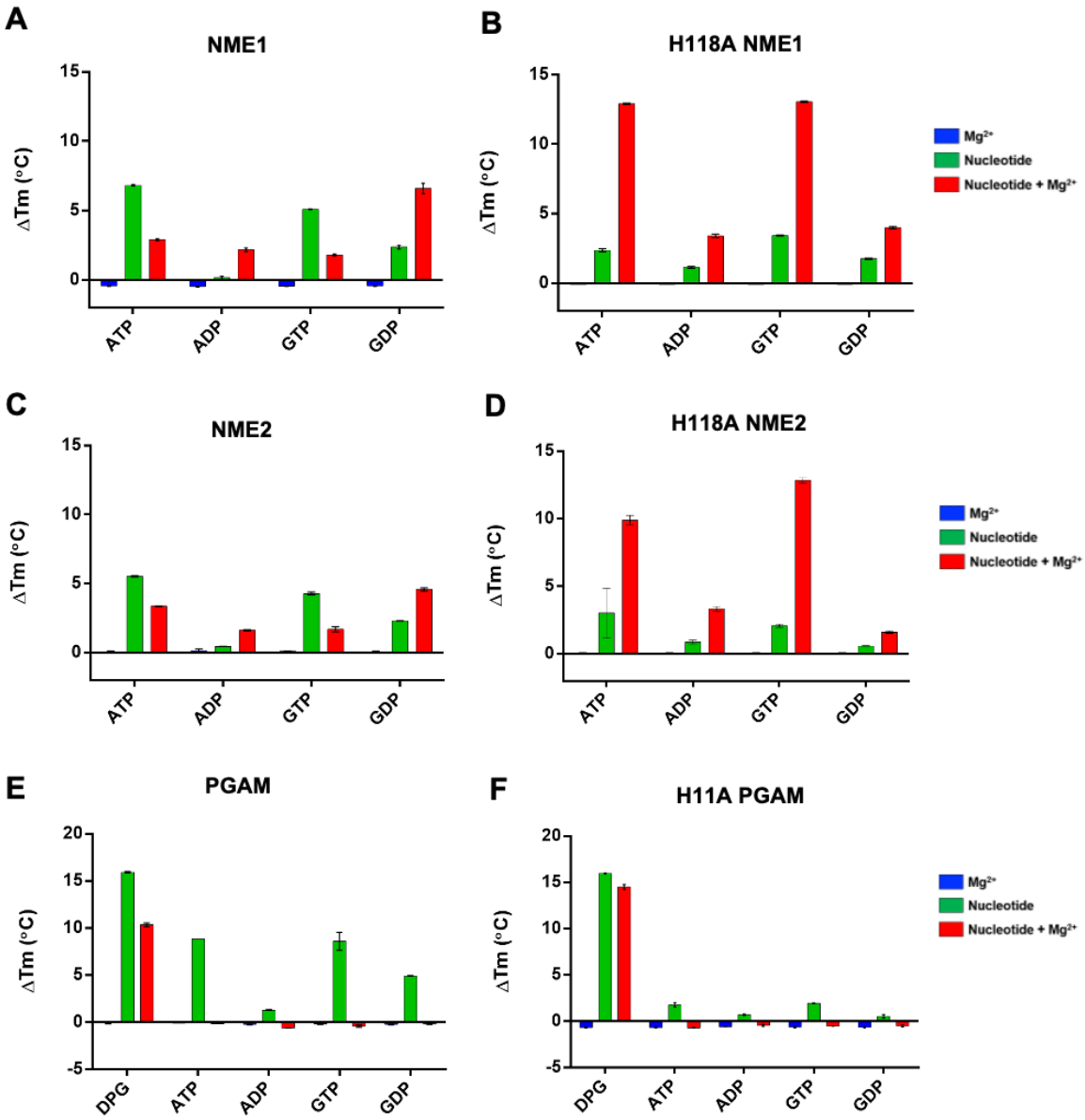

Figure 3.17. Comparative DSF analysis of NME1, NME2 and PGAM histidine active site mutants. The purified recombinant proteins were incubated for 5 minutes in the presence or absence of 1 mM of the indicated nucleotides and/or 10 mM $MgCl_2$ and then subjected to differential scanning fluorimetry (DSF) to analyse the thermal stability of each protein mixture relative to a solvent control. The average (N=2) change in melting temperature (ΔTm) of (5 µM) enzymes (A) NME1, (B) H118A NME1, (C) NME2, (D) H118A NME2, (E) PGAM and (F) H11A PGAM are presented. Thermal unfolding profiles and ΔTm values were calculated as described in Figure 3.5.

Comparative DSF analysis of R105A NME1 and NME2 mutants (Figure 3.18) revealed that magnesium no longer effected the thermostability of the mutants when incubated in the presence of nucleotides, in a similar manner to that established for H118A NME mutants. R105A NME1 displayed a reduced T_m shift compared to WT NME1 when incubated with all nucleotides. For instance, a T_m shift of 6.8 °C was reduced to 1.7 °C for R105A NME1 with ATP, whereas ADP, GTP and GDP failed to induce a T_m shift above 0.5 °C. Unlike WT NME1, for ATP, GTP and GDP the stability of the protein was increased in the presence of Mg^{2+} ions.

Likewise, the T_m shift, and proposed stability of R105A NME2 was greatly increased by the addition of Mg^{2+} ions in the presence of nucleotides. The T_m shift observed for ATP alone was + 2.1 °C, whereas with the addition of $MgCl_2$, this increased to + 11.94 °C. This large increase in T_m in the presence of $MgCl_2$ is repeatedly shown when incubated with the nucleotide ligands, particularly GTP, with a Tm shift of + 11.67 °C. In contrast to WT NME1 and NME2, it is clear that the affinity of the R105A mutants for these nucleotides increased in the presence of $MgCl_2$ as the resultant stability is increased. As the R105A mutants were shown to be dimers (Figure 3.14 and 3.15), the presence of nucleotide and Mg^{2+} ions may induce a higher order oligomer formation which therefore increases the stability of the protein.

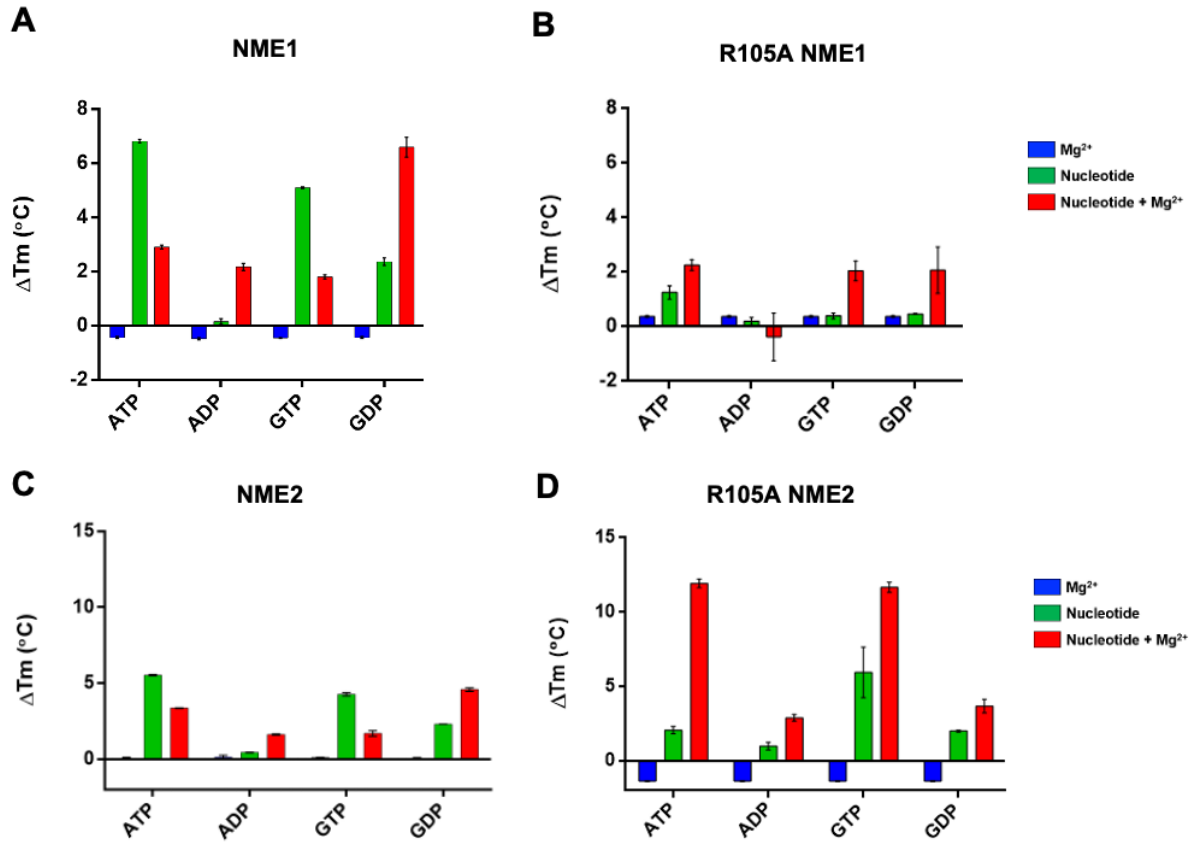

Figure 3.18. Comparative DSF analysis of NME1, NME2 and arginine active site mutants. The purified recombinant proteins were incubated for 5 minutes in the presence or absence of 1 mM of the indicated nucleotides and/or 10 mM $MgCl_2$ and then subjected to differential scanning fluorimetry (DSF) to analyse the thermal stability of each protein mixture relative to a solvent control. The change in melting temperature (ΔTm) of (5 μM) enzymes (A) NME1, (B) R105A NME1, (C) NME2 and (D) R105A NME2 are presented.

To evaluate the His phosphosites on NME1, NME2 and PGAM it was necessary to assess specific histidine point mutants by immunoblot. Purified recombinant proteins were incubated with ATP or DPG and any N1 histidine phosphorylation or N3 histidine phosphorylation was probed by immunoblotting (Figure 3.19). Wild-type (WT) NME1 and H118A NME1 were

incubated with ATP, along with WT PGAM and DPG as a N3 pHis positive control (Figure 3.19A). In the presence of ATP, WT NME1 was detected using the N1 pHis antibody, unlike H118A NME1. Only N3 pHis PGAM in the presence of DPG was observed when probed with the N3 pHis antibody. In Figure 3.19B, WT NME2 and H118A NME2 were processed in the same way as NME1 and only WT NME2 exhibited N1 histidine phosphorylation. To test the enzyme activity of H11A PGAM, the protein was incubated with the phosphate donor DPG and when analysed by immunoblot, it revealed no N3 pHis PGAM. As expected, this demonstrated that the site of N1 phosphorylation is indeed His118 on NME1 and NME2 (382, 383) and His11 on PGAM (384), as when substituted to Ala, autophosphorylation is negated. As the production of the enzyme intermediate is created through autophosphorylation, it is evident that these mutants are enzymatically inactive for phosphate transfer.

To evaluate the His autophosphorylation activity of the additional NME1 and NME2 active site mutants, they were compared side-by-side using by immunoblotting (Figure 3.19D and E). Other than R105A/H118A NME1, all mutants were thermally-shifted by ATP (Figure 3.19). As the cysteine residues are not directly involved in nucleotide binding and enzyme activity (199), it was hypothesized that these mutants would maintain their autophosphorylation activity, and to evaluate this, they were also subjected to immunoblot analysis. N1 pHis was detected at a near similar level as WT NME1 in C109A NME1 and the N1 pHis signal displayed by C109A/C145A NME1 was greater than in WT NME1. As expected, however, His phosphorylation was greatly reduced in R105A NME1. Figure 3.18E also revealed that R105A NME2 had a reduced ability to autophosphorylate compared to that of WT NME2. Not surprisingly, the R105A/H118A NME1 mutant was also unable to autophosphorylate based on N1 pHis antibody signals.

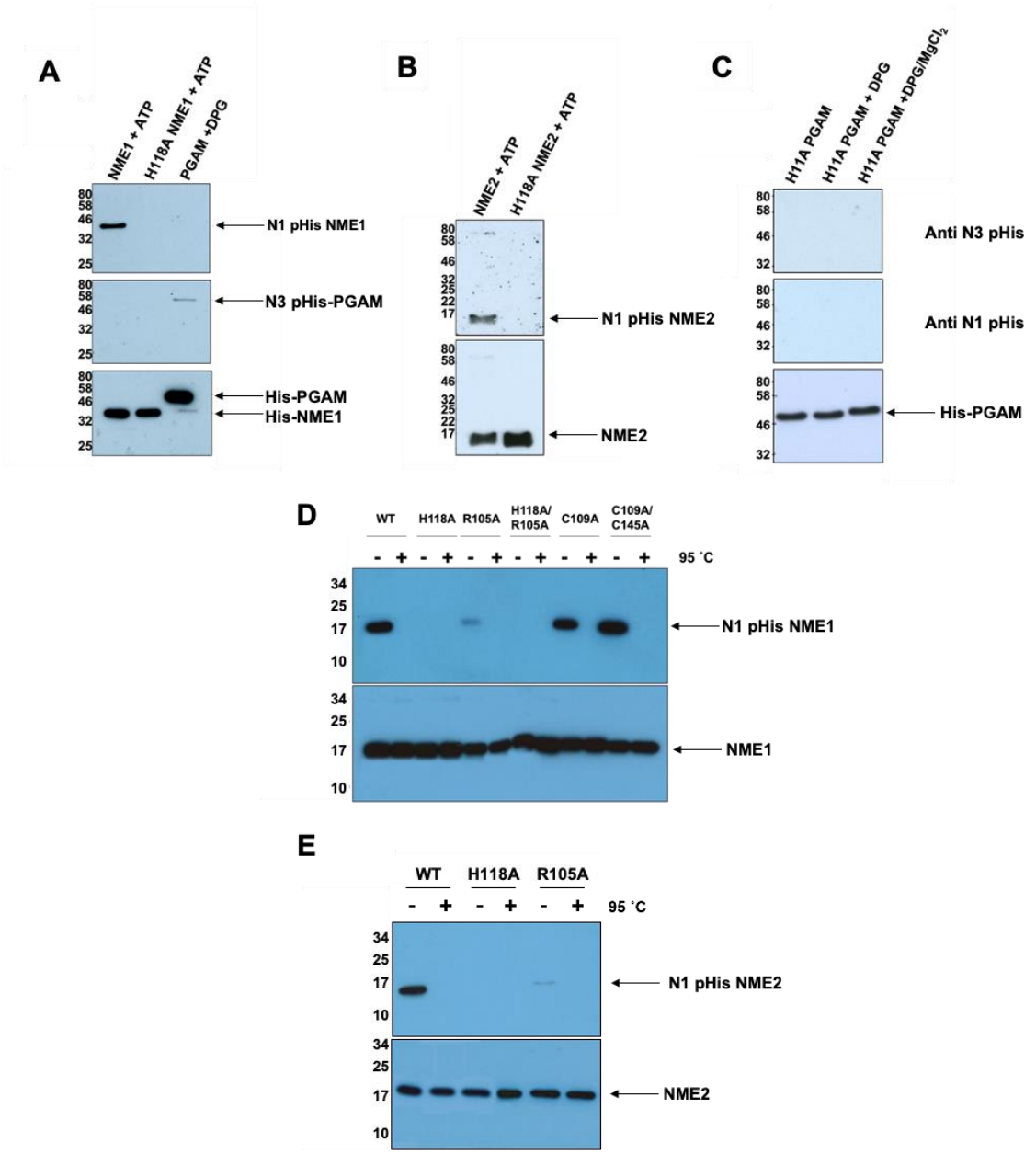

Figure 3.19. Selectivity of histidine phosphorylation for N1 and N3 phosphosites and the analysis of NME mutant proteins His autophosphorylation. The indicated proteins (200 ng) (A) His-GST NME1 and H118A NME1, (B) (non-tagged NME2) and H118A NME2 and (C) His-GST H11A PGAM are shown. All proteins were incubated with 10 µM of the indicated phosphate donor. Enzymes (1 µg) (D) NME1 and active site mutants and (E) NME2 and active site mutants were incubated with 1 mM of the indicated nucleotide in the presence or absence of 10 mM $MgCl_2$ and subjected to western blot analysis using the monoclonal anti-N1pHis antibody to detect phosphorylated histidine. Samples were divided into two aliquots, and one was heated at 95°C for 5 minutes. Unheated samples were processed for immunoblotting with either N1-pHis or N3-pHis antibodies and heated samples were probed using anti-His or anti-NME1 antibody to determine the total protein. A representative immunoblot is shown from N=3.

To further corroborate findings on the enzyme activity of the NME proteins shown in Figure 3.8, intact MS was carried out after incubation with ATP and $MgCl_2$. A mass shift of +80 Da is

consistent with the commonly analysed post-translational modification (PTM), phosphorylation (385). From Figures 3.20 to 3.24, it can be deduced that WT NME1 and C109A NME1 both contain phosphate, since WT NME1 exhibits an +80 Da shift and C109A NME1 exhibits a +79 Da shift in the presence of ATP. In the presence of $MgCl_2$, WT NME1 (Figure 3.20) and C109A NME1 (Figure 3.24) are only partially phosphorylated, indicated by observing two fragments, one corresponding to the mass of the proteins in the absence of any phosphate and another containing a phosphate group. This supports the hypothesis that Mg^{2+} ions are inhibitory to NME autophosphorylation. In the case of the NME1 mutants, H118A NME1 and R105A/H118A NME1, no such mass shift was detected, confirming their lack of, or markedly-reduced catalytic activity.

Furthermore, analysis of the NME2 proteins corresponded to the results observed for the NME1 (Figures 3.25 to 3.27), as WT NME2 (Figure 3.25) displayed a +81 Da mass shift in the presence of ATP and an +80 Da shift in the presence of ATP and $MgCl_2$, suggesting the addition of a phosphate group to the protein. An additional species of NME2, with a mass shift of 21 Da, was revealed in the presence of ATP and $MgCl_2$. A 21 Da shift indicates the presence of sodium adducts in the sample, which are generally obtained in sample preparation, for example from glassware. Consistent with previous findings (Figure 3.7), NME2 appeared to possess a lower level of autophosphorylation compared to NME1, as in both conditions, NME2 underwent partial phosphorylation. In contrast, H118A NME2 (Figure 3.26) displayed no mass shift on the addition of either ATP or $MgCl_2$.

Intriguingly, intact MS analysis of the R105A NME1 and R105A NME2 proteins revealed that in the presence of ATP, no mass shift was observed. However, in the presence of ATP and $MgCl_2$, ~10% of a species containing phosphate was detected for R105A NME1. When R105A NME2 was analysed, a peak attributable to ~50% of a phosphorylated NME2 species was also detected. Although this phosphosite cannot be determined by intact MS, this analysis suggests strongly that the R105A mutant proteins possess partial enzyme activity.

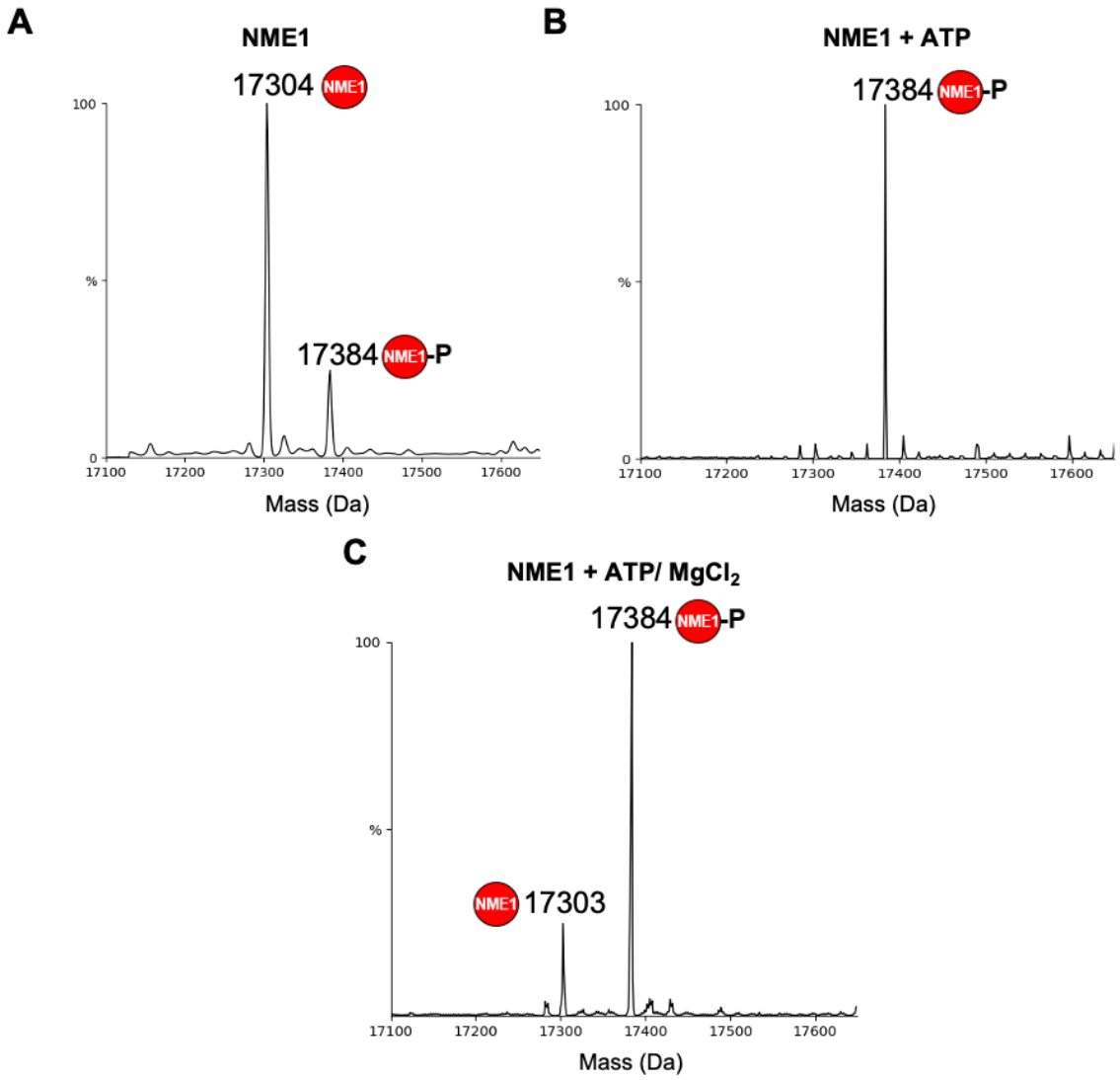

Figure 3.20. Intact mass spectrum of NME1 in (A) the absence or (B) the presence of ATP and (C) ATP/ $MgCl_2$. 1 µg of purified recombinant NME1 was incubated with or without 1 mM nucleotide in 50 mM Tric-HCl, pH 8.0, 100 mM NaCl for 5 minutes at room temperature. Samples were analysed by LC-MS using a Waters Synapt G2Si. Data were processed using MassLynx (4.1) and deconvoluted using MaxEnt1. Deconvolution settings were as follows: 0.5 Da/channel resolution; Uniform Gaussian distribution with a width at half height of 0.500 Da. The phosphorylated and non-phosphorylated NME proteins are indicated by black circles coloured red (NME1) or blue (NME2). Representative spectra are shown from N=3.

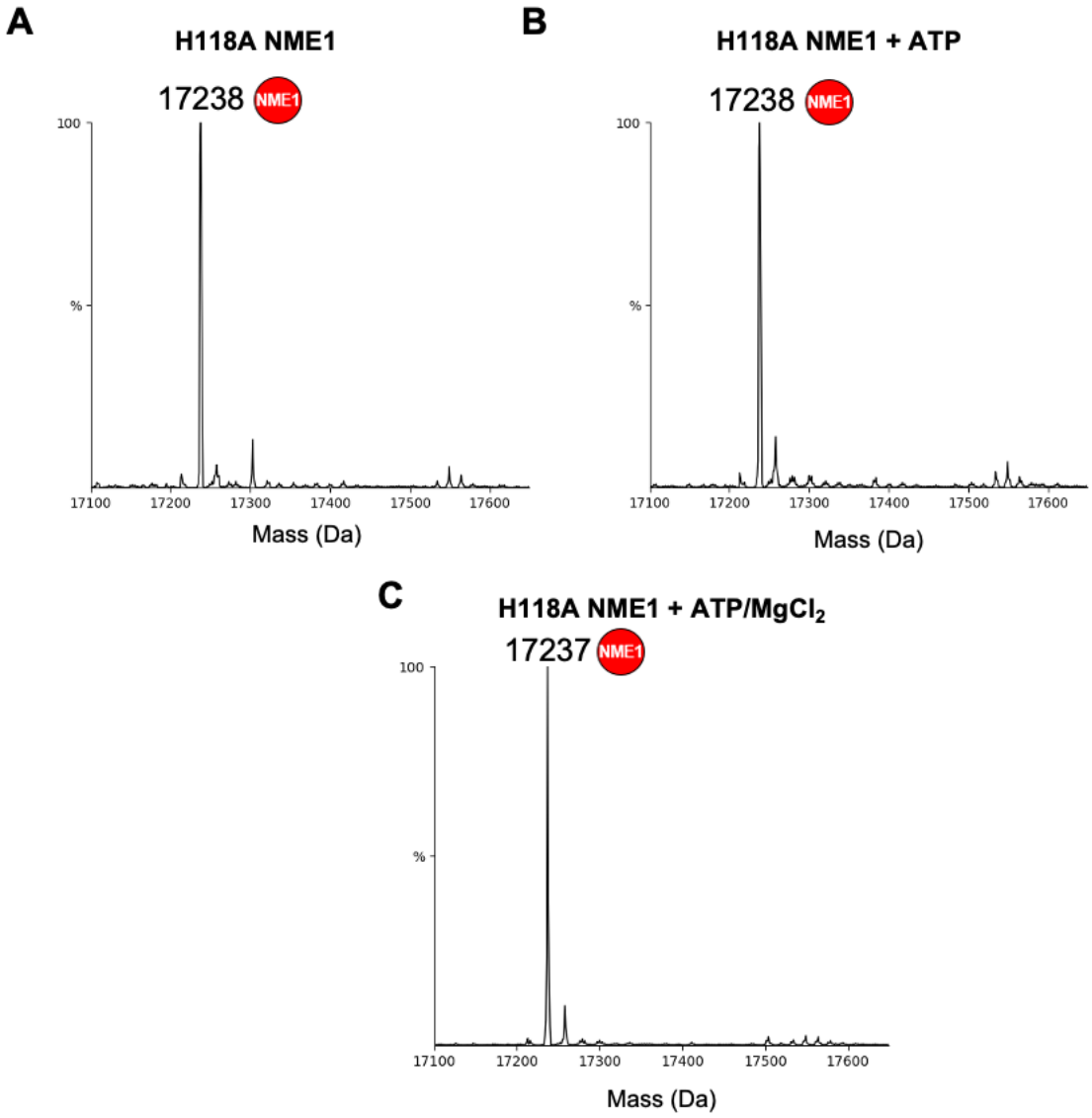

Figure 3.21. Intact mass spectrum of H118A NME1 in (A) the absence or (B) the presence of ATP and (C) ATP/ $MgCl_2$. 1 µg of purified recombinant NME1 was incubated with or without 1 mM nucleotide in 50 mM Tric-HCl, pH 8.0, 100 mM NaCl for 5 minutes at room temperature. Samples were analysed by LC-MS using a Waters Synapt G2Si. Data were processed using MassLynx (4.1) and deconvoluted using MaxEnt1. Deconvolution settings were as follows: 0.5 Da/channel resolution; Uniform Gaussian distribution with a width at half height of 0.500 Da. The phosphorylated and non-phosphorylated NME proteins are indicated by black circles coloured red (NME1) or blue (NME2). Representative spectra are shown from N=3.

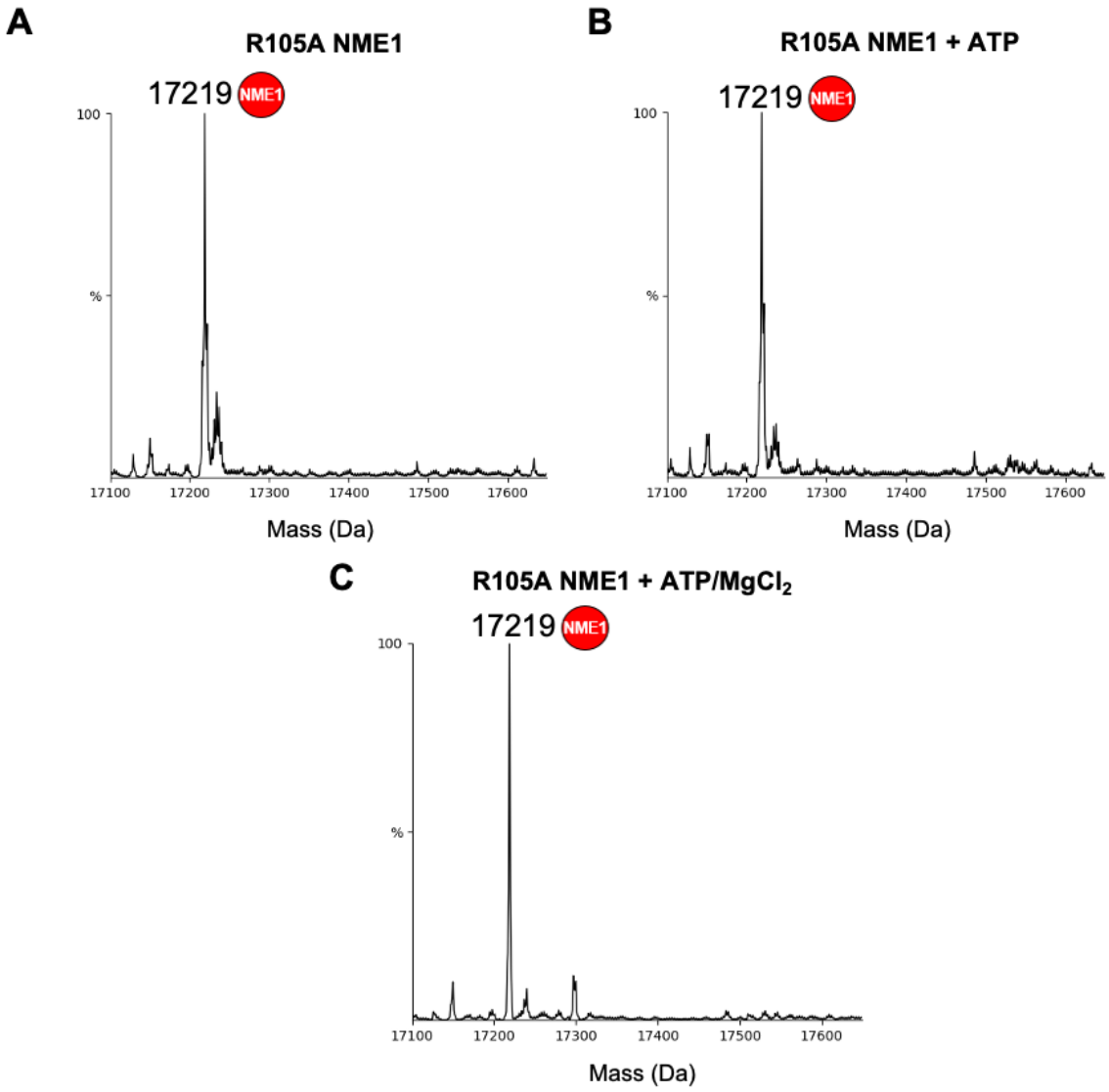

Figure 3.22. Intact mass spectrum of R105A NME1 in (A) the absence or (B) the presence of ATP and (C) ATP/ $MgCl_2$. 1 µg of purified recombinant NME1 was incubated with or without 1 mM nucleotide in 50 mM Tric-HCl, pH 8.0, 100 mM NaCl for 5 minutes at room temperature. Samples were analysed by LC-MS using a Waters Synapt G2Si. Data were processed using MassLynx (4.1) and deconvoluted using MaxEnt1. Deconvolution settings were as follows: 0.5 Da/channel resolution; Uniform Gaussian distribution with a width at half height of 0.500 Da. The phosphorylated and non-phosphorylated NME proteins are indicated by black circles coloured red (NME1) or blue (NME2). Representative spectra are shown from N=3.

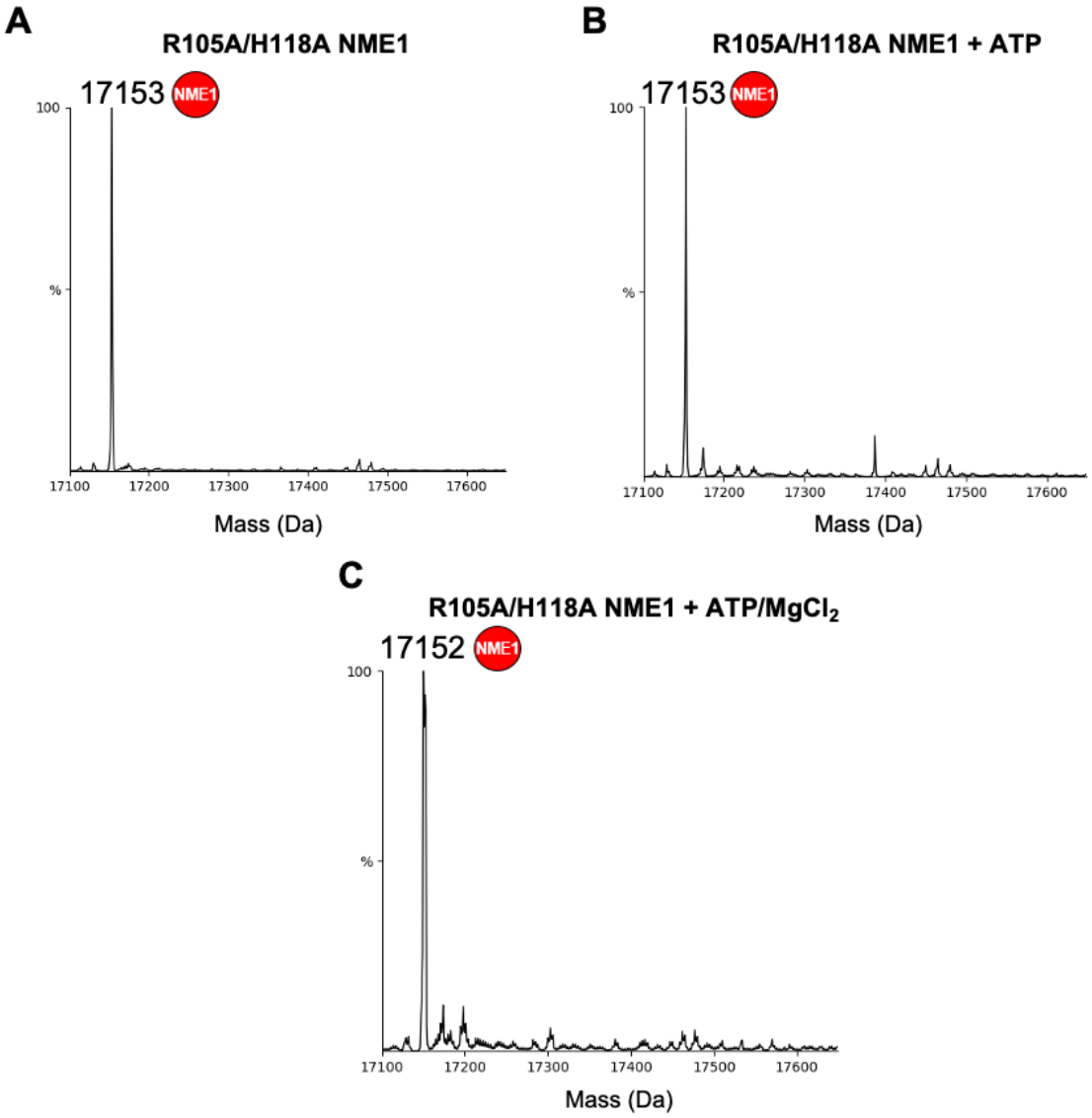

Figure 3.23. Intact mass spectrum of R105A/H118A NME1 in (A) the absence or (B) the presence of ATP and (C) ATP/ $MgCl_2$. 1 µg of purified recombinant NME1 was incubated with or without 1 mM nucleotide in 50 mM Tric-HCl, pH 8.0, 100 mM NaCl for 5 minutes at room temperature. Samples were analysed by LC-MS using a Waters Synapt G2Si. Data were processed using MassLynx (4.1) and deconvoluted using MaxEnt1. Deconvolution settings were as follows: 0.5 Da/channel resolution; Uniform Gaussian distribution with a width at half height of 0.500 Da. The phosphorylated and non-phosphorylated NME proteins are indicated by black circles coloured red (NME1) or blue (NME2). Representative spectra are shown from N=3.

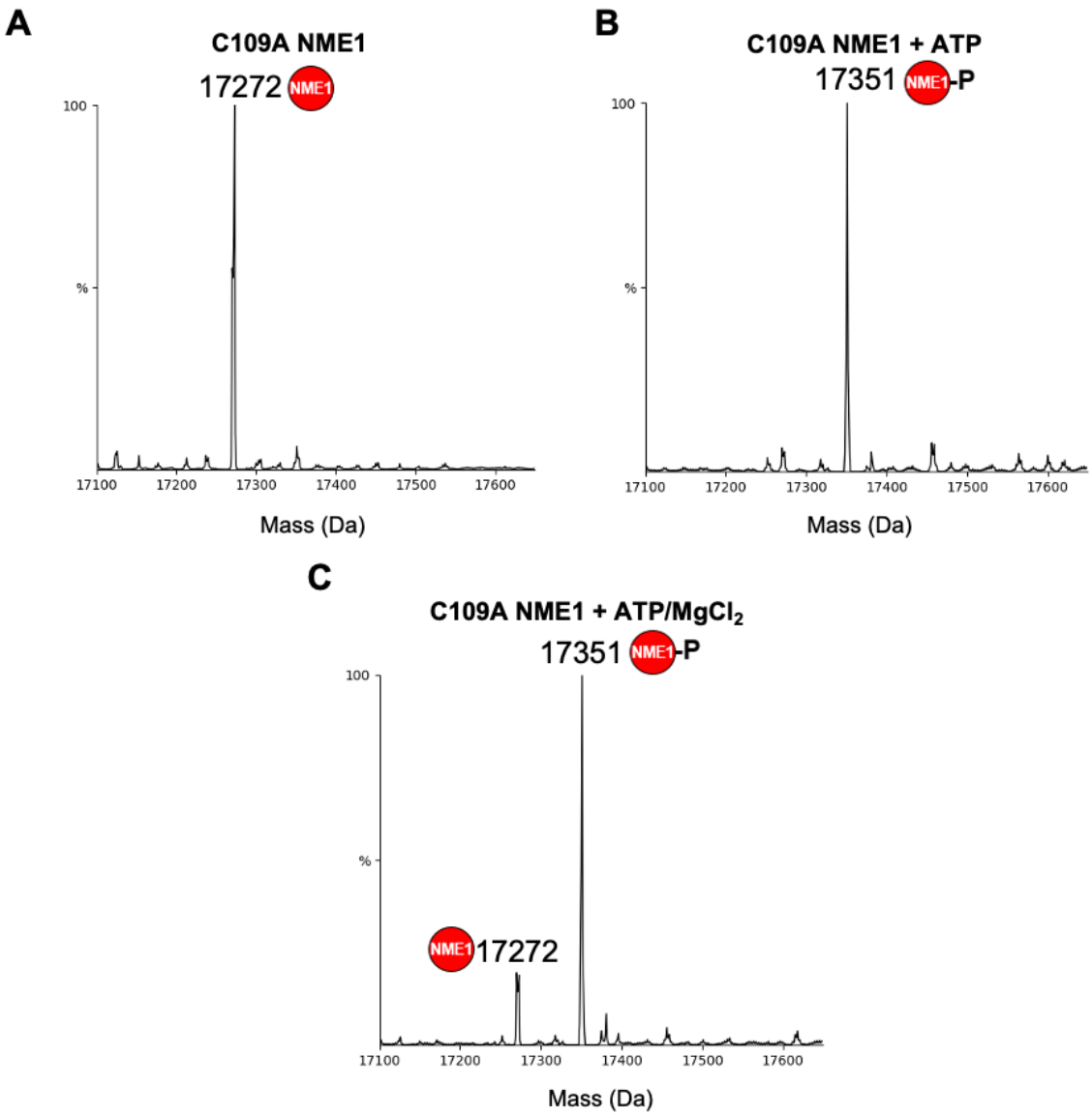

Figure 3.24. Intact mass spectrum of C109A NME1 in (A) the absence or (B) the presence of ATP and (C) ATP/ $MgCl_2$. 1 µg of purified recombinant NME1 was incubated with or without 1 mM nucleotide in 50 mM Tric-HCl, pH 8.0, 100 mM NaCl for 5 minutes at room temperature. Samples were analysed by LC-MS using a Waters Synapt G2Si. Data were processed using MassLynx (4.1) and deconvoluted using MaxEnt1. Deconvolution settings were as follows: 0.5 Da/channel resolution; Uniform Gaussian distribution with a width at half height of 0.500 Da. The phosphorylated and non-phosphorylated NME proteins are indicated by black circles coloured red (NME1) or blue (NME2). Representative spectra are shown from N=3.

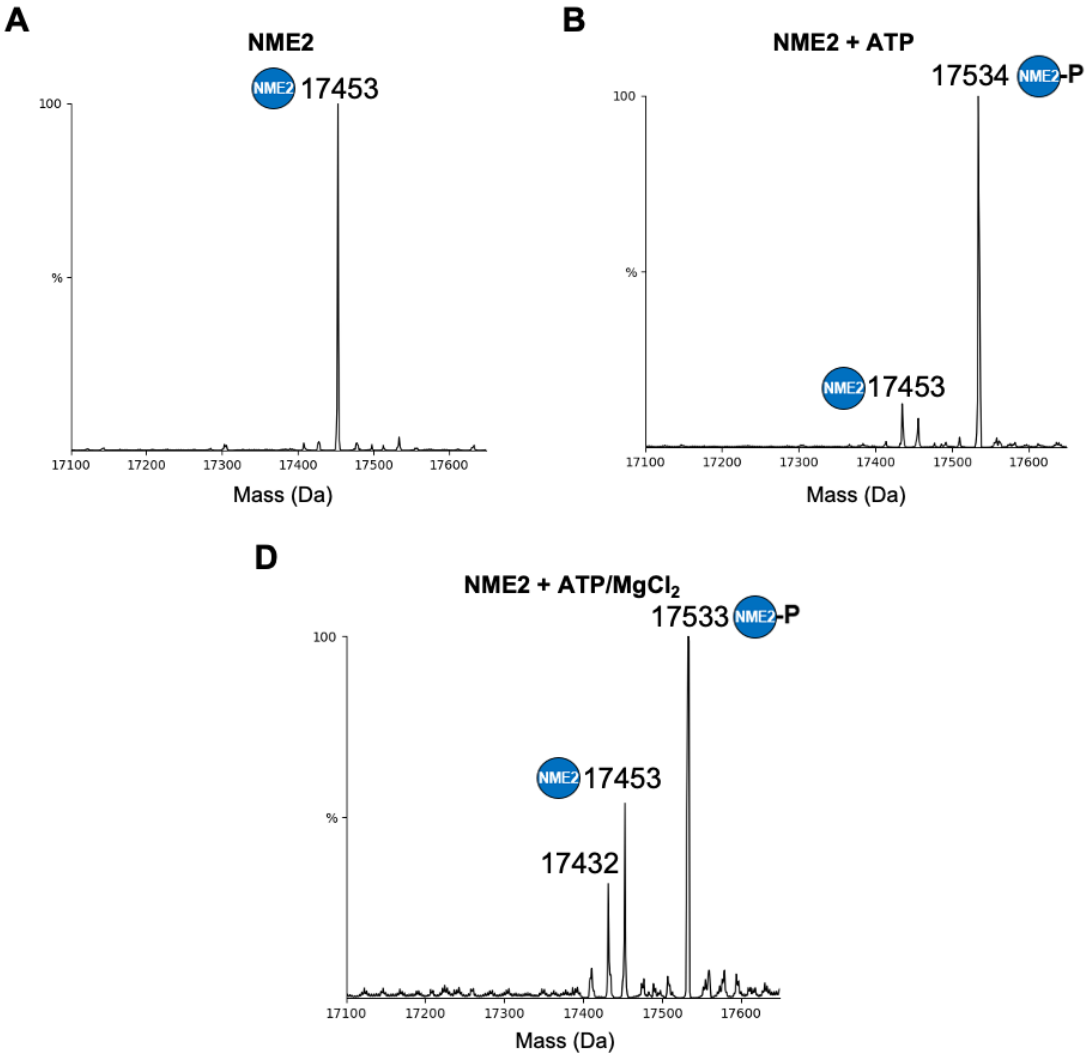

Figure 3.25. Intact mass spectrum of NME2 in (A) the absence or (B) the presence of ATP and (C) ATP/ $MgCl_2$. 1 µg of purified recombinant NME2 was incubated with or without 1 mM nucleotide in 50 mM Tric-HCl, pH 8.0, 100 mM NaCl for 5 minutes at room temperature. Samples were analysed by LC-MS using a Waters Synapt G2Si. Data were processed using MassLynx (4.1) and deconvoluted using MaxEnt1. Deconvolution settings were as follows: 0.5 Da/channel resolution; Uniform Gaussian distribution with a width at half height of 0.500 Da. The phosphorylated and non-phosphorylated NME proteins are indicated by black circles coloured red (NME1) or blue (NME2). Representative spectra are shown from N=3.

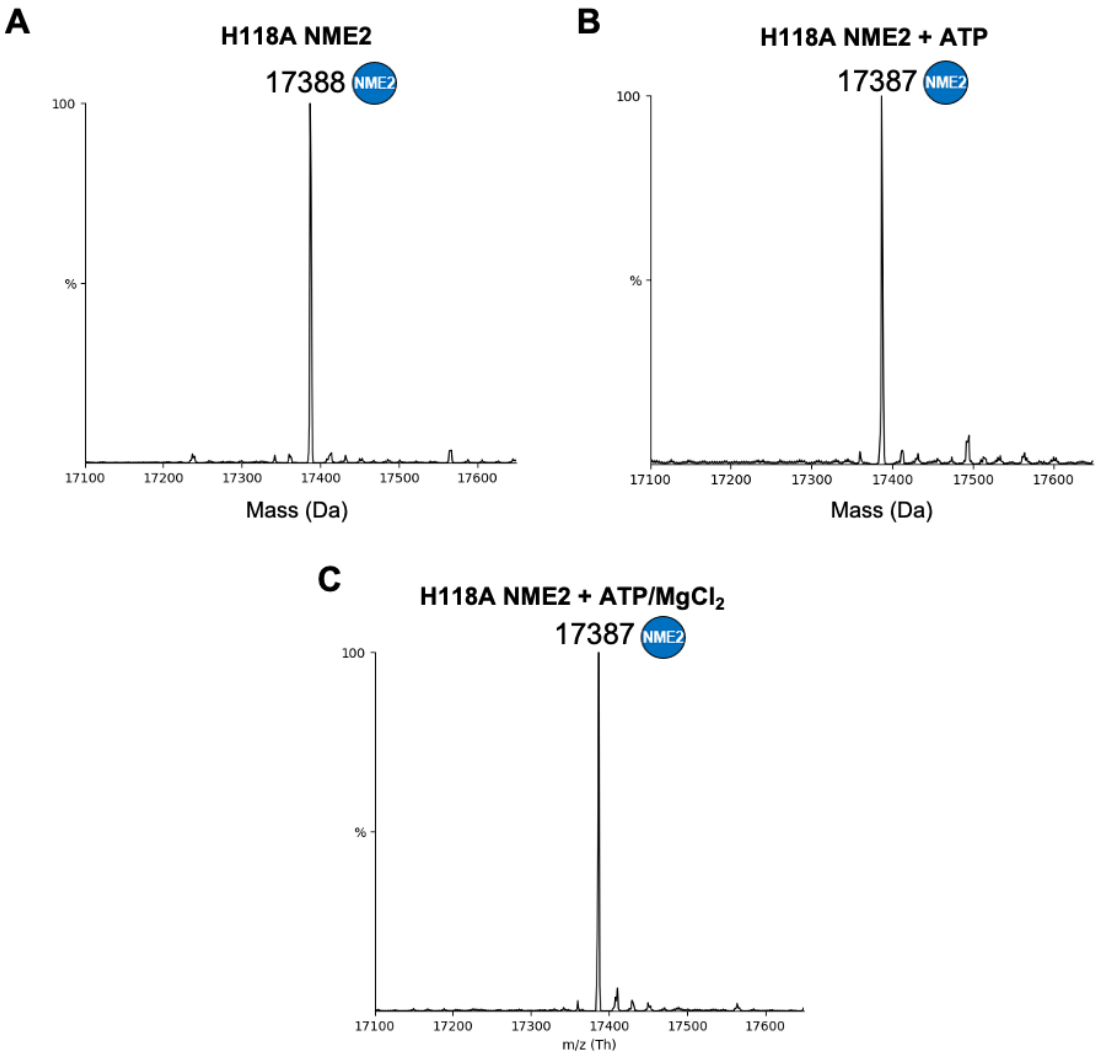

Figure 3.26. Intact mass spectrum of H118A NME2 in (A) the absence or (B) the presence of ATP and (C) ATP/ $MgCl_2$. 1 µg of purified recombinant NME2 was incubated with or without 1 mM nucleotide in 50 mM Tric-HCl, pH 8.0, 100 mM NaCl for 5 minutes at room temperature. Samples were analysed by LC-MS using a Waters Synapt G2Si. Data were processed using MassLynx (4.1) and deconvoluted using MaxEnt1. Deconvolution settings were as follows: 0.5 Da/channel resolution; Uniform Gaussian distribution with a width at half height of 0.500 Da. The phosphorylated and non-phosphorylated NME proteins are indicated by black circles coloured red (NME1) or blue (NME2). Representative spectra are shown from N=3.

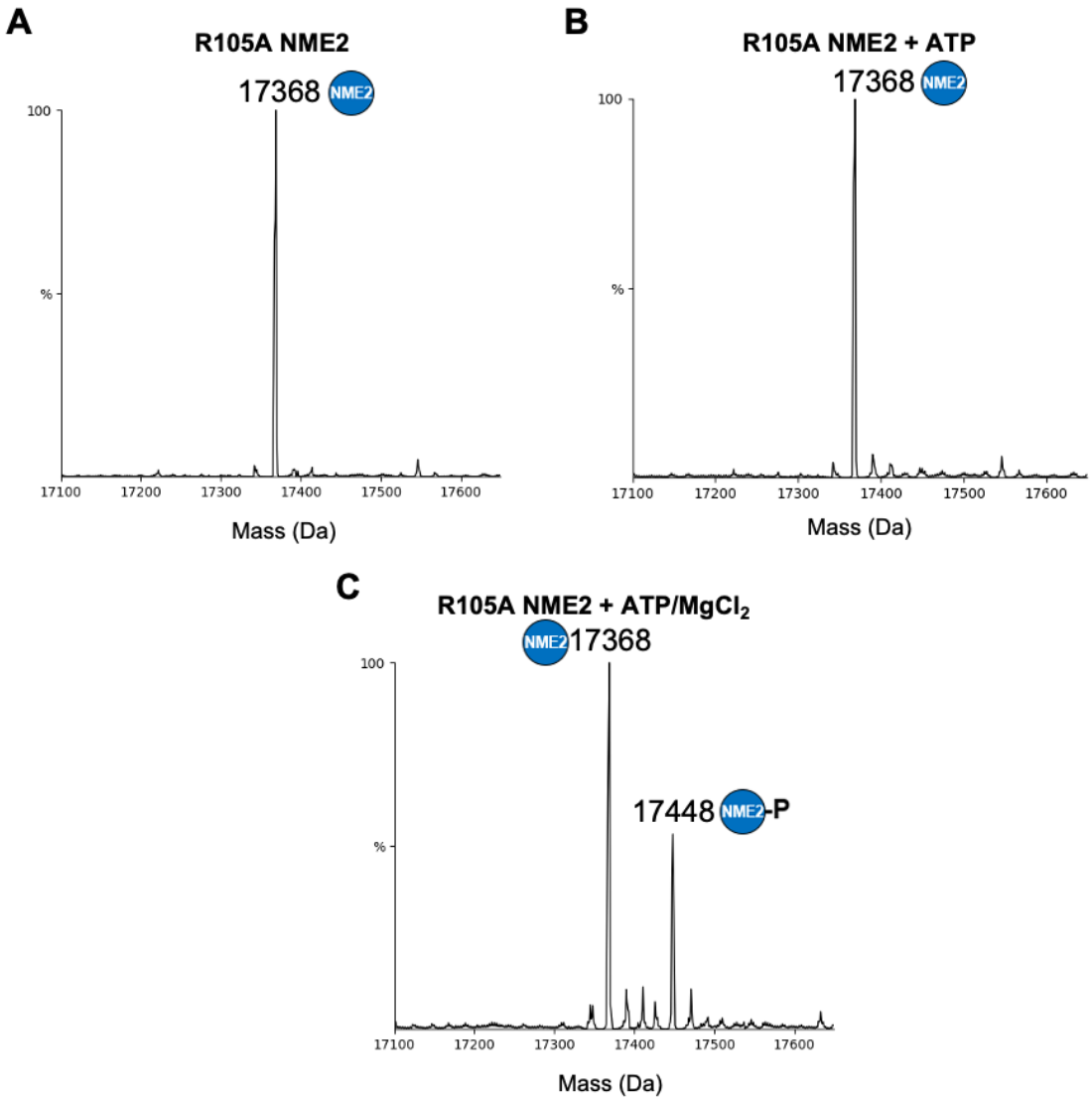

Figure 3.27. Intact mass spectrum of R105A NME2 in (A) the absence or (B) the presence of ATP and (C) ATP/ $MgCl_2$. 1 µg of purified recombinant NME2 was incubated with or without 1 mM nucleotide in 50 mM Tric-HCl, pH 8.0, 100 mM NaCl for 5 minutes at room temperature. Samples were analysed by LC-MS using a Waters Synapt G2Si. Data were processed using MassLynx (4.1) and deconvoluted using MaxEnt1. Deconvolution settings were as follows: 0.5 Da/channel resolution; Uniform Gaussian distribution with a width at half height of 0.500 Da. The phosphorylated and non-phosphorylated NME proteins are indicated by black circles coloured red (NME1) or blue (NME2). Representative spectra are shown from N=3.

3.7 Development of an enzyme assay in order to measure the nucleoside diphosphate activity of NME

NME proteins catalyse the transfer of a phosphate group from one nucleotide to another, using a ping-pong mechanistic reaction and a pHis intermediate (352). In contrast to protein kinases, which readily phosphorylate other proteins, the substrate for NME proteins is not generally thought to be a separate protein that elicits downstream effects, potentially making the reaction somewhat bidirectional depending upon nucleotide concentrations. (5). This potentially makes measuring the absolute catalytic activity of NME proteins challenging, as both the triphosphate nucleotides or diphosphate nucleotides and the NME enzyme itself are substrates. A reliable way to measure the NDPK activity of the purified recombinant proteins would be useful for further characterisation and analysis of NME proteins as well as for studies aimed at exploring inhibitory effects of small molecules and compounds on histidine kinase, and therefore NDPK activity.

3.7.1 Immunoblot analysis

As previously shown (Section 3.5), NME1 and NME2 are enzymatically active, in that each kinase autophosphorylates on His118. However, using the techniques described above, the protein's ability to transfer a phosphate from His118 in the active site to a nucleoside diphosphate cannot be readily demonstrated. In light of the recent development of monoclonal antibodies against phosphohistidine (pHis), which are specific for the N1 and N3 position (9), I employed these antibodies to determine if NME1 and NME2 possess NDPK activity. However, in order to only measure the forward reaction (Figure 1.10) of phosphate transfer to the nucleoside diphosphate (NDP), pre-phosphorylated (pNME) was generated and repurified, (Section 2.14) so that excess nucleoside triphosphate (NTP) was removed to help mitigate the 'reverse' reaction.

To assess the NDPK activity of NME1, pNME1 was generated, purified, and then incubated with increasing concentrations of ADP prior to immunoblot analysis with N1pHis antibodies (Figure 3.28). When immunoblotted with anti-N1 pHis, in the absence of any ADP, the signal displayed by N1 pHis NME1 was strong. However, as little as 20 µM ADP reduced the pNME1 signal and as the concentration of ADP increased, the level of pNME1 reduced, indicative of the NDPK reaction. At 625 µM ADP, and up to 5 mM ADP, pNME1 was no longer observed. Through this analysis, it was discovered that pNME1, at a concentration of 5.8 mM transferred most of the His118 bound-phosphate to ADP, despite the concentration of ADP being nearly 10-fold lower than NME1, at 625 µM. This verified that NME1 had a high level of NDPK activity and a high affinity for the ADP substrate.

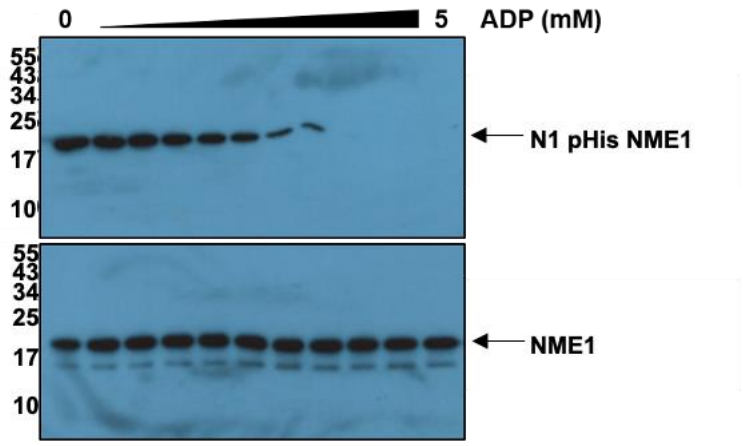

Figure 3.28. Transfer of phosphate from phosphorylated NME1 to ADP. Purified recombinant NME1 was incubated with 2 mM ATP to obtain pHis NME1. Excess ATP and ADP was removed by diluting pNME1 in Tris buffer and centrifugation. 1 µg of pHis NME1 (Section 2.14) was then incubated with increasing ADP at 2-fold increments and subjected to immunoblotting with N1-phosphohistidine antibody. Half the sample was heat treated and immunoblotted with the anti-NME1 antibody to determine total protein.

3.7.2 Can an ADP-Glo assay be used to assay NDPK activity?

The ADP-Glo assay exploits the enzyme luciferase, which employs ATP to create luminescence; the amount of light produced in the assay is therefore an indirect measurement of the kinase reaction products (Figure 3.29A). To explore this assay further in the context of kinases, reactions were set up that mimicked the conversion of ATP to ADP in a standard protein kinase assay, which transfers a phosphate group from ATP to a protein substrate, generating ADP (Figure 3.29C). The more ADP produced in the assay as a result of a high rate of enzyme activity, the greater the amount converted back to ATP (by an ADP-Glo assay reagent) for the luciferase reaction. Since ATP is a luciferase substrate, the greater the relative luminescence units (RLUs) detected and quantified. Due to the lack of a standard NME protein substrate, ADP and GTP were utilised in order to measure NDPK activity. The reaction produces ATP and GDP, and therefore the rate of the reaction would be measured by a reduction in RLUs as opposed to an increase in RLUs, as the ATP product is depleted in step 2 of the assay (Figure 3.29B). However, as Figure 3.29D shows, little to no change in luminescence was displayed, or the assay could not detect any change. This is likely due to the signal to noise ratio being high, because the levels of measured ADP are at such low concentrations.

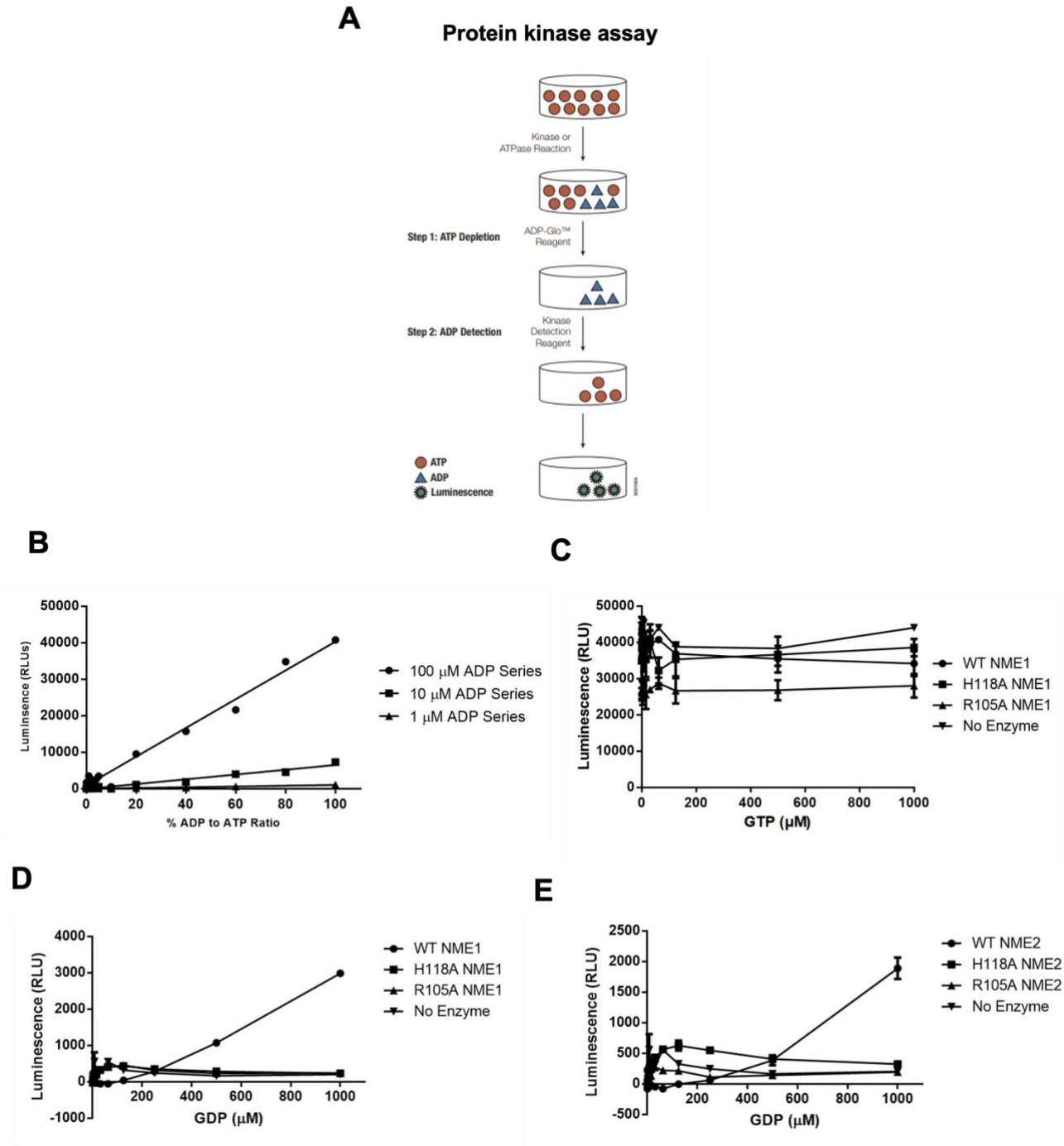

Figure 3.29. Development of a NDPK activity assay adapted from the ADP-Glo assay (Promega) to measure the nucleoside diphosphate kinase activity of purified recombinant NME proteins. (A) Schematic of the mechanism of ADP-Glo assay as instructed by Promega, used accordingly in panel B. (B) Luminescence at increasing ratios of ADP to ATP at different ADP concentrations was measured to test the efficacy of the assay as followed by the manufacturers instructions shown in (A). (C) 100 nM of NME1 was incubated with an increasing concentration of GTP and the assay was carried out as followed by the manufacturers instructions shown in (A). (D) NME1 and (E) NME2 were assayed as followed by (B) with an increasing concentration of GDP. Panels C, D and E were carried out using the ADP-Glo assay system adapted to the NDPK reaction as shown in Figure 2.4. Representative assays are shown from N=3.

To combat this, and to better mimic a protein kinase assay and elicit a detectable increase in RLU instead of a decrease, GDP and ATP were used in order to generate ADP as a product of the NDPK reaction (Figure 3.29E and F). WT NME1 and NME2, along with H118A and R105A mutants were incubated with increasing concentrations of GDP and a static ATP concentration. A dose dependent response was elicited for WT NME1 and NME2 as increasing GDP concentrations resulted in increased luminescence. Although it is clear that a level of NDPK activity was measured using this technique, the background noise of this assay when NME was introduced is greatly increased. Furthermore, Figure 3.29C shows that when 100 µM of ADP was produced, luminescence values reached ~ 40,000 RLUs, whereas if 100% of ATP was converted to ADP from GDP in assays (Figure 3.29E and D), the level of luminescence would be expected to be above that seen in Figure 3.29C, however at 100 µM GDP, the RLU was around zero. Therefore, a more appropriate sensitive method to measure NDPK activity of the purified recombinant NME proteins was designed, as described below.

3.7.3 The pyruvate kinase-lactate dehydrogenase coupled assay

The pyruvate kinase-lactate dehydrogenase (PK-LDH) coupled assay detects changes in enzyme activity based upon changes in absorbance of NADH at 340 nm. Here, NDPK activity is measured through phosphate transfer from ATP to any nucleoside diphosphate that pyruvate kinase does not utilise. The ADP product is then fed into a coupled assay system exploiting the enzymes pyruvate kinase (PK) and lactate dehydrogenase (LDH) described in Figure 3.30A. The final product of the assay system is NAD^+, which does not absorb at 340 nm. Thus, a change in enzyme activity in the PK-LDH assay is demonstrated by a reduction in the absorbance at $OD_{340nm.}$

To confirm that PK and LDH in the secondary reaction mechanism of the coupled assay were active, the OD_{340nm} was also measured at different ADP concentrations in the absence of NME (Figure 3.30B). As the ADP concentration increased, the rate at which the OD_{340nm} reduced over time also increased. This data was plotted, and the linear portion of the graph in Figure 3.30B is also presented as a bar chart in Figure 3.30C. From this, a 25-fold increase in the rate of reaction was observed when increasing the concentration of ADP from 0.1 mM to 1 mM, which verified that the secondary coupled assay was functioning.

To determine whether this assay could be used to measure NDPK activity of NME1, the assay was repeated in the presence of NME1. In this case, the substrates for NME1 were thymidine diphosphate (TDP) and adenosine triphosphate (ATP). The NDPK reaction with the aforementioned substrates catalysed by NME1 would therefore produce ADP to be fed into the PK reaction (Figure 3.30A). To try to obtain optimal reaction conditions, different

concentrations of ATP and TDP were tested (Figure 3.30D, E and F) and Figure 3.30G summarises the data. Compared to the negative control (no enzyme, grey), a reduction in the absorbance at 340nm over time was demonstrated in all enzyme assays. Figure 3.30G shows that with increasing concentrations of TDP and ATP, the rate of the reaction increased. At 0.1 mM TDP, regardless of the ATP concentration, the reaction rate was limited. At a concentration of 0.3 mM TDP and 0.3 mM ATP, a clear increase in reaction rate was seen, demonstrating that experiments carried out at these concentrations for the two substrates is sufficient to measure the NDPK activity of the purified recombinant NME proteins and is a suitable method to explore the different conditions under which enzyme activity might be affected.

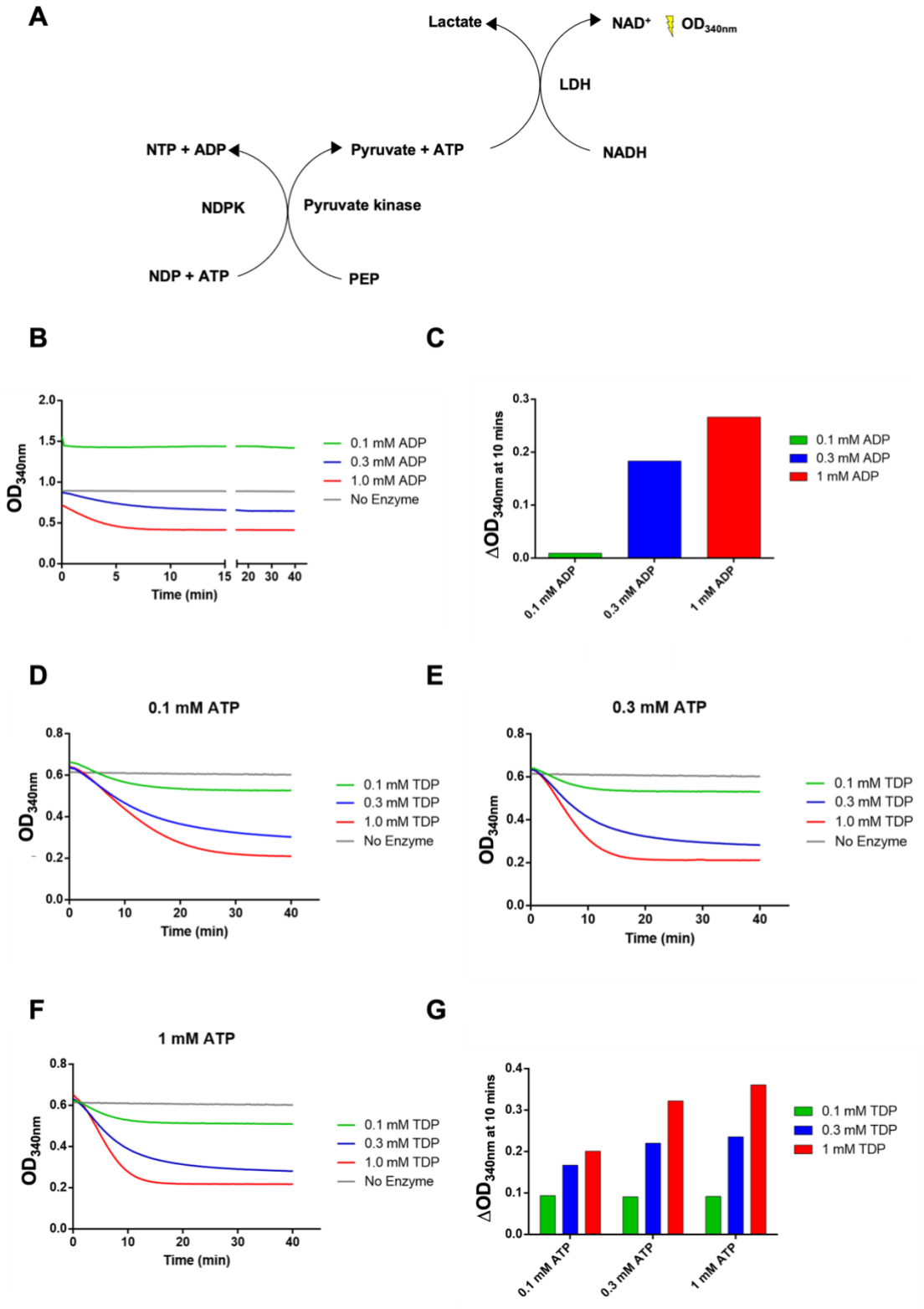

Figure 3.30. Evaluating a pyruvate kinase/lactate dehydrogenase coupled assay to quantify nucleoside diphosphate kinase activity (NDPK) of purified recombinant NME proteins. (A) Reaction mechanism of the NDPK and pyruvate kinase/lactate dehydrogenase coupled assay, which also quantifies ADP levels, but results in a read out at 340nm. (B) PK/LDH assay in the absence of NME1 at the indicated substrate ADP concentrations (C) the rate of the combined PK/LDH reaction calculated from (B). The PK/LDH assay in the presence of 25 nM NME1 at indicated substrate TDP concentrations in the presence of (D) 0.1 mM ATP, (E) 0.3 mM ATP and (F) 1 mM ATP and (G) displays the rates of reactions in (D), (E) and (F).

3.8 Discussion

3.8.1 Biochemical characterisation of recombinant NME proteins and PGAM

NME1, NME2 and PGAM have recently been at the forefront of research attempting to understand regulatory protein histidine phosphorylation (8, 9). Several studies have shown that each of these proteins contains a single His autophosphorylation site (His118 for NME and His11 for PGAM) and that His autophosphorylation activity is abolished when the His is mutated to an Ala (13, 132). However, for NME1/2, mutation of His does not appear to result in the loss of function for all roles in the cell. For example, NDPK activity is not required for either DNA binding nor cleavage, several transcriptional roles and in some reported cases suppression of metastasis (386, 387). The functions of NME1 and NME2 proteins are likely to require productive protein:protein interactions. Due to this, and the variety of functions NME1 and NME2 perform, including metastasis suppression (14), the evaluation of NME1 nucleotide ligands and nucleotide analogues has been reported (388). The aim of the studies described in this chapter was to carefully characterize recombinant human NME1, NME2 and PGAM, and to analyse nucleotide analogue interactions using thermal shift-based DSF, an established technique to study nucleotide and drug binding to protein kinases. In addition, a series of NME mutations were generated in order to further explore their significance in maintaining nucleotide-binding protein multimerisation and enzyme activity. To this end, recombinant full-length human tandem His-GST tagged NME1, NME2 and PGAM were expressed in *E. coli* and purified by IMAC and SEC. The His-GST tag used to purify the proteins was removed by proteolytic cleavage to reduce the risk of GST interfering in experimental procedures and to generate homogenous protein. Purified proteins were carefully analysed by exploiting a combination of SDS-PAGE, intact and native mass spectrometry (MS) and immunoblotting.

The thermal stability of each purified protein was assessed using DSF, which demonstrated that the proteins were likely to be folded, based on their possession of a characteristic unfolding profile as the temperature increased, with a clear midpoint transition. An unfolded protein is unlikely to display a large change in fluorescence upon heating, since more hydrophobic regions are already likely to be exposed to the surface (371). As discussed in previous studies from our group (368, 369, 371), this confirmed that the NME proteins bound to, and were stabilised by, ATP in a dose-dependent manner. In addition, PGAM was stabilised by DPG, as well as ATP (Figure 3.5), although NME1/2 did not appear to bind DPG. Adenosine diphosphate (ADP) and guanosine di- and triphosphates (GDP and GTP) were also tested, and NME1 and NME2 were stabilised by these nucleotides, with a similar profile to that of ATP. As expected, PGAM showed the biggest thermal stabilisation in the presence

of DPG, and similarly to NME1 and NME2, this was reduced in the presence of Mg^{2+} ions, in contrast to the known effects of Mg^{2+} ions on protein kinases, which promote nucleotide/co-factor (but not small molecule) binding. Furthermore, PGAM also bound to ATP, GTP and GDP and in the presence of ADP a small thermal shift was shown, which has not been previously studied in detail. The presence of magnesium for these nucleotides yielded no change in thermal stabilisation of PGAM in the presence of nucleotides. Whereas in the presence of Mg^{2+} ions, binding to the diphosphate nucleotides, ADP and GDP, was increased, as shown in Figure 3.5. One or two magnesium ions are favoured by the majority of kinases for supporting ATP binding and productive protein phosphorylation (389-391). However, in contrast to canonical kinases such as cAMP dependent kinase (PKA), binding to the triphosphate nucleotides was clearly reduced in the presence of Mg^{2+} ions in both NME1, NME2 and PGAM. Due to its aromatic imidazole ring, histidine can take part in cation interactions (392-394) and the protonated His form is likely capable of stabilizing metal cations alongside aromatic amino acids such as Phe, Tyr or Trp (395-398). This is a well-known phenomenon in the conserved HxD motif in the catalytic loop of protein kinases, as interactions between the HxD-His and DFG-Phe help position the catalytic loop and magnesium binding loop (399). Therefore, the inhibitory effects of magnesium may be a result of His118 cationic interactions in NME1/2, potentially leading to displacement of ATP. On the other hand, the conformation of the protein and the nucleotide binding pocket in the absence of Mg^{2+} ions may be more favourable for nucleoside triphosphate (NTP) binding, since a more favourable NDPK domain environment for nucleoside diphosphate (NDP) is seen in the presence of Mg^{2+} ions, demonstrated by higher thermal shifts.

Crystal structures have been solved for human NME1 in complex with ADP (400) and human NME2 in complex with GDP (345), but not ATP, and these complexes highlight that although Mg^{2+} ions are found in crystallographic the active site, only weak density peaks were observed in the vicinity of the α and β phosphates of ADP (345, 400), in contrast to binding of phosphates by Asp and Asn residues in canonical kinases. Crystallographic studies on tetrameric bacterial NME1 show that in the presence and absence of Mg, the structures are essentially identical, with Mg bound via an Asp residue, whilst interacting with the pyrophosphate of ADP (401). However, it is clear from data presented here, that phosphotransfer to the catalytic His, creating the phosphohistidine enzyme intermediate (Figure 3.6), and subsequent transfer to ADP (Figure 3.28), can be achieved in the absence of Mg ions. The finding that shifts in melting temperature of each enzyme is higher when incubated with diphosphate nucleotides and Mg^{2+} ions (Figure 3.5) compared to that in the absence of magnesium may also suggest that only the second step of the reaction, whereby

a phosphate group is transferred to the phosphate acceptor, is promoted by magnesium, but is still not essential.

3.8.2 Are recombinant NME1, NME2 and PGAM enzymatically active?

The utilisation of pHis as a means for catalysis in cell signalling and cell biology is not uncommon (8). For example, as well as NME1, NME2 and PGAM, succinyl-CoA synthetase (11) and ATP citrate lyase (402, 403) exploit a pHis enzyme intermediate in order catalyse a reaction. NME1, NME2 and PGAM have only been shown to transfer the phosphate moiety from a nucleoside triphosphate (GTP/ATP) to nucleoside diphosphate (ADP/GDP) (334). As previous findings suggest that NME1 and NME2 bind to adenosine and guanosine nucleotides, and PGAM binds DPG, it was important to determine whether this interaction resulted in productive autophosphorylation, the hallmark of enzyme activity in these proteins. To this end, immunoblot analysis and monoclonal N1-pHis and N3-pHis antibodies were employed to study proteins generated in bacteria. It was apparent that NME1, NME2 and PGAM possessed autophosphorylation activity when incubated with ATP or GTP and for PGAM and that DPG was sufficient for autophosphorylation in PGAM. Consistent with DSF findings, the level of pHis NME1 and NME2 detected by immunoblot analysis was reduced in the presence of Mg^{2+} ions, which further supports the theory that Mg^{2+} ions are not required for pHis autophosphorylation but rather impose an inhibitory effect.

These experiments also highlighted that in NME1 and NME2 pHis autophosphorylation was not specific to a particular biological triphosphate base (Figure 3.9). Although the roles of NME1 and NME2 have been previously attributed to ATP and GTP, for example NME2 activates G-proteins through the synthesis of GTP from GDP (404), these nucleoside diphosphate kinases bind to both purine and pyrimidine base nucleotides within the cell (352). I also established that the purified recombinant proteins behave similarly to those reported in the literature, as it was demonstrated the purified proteins can bind and utilise all nucleotides for pHis autophosphorylation. Interestingly, in Figure 3.9, I identified that although CTP and GTP display the smallest shift in melting temperature, and in the presence of CTP and GTP, the highest level of pHis NME1 and NME2 are detected (Figure 3.6 and 3.9), which suggests that thermal stability and binding is not necessarily indicative of the ability for the autophosphorylation reaction to occur. The ability to use any nucleoside triphosphate as a phosphate donor for autophosphorylation is likely attributed to NME's very central role in nucleotide sensing, interconversion and homeostasis. Crystal structures of NME1 and NME2 in complex with different NDP substrates such as ADP, GDP and TDP have been reported and have established that the NME proteins bind both di and triphosphorylated substrates at the same site with the phosphate moiety possessing the same conformation in the NDPK

domain (197, 199, 201). Both ADP and TDP interact with Arg88 and Arg105, whereas the guanine group only interacts with Arg88 but additionally interacts with the carboxylate Glu152 in an adjacent subunit (199). Whilst the co-crystallisation of NME with CDP has not been reported, one study has shown that CDP exhibits very low affinity (199), in accord with my DSF data (Figure 3.9).

The isolation of folded and enzymatically active NME and PGAM recombinant proteins was required for future experiments. As a consequence of this exploratory work, the development of medium-throughput DSF screens to explore small molecules as potential targets for NME1 and NME2 is now made possible, alongside investigations into the putative histidine kinase activity of NME1 and NME2 towards other proteins, which could reveal if these enzymes are indeed protein His kinases.

3.8.3 How do amino acid substitutions in the active site affect NME structure and function?

In addition to the native, wild-type proteins, active site mutants were produced to expand on the biochemical and mechanistic understanding of the proteins. The effects of mutations on native structure were compared using both SEC-MALLS and native MS. SEC-MALLS analysis revealed that wild-type NME1 and NME2 were likely to be hexameric in solution, in agreement with previous findings, and clear evidence that these recombinant proteins are folded and able to multimerise (Figure 3.1 and Figure 3.2). Whilst H118A NME1 was also found to be a hexamer, R105A NME1 possessed a molecular mass indicative of a homodimer at ~34 kDa, suggesting an important functional role for this highly conserved Arg residue in the assembly of higher order structures (see below).

To build on SEC-MALLS analysis in solution, native MS was also performed on purified NME1/2. Wild-type NME1 and NME2, H118A NME1, H118A NME2 and C109A NME1 were all present as hexamers in the gas phase. It was clear that the substitution of Arg to Ala at position 105 had the greatest effect on the oligomeric state of the protein, consistent with SEC-MALLS findings. In accord, R105A NME2 was also dimeric, and analysis of a R105A/H118A NME1 double mutant showed that due to the R105A mutation, this protein also presented as a dimer. Arg105, along with Lys12, Arg88 and Gly119, all donate hydrogen bonds to the phosphate groups of the nucleotide substrate (199). However, Arg105 is also located within the Kpn loop, which is a flexible region of the C-terminal tail, spanning residues 96-117 (Figure 1.8 and 1.9) (179). The importance of the Kpn loop was initially reported when the first residue of the loop, Pro96 (Pro97 in Drosophila) a residue conserved in all NDPKs, was mutated to a Ser residue. This is associated with a downstream dysfunction in the *plum* gene encoding

phosphodiesterase activity, which was shown to be lethal (179, 405, 406) and was since named ‘killer of prune’ (188). Furthermore, the Kpn loop was found to be important for oligomerisation, as it is located in the area between subunits and forms extensive hydrophobic and hydrogen bonds with different subunits within the oligomer (Section 1.8.2.1) (186).

Previous structural analysis has highlighted the effects of mutating the Arg105 in the Kpn loop (407). For example, when the Arg105 of NME was mutated to a Lys, the protein remained a hexamer, like the wild-type protein, but no data for an Arg105 to alanine mutant was presented. Thus, it is likely that the guanidinium group of the arginine side chain contributes to maintaining the position of the Kpn loop and in particular, the length of the side chain may be important in anchoring the Kpn loop in the correct secondary structure conformation through a fully extended arginine side chain as the R105K mutant was in the native hexameric fold. Regardless, the destabilising effect of the R105A mutation on both NME1 and NME2 highlights its role in stabilising the interactions at the trimer interface.

Based on these findings, it was important to ensure the active site mutants were appropriately folded and to assess their ability to bind to ATP (Figure 3.16). The melting temperature of the active site mutant proteins differed somewhat from their wild-type counterparts (Table 3.1). For example, R105A NME1 and R105A NME2 displayed a lower melting temperature than the wild-type proteins, consistent with a dimer unfolding at a lower melting temperature. This is particularly true for R105A/H118A NME1, which exhibits a T_m some 15 °C lower than wild-type NME1, suggesting that the substitution of both amino acids has an additional effect on thermal stability. Interestingly, a positive shift (and higher ΔT_m) in the presence of ATP was displayed by all proteins tested, with the exception of R105A/H118A NME1. However, the ΔT_m was lower for R105A NME1, R105A/H118A NME1 and R105A NME2 compared to wild-type NME1 and NME2, indicating that the nucleotide-binding pocket in these mutants is less favourable for ATP binding and explains why the increase in stability induced by ATP inclusion is much less prominent.

Cys109 and Cys145 are amino acids located outside of the nucleotide binding pocket (Figure 3.10), therefore it is not surprising that mutating these cysteine residues to alanine did not have a pronounced effect on ATP binding. However, the melting temperature (T_m) of C109A NME1 is ~4 ˚C higher than that of wild-type NME1 and C109A/C145A NME1 is ~1 °C higher, evident of a more stable protein structure. Although Cys109 is part of the residues forming the Kpn loop in NME, it is clear that any interactions made with C109 are not crucial for hexamer assembly, as C109A NME1 remained a hexameric (Figure 3.15). The Cys109 residue is buried in the protein structure although it was demonstrated by Song *et al* that under oxidative

stress, the Cys109 can form disulfide bridges with either Cys4 or Cys145, contributing to a ‘less stable; oligomer (192). It is inevitable that some sample oxidation occurs over time, and this could therefore provide an explanation as to why the C109A mutant is more stable than WT NME1. In the same way, Cys145 forms disulphide cross-linkages with Cys4 under oxidative conditions, which in turn stabilises the dimer oligomeric state. When the Cys145 residue is mutated to Ala, these intramolecular disulfide bonds can no longer be formed, which are thought to be important to stabilise the hexamer structure. This further validates data presented in Figure 3.16 as Cys145 was more stable (higher T_m value) than wild-type proteins in both the presence and absence of ATP (192, 408).

Active site mutants generated and purified were H118A and R105A NME1 and NME2 and R105A/H118A NME1 and C109A and C109A/C145A NME as well as H11A PGAM. The capacity of each to autophosphorylate on a histidine was also compared utilising immunoblot analysis (Figure 3.18). When compared side-by-side with wild-type proteins, histidine autophosphorylation in the His to Ala mutants was abolished, confirming that there is likely only one pHis site at His118 in NME1/2 and His11 in PGAM. This was validated by intact MS analysis on recombinant NME proteins, since in the presence of ATP, an ~80 Da mass shift was detected which is equivalent to the addition of a single phosphate group. The level of autophosphorylation activity was significantly reduced for Arg105 to Ala mutants. When analysed by DSF (Figure 3.16), it was found that they had a decreased temperature shift with ATP. This could likely be an explanation for the decrease in pHis autophosphorylation, since Arg105 is involved in nucleotide binding, orienting the phosphate group in position for transfer to His118 (197, 199). Therefore, it is reasonable to conclude that His118 and Arg105 are both important in the binding and more importantly the phosphate transfer from ATP to the NME protein, whereas since the substitution of the Cys109 and Cys145 residues to Ala has a less pronounced effect on phosphate transfer to His118, they are not critical. Any N1-pHis NME1 or NME2 detected in Figure 3.18D and E was abolished when heated at 95°C, further verifying the identity of heat-labile pHis. Through both SEC-MALLS and native MS analysis, R105A NME1 and R105A NME2 were both discovered to be dimers as opposed to the native hexameric structure of human wild-type NME1 and NME2 (182) therefore it is to be expected that the capacity of these proteins to function like their wild-type counterparts is diminished as the stability of the protein may affect autophosphorylation activity.

3.8.4 Can the enzyme activity of NME proteins be measured *in vitro*?

Although the NDPK activity is needed to maintain the nucleotide pools, this is just one potential function for NME proteins. Phosphate transfer, as a function of NDPK activity of NME proteins, was evaluated in Figure 3.28, and the levels of pNME1 gradually decreased as the

concentration of phosphate acceptor increased, providing evidence for His phosphorylation. However, a more high-throughput method was desired to screen for competitive inhibitors and so an ADP-Glo assay was pursued next (Figure 3.29). Unfortunately, each step in the ADP-Glo assay required a 40-minute incubation period (Section 2.15) and the turnaround for NME1 autophosphorylation is <10 seconds and phosphate transfer of the enzyme is <5 minutes (Figure 3.8). This approach is therefore not useful for determination of NDPK activity, since it is likely the reaction very rapidly reaches an equilibrium; rapid stopped flow kinetics will be needed to assess this process more carefully (409).

To address these issues further, NME activity was monitored using a pyruvate kinase-lactate dehydrogenase (PK-LDH) coupled assay and this allowed NME1 to be established as enzymatically active in terms of autophosphorylation activity, through phosphotransfer activity onto an NDP. By coupling the NDPK activity of the enzyme to the PK-LDH reactions, phosphate transfer from NTP to NDP becomes unidirectional, as the product is directly fed into the secondary reaction system. Developing a method to measure the NDPK activity of the enzymes was critical in order to obtain a high-throughput assay for studying mutations, and for the analysis of effects of small molecules under different conditions.

In Chapter 4, I go on to utilise DSF and enzymatic assays described in this chapter to search for new types of NME small molecule binder/inhibitory ligand. In the case of DSF, this represents a new high-throughput approach for small molecule discovery.

Chapter 4: Investigating NME1 for small molecule ligands and drug targets

Introduction

The NME family of proteins utilise a number of nucleotide co-factors in their roles as NDPKs, alongside a major contribution to a variety cellular processes; in some cases the appropriate co-factor(s) and targets that support these outputs are not known. In comparison to protein kinases, the nucleotide binding pocket of NME proteins employ an intramolecular hydrogen bond between the 3'OH group of the ribose forms with the oxygen of the β-phosphate (407). This led to the hypothesis that replacement of the 3'OH group with a phosphate might inhibit NDPK activity, which was very recently found to be true for the 3'-phosphorylated nucleotide inhibitors PAP and PAPS using NME1 from *Dictyostelium* as the target (410). In addition, it was recently shown that NME proteins might also be regulated through Cys-based redox mechanisms. Under experimentally-induced oxidizing conditions, structural modifications on redox-active cysteines take place, leading to a change in the enzyme quaternary structure as the hexamer is dissociates into dimers (411). Known modifications on protein Cys thiols also include glutathionylation and oxidation to sulfonic acid within the proteome (412). Cys S-glutathionylation is an additional cellular response to oxidative stresses, and in some cases, this reversible post-translational modification is essential for the function of signalling proteins (413-415). In response to H_2O_2, disulfide bond cross-links are thought to form between Cys109-Cys109 in NME, and this is reversibly reduced by DTT in vitro (408). This site of oxidation between the Cys109 residues was identified by mass spectrometry and these modifications drive hexamer dissociation (192). Residues Cys4 and Cys145 have also been shown to form an intramolecular disulfide bond under oxidative conditions and these cross-links and subsequent hexamer dissociation have been shown to result in a loss in enzyme activity (416).

Very recently, the universal acetyl group carrier Coenzyme A (CoA) was reported to bind to human NME1 through both covalent and non-covalent mechanisms *in vitro* (417). The low molecular weight thiol CoA is produced enzymatically by conjugation of ATP, cysteine and pantetheine and is generated in all living cells from dephosphorylated CoA, and can then be converted to acetyl CoA to feed into the TCA cycle and fatty acid metabolism (Figure 4.1) (418-420). It was also reported that CoA binding and inhibition of NME1 enzyme activity was induced under oxidative conditions (417). Solvent exposed cysteines in protein targets are modified by the antioxidant function of CoA by exploiting the highly reactive thiol group. This novel PTM has been termed protein 'CoAlation' and this has since been shown to be

widespread in metabolic processes and protein synthesis, functioning as a reversible mechanism for redox regulation (421-423). Broadly, CoAlation is proposed to function through regulation of the activity, conformation and/or subcellular localisation of the modified protein, and also serves to 'protect' Cys residues from irreversible over-oxidation (423, 424).

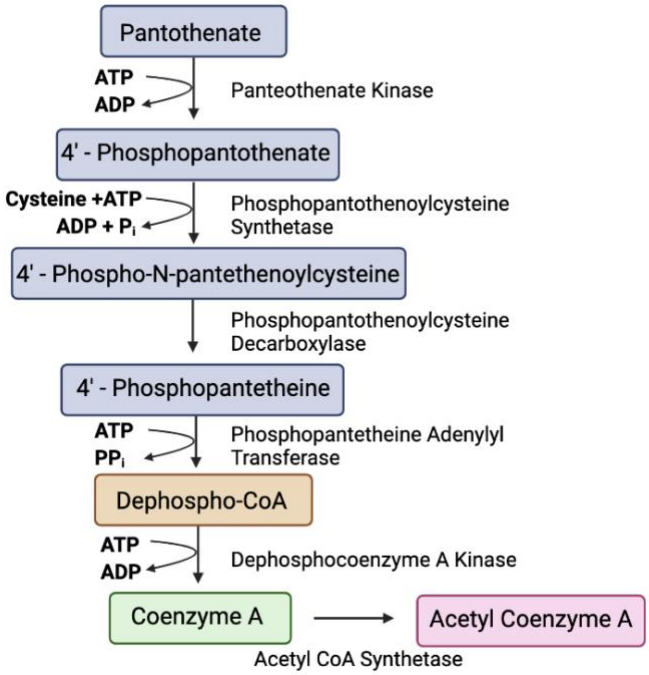

Figure 4.1. Reaction scheme of the synthesis of Coenzyme A and its derivatives. The flow diagram shows the process of Coeznyme A (CoA) production from dephosphorylated CoA and subsequent production of acetyl CoA and was developed using BioRender.

To date, no tight binding inhibitors or activators for human NME1 or NME2 have been described, although the biological functions of NME proteins suggest that it may be a potential therapeutic target. The discovery of efficient compounds is the first step toward designing specific drugs targeted to NME proteins and the NDP kinase activity. Furthermore, such compounds could shed light on the specific mechanisms by which the NME proteins carry out their functions and how these mechanisms relate to or rely on NDPK activity and/or structure. Therefore, in this chapter a variety of clinically approved inhibitors and compounds were explored to determine any effect on activity and multimerization of NME proteins, including a set of NME mutants that are predicted to influence their biological functions.

The experimental objectives of work described in this chapter are:

1. Biochemical analysis of purified proteins in the presence of nucleotides and comparative analysis with active-site and structural mutants
2. Determination of whether redox regulation affects the overall structure and catalytic activity of NME proteins

3. Identification of small molecule compound(s) that interact with NME1, in order to understand connections between NME structure and function in the cell.

4.1 Biochemical analysis of NME1 and NME2 with nucleotide test ligands

The nucleotide test ligands described in this section are presented in Figure 4.2. As discussed in Chapter 3, NME1 and NME2 have affinity for all nucleotides tested, based on their thermal responses, and in particular adenosine nucleotides (Figure 3.5). The nucleotide test ligands investigated in this Chapter all possess an adenosine or guanosine ring (Figure 4.2) and were therefore deemed appropriate to analyse as potential ligands for the purified recombinant proteins NME1, NME2 and PGAM, described in Chapter 3. To determine how changes in nucleotide structure and additional side chains and ions affect binding, differential scanning fluorimetry (DSF) was employed, as introduced in Chapter 3 (Figure 4.3).

In order to obtain a better understanding of how nucleotides may bind to NME1, NME2 and PGAM and to elucidate the importance of the His residue that becomes phosphorylated, mutant NME proteins were generated and analysed by DSF in the presence of nucleotides. A comparison of wild-type (WT) NME1 and H118A NME1 in the presence of ATP, ADP, GTP and GDP is shown in Section 3.6. Along with each nucleotide, adenosine monophosphate (AMP), cyclic AMP (cAMP) and cyclic guanosine monophosphate (cGMP) were also evaluated (Figure 4.3A). In the presence of AMP, in the presence and absence of Mg^{2+} ions, the change in melting temperature (ΔT_m) of NME1 was negligible, below +/- 0.1 °C. This was also observed for H118A NME1, with the ΔT_m near zero, suggesting that AMP does not induce a change in conformation and/or stability of either NME1 or H118A NME1, and therefore most likely does not bind. Although the adenosine ring of the nucleotide has been shown to interact with residues of the NME1 active site (197), it is clear that the presence of at least two phosphate moieties, as found in ADP and ATP, are important for high-affinity binding. This is further demonstrated by the cyclic monophosphate nucleotides, cAMP and cGMP. Although these cyclic nucleotides induce a ΔT_m indicative of binding, albeit of a lower affinity, compared to the diphosphate and triphosphate nucleotides, in the presence of cAMP and cGMP, NME1 appeared to have the lowest ΔT_m shift at +1.2 °C and +1.8 °C. This was reduced to +0.38 °C and +0.89 °C in the presence of $MgCl_2$.

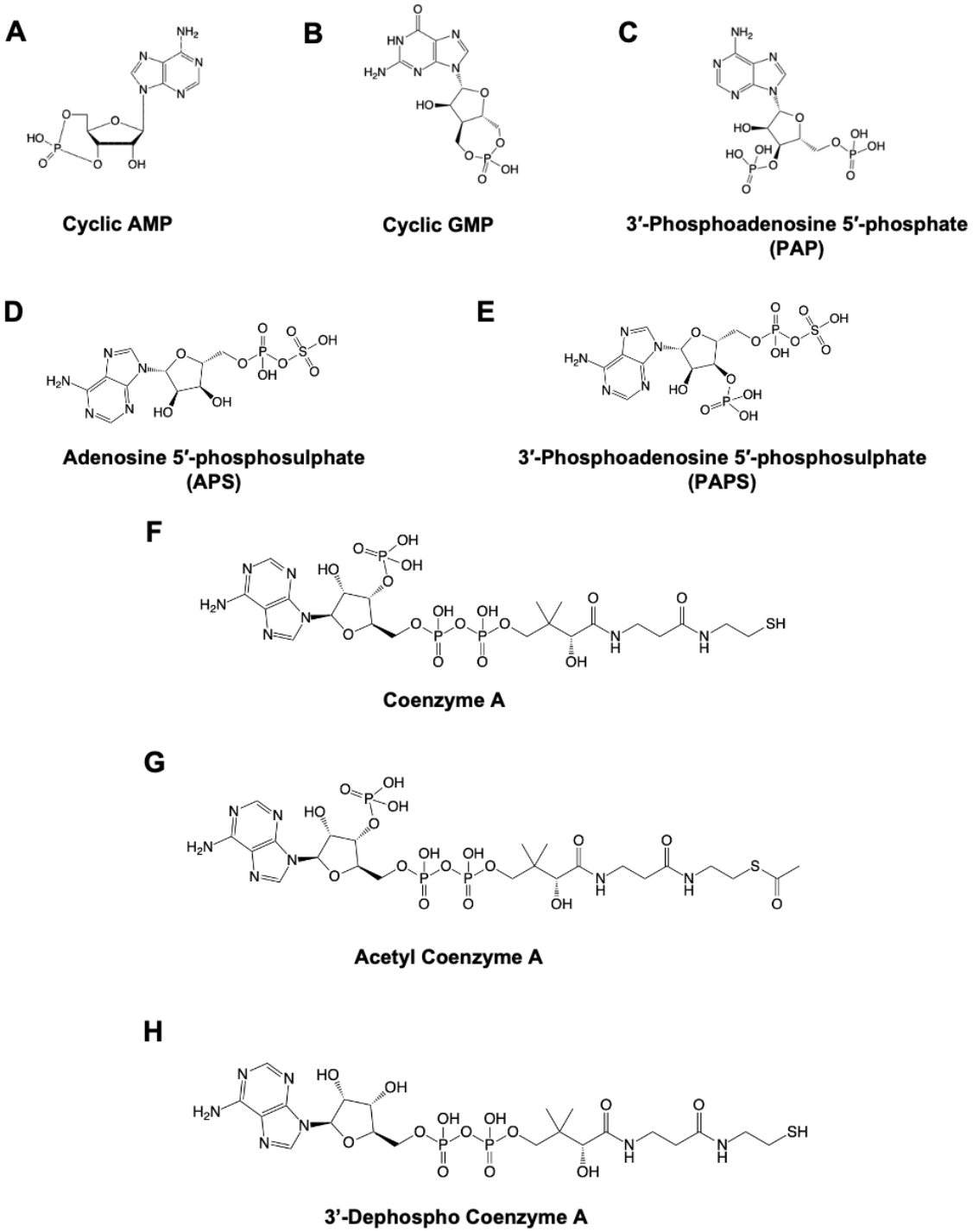

Figure 4.2. Chemical structures of nucleotide test ligands. Chemical structures were produced in ChemDraw 19.1.

When H118A NME1 was analysed in the presence of the same panel of nucleotides (Figure 4.2C), similar results to those observed previously were found, in that Mg^{2+} ions alone appear to stabilise the His mutants compared to a destabilising effect seen in wild-type proteins. The ΔT_m observed for H118A NME1 in the presence of cAMP and cGMP alone was +3.8 °C and + 4.1 °C. In contrast to ATP, ADP, GTP and GDP, where the presence of Mg^{2+} ions increased

the stability of the H118A NME1 protein, for cAMP and cGMP, the presence of Mg^{2+} ions had little effect as the ΔT_m only increased up to +0.45 °C, which is close to the error margins within the assay. His amino acid substitution to a smaller, uncharged side chain may provide a more suitable environment for the cyclic nucleotides to occupy, which is unchanged in the presence of Mg^{2+} ions and may be a result of the oxygen group of the phosphate group no longer being free to interact with active site residues in the cyclic structure.

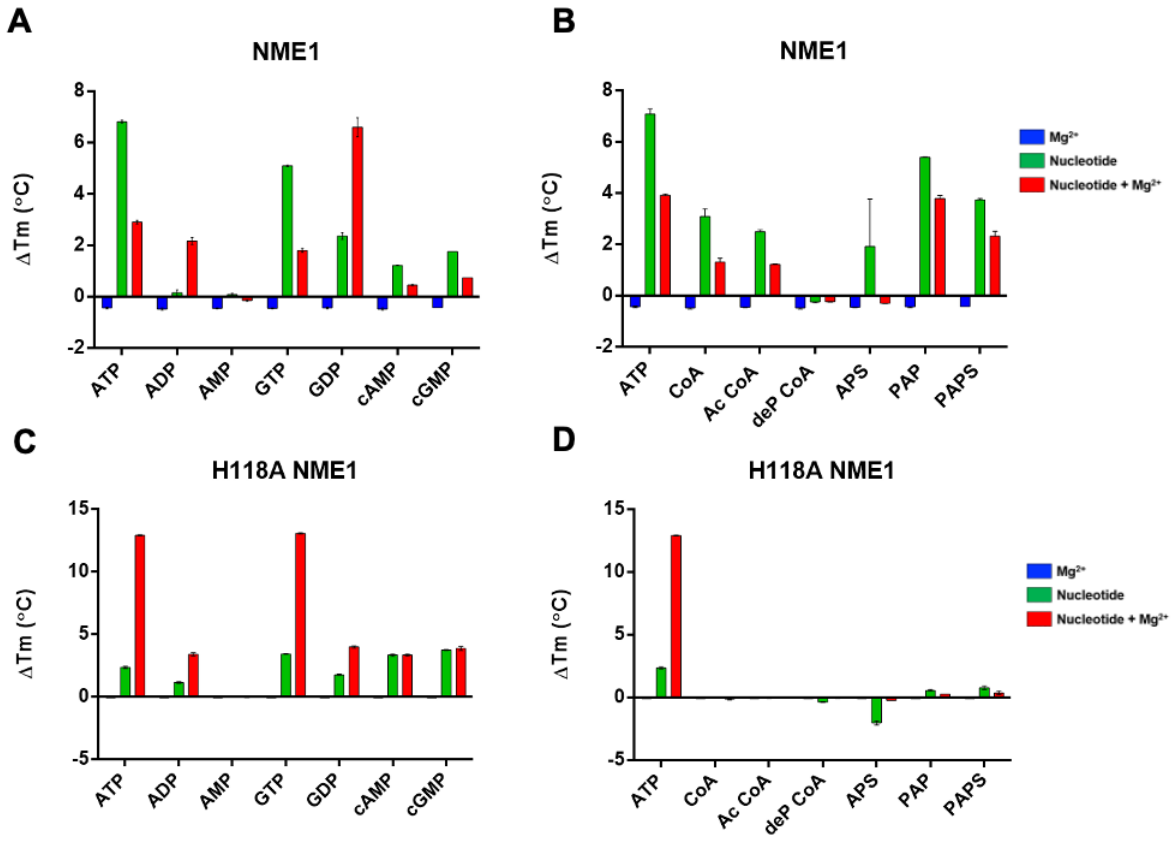

Figure 4.3. DSF analysis of potential NME1 nucleotide ligands. Purified recombinant proteins were incubated for 5 minutes in the presence or absence of 1 mM of the indicated nucleotides and/or 10 mM $MgCl_2$ and then subjected to differential scanning fluorimetry (DSF) to analyse the thermal stability of each protein mixture relative to a solvent control. The average (N=2) change in melting temperature (ΔTm) of (5 µM) enzymes (A) and (B) NME1 compared to (C) and (D) H118A NME1 are presented.

CoA and its derivatives acetyl CoA and dephosphorylated CoA, which lacks the 3' phosphate (Figure 4.2 and Figure 4.3) were also analysed by DSF in the presence of NME1 (Figure 4.3B) and H118A NME1 (Figure 4.3D). The ΔTm observed in the presence of CoA was +3.3 °C, which reduced to +1.2°C in the presence of CoA and $MgCl_2$. Incubation with acetyl CoA (Ac CoA) yielded similar results, as the T_m of NME1 increased by +2.8 °C for acetyl CoA alone and +1.5 °C for acetyl CoA plus $MgCl_2$. In contrast to this, in the presence of dephosphorylated CoA, the T_m of NME1 reduced only marginally to -0.15 °C. Collectively, this data suggests that CoA and acetyl CoA increase the stability of NME1 and are likely binding to the protein via the

phosphate on the adenosine ring. This is indicated by the absence of any significant change in T_m when this phosphate is removed in dephosphorylated CoA. Furthermore, the phosphate group attached to the ribose sugar maintains the strongest structural similarities to nucleoside di- and triphosphates.

3'-phosphorylated nucleotides are known binding partners of bacterial NME1 (410) and to confirm that this interaction could be recapitulated with purified human NME1 and NME2 purified, APS, PAP and PAPS were incubated with NME1 and NME2 and analysed by DSF (Figure 4.3 and 4.4). PAP and PAPS induced large changes in T_m, with the ΔT_m value of NME1 in the presence of PAP being similar to that induced by GTP at +5.6 °C. In the presence of PAPS, a ΔT_m shift of +4.9 °C was observed and the lowest ΔT_m shift was revealed to be +1.9 °C when incubated with APS. This verified that the 3'-phosphate group contributes to NME binding and increased the affinity of these nucleotides. Like the majority of the ligands tested in the presence of Mg^{2+} ions, the stability of the protein was reduced for APS, PAP and PAPS with ΔT_m shifts of -0.5 °C, +4.9 °C and +2.1 °C respectively. This data is in agreement with the literature describing PAP and PAPS as NME binding ligands, although the biological relevance of this finding is unknown, since PAPS is best known as a sulfate donor for protein, glycan and hormone sulfotransferases (410).

Strikingly, Figure 4.3D, revealed that NME1 binding to CoA and its derivatives, as well as the 3'-phosphorylated nucleotides PAP and PAPS, was abolished when the active site His118 residue was replaced with Ala, since the T_m changed no more than +0.5 °C in H118A NME1. In the presence of APS however, binding indicative of inducing a destabilising effect was observed, as a ΔT_m shift of -2.0 °C was seen. These findings suggest that the active site His118 residue plays an important role in the binding of all these ligands through the imidazole ring may forms polar interactions and contributes to neutralisation of the negative charge of the 3'-phosphate moiety.

Next, NME2 was analysed by DSF with a panel of nucleotide ligands, where it displayed a similar thermal melt profile to NME1 (Figure 4.4). For example, there was no evidence that AMP bound to either WT NME2 or H118A NME2, since no change in T_m was observed. An additional possibility is that binding did not induce a change in stability measurable by DSF. However, for NME2, the cyclic monophosphates cAMP and cGMP did show evidence of binding, but to a lesser extent than ATP and GTP in the presence of nucleotide alone with ΔT_m shifts of +1.7 °C and + 2.1 °C. The stability and resultant ΔT_m shown with these nucleotides reduced to +0.9 °C and +1.3 °C when Mg^{2+} ions were included, in marked contrast to the

effects of Mg ions for protein kinases. When cAMP was incubated with H118A NME2, the ΔT_m for both nucleotide alone, and nucleotide with $MgCl_2$ was +0.4 °C. On the other hand, in the presence of cGMP, the Tm of H118A NME2 increased more than WT NME2, by +4.0 °C. This ΔT_m was unchanged when $MgCl_2$ was also added to the assay mixture, further corroborating the hypothesis that $MgCl_2$ has no detectable effect on H118A NME1 or H118A NME2 on the binding of cAMP and cGMP.

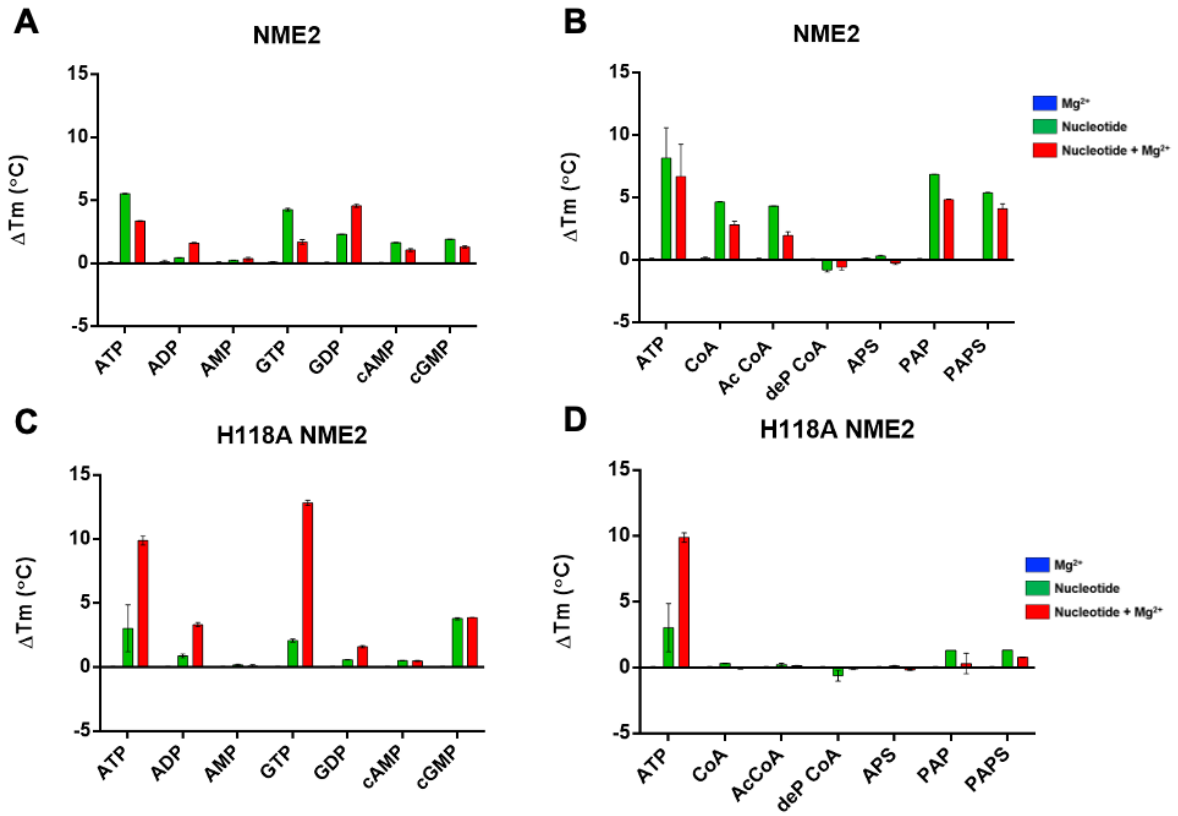

Figure 4.4. DSF analysis of potential NME2 nucleotide ligands. Purified recombinant proteins were incubated for 5 minutes in the presence or absence of 1 mM of the indicated nucleotides and/or 10 mM $MgCl_2$ and then subjected to differential scanning fluorimetry (DSF) to analyse the thermal stability of each protein mixture relative to a solvent control. The average (N=2) change in melting temperature (ΔTm) of (5 µM) enzymes (A) and (B) NME2 compared to (C) and (D) H118A NME2 are presented.

In the presence of CoA, acetyl CoA, PAP and PAPs, the T_m of NME2 increased, confirming that these nucleotides are also NME2 ligands (Figure 4.4B). For example, in the absence of Mg^{2+} ions, CoA induced a ΔT_m shift of +4.9 °C whereas the ΔT_m shift was decreased to + 2.7 °C in the presence of Mg^{2+} ions. Similarly, a ΔT_m shift of +4.8 °C in the presence of acetyl CoA alone and a ΔT_m shift of +1.8 °C with $MgCl_2$, was observed. Dephosphorylated CoA (deP CoA) showed a ΔT_m of - 0.6 °C, suggesting that it had a small destabilising effect on the protein, which reduced to – 0.5 °C in the presence of $MgCl_2$. APS displayed changes below the error envelope of the assay (± 0.3 °C), therefore it had no effect on the stability of NME2 or did not bind, which given the large shifts displayed with PAP and PAPS, is likely due to the absence

of the 3' phosphate group (Figure 4.2). PAP and PAPS had the greatest effect of all the nucleotides tested on the thermal stability of NME2. When incubated with PAP, DSF analysis revealed a +6.5 °C increase in T_m with nucleotide alone, and +4.5 °C increase with Mg^{2+} ions added. For PAPS, the observed ΔT_m was +5.3 °C and when Mg^{2+} ions were added, this reduced to +3.8 °C. As seen with H118A NME1, the binding of these nucleotides to H118A NME2 compared to WT NME2, and subsequent changes in melting temperature, was greatly reduced (Figure 4.4D). The ΔT_m shifts previously displayed by WT NME2 in the presence of CoA and acetyl CoA was near zero, whilst the ΔT_m shifts of PAP and PAPS were reduced to +1.0 °C.

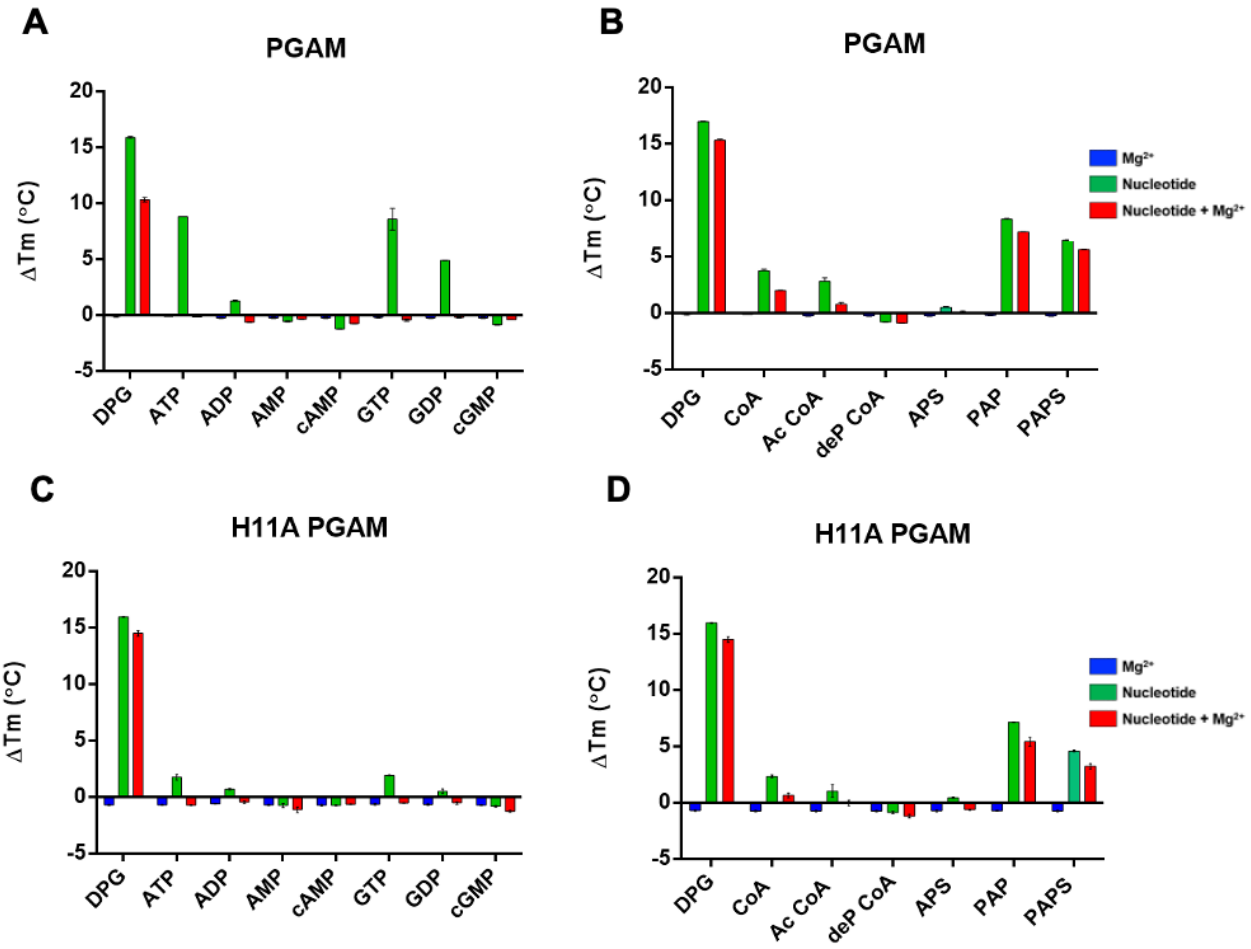

Figure 4.5. DSF analysis of potential PGAM nucleotide ligands. Purified recombinant proteins were incubated for 5 minutes in the presence or absence of 1 mM of the indicated nucleotides and/or 10 mM $MgCl_2$ and then subjected to differential scanning fluorimetry (DSF) to analyse the thermal stability of each protein mixture relative to a solvent control. The average (N=2) change in melting temperature (ΔTm) of (5 μM) enzymes (A) and (B) PGAM compared to (C) and (D) H11A PGAM are presented.

Next, the interaction of nucleotides with PGAM was investigated (Figure 4.5). This revealed that AMP, cAMP and cGMP had very little, or no, effect on the thermal stability of the purified human PGAM. In the presence of these nucleotides alone, ΔT_m shifts of ≤ -0.5 °C were

observed, suggesting negligible binding. When the ligands were analysed in the presence of H11A PGAM (Figure 4.5C), no binding was detected, as expected. In contrast, the ligands CoA, acetyl CoA and PAP and PAPS, displayed ΔT_m shifts indicative of ligand binding as the stability of the protein was increased in the presence of these nucleotides, like that seen for NME1 and NME2. For instance, the T_m of PGAM increased by +3.8 °C in the presence of CoA, and +3.1 °C in the presence of acetyl CoA. These were both reduced by the addition of Mg^{2+} ions. In the presence of PAP, the observed ΔT_m shift was +7.2 °C and for PAPS, the ΔT_m was +5.8 °C and the addition of $MgCl_2$ in the presence of both these nucleotides reduced the ΔT_m by ~1.0 °C. In comparison to the NME histidine mutants, the His to Ala substitution in PGAM had a less profound effect on the binding of these nucleotides. Although the ΔT_m shifts were reduced by ~1.5 °C in all instances, they were not abolished or reduced to near zero as shown for NME1 and NME2. This was particularly true for PAP and PAPS, and therefore demonstrates that although the His11 in PGAM may not be involved in binding of these ligands, rather the reduction in T_m may be a result of a change in protein conformation. However, using this technique, this suggestion cannot be determined unequivocally.

To further explore the effect of nucleotide ligands on NME proteins, the NDPK activity of NME1 was analysed using the pyruvate kinase/lactate dehydrogenase (PK/LDH) coupled assay described in Chapter 3 (Figure 3.30). NME has been reported to undergo structural changes under oxidative conditions, such as in the presence of hydrogen peroxide (H_2O_2), which is a reactive oxygen species, which typically transfers an oxygen atom to a chemical species (192). It was proposed that the Cys residues in NME were sensitive to oxidative stress and when incubated with H_2O_2, formed disulfude linkages which led to NME1 hexamer dissociation, which reduced NDPK activity. Because of this, NME1 was incubated in the presence of the nucleotide test ligands, with the addition of 1 mM H_2O_2 (Figure 4.6), which is commonly used to interrogate protein kinases at concentrations below 1 mM, up to ~ 100 µM (425, 426), to explore how oxidative stress affects NDPK activity and structure. In order to ensure that none of the nucleotides were inhibiting the latter part of the coupled assay system (Figure 3.30A), a control PK/LDH assay with these nucleotides and test ligands, in the absence of NME1 and its TDP substrate, was carried out in parallel. The change in absorbance reflects the reaction turnover, therefore the greater the change in absorbance, the greater the enzyme activity and rate of reaction. In the absence of any nucleotide test ligand, the change in absorbance over ten minutes was 0.31 AU for NME1. This was greatly reduced to 0.01 AU in the presence of Coenzyme A (CoA), indicating very little change in absorbance over time. This is indicative of CoA inhibiting the catalytic transfer of a phosphate from ATP to TDP by NME1, and so very negligible ADP is produced for consumption by pyruvate kinase

in the second part of the coupled assay system in order to produce NAD^+ (Figure 3.30). As the reaction rate of the PK/LDH reaction is largely unaffected by the presence of CoA, it is fair to assume the CoA is specifically inhibiting the NDPK reaction catalysed by NME1.

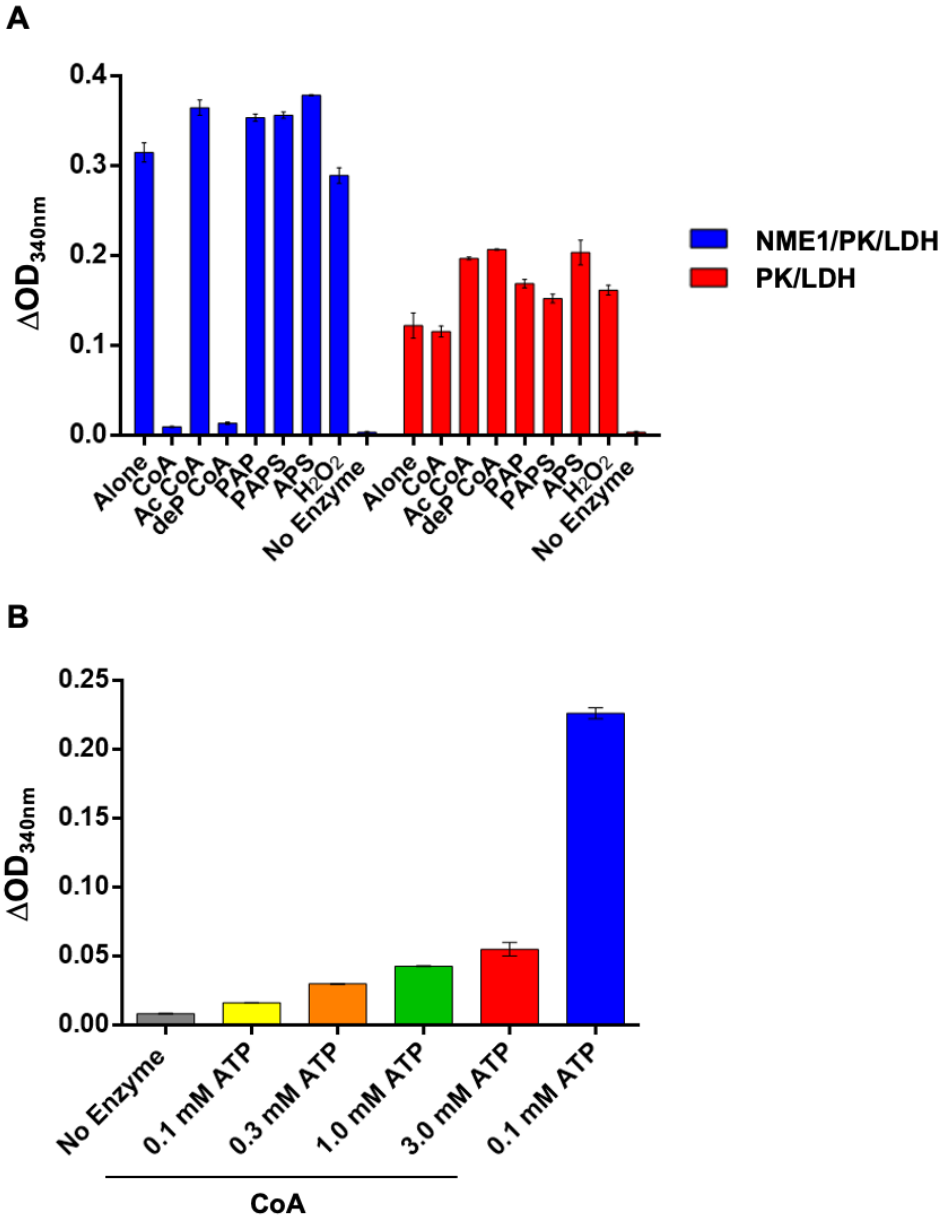

Figure 4.6. Analysis of NME1 enzyme activity in the presence of nucleotide ligands by the pyruvate kinase/lactate dehydrogenase coupled assay. (A) Purified recombinant NME1 was incubated for 5 minutes in the presence or absence of 1 mM of the indicated nucleotides prior to the addition of the assay reaction mix containing 300 μM substrate (TDP for NME1 and ADP for the PK control) then subjected to analysis using the PK/LDH coupled assay (Section 2.16). The mean change (N=2) in OD at 340 nm over 10 mins is presented. (B) 10 mM CoA was incubated with 25 nM NME1 and TDP was titrated in before analysing the rate of NDPK reaction by the PK/LDH coupled assay.

In the presence of PAPS, PAP, APS and acetyl CoA, the rate of the reaction appeared to increase. However, as the turnover for phosphate transfer to a diphosphate nucleotide by

NME1 is <10 seconds (Figure 3.8), it is unclear whether this is a result of differences in the time it takes to add the assay mixture and measure the reaction plate. Furthermore, these slight differences were also observed in the PK/LDH control. Intriguingly, deP CoA also reduced the rate of the NME1 reaction from a ΔOD_{340nm} of 0.31 to 0.02 AU, demonstrating a potent inhibitory effect. In the presence of H_2O_2, the ΔOD_{340nm} was reduced from 0.31 to 0.29, but this result does not appear to be significant, and this would need to be further explored at higher concentrations or using a more rapid (stopped-flow) technique. To further validate inhibition of NME1 NDPK activity by CoA, ATP substrate was titrated into a reaction assay that contained a set concentration of 10 mM CoA, and the ΔOD_{340nm} was measured (Figure 4.6B). The ΔOD_{340nm} increased in parallel with increasing ATP concentrations. At the highest concentration of ATP, the ΔOD_{340nm} was highest, and as the level of CoA was still much higher than ATP, the ΔOD_{340nm} did not come close to that observed in the absence of CoA addition (blue). This suggests that CoA competitively inhibits the NDPK activity of NME1 through the canonical ATP substrate. This finding is in accord with the literature (417), whereas inhibition of NME by deP CoA is a new finding and may suggest an alternate mode of inhibition and binding that doesn't rely on phosphorylation.

4.2 Analysing the effect of cysteine mutations in NME1 and effects on ligand binding and enzyme activity

In the previous chapter, C109A and C109A/C145A NME1 mutants were purified in order to evaluate whether these amino acids contribute to assembly or stability of the NME1 oligomeric state, which subsequently influences enzyme activity. Cys109 is located in close proximity to the nucleotide-binding pocket in the Kpn loop and Cys145 is located in the C-terminal tail, and these specific residues are not thought to be involved in direct nucleotide binding (183, 191). However, these regions are associated with catalysis through oligomer assembly, (186) and I first established that both C109A NME1 and C109A/C145A NME1 were hexameric (Figure 3.15) in solution. Under oxidative conditions, these Cys residues have been reported to play an important role in hexamer dissociation, through increasing the stability of the homodimers that generate native hexameric NME (191, 408). CoA has previously been shown to employ its reactive thiol group for covalent modification of solvent-exposed Cys residues in cellular response to oxidative or metabolic stress. This antioxidant function of CoA in redox regulation was discovered to be a widespread and reversible mechanism (422, 423, 427). Therefore, I analysed nucleotide binding, including CoA and its derivatives, for NME1 Cys mutants using DSF (Figure 4.7). The data previously shown in Figure 4.3B is shown again in 4.7A to allow simple comparative analysis.

The melting temperature of the purified recombinant C109A NME1 in the presence of CoA increased by +1.7 °C, which is 1.3 °C lower than that observed for WT NME1. Similar to WT NME1, when incubated with acetyl CoA, the effect on T_m was less than that of CoA, with a ΔT_m of +0.7 °C. In contrast to CoA and acetyl CoA, dephosphorylated CoA yielded a negative ΔT_m of -1.3 °C demonstrating a reduction in protein stability when incubated with dephosphorylated CoA. This is 1.0 °C higher than that observed for WT NME1. Furthermore, unlike CoA and acetyl CoA, the ΔT_m remained the same in the presence of Mg^{2+} ions as well as dephosphorylated CoA. The ΔT_m across the nucleotides APS, PAP and PAPS, in particular PAP and PAPS, was markedly lower than WT NME1. When incubated with APS, the ΔT_m of C109A NME1 was + 0.4 °C, and + 2.1 °C and + 0.6 °C for PAP and PAPS. For both APS and PAPS in the presence of $MgCl_2$ the ΔT_m was negligible, and for PAP the ΔT_m reduced to +1.0 °C.

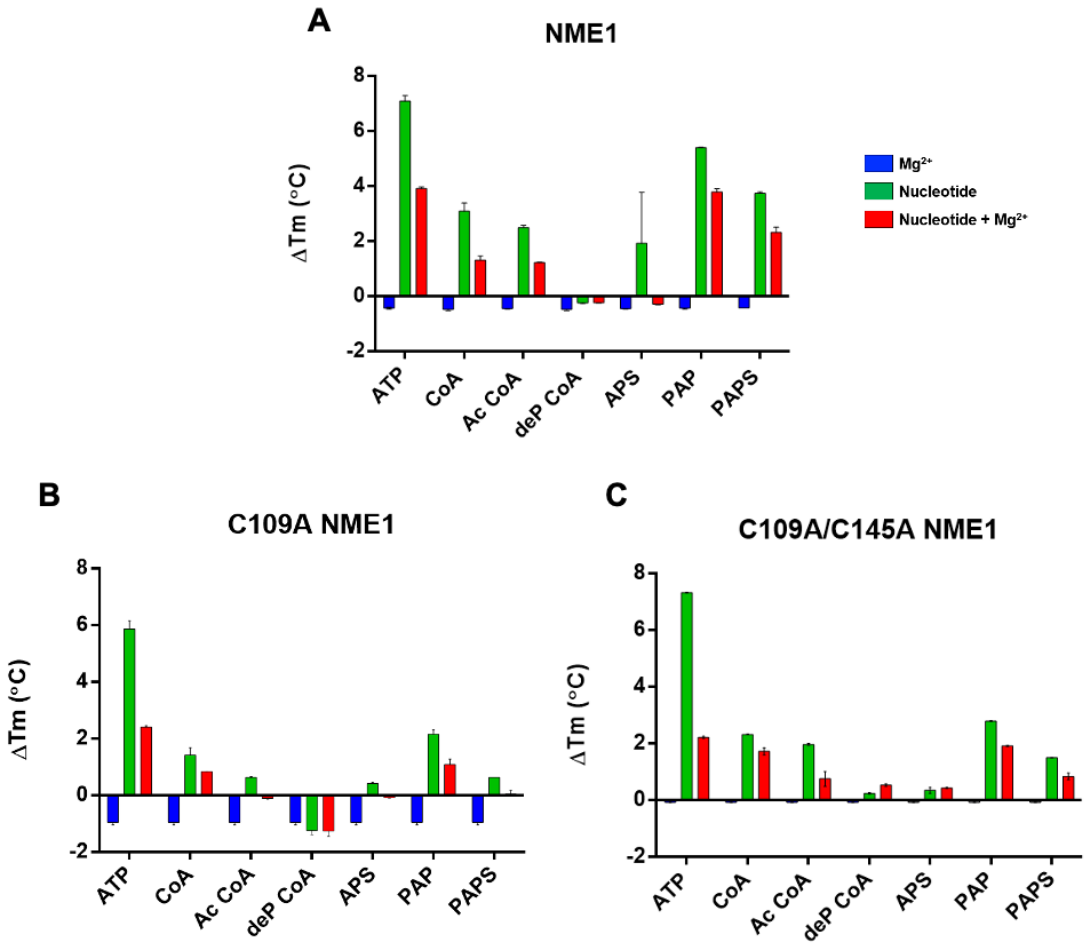

Figure 4.7. Comparative DSF analysis of NME1 and NME1 cysteine mutants in the presence of nucleotide test ligands. Purified recombinant proteins were incubated for 5 minutes in the presence or absence of 1 mM of the indicated nucleotides and/or 10 mM $MgCl_2$ and then subjected to differential scanning fluorimetry (DSF) to analyse the thermal stability of each protein mixture relative to a solvent control. The average (N=2) change in melting temperature (ΔTm) of (5 µM) enzymes (A) NME1, (B) C109A NME1 and (C) C109A/C145A NME1 are presented.

Figure 4.7C presents the ΔT_m values calculated from the DSF analysis of C109A/C145A NME1. Like the majority of the nucleotides tested with C109A NME1, the ΔT_m values for C109A/C145A NME1 were reduced compared to WT NME1, however this was less prominent for C109A/C145A NME1 compared to C109A NME1. Notably, the T_m of C109A/C145A NME1 in the presence of $MgCl_2$ was also largely unchanged, whereas the T_m of C109A NME1 was reduced by -1.0 °C, suggesting that C109A/C145A NME1 was more resistant to destabilisation by Mg^{2+} ions. In the presence of CoA, the ΔT_m shift was revealed to be +2.2 °C, and in the presence of CoA and $MgCl_2$, the ΔT_m shift was +1.8 °C. Acetyl CoA yielded a ΔT_m shift of +1.9 °C and when incubated with $MgCl_2$ alongside, this reduced to +0.8 °C. In contrast to the inhibition of nucleotide binding by $MgCl_2$ seen for the previously mentioned nucleotides, the pre-incubation of dephosphorylated CoA with $MgCl_2$ compared to dephosphorylated CoA alone was largely unchanged. A similar result was observed with APS and therefore may not indicate that these nucleotides have any effect on protein stability. On the other hand, incubation with these nucleotides may simply result in a less pronounced effect compared to the other nucleotides.

When analysed in the presence of PAP and PAPS, changes in the T_m values of C109A/C145A NME1 indicative of nucleotide binding were also observed. When incubated with PAP, C109A/C145A NME1 was determined to have a ΔT_m shift of +2.9 °C, which decreased in the presence of $MgCl_2$ by 1.0 °C. Pre-incubation with PAPS revealed a ΔT_m shift of +1.5 °C and +1.1 °C with the addition of $MgCl_2$. Overall, the data presented in Figure 4.7 suggest that the observed stability of NME1 in the presence of the nucleotides CoA, acetyl CoA, PAP and PAPS, was reduced when the Cys residues were mutated, most notably in the C109A mutant. Thus, the highly conserved Cys109 is most likely involved in stabilising interaction of these nucleotides due to its location within the Kpn loop.

There are a total of three Cys residues in NME1; Cys4, Cys109 and Cys145. Cys4 and Cys145 can form disulfide bridges with one another and under oxidising conditions, Cys109 cross-links can also be formed intermolecularly (191, 416). As previously discussed, these Cys residues are located within conserved domains of the protein involved in oligomer formation. To assess the effect that they have on NME1 oligomer formation and structure, the wild-type protein, along with the Cys mutants, were analysed by gel electrophoresis under non-reducing conditions (Figure 4.8). Figure 4.8A shows wild-type (WT) NME1 in the absence and presence of the nucleotide test ligands investigated in this chapter. In the absence of any nucleotide or binding partner, three stained bands are observed, at ~36 kDa, ~19 kDa and ~17 kDa. The slowest migrating band at ~36 kDa, is most likely a dimer of NME1, as this is close to the

molecular mass of two NME1 monomers. The bands at 19 kDa and 17 kDa are NME1 monomers, and the fastest migrating band at ~17 kDa observed was predicted to be a monomer with an intramolecular disulfide bond. A similar band pattern was revealed in the presence of ATP, however at ~19 kDa a very faint doublet band was apparent, indicative of a phosphorylated protein with reduced electrophoretic mobility. Furthermore, the three stained bands became less prominent, which might be due to high order oligomers becoming more stable in the presence of ATP, although if this is the case, these are not detectable using this semi-quantitative method.

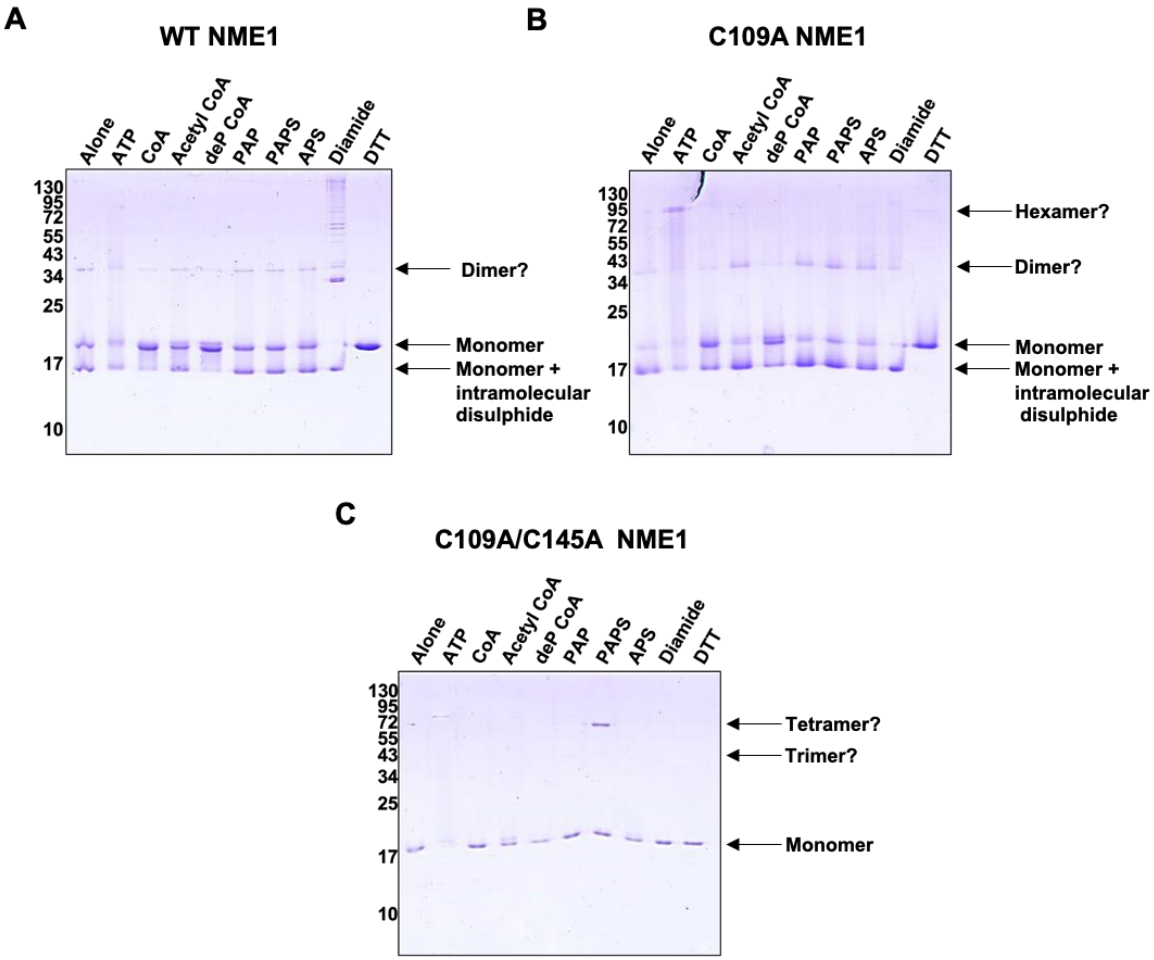

Figure 4.8. Analysis of NME1 and NME1 cysteine mutants in the presence of nucleotide test ligands by non-reducing PAGE. 2 µg purified recombinant proteins (A) NME1 (B) C109A NME1 and (C) C109A/C145A NME1 were incubated for 1 hour at 37 ºC in the presence or absence of 1 mM of the indicated nucleotides and then subjected to electrophoresis on a 15% acrylamide gel under non-reducing conditions.

When pre-incubated with CoA and subjected to electrophoresis under non-reducing conditions, the NME1 band previously seen in the absence and presence of ATP at ~17 kDa was no longer detectable or was at a level undetectable using this method. On the other hand, the ~19 kDa band increased in density, suggesting that the intramolecular disulfide bond, or one of, was abolished in the presence of CoA. From Figure 4.7, it is clear that WT NME1 had

a high affinity for CoA, with a ΔT_m of +3.3 °C and is likely binding to NME1. In Figure 4.8A, the change in the band pattern of native NME1 seen in the presence of CoA provides further evidence for this. Staining at the same molecular mass as those seen with CoA were also displayed by NME1 in the presence of dephosphorylated CoA. Acetyl CoA is the only CoA derivative that appeared to not disturb the band at ~17 kDa. Acetyl CoA and dephosphorylated CoA however result in a doublet band at the molecular mass of ~19 kDa. As no ATP was present, it is unlikely that this is phosphorylated protein, but may be a result of a faster migrating band due to modifications induced through nucleotide binding. In addition, for all the CoA derivatives incubated with NME1, the ~36 kDa band was less pronounced, suggesting that these nucleotides may also disrupt the stability of the dimer.

In the presence of PAP, PAPS and APS the protein behaved in a similar manner with or without nucleotide. Although PAP and PAPS yielded the greatest change in NME1 T_m of the nucleotides tested, there was no detectable change when subunit migration was analysed by native-PAGE. It remains possible that the hexameric structure of the protein, which may be stabilised by these nucleotides, is at a concentration too low to detect by gel electrophoresis. In the cell, diamide decreases the concentration of reduced glutathione (GSH) (428), and *in vitro* it can react with free thiols in protein and lead to disulfide bond formation (429). In the presence of diamide, NME1 appeared to undergo extensive disulfide bond formation, with the most notable bands migrating at ~17 kDa and ~32 kDa, with weaker bands at ~36 kDa, ~57 kDa and ~60 kDa. The band at ~17 kDa is most likely the NME1 monomer containing an intramolecular disulfide. The band at ~32 kDa and ~36 kDa both appeared to be at dimer molecular mass, however the band at ~32 kDa could also likely contained an intramolecular disulfide, resulting in faster migration in the gel. Dithiotreitol (DTT) is a commonly used reducing agent and incubation with DTT resulted in NME1 migrating as a single ~19 kDa monomer band. This further demonstrates that the ~17 kDa band does likely possesses an intramolecular disulfide bond and furthermore, that the ~36 kDa dimer is likely formed and stabilised by disulfide bonds.

When C109A NME1 was analysed by native-PAGE, differences in the native structure and oligomers compared to WT NME1 were clearly revealed. In contrast to WT NME1, a very weak band at ~94 kDa was observed alongside weak bands at ~36 kDa and ~19 kDa and a strong band at ~17 kDa. It is likely that the band at ~94 kDa is a C109A NME1 hexamer, suggesting that the C109A mutant possessed a more stable higher order oligomeric state. This is corroborated by data shown by DSF analysing the thermal stability of the protein (Figure 3.16) as C109A NME1 had a melting temperature 4.4 °C higher than WT NME1. In the presence of ATP, this band at a molecular mass inducive of a hexamer became stronger and the

monomeric bands at ~17 kDa and ~19 kDa were weaker. Furthermore, the ~94 kDa C109A NME1 hexamer migrated as a doublet, indicating that the protein was potentially phosphorylated.

The migration pattern of the C109A NME1 oligomers changed when pre-incubated with CoA. Compared to incubation alone and ATP incubation, the band at ~19 kDa was much stronger with CoA pre-incubation. In contrast to WT NME1 in the presence of CoA, a ~17 kDa C109A NME1 monomer is present. The greatest difference between WT NME1 and C109A NME1 was observed in the presence of diamide. C109A NME1 did not seem to form as many disulfides compared to WT NME1, as less bands were revealed, most likely to do with the removal of a Cys residue on which thiols can be produced. Unsurprisingly, incubation with DTT resulted in the absence of the band at ~17 kDa, as the intramolecular disulfide bond is no longer formed. However, a band at a molecular mass of ~94 kDa, therefore most likely a hexamer, was resistant to the reducing agent, and could be a result of the absent Cys residue further stabilising the NME hexamer. As two out of the three Cys residues in NME1 are mutated in C109A/C145A NME1, it is not surprising that when analysed by native-PAGE, the lower migrating monomeric band, representing a monomer with an intramolecular disulfide, is no longer present across all conditions analysed. When pre-incubated with ATP in the absence of Mg^{2+} ions, a band migrating at ~84 kDa was observed in addition to a very faint ~17 kDa monomer doublet. Although 84 kDa is lower than the molecular weight of an NME1 hexamer, the mutations introduced, and in addition to His phosphorylation, may actually result in a faster migrating NME1. When incubated with CoA and dephosphorylated CoA, a monomeric NME1 was revealed, and in the presence of acetyl CoA, a monomeric doublet band like that seen for WT NME1 and C109A NME1 was present.

Analysis of C109A/C145A NME1 in the presence of PAP and PAPS revealed a very faint NME1 band at ~43 kDa, in addition to the monomer at ~17 kDa, which is likely to be a fast-migrating C109A/C145A NME1 trimer. Furthermore, an additional ~68 kDa band was seen in the presence of PAPS. These bands, which are absent when WT or C109A NME1 are analysed, may be reflective of the disruption that the two mutations of the Cys residues have on oligomer formation. When incubated with APS, a monomer doublet, similar to that seen in the presence of acetyl CoA was observed. It is clear that these two residues are vital for disulfide linkages as there is no change in C109A/C145A NME1 in both the presence and absence of diamide and DTT. Song *et al* proposed two methods of CoA binding, one that involved non-covalent bonds between the adenosine ring and the nucleotide binding pocket and the other that covalently bound the thiol group of the CoA to the previously buried Cys109 that becomes exposed under oxidative conditions (417). This thiol group is also present in

dephosphorylated CoA and the acyl group of acetyl CoA disturbs this and could therefore provide an explanation for NME1 binding and inhibition of CoA and dephosphorylated CoA, but not acetyl CoA. However, the experiments done here were not carried out under oxidative conditions, although it is difficult to completely avoid this in an open-air environment.

To further analyse the effects of Coenzyme A and to better understand how oxidising agents affect NME1, wild-type NME1 and C109A NME1 were analysed by DSF after pre-incubation with titrated CoA (Figure 4.9A) and H_2O_2 (Figure 4.9B). It was found that only at a concentration of 0.75 mM did CoA yield a change in melting temperature of WT NME1 or C109A NME1 above the assay threshold of significance, at +1.8 °C for both proteins. A dose dependent ΔT_m was then observed as the concentration of CoA increased to 3.0 mM with the ΔT_m of WT NME1 reaching +6.7 °C and C109A NME1 reaching +6.3 °C. These changes in melting temperature are similar to those seen in the presence of 1 mM ATP, demonstrating decreased CoA affinity compared to ATP, although a quantitative technique such as calorimetry is needed to reveal the absolute difference. In contrast to CoA, H_2O_2 induced a negative ΔT_m, indicative of binding and in doing so inducing a destabilising effect on the protein structure. Again, as the concentration of H_2O_2 increased, destabilisation increased. At 0.25 mM H_2O_2 the ΔT_m of WT NME1 was negligible and decreased to -1.0 °C at 0.5 mM. At a concentration of 1.0 mM H_2O_2, a ΔT_m of -3.1 °C in WT NME1 was induced. C109A NME1 appeared to be resistant to destabilisation as it remained at ~0.8 °C until the concentration of H_2O_2 reached 2.0 mM. However, at 2.0 mM H_2O_2, the ΔT_m was revealed to be -5.5 °C for WT NME1 and -4.5 °C for C109A NME1. The highest ΔT_m shift for C109A NME1 was a result of pre-incubation with 5.0 mM, rather than 10 mM H_2O_2 at -5.2 °C. In contrast, for WT NME1 the ΔT_m continues to decrease up to -8.5 °C at 10 mM H_2O_2. This greatly differs to the protein kinase, Aurora A for example, in which the T_m is unchanged in the presence of 1 mM H_2O_2 (425).

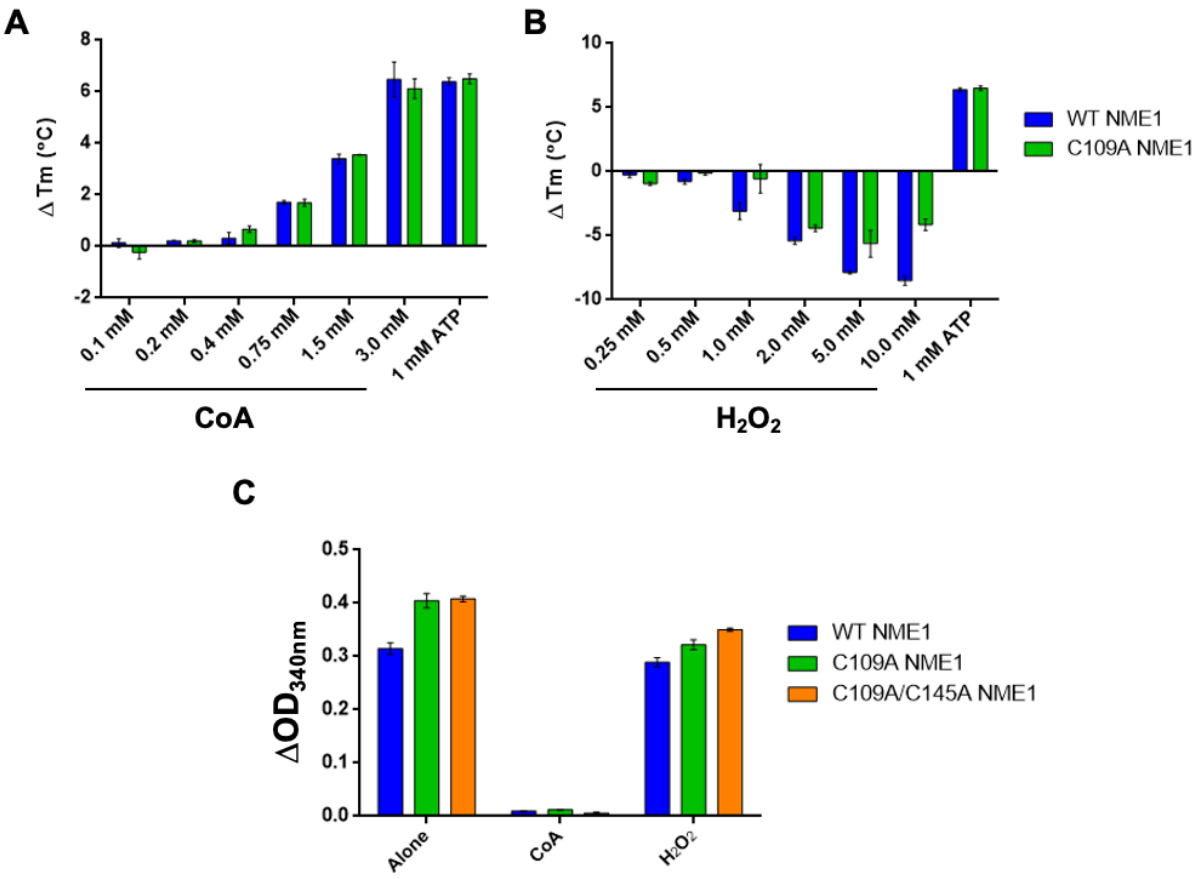

Figure 4.9. Analysis of NME1, C109A NME1 and C109A/C145A NME1 in the presence of Coenzyme A and H_2O_2 by DSF and the PK/LDH coupled assay. (A) and (B) purified recombinant proteins were incubated for 5 minutes in the presence or absence of 1 mM of the indicated nucleotides and subjected to differential scanning fluorimetry (DSF) to analyse the thermal stability of each protein mixture relative to a solvent control. The average (N=2) change in melting temperature (ΔTm) of (5 μM) enzymes is presented. (C) 25 nM purified recombinant proteins were incubated in the presence or absence of 2 mM of CoA or H_2O_2 before the rate of NDPK reaction was analysed using the PK/LDH coupled assay (Section 2.14). The mean change (N=2) in OD at 340 nm over 10 mins is presented.

Together, Figure 4.9A and B, demonstrate that C109A NME1 possessed some resistance to CoA binding and stabilisation and H_2O_2 destabilisation, compared to WT NME1. The reduced stability of CoA in the presence of CoA may be a result of a disruption in the bonds formed at the CoA binding site. Whereas resistance to H_2O_2 destabilisation could be due to a number of different oxidation events on Cys4 or Cys145 that in turn stabilises the C109A mutant. As it was determined that these compounds, particularly CoA, bind and induce structural changes that are different in WT NME1 and the cysteine mutants (Figure 4.8), it was possible they might directly affect NDPK activity. To this end, NDPK activity was measured using the PK/LDH coupled assay system and WT NME1, C109A NME1 and C109A/C145A NME1 were analysed for NDPK activity in the absence and presence of CoA and H_2O_2 (Figure 4.9C). In the absence of any compound, WT NME1 had the lowest activity, as C109A NME1 and

C109A/C145A NME1 both exhibited a ΔOD_{340nm} after 10 minutes of 0.4 AU, which is ~0.1 AU higher than WT NME1. For all purified proteins, this change is diminished to near zero in the presence of 1 mM CoA, indicating that from the point of measurement, a nearly undetectable amount of phosphate was being transferred from ATP to TDP by NME1 and the cysteine mutants. In contrast, H_2O_2 did not have as profound effect. WT NME1 in the presence of H_2O_2 did not appear to significantly reduce the change in absorption and did so only marginally for C109A NME1 and C109A/C145A NME1 with a ΔOD_{340nm} of 0.7 and 0.5 AU respectively.

In order to further explore enzyme activity of NME proteins in the presence of CoA and H_2O_2, the extent of autophosphorylation was analysed using monoclonal antibodies against N1 pHis (Figure 4.10). Figure 4.10A demonstrated the effect of CoA pre-incubated with WT NME1, C109A NME1 and C109A/C145A NME1 prior to adding ATP in order to analyse N1 histidine phosphorylation. In the absence of ATP, no band was detected for any of the proteins tested. The level of N1 pHis NME1 did not appear to change significantly when incubated with CoA and ATP, compared to ATP alone. This result was replicated for the cysteine mutant proteins. In conjunction with the data shown in Figure 4.9, this data suggests that CoA binds to NME1 in a dose-dependent manner, despite the Cys mutations, and inhibits transfer of a phosphate from NME to the nucleotide acceptor (Figure 4.9) but not transfer of a phosphate to NME, since His 118 autophosphorylation remained unaffected.

When analysed in the presence of H_2O_2, the signal detected for the WT NME1 monomer was slightly reduced compared to the ATP control. This could be due to the presence or increase in a detectable amount in a N1 pHis NME1 dimer. Furthermore, this N1 pHis SDS-resistant dimer is also presented in C109A NME1 with H_2O_2, however the level of autophosphorylated C109A NME1 monomer is greatly reduced, indicating an inhibitory effect of H_2O_2 on the C109A NME1 monomer. The signal for N1 pHis C109A/C145A NME1 was unaffected in the presence of H_2O_2, and no pHis dimer was observed. This suggests that Cys145 is involved in dimerization of the NME protein in the presence of H_2O_2 and most likely oxidative stress. In addition, the Cys109 may provide some protection from H_2O_2 induced oxidative stress and subsequent loss of autophosphorylation activity.

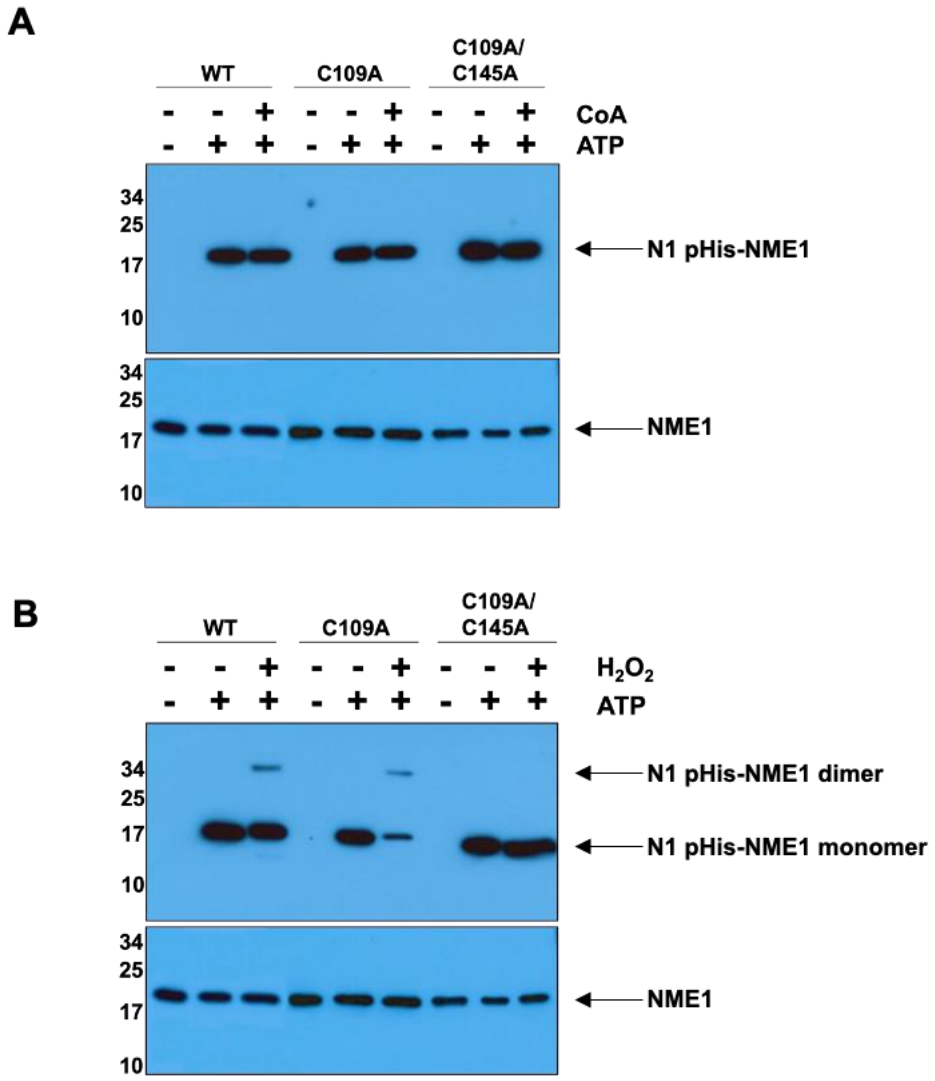

Figure 4.10. Analysis of the autophosphorylation activity of NME1, C109A NME1 and C109A/C145A NME1 in the presence of hydrogen peroxide (H2O2) and Coenzyme A. Purified recombinant proteins (1 µg) were incubated in the presence or absence of 10 mM of CoA or H_2O_2 for 1 hour at 37 ˚C before the addition of 1mM ATP. Samples were then resolved by SDS PAGE on a 15% acrylamide gel and analysed by western blot. Samples were divided into two aliquots, and one was heated at 95°C for 5 minutes. Unheated samples were processed for immunoblotting with an N1-pHis antibody and heated samples were probed using anti-NME1 antibody to determine the total protein. Similar results were observed in repeat experiments.

4.3 A DSF screen for NME1 interaction with clinically approved kinase and TPST inhibitors

NME1 can be described as a moonlighting enzyme, whereby it has one or more functions independent of its catalytic function (430) and it appears to interact with various binding partners to allow the regulation of cellular processes including nucleotide homeostasis, endocytosis, intracellular trafficking, stress-response signalling, cell motility and tumour metastasis (172). Despite diverse effects on cell biology, for the majority of processes, the

mechanisms by which NME1 drives biology are not understood. In addition, NME1 might be an interesting chemical biology target in terms of both activation as well as inhibition, which might help to gain a better insight into its cellular actions. To this end, and recognising that protein kinase inhibitors can inhibit other classes of enzymes such as sulfotransferases that employ PAPS as a co-factor (326), a broad panel of kinase inhibitors were screened to look for binding to NME1 (Figure 4.11).

To semi-quantify interactions, NME1 was pre-incubated with the indicated kinase inhibitors and analysed by DSF in order to evaluate thermal stability in the presence of each compound (Figure 4.11A). Staurosporine is a non-specific kinase inhibitor, and Byrne *et al* demonstrated that when incubated with the purified protein kinase PKA at a 20 fold molar excess, and analysed by DSF, a ΔT_m of ~12 °C was evident (327). When NME1 was incubated with 200 µM staurosporine a ΔT_m of -0.7 °C was calculated, suggesting a lack of binding. Interestingly, negligible ΔT_m values were also observed for other (target-specific) protein kinase inhibitors tested, including erlotinib, an epidermal growth factor receptor (EGFR) inhibitor (431). Of the kinase inhibitors tested, those that yielded the largest ΔT_m were selumetinib, vemurafenib, sorafenib and dabrafenib, with ΔT_m values of +1.0 °C, -3.4 °C, -3.8 °C, and -2.6 °C respectively. Furthermore, mining the RAF-inhibitor class more carefully for NME1 ligands by DSF revealed that rottlerin, suramin, RAF-265 and ZM336372 all induced significant negative changes in the melting temperature of NME1 with ΔT_m shifts of -0.8 °C, -1.0 °C, -4.3 °C and -2.7 °C respectively. The changes in melting temperature for NME1 in the presence of these compounds are generally indicative of destabilisation of the protein structure, as negative shifts were observed. This is in contrast to canonical protein kinases like PKA and sulfotransferases such as HS2ST and TPST1, where these compounds all elicit a positive shift in T_m when tested by DSF (367, 369, 371).

To explore whether catalogued changes in NME1 melting temperature correlate in changes in NDPK activity, an NDPK reaction assay was set up in the presence of several inhibitors that demonstrated the largest ΔT_m shifts, and the reaction was analysed using the PK/LDH coupled assay system (Figure 4.11B). As described previously (Figure 4.9), CoA is an inhibitor of NDPK activity in NME1 and was therefore used as a positive control. No decrease in the ΔOD_{340nm} indicative of a reduced rate of NDPK activity was seen in the presence of any protein kinase inhibitor tested. Vemurafenib elicited a large increase in the ΔOD_{340nm} after 10 minutes, however this increase was also observed in the PK/LDH control, so the effect of this compound

was not specific to the NME1 part of the reaction, and is therefore likely interfering with the absorbance at 340 nm.

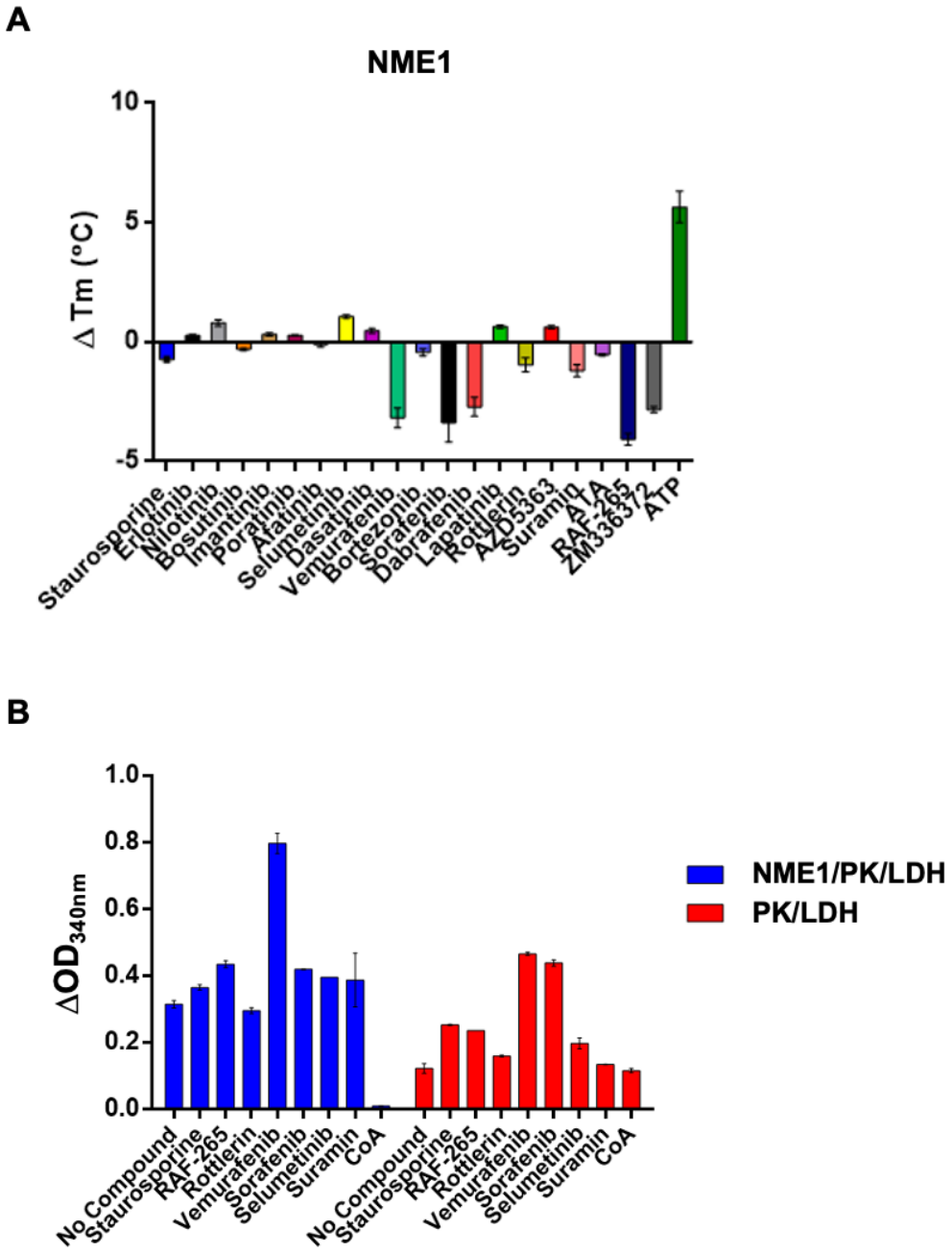

Figure 4.11. Screening NME1 with protein kinase inhibitors and drug-like compounds by DSF. The purified recombinant protein was incubated for 5 minutes in the presence or absence of 200 μM of the indicated drug then subjected to differential scanning fluorimetry (DSF) to analyse the thermal stability of each protein mixture relative to a solvent control. The average (N=2) change in melting temperature (ΔTm) of (5 μM) enzymes are presented. (C) 25 nM NME1 was incubated in the presence or absence of 200 μM of the indicated drug before the rate of NDPK reaction was analysed using the PK/LDH coupled assay (Section 2.14). The mean change (N=2) in OD at 340 nm over 10 mins is presented.

4.4 DSF screen for NME1 interaction with compounds assembled from an FDA-approved drug library

Since NME1 does not possess the classical bilobal domain structure and catalytic elements found in protein kinases, it is perhaps not surprising that broad-spectrum kinase inhibitors such as staurosprone do not block NME1 enzyme activity. Therefore, to further investigate and identify a broader range of potential NME1-binding compounds, a commercial FDA-approved drug library was purchased from SelleckChem. The library contains a variety of unique and biodiverse drugs related to oncology, cardiology, anti-inflammatory, immunology, neuropsychiatry, analgesia and includes several other kinase inhibitors. Thus, it was deemed an appropriate source for an initial library screen.

The FDA-approved library collection is named and ordered via a SX000 (X = 1, 2, 3 or 4) nomenclature and this is also used here. An initial screen of NME1 in the presence of library compounds was carried out and the ΔT_m values obtained were plotted alongside positive controls, including ATP and CoA, which induce a stereotypical shift in T_m as presented in Figure 4.12A. All compounds that resulted in a ΔT_m above ± 1.0 °C were then re-analysed in duplicate, and the mean ΔT_m for these results were plotted in Figure 4.12B. The data highlighted in red indicates compounds in the library that caused the melting temperature of NME1 to increase or decrease by 1.0 °C and will be referred to as FDA-library 'hits'. A threshold of 1.0 °C was determined for compounds to be taken for further analysis as below this the data is generally less reliable in suggesting binding. An exception to this was S1730, in which the ΔT_m of NME1 was +0.7 °C, and this was selected for further analysis as it was the only compound that yielded a positive shift above the 'error envelope' of the assay. From DSF analysis, it was observed that many of the FDA-library hits (chemical structures displayed in Figure 4.13) contained functional groups capable of accepting electrons, which are potentially able to act as protein oxidising agents. In fact, S1949, better known as menadione, is a very well-known oxidising agent (432), and resulted in a ΔT_m of -5.7 °C. This pattern was also seen for compound S1808 for example, which caused a ΔT_m shift of -3.1 °C.

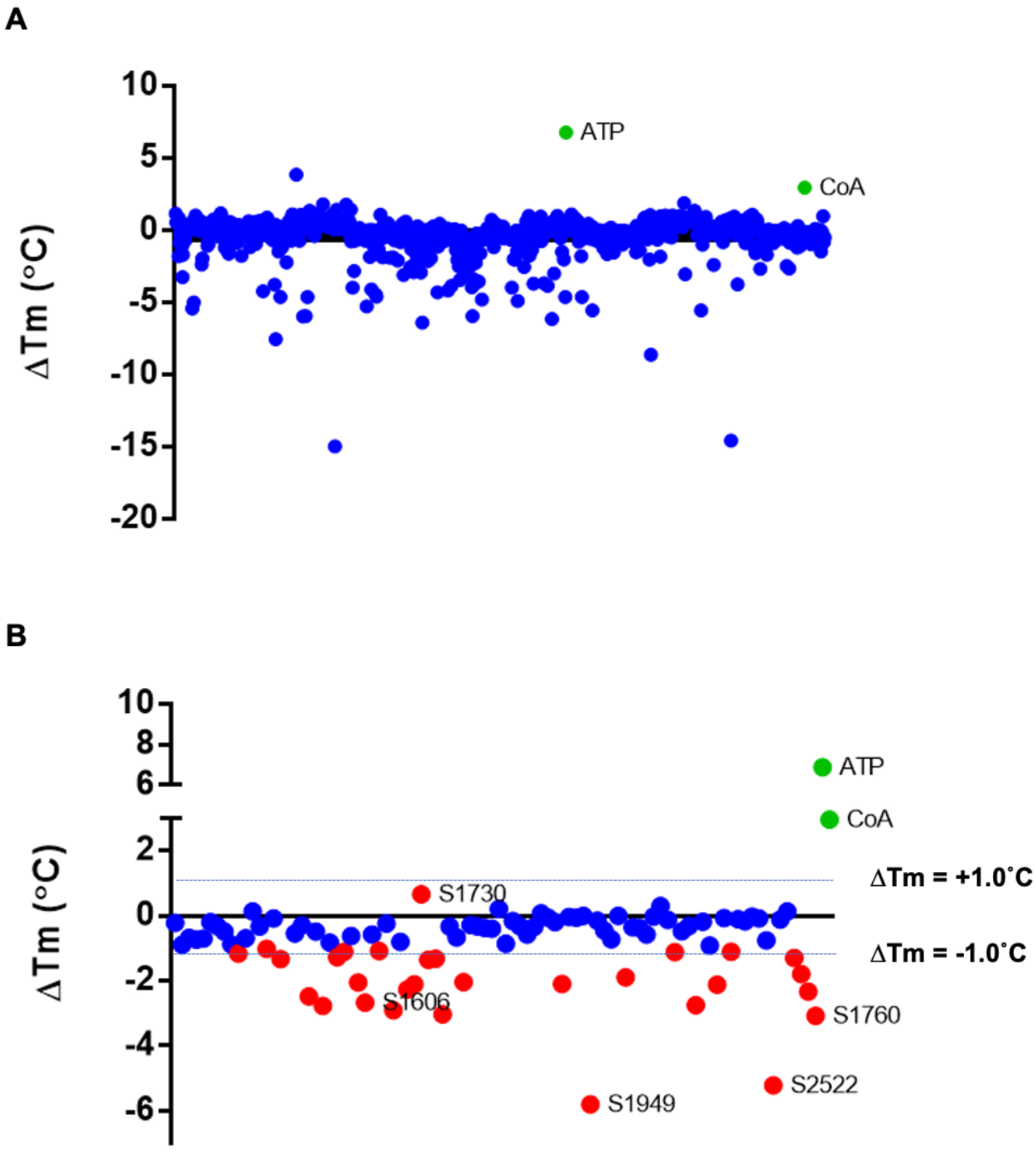

Figure 4.12. Screening NME1 with the food and drug administration (FDA) approved drug library by DSF. (A) Purified recombinant protein was incubated for 5 minutes in the presence of 200 µM of the indicated drug then subjected to differential scanning fluorimetry (DSF) to analyse the thermal stability of the protein mixture relative to a solvent control. The change in melting temperature (ΔTm) of NME1 in the presence of these drugs presented. (B) FDA hits with a ΔTm above and below +/-1.0 ˚C was repeated in duplicate and the average ΔTm of these are presented. Compounds that elicited a ΔTm above and below +/-1.0 ˚C are highlighted in red.

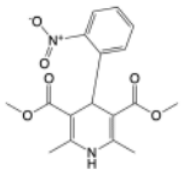

S1808, Nifedipine

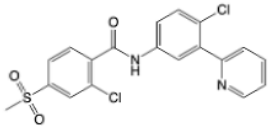

S1082, Vismodegib

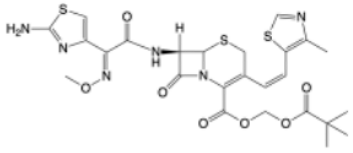

S1768, Cefditoren pivoxil

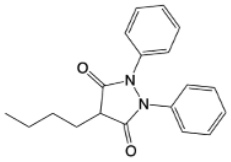

S1654, Phenylbutazone

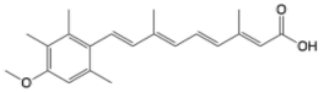

S1368, Acitretin

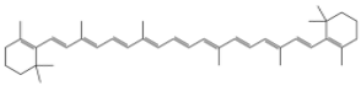

S1767, Beta-Carotene

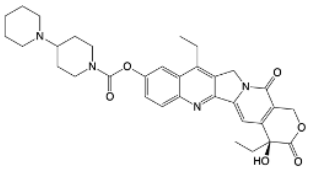

S1198, Irinotecan

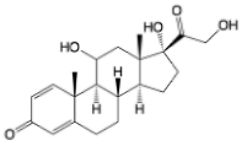

S1737, Prednisolone

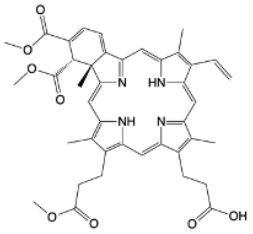

S1786, Verteporfin

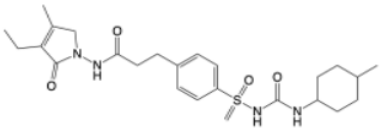

S1344, Glimepiride

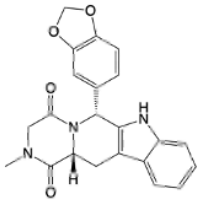

S1512, Tadalafil

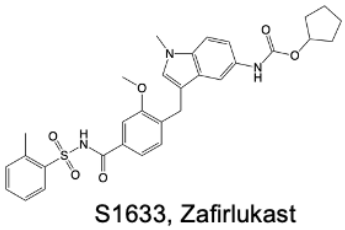

S1633, Zafirlukast

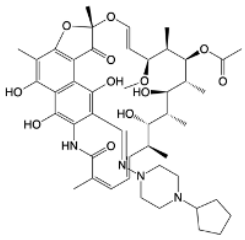

S1760, Rifapentine

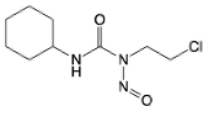

S1840, Lomustine

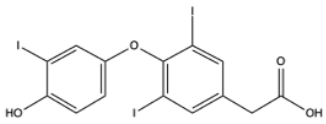

S4185, Tiratricol

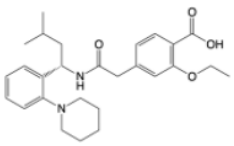

S1426, Repaglinide

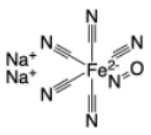

S4059, Sodium Nitroprusside

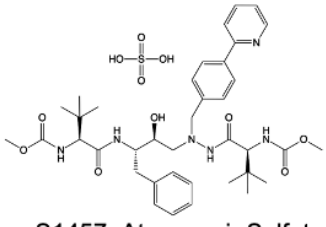

S1457, Atazanavir Sulfate

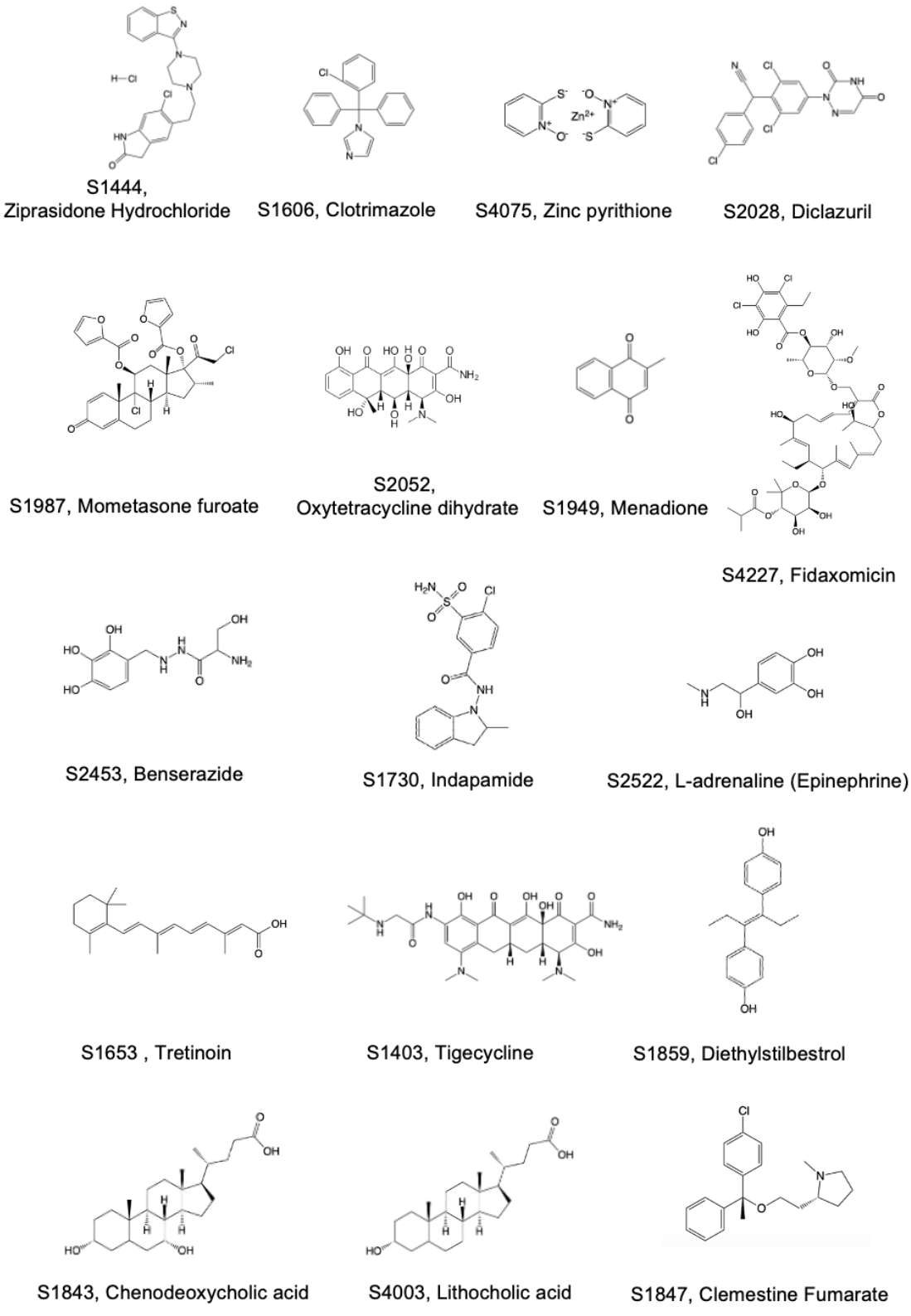

Figure 4.13. Chemical structures of FDA library hits. Chemical structures were generated using ChemDraw 19.1, with common names indicated alongside.

To further verify the data, several FDA-library 'hits' at increasing concentrations between 10 µM to 200 µM, were incubated with NME1 and analysed by DSF (Figure 4.14). For more than half the compounds tested, it was revealed these compounds elicit a reduction in NME1 stability in a dose-dependent manner as the higher the concentration, the greater the negative T_m shift observed. In some cases, only the highest concentration of 200 µM resulted in a ΔT_m. This was observed for the compounds S2028, S1987 (Figure 4.14A), S1737, S4059 (Figure 4.14B), S1444, S1808, S1847 (Figure 4.14C), S1082, S1198, S1344, S1654, S1767 and S1512 (Figure 4.14D). This suggested that NME1 had a lower affinity for these compounds compared to those that showed a T_m shift at 10 µM for example.

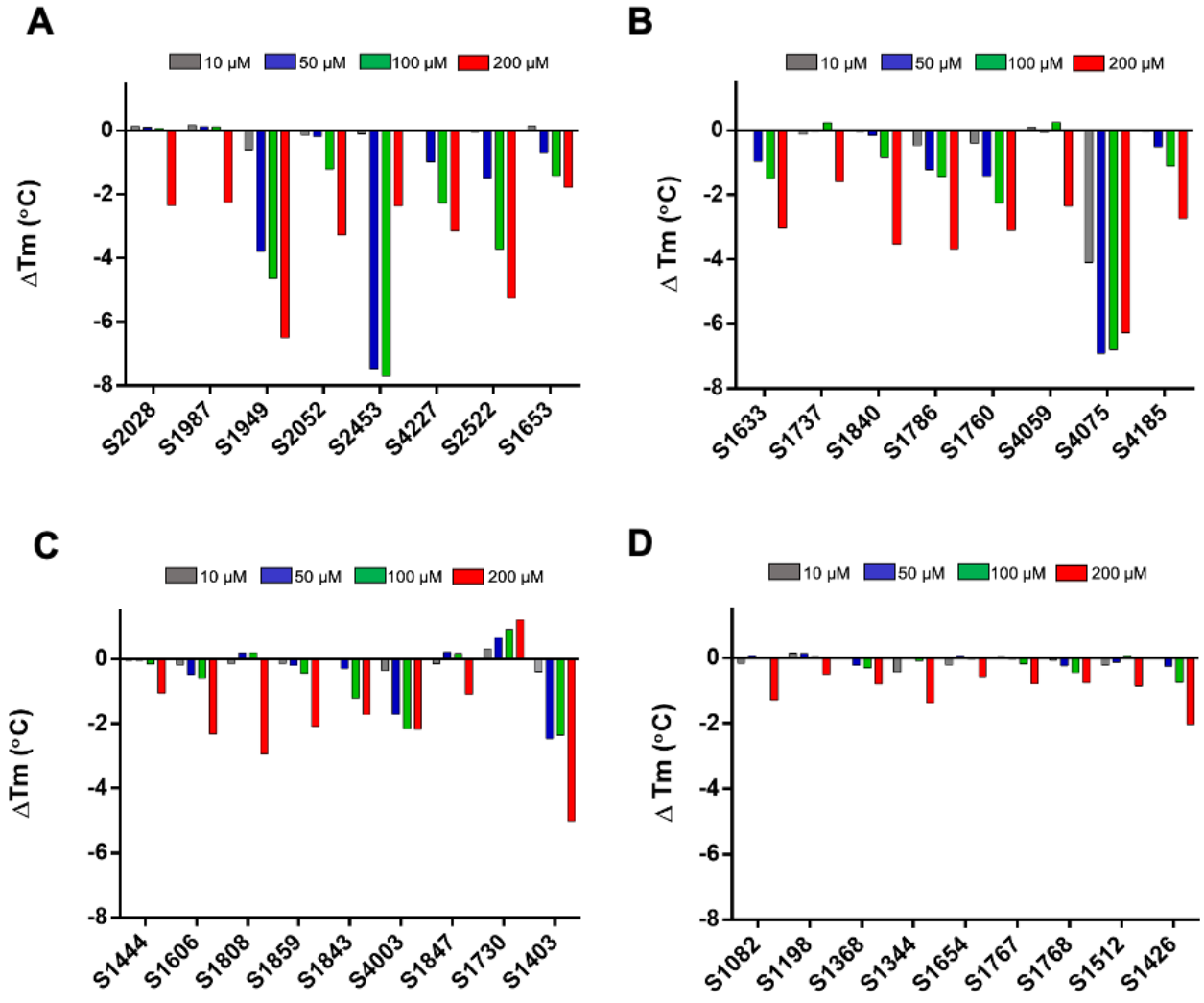

Figure 4.14. DSF analysis of NME1 with titrated FDA library hits. 5 µM purified recombinant NME1 was incubated for 5 minutes in the presence of 200 µM of the indicated FDA hit and then subjected to differential scanning fluorimetry (DSF) to analyse the thermal stability of each protein mixture relative to a solvent control. The average (N=2) change in melting temperature (ΔTm) is presented.

4.5 Analysis of NME1 protein structure in the presence of FDA-approved drug library hits

Given that NME1 is redox regulated and the hexamer has been shown to dissociate under oxidative stress (191, 192, 408, 416, 433), it was reasonable to question whether the destabilising effect of FDA for NME1 was due to a link between the detection of oxidative stress by NME1 and multimerisation (e.g. hexamer breakdown). In order to determine if some compounds might be hexamer 'degraders', comparative DSF analysis was carried out with R105A NME1, which is normally a dimer, and the supposedly 'oxidative-resistant' C109A NME1 hexamer. Those compounds that yielded the largest differences in ΔT_m of WT NME1 compared to R105A NME1 and C109A NME1 are plotted in Figures 4.15A and B. In Figure 4.15C, a PKA counter-screen was performed to highlight the differences for a canonical protein kinase and an NDP kinase such as NME1, and also to discover any that are specific to NME1.

As shown in Figure 4.15, pre-incubation of C109A NME1 and R105A NME1 with some of the compounds resulted in higher ΔT_m shifts than WT NME1. In order to thoroughly explore how these compounds are affecting protein structure and stability; these compounds were also selected for further analysis on the protein. For instance, although S1082 induced a small change in ΔT_m in WT NME1, for C109A NME1 a ΔT_m of -19.0 °C was observed. Similarly, in the presence of S1457, for both R105A NME1 and in particular C109A NME1, the ΔT_m was higher than that displayed by the wild-type protein. In the presence of S1512 and S1606, C109A NME1 appeared to be resistant to destabilisation, whereas R105A NME1 in the presence of S1606 had a higher ΔT_m than WT NME1 at -4.2 °C. Again, in the presence of S1633, C109A NME1 had a slightly lower ΔT_m shift compared to WT NME1, suggesting the protein stability was not as affected. Unlike WT NME1 and C109A NME1, when pre-incubated with S1730, R105A NME1 had a negative change in T_m. In the presence of S1737, the ΔT_m of C109A NME1 and in particular R105A NME1 was greatly reduced, with ΔT_m's of -1.0 °C and near zero respectively, compared to WT NME1 at -5.0 °C. In contrast to this resistance shown, C109A NME1 displayed a greater effect on protein instability than WT NME1 in the presence of S1760, whereas R105A NME1 yielded a positive thermal shift of +4.3 °C. S1198 and S1344 are shown here and selected for further analysis as well as those displayed in Figures 4.14A and B to compare the differences between compounds that cause a negligible ΔT_m to those that cause larger ΔT_m shifts and act as a control.

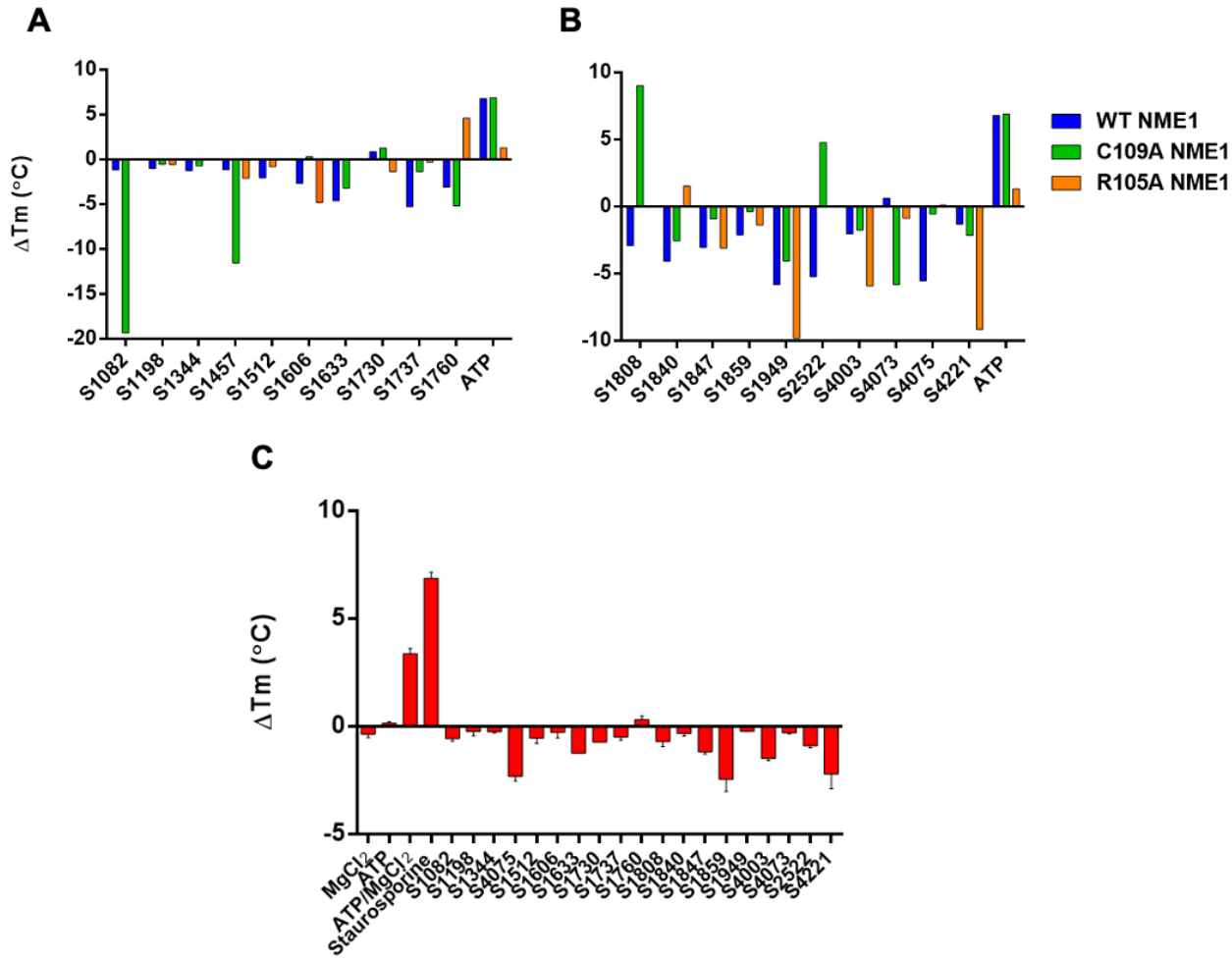

Figure 4.15. Comparative DSF analysis of NME1 and NME1 mutants in the presence of FDA library hits. 5 µM purified recombinant proteins were incubated for 5 minutes in the presence of 200 µM of the indicated FDA hit and then subjected to differential scanning fluorimetry (DSF) to analyse the thermal stability of each protein mixture relative to a solvent control. The average (N=2) change in melting temperature (ΔTm) of the NME proteins (A) and (B) is presented. The average (N=2) change in melting temperature (ΔTm) of (C) PKA in the presence of FDA library hits is presented.

C109A NME1 displayed 'resistance' to destabilisation in this assay based on lower ΔT_m values in the presence of S1808, S1840, S1847, S1859, S1949, S2522 and S4075. In the same way, R105A NME1 displayed resistance when analysed with S1840, S1859 and when pre-incubated with S1847 the ΔT_m of R105A NME1 was similar to WT NME1. S1949 induced a ΔT_m value of -8.9 °C in R105A NME1, which was much greater than that seen for the other proteins tested. Lastly, analysis in the presence of S4221 revealed that R105A NME1 had the greatest ΔT_m of -9.6 °C and the ΔT_m observed for WT NME1 and C109A NME1 was -1.2 °C and -2.0 °C respectively. From Figure 4.15C, I conclude that these compounds have some specificity in inducing an effect on NME1, since a standard protein kinase (PKA) displayed ΔT_m values of -1.0 °C in the presence of the majority of the compounds tested. The exception

to this was in the presence of S4075, S1859 and S4221 and only S4221 have a reduced stabilising effect on WT NME1 when compared to PKA.

Differential scanning fluorimetry (DSF) analysis is a useful technique to determine whether a test ligand can bind. However, a change in melting temperature may not always be a reflection of binding. Furthermore, destabilisation or stabilisation of a proteins melting temperature may not be indicative of quaternary structural changes such as subunit dissociation, just as a positive ΔT_m does not necessarily mean higher order oligomers are forming. Therefore, to gain a better understanding of whether these compounds do in fact cause structural changes and effect native oligomer formation native (non-reducing) PAGE was performed after incubation of with FDA-library hits (Figure 4.16 to Figure 4.18).

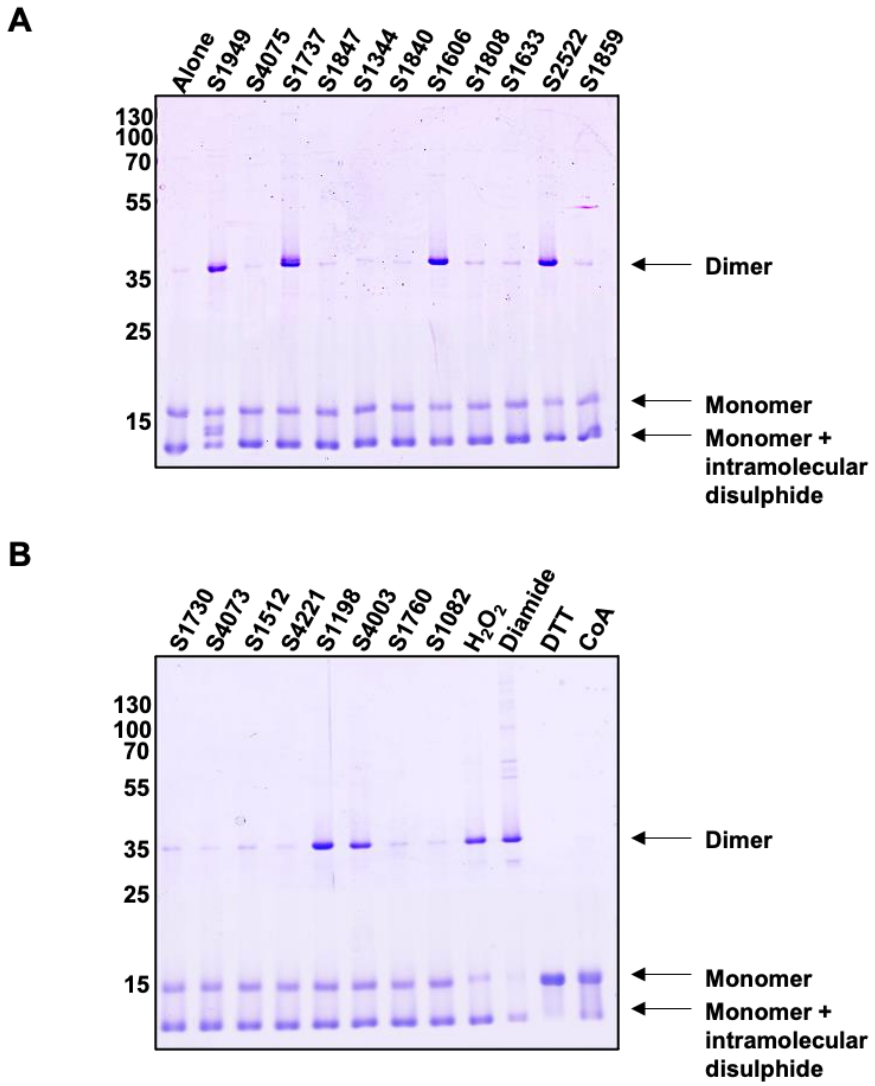

Figure 4.16. Analysis of NME1 by native PAGE after incubation with FDA library hits. 2 ug of purified recombinant wild-type NME1 was incubated for 30 minutes in the presence 200 µM of the indicated drug ad subjected to electrophoresis on a 15% acrylamide under non-reducing conditions.

Figures 4.16A and 4.16B demonstrate the oligomerisation status of wild-type NME1 after FDA-library hits pre-incubation. As previously shown in Figure 4.8A, when analysed in the absence of any compound or co-factor, three NME1 bands are typically resolved; a faint band at ~36 kDa, and two stronger bands at ~17 kDa and ~13 kDa, depicting a dimer and two monomers, one of which likely contains an intramolecular disulfide. When analysed in the presence of S1949 (menadione) however, an additional doublet migrated at a predicted mass between the ~17 kDa and ~13 kDa band, at ~15 kDa. Furthermore, the density of the dimer ~36 kDa band greatly increased. Since the strength of the lower band at ~13 kDa was reduced, it was hypothesised that the ~15 kDa doublet band had decreased mobility, which may be a result of a reduction in thiols due to compound modifications. In addition, the increase in the strength in staining of the dimer band in the presence of menadione is probably due to hexamer dissociation as a direct result of dimer stabilisation through disulfide bonds between Cys109, Cys145 and/or Cys4.

For the remaining compounds pre-incubated with NME1 in Figure 4.16A and B, the signal for the two monomeric bands was similar, suggesting that the monomer, and notably the intramolecular disulfide, likely forming between the Cys145 and Cys4 residues of NME1, was unaffected by these compounds. An additional NME1 band that was unaffected by the compounds was a very faint band at ~72 kDa, most notably in Figure 4.16A. In contrast, the population of the NME1 dimer appeared to be the most susceptible to change. Like S1949, S1737, S1606, S2522, S1198 and S4003 increased the density of the band migrating to ~36 kDa. Interestingly, the dimer of NME1 in the presence of S1737 migrated as a doublet, suggesting that the disulfide linkages involving Cys109, which stabilises the NME1 dimer are affected, as opposed to S1949, which appeared to affect the Cys145 disulfide linkages.

Strikingly, when C109A NME1 was analysed in the presence of these FDA-library hits (Figure 4.17), S1949 appeared to be the only compound that induced high levels of dimer population. Unlike NME1, the hexamer band at ~95 kDa was more prominent for C109A NME1, which was also the case for the native-PAGE results displayed in Figure 4.8B. When incubated with S1949, not only was the dimer band strength increased compared to C109A NME1 alone, but the hexamer band also increased and migrated as a doublet. Similar to WT NME1, an additional band between the two monomers at ~17 kDa and a weak ~14 kDa NME1 band, migrated to ~15 kDa, but did not appear as a doublet. A similar band pattern for the higher order C109A NME1 oligomers was displayed in the presence of S2522, with a stronger band at ~95 kDa. Furthermore, the density of C109A NME1 at ~17 kDa, indicative of a C109A NME1 monomer without an intramolecular disulfide bond, was reduced. In the presence of the oxidising agent H_2O_2, NME1 migrating at ~95 kDa and ~36 kDa increased in signal strength,

whereas the lower monomeric bands both appeared weaker. When incubated with diamide, it was observed that the ~95 kDa C109A NME1 hexamer band was stronger and migrated as a doublet. It was also noted that the monomeric C109A NME1 at ~17 kDa was almost undetectable.

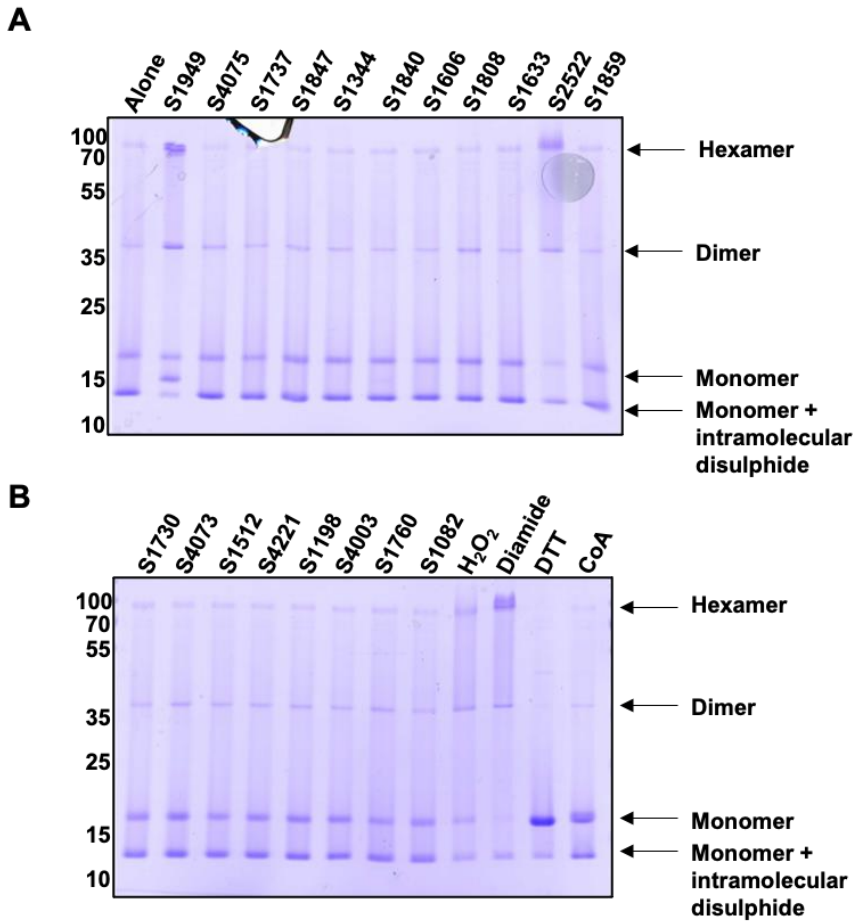

Figure 4.17. Analysis of C109A NME1 incubated with hits from the FDA-library by non-reducing PAGE. 2 ug of purified recombinant C109A NME1 was incubated for 30 minutes in the presence 200 µM of the indicated drug ad subjected to electrophoresis on a 15% acrylamide under non-reducing conditions.

As previously discussed in Chapter 3, the purified recombinant R105A NME1 mutant is a dimer under native conditions and in solution (Section 3.6.2). Because of this, it was necessary to analyse the impact of library hits on the native structure of R105A NME1 in comparison to WT NME1 by subjection to electrophoresis under non-reducing conditions. Firstly, in the absence of any FDA-library hit, R105A NME1 exhibits a very different migration pattern of R105A NME1 oligomers to WT NME1. For instance, several bands were observed surrounding both dimeric and monomeric molecular masses. Between ~33 kDa and ~37 kDa, three bands were revealed, with the strongest at ~36 kDa. Furthermore, three polypeptide bands were presented for R105A NME1 monomers at ~16 kDa, ~17 kDa and ~19 kDa. These additional bands displayed by R105A NME1 are likely due to more surface residues being

exposed as a result of the dimeric structure and changes in the hydrophobicity and charges of the secondary structure. When incubated with the FDA-library hits, the ~17 kDa band and the ~37 kDa band are much less pronounced or undetectable and for the majority of compounds, the bands surrounding the dimer mass were weaker. The exception to this was S1633, where a strong ~34 kDa NME1 band was observed and may therefore stabilise the dimer.

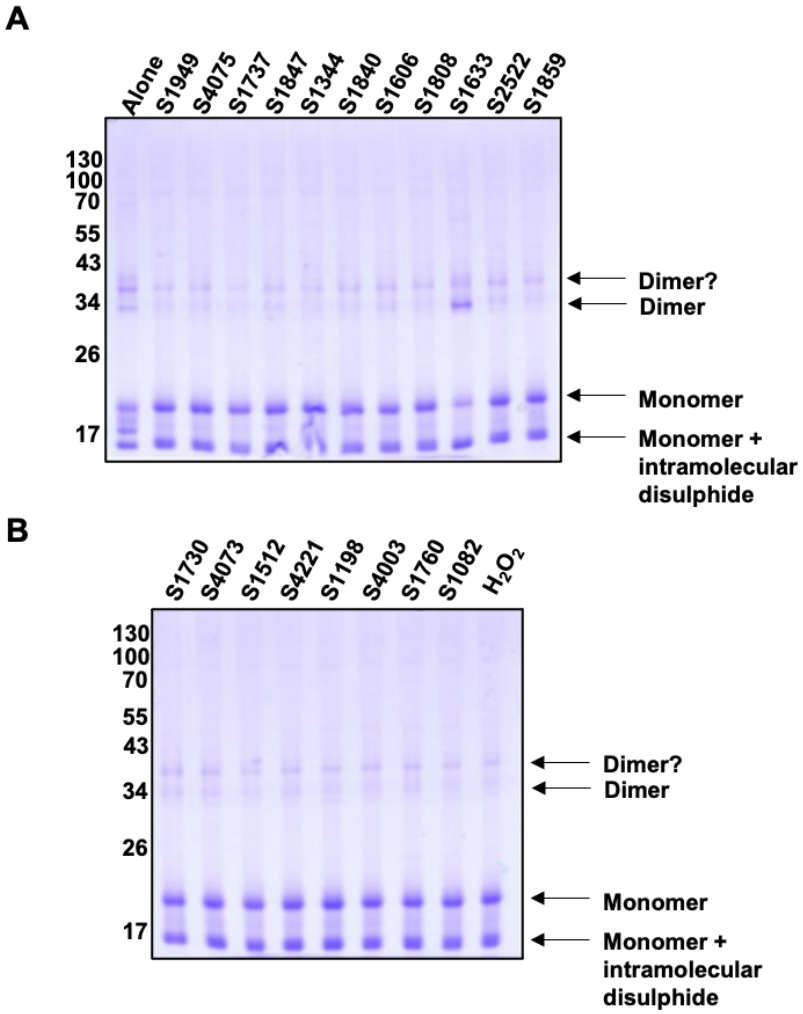

Figure 4.18. Analysis of R105A NME1 incubated with hits from the FDA-library by non-reducing PAGE. 2 μg of purified recombinant R105A NME1 was incubated for 30 minutes in the presence 200 μM of the indicated drug ad subjected to electrophoresis on a 15% acrylamide under non-reducing conditions.

To validate this data further and to assess the native structure of NME1 and these mutants in the presence of FDA-library compounds using an unrelated technique, native mass spectrometry (MS) was exploited. To do this, it was first necessary to determine how the protein structure is affected in the presence of a known binding partner and NTP substrate, ATP (Figure 4.19). After native MS analysis in the absence (Figure 4.19A) or presence (Figure 4.19B) of ATP, the hexamer structure of WT NME1 was maintained. This confirmed that higher order multimers and homohexamers are not formed in the presence of ATP. The small peak

identified with a molecular mass of ~109 kDa is most likely caused by a lack of resolution and overlapping peaks in the MS spectra (see appendix). When C109A NME1 and R105A NME1 were analysed in the absence and presence of ATP (Figure 4.19C to F), their protein structure was also preserved.

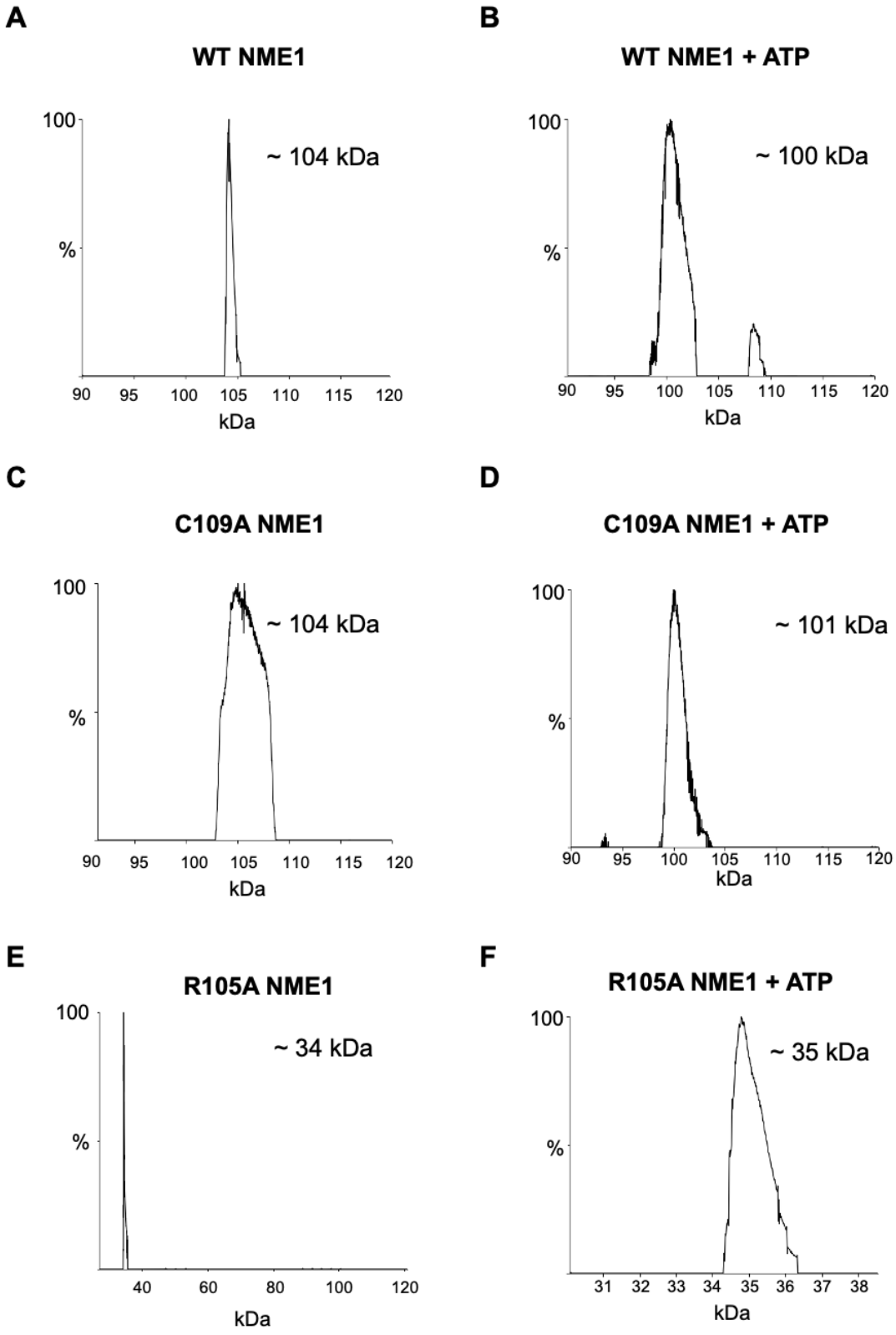

Figure 4.19. Oligomeric state of NME1 proteins determined by native mass spectrometry in the presence of ATP. 1 µg of purified recombinant (A) and (B) WT NME1, (C) and (D) C109A NME1 and (E) and (F) R105A NME1 were incubated in the presence of absence of 1 mM ATP for 10 mins at ambient temperature. Proteins were then buffer exchanged into 150 mM ammonium acetate using Amicon 10 kDa cut-off spin columns prior to MS analysis. Data analysis carried out using MassLynx 4.1 and figures created using UniDec.

NME1, C109A NME1 and R105A NME1 were also analysed in the presence of members of the FDA-library and a control DMSO solvent. FDA-library hits that in C109A NME1 displayed resistance to hexamer dissociation compared to WT NME1, are presented in Figure 4.20, and the results of all FDA-library hits are summarised in Table 4.1. In Figure 4.20, the output of the data deconvolution to determine the molecular mass of NME1 and C109A NME1 in the presence of S1949 (A and B), S1082 (C and D) and S4073 (E and F) were plotted. As shown in Figure 4.19A, the oligomeric structure of NME1 in the presence of S1949 under native conditions was revealed to be indicative of dimer of mass ~32 kDa, whereas C109A NME1 was identified as a m/z peak with a trimer mass of ~52 kDa. Similarly, in the presence of S1082, NME1 was observed to be a dimer at ~38 kDa and C109A NME1 a trimer at ~56 kDa. This resistance to hexamer dissociation displayed by C109A NME1 in the presence of potentially oxidising agents, was further exemplified when incubated with S4073, which remained a hexamer. In contrast, NME1 dissociated to a dimer in the presence of S4073.

The results obtained after native MS are summarised in Table 4.1 and in contrast to my native PAGE analysis, it was apparent that the majority of FDA-library hits resulted in the NME1 hexamer dissociating to a dimer, with the exception of S1198 (tetramer), S1344 (trimer), S1808 (trimer), S1840 (trimer), S4003 (trimer), S4073 (hexamer) and S4221 (trimer). Although dissociation of C109A NME1 to a dimer was only seen upon pre-incubation with S1457, S1730, S1760, S1808, S1847 and S4073, a change in the native C109A NME1 structure was revealed for most of the compounds. Furthermore, the R105A NME1 dimer is preserved in the presence of all compounds except S1457, S1082, S1737 and S4075, in which the latter three result in the identification of a hexamer, which is difficult to detect by native-PAGE analysis.

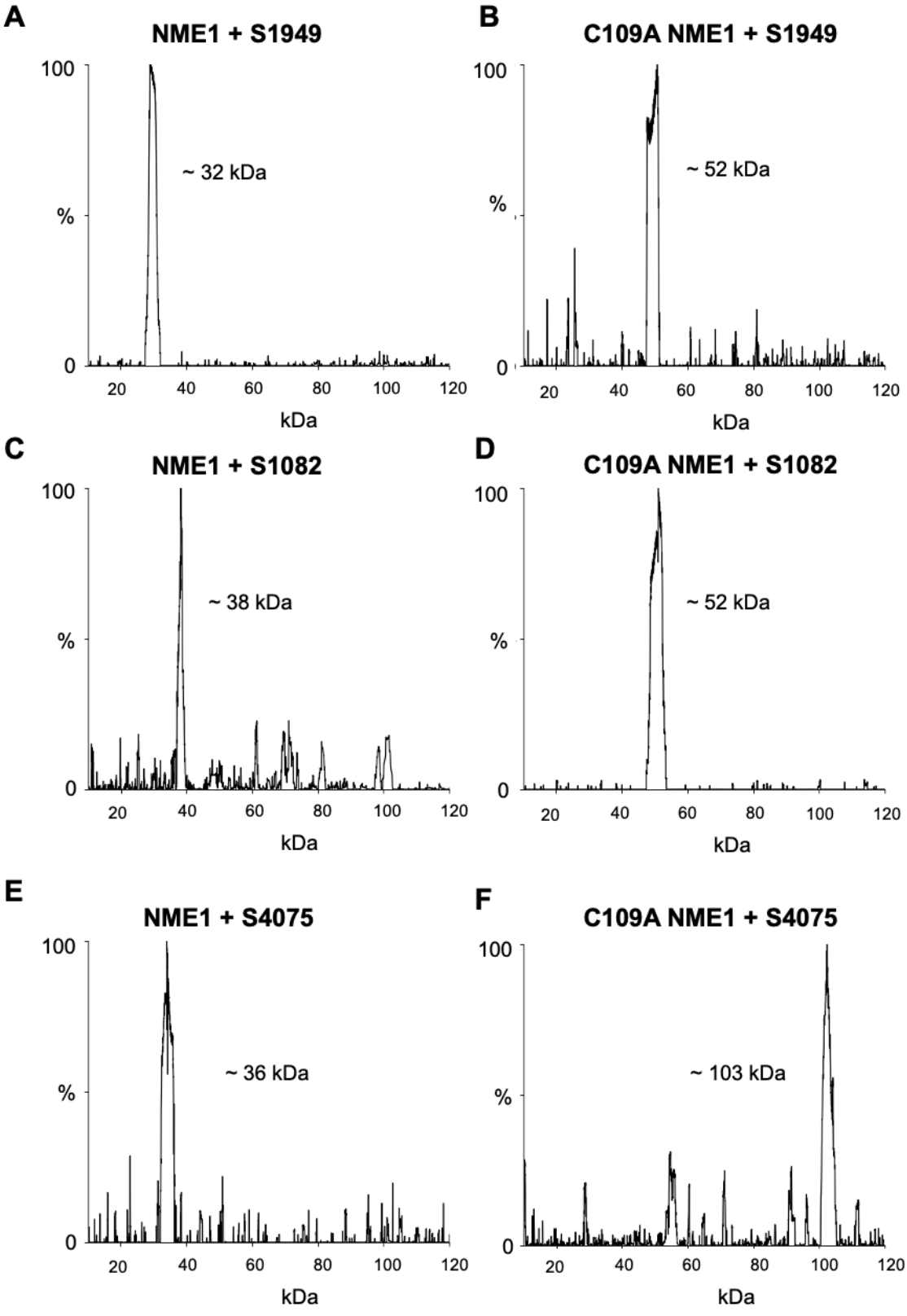

Figure 4.20. Oligomeric state of NME1 proteins with selected FDA drugs. Oligomeric determination for 10x excess compound with NME1 WT or C109A. Data analysis carried out using MassLynx 4.1 and figures created using UniDec. Protein buffer exchanged into 150 mM ammonium acetate using Amicon 10 kDa cut-off spin columns prior to MS analysis.

Compound	NME1	C109A NME1	R105A NME1
S1082 (Vismodegib)	Dimer	Trimer	Hexamer
S1198 (Irinotecan)	Tetramer	Hexamer	Dimer
S1344 (Glimepiride)	Trimer	Trimer	Dimer
S1457 (Atazanavir sulfate)	Dimer	Dimer	Monomer
S1512 (Tadalafil)	Dimer	Trimer	Dimer
S1606 (Clotrimazole)	Dimer	Trimer	Dimer
S1633 (Zafirlukast)	Dimer	Trimer	Dimer
S1730 (Indapamide)	Dimer	Dimer	Dimer
S1737 (Prednisolone)	Dimer	Tri/Hex	Hexamer
S1760 (Rifapentine)	Dimer	Dimer	Dimer
S1808 (Nifedipine)	Trimer	Dimer	Dimer
S1840 (Lomustine)	Trimer	Tetramer	Dimer
S1847 (Clemastine fumarate)	Dimer	Dimer	Dimer
S1859 (Diethylstilbestrol)	Dimer	Trimer	Dimer
S1949 (Menadione)	Dimer	Trimer	Dimer
S2522 (Adrenaline)	Dimer	Trimer	Dimer
S4003 (Lithocholic acid)	Trimer	Trimer	Dimer
S4073 (Aminosalicylate sodium)	Hexamer	Dimer	Dimer
S4075 (Zinc pyrithione)	Dimer	Hexamer	Hexamer
S4221 (Benzbromarone)	Trimer	Trimer	Dimer

Table 4.1. Oligomeric state of NME1 proteins with selected FDA library drugs determined by native mass spectrometry. Oligomeric determination for 10x excess compound with NME1 WT, C109A or R105A. Data analysis carried out using MassLynx 4.1. Protein buffer exchanged into 150 mM ammonium acetate using Amicon 10 kDa cut-off spin columns prior to MS analysis.

4.6. Analysis of NME1 nucleotide transferase activity in the presence of FDA-approved drug library drugs

To determine if library hits change the activity of wild-type NME1 protein as a function of the structural changes they elicit based on MS analysis, His118 autophosphorylation activity was analysed, both under non-reducing conditions and by using the monoclonal N1 histidine phosphorylation (N1 pHis) antibodies (Figure 4.21). In the absence of ATP, no band was seen for N1 pHis-containing NME1. In contrast, in the presence of ATP, three proteins were detected at ~15 kDa, ~18 kDa and ~32 kDa. NME1 at ~18 kDa and ~32 kDa possessed the strongest N1 pHis NME1 signal. The presence of three differentially-migrating NME1 proteins suggested that either each monomer within the multimer is histidine phosphorylated (199, 373), or that any N1 pHis present in the native structure prior to analysis was maintained under reducing conditions. As previously suggested, it was clear that these compounds had a greater effect on the NME1 dimer, however total loss of autophosphorylation activity was not observed in the presence of any of the compounds by western blot analysis.

The effects of compounds on NME1 autophosphorylation were further investigated by immunoblotting. For example, when the N1 pHis signal dropped for the NME1 dimer in the presence of a number of compounds, most notably S4073 (Figure 4.21B), it was difficult to determine whether autophosphorylation dropped for other higher order oligomer species as particularly in the case for S4073, the protein showed no sign of hexamer dissociation by native-PAGE or native-MS. However, the hexamer species was undetectable in both native-PAGE and western blot analysis. Furthermore, the level of monomeric N1 pHis signal varies in the ATP controls, making it difficult to clarify how the compounds changed it. On the other hand, it is apparent that the majority of those compounds that increased the population of NME1 dimer species, such as S1737, did not inhibit the level of autophosphorylation activity detectable by western blot analysis.

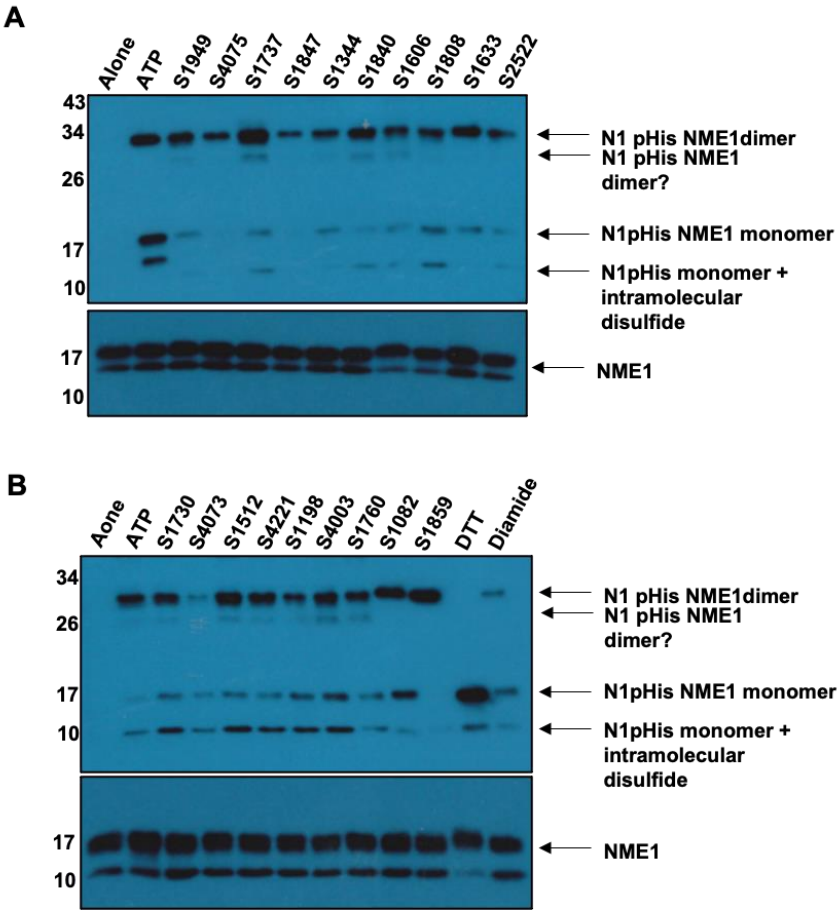

Figure 4.21. Western blot analysis of NME1 autophosphorylation in the presence of FDA-approved drug library hits under non-reducing conditions. 1 µg of purified recombinant NME1 was incubated in the presence or absence of 200 µM of the indicated drug for 30 mins at ambient temperature before the addition of the 50 µM ATP. One half of the reaction was split and heated to 95 ºC. The samples were then subjected to electrophoresis on a 15% acrylamide gel and immunoblotted using anti-N1 pHis antibody under non-reducing conditions. Total protein was determined using anti-NME1 antibody against the heat-treated samples.

The level of NME1 autophosphorylation activity appeared to be variably altered in different oligomer species in the presence of these FDA-library hits. As previously demonstrated by analysis of NME1 in the presence of CoA (Figure 4.10), pHis autophosphorylation is both rapid and very robust, and immunoblot analysis may not therefore be a reliable method to assess inhibition. Therefore, to further elucidate the extent of changes in NME1 enzyme activity that these compounds could elicit and whether these changes in autophosphorylation activity impact the NDPK activity of NME1, the PK/LDH coupled assay was employed (Figure 4.22). Additional compounds that were originally identified in the DSF screen and resulted in a change above 1.0 °C were also analysed. To ensure the assay was working efficiently, a no enzyme control was set up, encompassing all other reagents except the active enzymes and no change in absorbance was revealed. In the positive no compound control, the ΔOD_{340nm} after 10 minutes of the reaction was 0.42 AU for NME1 and 0.21 AU for PK. When analysed

using the PK/LDH coupled assay, no significant reduction in OD_{340nm} (indicative of decreased enzyme activity) was observed across both NME1 and the PK control. The greatest ΔOD_{340nm} was in the presence of S2453, at 0.38 AU respectively. Compared to the known inhibitor, CoA, this effect was considered negligible. However, due to solubility issues with compounds, concentrations of higher than 200 µM could not be tested, and as the substrate concentration below 300 µM did not elicit a suitable ΔOD_{340nm} for reliable measurement (Figure 3.30), it is possible that the compounds were outcompeted by both TDP and ATP. Although, pre-incubation with the compounds, particularly those that induce dimerization such as S1949 and S2522, potentially negate this view. In the presence of S1949 and S2522, the NDPK activity of NME1 did not appear to be affected and this suggested that the dissociation of the hexamer and dimer stabilisation did not reduce NDPK activity.

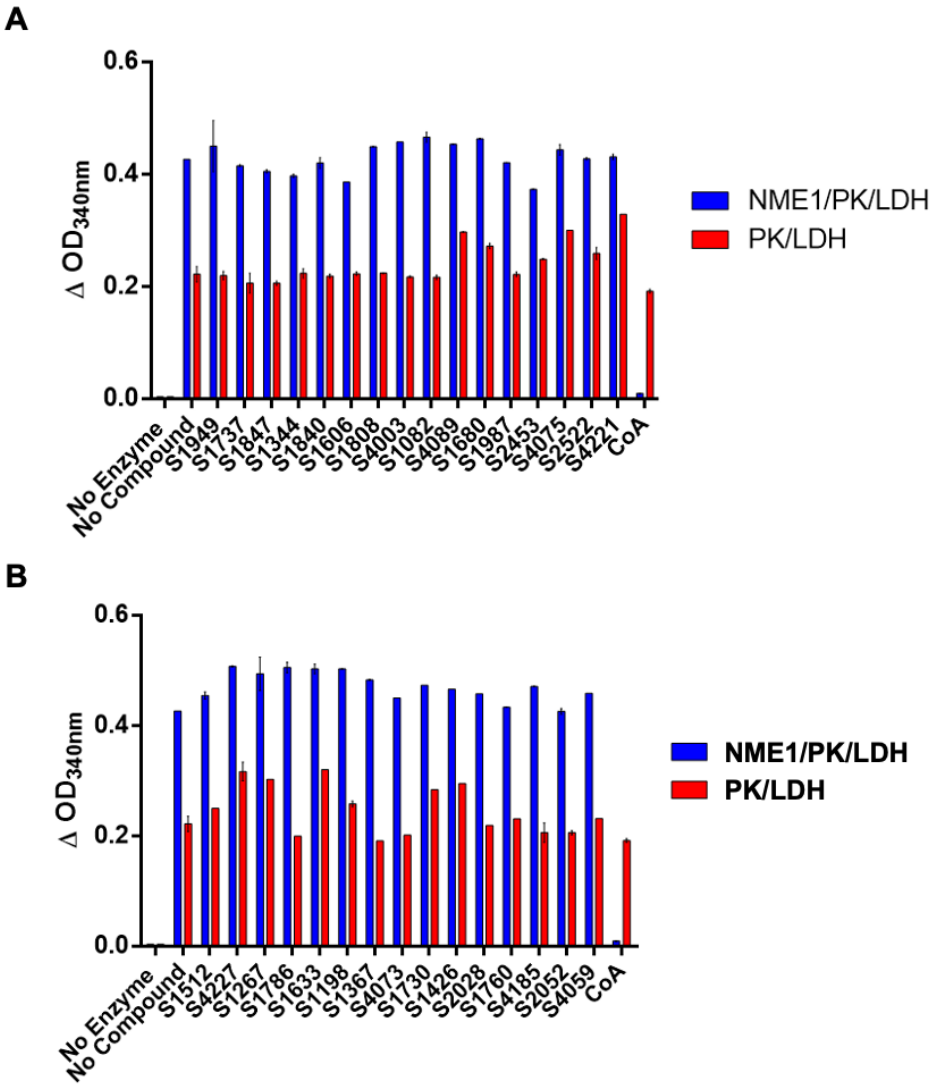

Figure 4.22. Analysis of the NDPK reaction rate of NME1 in the presence of FDA-approved drug library hits by the PK/LDH coupled assay. 25 nM NME1 was incubated in the presence or absence of 200 µM of the indicated drug before the addition of the 300 µM substrate (TDP for NME1 and ADP for the PK/LDH control) and the rate of NDPK reaction was analysed using the PK/LDH coupled assay (Section 2.14). The mean change (N=2) in OD at 340 nm over 10 mins is presented.

4.7 Proposed docking and binding methods of novel FDA-approved library drugs to NME1

To gain insight into how these known and novel NME1 ligands might interact with the NME protein structure, a collaboration was established with Jack Simpson, a PhD student in the group of Dr Neil Berry (School of Chemistry, University of Liverpool). The docking pose and binding interactions of CoA, S1949 (Menadione) and S2522 (Adrenaline), based on successful ADP docking replicated from the known NME1 crystal structure (PBD Code: 2HVD) (Section 2.23) and (Figure 4.23) was established. Due to this, this meant that the predicted binding site of these molecules was focussed to the known ADP binding site. The NME1 crystal coordinates were loaded into Spartan software, where the ADP molecule was removed and re-docked to ensure that the software mimicked the crystal structure pose accurately. Once this was done, the settings within the software were optimised until several poses of ADP in the NME1 crystal structure obtained RMSD's of $\leq$ 2.0. This ensured that the process was accurate and reliable enough to be brought forward for the docking of other molecules that currently do not have a solved crystal structure and to analyse and propose a method of binding for novel ligands.

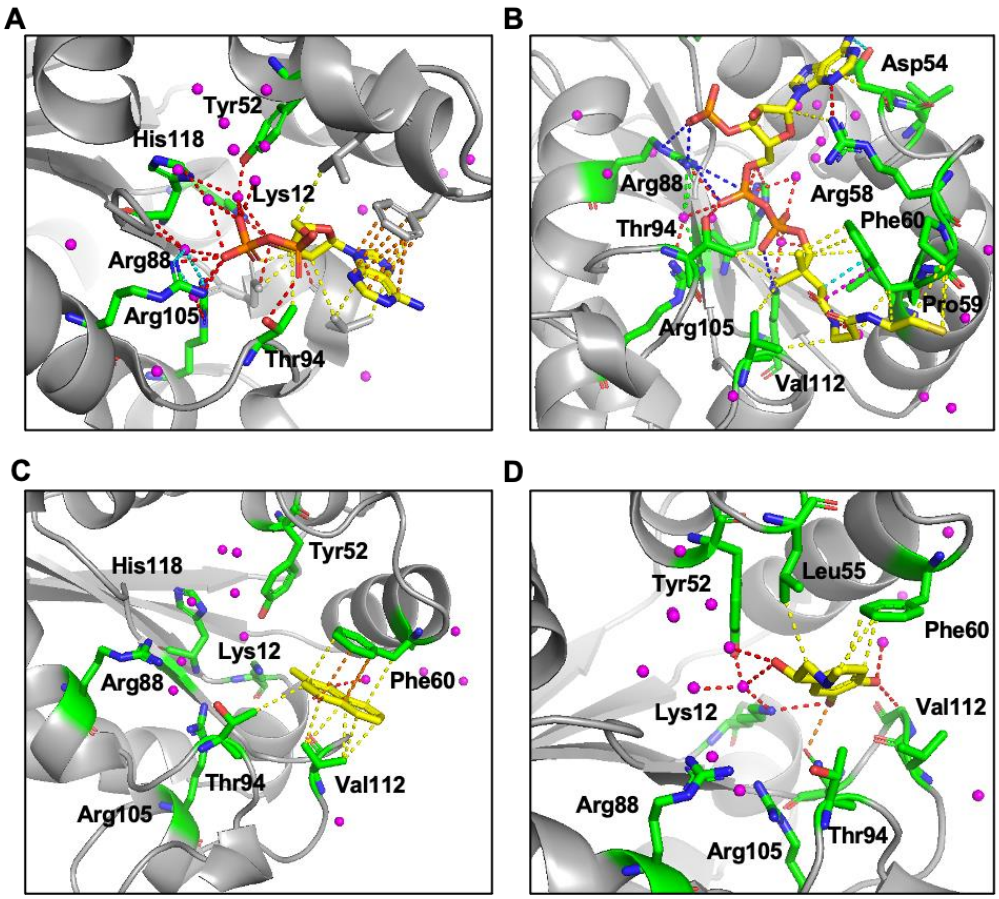

Figure 4.23. Computational modelling of NME1 ligand docking. (A) ADP (B) CoA (C) Menadione and (D) Adrenaline. Hydrogen bonds (red), cationic dip bond (cyan), pi-pi bonds (orange), van der waals (yellow) and water molecules (magenta) are shown. Residues of interest and that form interactions with the ligands are shown in green. PDB Code: 2HVD

Figure 4.23A displays likely interactions between a single ADP molecule and NME1 active site residues. In accordance with the literature, the adenosine ring is stacked against the aromatic ring of Phe60 and hydrogen bonds to Arg88 and Arg105 neutralise the phosphate groups (197-199). His118 also forms hydrogen bonds with the phosphate group of ADP, orienting the molecule for phosphate transfer (197, 407). As shown in Figures 4.23C and 4.23D, it was also observed that the stacking of the aryl rings present in both menadione and adrenaline might involve Phe60 and Val112, however the orientation of adrenaline appeared to be less favourable than menadione. Lys12, a key residue for NME1 enzyme activity (345), was not predicted to interact with menadione. In addition, the docking analysis showed that these molecules did not occupy as much space in the nucleotide binding pocket as ADP, and as a result, did not appear to interact with His118. Thus, the proposed method of binding that this analysis demonstrated may provide an explanation as to why they do not inhibit enzyme activity under the conditions tested.

In comparison to ADP, menadione and adrenaline, CoA is larger molecule. Surprisingly, in silico docking suggested that the adenosine ring did not occupy the same position as the adenosine ring does in ADP. Instead, hydrogen bonds and van der Waals interactions were observed between the adenosine ring of CoA and Arg58 and Asp54, which are not known to being involved in nucleotide binding. Furthermore, the sulfhydryl group of CoA may interact with Pro59. However, the orientation and binding of CoA in this model contradicts the evidence discussed here (Figure 4.6) since it suggests that the CoA binds to NME1 in a similar orientation to ADP which results in competitive inhibition of the NDPK activity. On the other hand, compared to menadione and adrenaline, this docking pose does highlight how CoA interacts with His118 and therefore could interfere with phosphate transfer to a nucleoside diphosphate.

4.8 Discussion

NME1 is an evolutionary conserved and multifunctional enzyme that was the first metastasis suppressor gene to be named; its downregulation is also indicative of poor patient prognosis (14). Despite extensive NME1 analysis there remains a lack of small molecule inhibitors with which to probe NME protein function *in vitro* or in cells. In this chapter, known co-factors, potential inhibitors and novel compounds identified in a screen were examined. Due to fundamental differences in NDP kinase structure and reaction mechanism when compared to protein kinases, a non-kinase focused library containing a panel of known drug chemotypes was used to screen for potential NME1 binders and inhibitors.

4.8.1 Comparative biochemical analysis of NME1 wild-type and NME1 active mutants

Through DSF, the thermal stability of wild-type and His active-site mutants of NME1, NME2 and PGAM were assessed in the presence of a number of different nucleotide derivatives. This demonstrated that the affinity displayed by NME1 and NME2, relative to ΔT_m values, was much greater for di- and tri-phosphorylated nucleotides than for monophosphorylated nucleotides. Indeed, when NME1 and NME2 were analysed in the presence of the nucleotides shown in Figure 4.2, ΔT_m values suggested that both proteins have a relatively high affinity for CoA, acetyl CoA and, most notably, PAP and PAPS. The established literature binding of PAP and PAPS (410), and much more recently CoA (417), is in accordance with these findings.
Investigating whether binding of nucleotides is affected by substitution of the active site His residue has not previously been evaluated. In this Chapter, I discovered that an Ala mutation at the conserved His118 residue in the active site of NME1 and NME2 negated ΔT_m values, suggesting abolition of binding. Although a H118A mutation does not change the hexameric nature of NME1 (Figure 3.15), loss in binding-affinity likely occurs through loss of an interaction with the phosphate moiety, which is transferred to His118 enzymatically (197). Unlike ADP and GDP, where binding to H118A NME1 and H118A NME2 increased in the presence of Mg^{2+} ions. CoA and its derivatives were unaffected by the presence of Mg^{2+} ions, meaning the added stability observed for ADP and GDP was not enough to maintain binding of these nucleotides, perhaps due to their larger size.

Evidence of the increased stability of PGAM, which likely infers the binding of PGAM to the 3'-phosphorylated nucleotides PAP and PAPS represents a new finding. These nucleotides appeared to bind to PGAM with a high affinity, yielding a change in melting temperature higher than, or equivalent, to that observed with NME1 and NME2 (Figure 4.5). Interestingly, this change in melting temperature was unaffected by the mutation of His11 to Ala, suggesting a novel mode of binding. A crystal structure in the presence of 2,3-DPG (DPG) has not been

reported for PGAM but interactions between the substrate and the protein can be inferred based on crystal structures of bacterial PGAM derived from *E. coli* in complex with the inhibitors vanadate and citrate (434-436). The key residues involved in substrate DPG and cofactor 3-PG binding include His11 and Tyr 92, as substitution of these amino acids abolish PGAM enzyme activity (436). Another residue involved in the regulation of catalytic activity was found to be Tyr26 (379). A highly disordered C-terminal tail and a loop segment which are mobile in solution, form a 'flexible gateway' to accommodate a variety of substrates and cofactors (436), which may account for the binding of the nucleotide test ligands described here that differ from the known physiological substrate, DPG. This would also provide an explanation as to why the H11A PGAM mutant still possesses affinity to PAP and PAPS. Furthermore, vanadate is an inhibitor of several other enzymes such as tyrosine phosphatases, sulfatases and sulfotransferases (437, 438), which also bind PAP and PAPS (439), suggesting that PAP and PAPS may bind in the same way as vanadate does to PGAM by mimicking a phosphate group in the substrate.

4.8.2 Investigating the effect of oxidising agents on NME1 structure and enzyme activity

The regulation of enzyme functions through oxidative modification is thought be a common adaptive mechanism in cells. For example, the oxidation of Cys to sulfenic or sulfonic acid is known to inactivate peroxiredoxins (440), phosphatases (441) and protein kinases (425). In comparison, oxidized Cys is essential for the proper function of matrix metalloproteases (442) and nitrile hydratases (443). NME1 is also thought to be redox sensitive *in vitro*, because oxidative stressors, such H_2O_2 have been shown to induce disulfide crosslinking (192). Inter- and intra-molecular disulfide bonds were discovered between Cys109, Cys145 and Cys4 (191) and to validate these findings and further investigate how NME1 is modified through redox regulation, cysteine mutants, C109A and C109A/C145A NME1 were purified and analysed.

To evaluate the impact of nucleotide derivatives on NDPK catalytic activity of NME1, the change in absorbance at 340nm was measured after pre-incubation with them and subjected to analysis via the PK/LDH coupled assay. In addition to nucleotide ligands reported previously, H_2O_2, an oxidative agent, was also analysed under similar conditions to determine how it affects NDPK activity. The data presented in Figure 4.6 revealed that the two nucleotides that decreased the NDPK activity of NME1, based on the lowest ΔOD_{340nm} after 10 minutes, were CoA and dephosphorylated (at the 3' position of the ribose sugar) CoA. Interestingly, acetyl CoA did not have the same effect. These results, including the analysis by DSF and the structural differences between the CoA derivatives (Figure 4.2) suggest that the increase in thermal stability of NME1, but not enzymatic activity, was dependent on the

phosphate group attached to the adenosine ring. Whereas the enzyme activity was subject to the presence of the sulfhydryl side chain in CoA and dephosphorylated CoA (deP CoA). This also highlights that analysis by DSF yielding a small ΔT_m value, particularly a negative value like that shown for deP CoA, does not necessarily indicate that a ligand is not binding or having a large impact on the protein, demonstrating the importance of exploiting a variety of techniques for experimental investigations.

The sulfhydryl group on CoA and deP CoA may be interacting with residues in NME1 important for phosphate transfer or interfere with enzyme activity through conformational changes. In order to further explore this, and to determine whether the sulfhydryl group interacts with residues within the active site or not, active site mutants, such as positively charged arginine residues that are most likely going to neutralise and interact with the sulphate group e.g. R88A, would need to be explored. In contradiction to the literature showing the 3'-phosphorylated nucleotides PAP and PAPS are inhibitors of NME1 enzyme activity, when tested here, activity was not detectably inhibited in their presence. However, as optimised previously (Figure 3.30), relatively high levels of NDP/NTP substrate were utilised in this assay, and as the K_d of PAP and PAPS is lower than NTP's or NDP's (410), PAP and PAPS may have been outcompeted by these in the assay mixture. What's more, this inhibitory effect was reported in NDPK from *Dictyostelium discoideum* (410), and may therefore not extend to the human NDPKs.

4.8.3 Utilising cysteine mutants to further explore NME1 structure and enzyme activity in the presence of nucleotide ligands

It is unclear whether CoA competitively inhibits NME1 by occupying the nucleotide binding pocket as if this were the case, acetyl CoA and not dephosphorylated CoA would likely reduce enzyme activity. However, Figure 4.6B confirms that in the presence of a set CoA concentration, the ΔOD_{340nm} increases relative to ATP concentration. Interestingly, CoA binding and inhibition of NME1 has been discovered previously in cells and *in vitro* (417), and this study concluded that CoA binds covalently and non-covalently to NME1, which might explain the findings in Figure 4.5, where the inhibition mechanism would likely be due to covalent (irreversible) inhibition. CoA binding was discovered to be dependent on experimental conditions, and the proposed covalent binding was evident under oxidative conditions and was reliant on Cys109. As previously stated, the cysteine residues of NME1 are important for response to oxidative stress, and Cys109 in NME1 could be a key redox regulator (408).

To gain further insights into this model, C109A and C109A/C145A NME1 mutants were also analysed by DSF in the presence of nucleotide analogues (Figure 4.7). The ΔT_m values

observed for C109A NME1 and C109A/C145A NME1 in the presence of the nucleotide test ligands decreased compared to WT NME1. This suggested that these residues are likely to be involved in binding. However, they are not critical as the changes in T_m were not abolished upon amino acid substitution. In fact, it may be that these nucleotides and CoA derivatives alter the conformation of the protein structure, yielding differences in T_m compared to the wild-type (WT). To verify this theory, native-PAGE analysis was carried out on these proteins in the presence of these ligands (Figure 4.8). Most notably, when proteins were analysed under non-reducing conditions, two monomeric bands in WT NME1 and C109A NME1 were observed, but one was absent for C109A/C145A NME1. This suggests that the fastest migrating band is likely a population of NME monomer with an intramolecular disulfide between Cys145 and Cys4.

The resistance to CoA interaction by mutation of Cys 109 to Ala reported by Song *et al* is likely due to prolonged pre-incubation with H_2O_2, since inhibition of C109A NME1 was evident under non-oxidative conditions and this is corroborated by my data, in which CoA inhibits both Cys mutants as well as the WT (Figure 4.9C). This revealed that inhibition is likely due to ATP/TDP competition and not inhibition by covalent binding. However, my data did suggest that another residue may play an additional role in thiol binding, as acetyl CoA does not inhibit the protein. To further explore this, the NDPK activity of the cysteine mutants pre-incubated with acetyl CoA and dephosphorylated CoA would need to be measured. When analysed by native-PAGE, CoA appeared to reduce WT NME1, as the monomeric band containing the Cys4/Cys145 disulfide was less apparent. This is further corroborated by the reduction in dimer population of WT NME1 with CoA whereas it increased with acetyl CoA.

In the presence of ATP, the density of the monomeric bands reduced, and higher order oligomers were stabilised, which is particularly prominent for C109A NME1. In fact, it appeared that in the absence of C109, the hexamer oligomer was stabilised. Lack of dimers in C109A/C145A NME1 indicated that Cys109 is not solely responsible for dimer stabilisation. The sulphide group in PAPS and APS does not seem to have the same effect on NME1 or C109A NME1 as in CoA. It is possible that under non-oxidative conditions, inhibition by CoA may be due to reduction of Cys4 as it is exposed on the surface of the protein structure and mutating Cys145 in addition to Cys109 does not cause resistance to CoA inhibition. Furthermore, the side chain of CoA could alter the conformation of the protein leading to an unfavourable position for disulfide cross linking.

In the presence of CoA and H_2O_2 the ΔT_m values of both WT NME1 and C109A NME1 change incrementally with increasing concentrations of both CoA and H_2O_2. In comparison to CoA,

H_2O_2 incubation resulted in ΔT_m values indicative of destabilisation. C109A NME1 was observed to be more resistant to the changes in T_m displayed by WT NME1. This is in accordance with the literature, as studies have demonstrated that due to the oxidative conditions induced by H_2O_2, Cys109 is thought to be exposed to the surface and in doing so forms disulfide bridges that promote hexamer dissociation. However, with the previous findings, this data demonstrates that mutating the Cys residue to Ala, does not result in a fully resistant protein, highlighting that there may be other factors involved. Furthermore, from Figure 4.9C, when the NDPK activity of NME1 and cysteine mutants was measured using the PK/LDH assay, CoA appeared to inhibit WT NME1 and both the cysteine mutants. This is likely due to the non-covalent binding of CoA and competitive inhibition with nucleotide substrates of NME1 and while my work was taking place, Gout and colleagues demonstrated that the NDPK activity of the catalytically active C109A mutant was still inhibited by CoA (417). However, in the presence of H_2O_2, the NDPK activity of WT NME1 was not affected, and as a result it was unclear whether the cysteine mutants were resistant to H_2O_2 oxidation. Other studies have demonstrated inhibition of NDPK activity by H_2O_2, however only substantial loss of activity was lost at 5 mM when pre-incubated for 2 hours prior to NDPK activity measurement (192), meaning a loss of NDPK activity may be undetectable for WT NME1 at 2 mM H_2O_2.

Although inhibition of NDPK activity in the presence of CoA was present (Figure 4.9), the autophosphorylation activity of NME1 in the Cys mutants did not appear to change, and was certainly not abolished (Figure 4.10). This may be due to the first half of the 'ping pong' reaction mechanism catalysed by NME1, in which the phosphate is transferred to the active site His118, not being greatly affected by CoA, or simply the differences in technique. On the other hand, when analysed in the presence of H_2O_2, an SDS resistant dimer was apparent for WT NME1 and C109A NME1. What's more, the level of autophosphorylation detected for the C109A NME1 monomer was reduced. This demonstrated that the dimer present under oxidative stress was stabilised by a disulfide link involving Cys145, and most likely Cys4, as the C109A/C145A NME1 protein was resistant to dimer formation, as well as a reduction in N1 pHis levels shown by WT NME1 and most notably, C109A NME1. However, it is difficult to determine if this is a true result. Due to the nature of the heat labile N1 pHis modification, samples processed for immunoblot analysis to detect N1 pHis are not heat-treated, although SDS is still present in order to denature the protein. As shown previously, the C109A NME1 hexamer is stabilised by the presence of ATP (Figure 4.8), meaning an SDS resistant N1 pHis hexamer undetectable by western blot may account for the reduction of N1 pHis monomer. This would explain why no reduction in NDPK activity was demonstrated by C109A NME1 in the presence of H_2O_2 in Figure 4.9.

Moreover, the dissociation of the hexamer does not necessarily result in a reduction in enzyme activity, particularly autophosphorylation activity. This is supported by the fact that the purified R105A NME1 mutant, which was found to be a dimer in solution, maintains its autophosphorylation activity. Therefore, in the presence of H_2O_2 or other oxidising agents, the N1 pHis signal across oligomers, may not be reflective of a reduction in activity.

4.8.4 Can small molecule NME1 inhibitors be discovered from unfocused libraries?

Published genetic work aimed at understanding molecular mechanisms underlying the ability of NME1 to suppress metastasis led to several observations demonstrating that NME1 binds to a variety of proteins and cofactors, for example the kinase suppressor Ras 1 scaffold protein. This, along with its role in metastasis suppression makes NME1 a desirable target for small molecules. To this end, a variety of clinically approved kinase inhibitors, including RAF inhibitors found to be novel inhibitors of TPST (326) and NME1's affinity for TPST substrates PAPS, were first analysed here by DSF (Figure 4.11A) and then analysed by the PK/LDH assay for NDPK activity (Figure 4.11B).

A selection of compounds that induced the largest ΔT_m values, such as vemurafenib, sorafenib, selemutinib and RAF-265, as well as staurosporine, a well-known broad spectrum protein kinase inhibitor, were pre-incubated with NME1 and the NDPK activity of the enzyme was measured. It was observed that rottlerin was the only compound that reduced the ΔOD_{340nm} and this did not appear to be a significant change. Vemurafenib greatly increased the change in absorbance after 10 minutes, however this was also revealed for the PK/LDH control, demonstrating that this change in absorbance is not specific to NME1.

As protein kinase and sulfotransferase inhibitors induced no detectable change in NDPK activity, despite evidence for thermal effects through DSF, a new analysis with an FDA-approved drug library was performed. When the structures of compounds that induced a ΔT_m value below -1.0 °C were studied (Figure 4.12), it became apparent that these compounds had the ability to oxidise NME1, for example S1949. Many other compounds, such as S2522 and S1082, that also resulted in the destabilisation of NME1, possess carbonyl groups that may cause oxidative stress and result in Cys-based modifications.

With this, and my data demonstrating that many FDA-library hits reduced the thermal stability of NME1 in a dose-dependent manner (Figure 4.14), it was necessary to analyse the more stable C109A mutant and the R105A NME1 dimer in the presence of a selection of compounds. Although in some cases, C109A NME1 and R105A NME1 were observed to

possess larger ΔT_m values than WT NME1 in the presence of compounds, many of the compounds were selected based on smaller ΔT_m values. These mutant proteins were thought to be more resistant to destabilisation, in particular hexamer dissociation in the presence of potentially oxidising compounds. Furthermore, the FDA-library hit counterscreen undertaken with a standard protein kinase, revealed that these selected compounds do not induce great changes in PKA thermal stability compared to NME1, reflective of selectivity towards NME1 (Figure 4.15C).

To analyse and obtain more qualitative data for purified recombinant NME1 and the mutants in the presence of these FDA-library hits, gel electrophoresis was carried out under non-reducing conditions (Figure 4.16 to 4.18). When analysed by native-PAGE, some compounds revealed an increase in the population of NME1 dimer, a similar result to pre-incubation with H_2O_2, suggesting that these compounds could be acting as oxidative stressors. However, in contrast to H_2O_2, the compounds did not affect the population of the monomers, as in the presence of H_2O_2 the band representing the monomer containing an intramolecular disulfide bond at ~12 kDa was stronger and in turn, the monomer at ~14 kDa was weaker. It is therefore likely that H_2O_2 induced disulfide cross-links between all Cys residues present, whereas the compounds may have had a greater effect on some Cys residues more than others. Cysteine residues can undergo different types of modifications and depending on the modification, migration during gel electrophoresis may be different. This may account for the differences seen in NME1 migration patterns of H_2O_2 and the FDA-library hits, however this could not be determined using this technique and would require mass spectrometry analysis for example.

The data presented in Figures 4.16, 4.17 and 4.18 determined the impact of mutating the residues Cys109 and Arg105 to Ala on protein structure and the consequence that this had on the protein response in the presence of the FDA-library hits. In contrast to WT NME1, C109A NME1 and R105A NME1 demonstrated resistance to increased dimer formation in the presence of S1737, S1606, S2522, S1198 and S4003 for example, whereas S2522 and S1949 increased the hexamer population of C109A NME1. This data confirms that NME1 is sensitive to redox regulation, in agreement with recent literature (408). In addition, the involvement of the Cys109 residue in dimer formation and stabilisation under oxidative conditions is verified (192) and that it is specific to the dimer oligomer as when R105A NME1 which still possessed Cys109, was analysed, no other higher order oligomers were produced. Furthermore, this data highlighted the importance of Cys residues in redox regulation and for NME1, in oligomer formation.

To further evaluate the impact of FDA-library hits on NME1, analysis by ion mobility mass spectrometry (MS) under native conditions was undertaken in the presence of ATP or compounds. NME1, C109A NME1 and R105A NME1 all demonstrate an ability to bind to ATP, and although it is clear that the oligomeric state of NME1 is dynamic and flexible under a variety of conditions and binding partners, pre-incubation with ATP did not alter the protein structure in a way that changed the quaternary and native fold of the protein (Figure 4.19). This was particularly true for the R105A NME1 'fixed' dimer, which did not form higher order oligomers after stabilisation by ATP (Figure 4.19), which could have been a possible explanation for its reduced autophosphorylation activity.

Strikingly, and in contrast to what was observed in the presence of ATP, when NME1 and the mutant proteins were pre-incubated with library hits, distinctive changes in the oligomeric state of NME proteins were clear. This data is summarised in Table 4.1, and selected compounds that revealed C109A NME1 resistance to dissociation compared to WT NME1 are presented in Figure 4.20. For example, in the presence of S4075, C109A NME1 remained a hexamer, whereas wild-type NME1 was identified with a molecular mass of a dimer. This was not detectable by native-PAGE, as the density of the dimeric NME1 band did not increase when incubated with S4075, however when analysed by DSF, the ΔT_m value of C109A NME1 was negligible compared to >5.0 °C for WT NME1 (Figure 4.15B). S4075, also known as zinc pyrithione, is known to dissociate to zinc salt and pyrithione in the cell (444, 445). Hyper-accumulation of zinc has been found to cause mitochondrial dysfunction associated with reactive oxygen species, which is linked to the reduction in ATP production (446-448). NME1 may detect the high levels of zinc and react to oxidative stress, dissociating the hexamer and this response may be inhibited in C109A NME1. On the other hand, the presence of sulphur and oxygen groups in S4075 may result in cysteine modification in WT NME1 but not C109A NME if zinc salts are formed when dissociated form pyrithione.

As discussed previously, S1949 is an oxidising agent, and from the data presented in this chapter, it is likely that S1949 is resulting in the oxidation of NME1, as supported by thermal destabilisation when analysed by DSF, and an increase in dimer population when analysed by native-PAGE. This was further corroborated through analysis by native MS, as when incubated with S1949, the molecular mass of the protein detected was ~ 32 kDa, distinctive of a NME1 dimer. C109A NME1 however, was revealed to have a molecular mass of ~54 kDa, which is representative of a trimer. When C109A NME1 was analysed by DSF in the presence of S1949, the ΔT_m value was lower than that displayed by WT NME1, but the thermal stability of C109A NME1 was reduced, suggesting that C109A NME1 maintained some resistance to dissociation. The dissociation of the hexamer to a trimer, as opposed to a dimer, may be due

to menadione yielding modifications in Cys145 and Cys4, as demonstrated by native-PAGE analysis and the presence of a monomer doublet migrating to ~ 13 kDa. This was not observed for any other compound tested and would explain why C109A NME1 was still affected. Dissociation to a trimer for C109A NME1 and a dimer for WT NME1 was also noted when pre-incubated with the compound S1082. Both S1949 and S1082 did not appear to interfere with trimer association in the C109A NME1 mutant protein, suggesting that the Kpn loop involved in trimer interaction remained intact in the presence of these compounds but was disordered in WT NME1, promoting dissociation to a dimer.

It also remains possible that in the gas phase, where 'native' MS is carried out, both wild-type NME1 and C109A NME1 were more sensitive to dissociation in the presence of these compounds compared to in solution. This would therefore shed light on the differences obtained by native MS and native-PAGE. However, the collective data does highlight the role of Cys109 in dimer stabilisation under oxidative stress, as it is clear that in the presence of compounds such as S1949 and S1737 for example, the C109A NME1 hexamer is less prone to dissociate, which is corroborated by both techniques.

4.8.5 In vitro analysis of NME1 with small molecule ligands

To further expand on these novel findings, the enzyme activity including autophosphorylation and NDP kinase activity of NME1 in the presence of the FDA-library hits were analysed. The autophosphorylation activity of NME1 was tested by immunoblot (Figure 4.21) and the NDP kinase activity was analysed through the PK/LDH coupled assay (Figure 4.22). It was revealed that under reducing (in the presence of DTT) and oxidising (diamide) conditions, N1 pHis autophosphorylation at His118 in the NME active site occurred, however this was reduced in the presence of diamide. This is most likely due to extensive cysteine modification and hexamer dissociation. Analysis by western blot clearly showed that the level of autophosphorylation on His118 varied in the different oligomeric species and under different conditions. For example, in reducing conditions, monomeric N1 pHis NME1 increased, and the N1 pHis dimer species was no longer present. Due to each monomer of the NME1 hexamer binding an ATP molecule, it is not surprising that each monomer becomes autophosphorylated at His118. However, this does make it difficult to make conclusions on the inhibitory effects of these compounds through western blot, as although the detected N1 pHis dimer species seemed to vary with different compounds it is not clear whether undetectable higher order oligomeric species maintain the activity of the enzyme in solution.

To combat this, the PK/LDH assay was employed and the NDPK activity was measured, which relies on the formation of the pHis enzyme intermediate. A ΔOD_{340nm} after ten minutes,

demonstrating the production of NAD^+ as a product of active enzymes within the assay system, was observed in the presence of all compounds. This indicated that the presence of these compounds, and apparent change in NME1 structure did not inhibit the NDPK activity in this assay. It is clear that the protein structure of NME1 can vary and the changes in the thermal stability of the protein, particularly negative shifts when analysed by DSF does not necessarily result in the enzyme activity of the protein being affected. For the library hits found here, the effects on the NME1 structure and stability may yield changes in the functional properties of NME1 that are unrelated to NDP kinase activity. The results found here therefore suggest that the catalytic activity of NME1 could be independent of its oligomerisation state.

Identifying new binding partners of NME proteins like these described in this Chapter could provide new insight into the cellular functions of the multi-faceted NME proteins, in particular with regard to oligomerisation linked to enzymatic activity. This might allow further exploration into the potential role of NME proteins role as elusive 'histidine kinases', as has been proposed through the transfer of phosphate in the NME1 pHis intermediate to other proteins *in trans*. However, pHis modifications and their roles within human cells are not very well understood. Chapter 5 utilises the knowledge gained from Chapters 3 and 4 to more thoroughly investigate NME1 and NME2 as putative protein histidine kinases.

Chapter 5: Investigating NME1 and NME2 as histidine protein kinases

Introduction

Despite the presence of Ser/Thr and Tyr phosphorylation in most prokaryotes and plants, it is believed that the dominant form of protein phosphorylation in these organisms is His phosphorylation catalysed by His protein kinases functioning as part of 'two-component' signal transduction systems (449-451). The imidazole ring of His contains two phosphorylatable N-containing atoms, so two possible isomers of phosphohistidine can be generated: N1 phosphohistidine (N1 pHis) and/or N3 phosphohistidine (N3 pHis) (11, 133). In bacteria and plants, pHis is critical for cell signalling, and plays a dominant role in the two-component signalling systems (TCS) (Figure 1.6) (12). In this system, a His kinase is linked to a membrane-bound receptor, which is activated through a sensor domain upon detection of an extracellular stimulus; this results in autophosphorylation on a conserved His residue in the receptor. Subsequently, the phosphoryl group is transferred enzymatically to a conserved Asp residue located in the regulatory domain of a response regulator protein (452-455). In bacteria, two-component signalling is important for environmental sensing, biofilm formation and in diseases and drug-resistance (456). In higher plants, pHis is connected to multiple regulatory mechanisms, including circadian rhythms, osmoregulation, cytokine and ethylene signalling (457, 458).

The activation of the response regulator protein, which is often a transcription factor, modulates the cellular response, or in more complex systems typically found in plants, the histidine kinase activates multiple phospho-relay reactions (459). The 'thermodynamic instability' of the phosphoramidate bond in N1 pHis or N3 pHis (133), as well as the phosphoanhydride bond in phosphoaspartate (460, 461), is postulated to facilitate these phosphoryl transfer reactions. However, the unstable nature of these bonds significantly impedes biochemical investigation into pHis-based cell signalling, since standard gel-based analysis and phosphoproteomics workflows both rely on acidic conditions or elevated temperatures for analysis, which are incompatible with the acid and heat-labile nature of pHis (133). As a consequence, eukaryotic studies into non-canonical phosphorylation have fallen behind compared to the study of heat-stable pSer/Thr/Tyr, and the extent to which pHis, pLys, pArg (and other non-canonical phosphorylation) on proteins contribute to mammalian cell signalling remains unclear.

However, with the development of new tools and protocols for experimental analysis, recent studies have shed some light on the characteristics and mechanisms of pHis in mammalian

cells (7-10). Indeed, phosphorylation on a His residue in histone H4 was one of the earliest described events driven by a still-unidentified histidine kinase (135, 279, 462). Moreover, the NME1 and NME2 enzymes have been proposed to function as His protein kinases, perhaps consistent with their well-characterised ability to employ a pHis intermediate during catalysis in their well-established roles as nucleoside diphosphate kinases. Moreover, to date, NME proteins are the only putative mammalian histidine kinases that have been characterised in any detail (7, 13).

Protein	His site	pHis isoform	Putative His Kinase	Reference
NME1	His118	N1 pHis	-	Wagner et al, 1995
NME2	His118	N1 pHis	-	Wagner et al, 1995
PGAM	His11	N3 pHis	-	Cantley et al, 2010
KCNN4 (KCa3.1)	His358	N3 pHis	NME2	Srivastava et al, 2006
Histone H4 (HisH4)	His18	N1/N3 pHis	Unknown	Chen et al, 1977
TRV5 (TRPV5)	His711	N3 pHis	NME2	Srivastava et al, 2014
SUCLG2	His105	N1 pHis	NME1	Kee and Muir, 2012

Table 5.1. List of pHis containing proteins and site of phosphorylation

NME1 and NME2 share 88% identity (463) and both bind to a variety of nucleotides including ATP (Chapters 3 and 4) however, they do not possess conventional substrate-binding features found in protein kinases. Moreover, these putative histidine protein kinases have been reported to phosphorylate different protein substrates on His residues (Section 1.8.3). For example, NME1 has been reported to phosphorylate succinate CoA synthetase (264, 464, 465), ATP-citrate lyase (466) and annexin A1 (8, 467), whilst NME2 phosphorylates the β-subunit of trimeric G proteins (296), the potassium channel KCa3.1 (243, 468) and the calcium channel TRPV5 (273). To evaluate this further, peptide sequences derived from a select few of these substrates, containing the pHis sites, were utilised for the experimental procedures described in this chapter (Table 5.1).

The aims of the work described in this chapter are:

1. Determine experimental conditions under which pHis can be detected in human cell extracts.
2. Explore the enzymatic activity of recombinant NME and NME isolated from human cells lines and establish whether phosphate can be transferred to an unphosphorylated His residue

3. Investigate the interaction and potential phosphorylation of NME1 and NME2 with peptides derived from putative His-containing substrates

5.1 Detecting global phosphohistidine (pHis) levels in human cell lines

To carefully investigate the ability of NME1 and NME2 to transfer a phosphoryl group onto a His residue in a protein substrate, both bacterially and human cell sources of NME1 and NME2 were utilised. To determine an appropriate human cell line in which to express NME, endogenous pHis levels were determined in human HeLa and HEK293T mammalian cell lines, both of which are ideal for transfection. To help understand conditions under which pHis can be detected and in order to generate appropriate controls and optimise experimental procedures, both cell lines and different lysis conditions were explored.

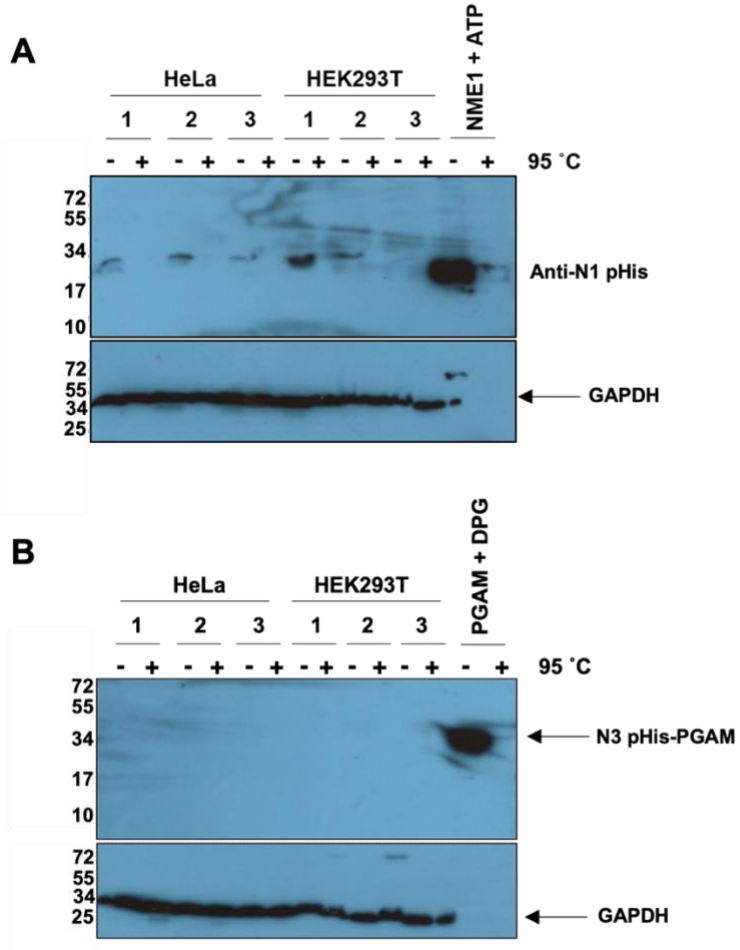

Figure 5.1. Thermal analysis of global pHis levels in human HEK293T and HeLa cells under different lysis conditions and blocked with 5% milk-TBST solution. HeLa or HEK293T cells were lysed in 2% SDS and 1% Triton-X100 (Condition 1), 2% SDS (Condition 2) or 1% Triton X-100 (Condition 3) (Section 2.21). Samples were split into two and one was heat-treated to 95 ºC for 30 mins. Recombinant NME1 and PGAM in the presence of phosphate donors ATP and DPG were used as positive controls. 50 µg samples of cell lysate were subjected to electrophoresis on a 15% acrylamide gel and processed for immunoblotting. The nitrocellulose membranes were blocked in 5% milk-TBST solution before being probed with (A) N1-phosphohistidine antibody or (B) N3-phosphohistidine antibody. Total cell lysate loaded was determined by stripping and reprobing the membrane for anti-GAPDH. A representative immunoblot is shown.

Figure 5.1 demonstrates three different conditions in which HeLa and HEK293T mammalian cells were lysed and lysates analysed by immunoblotting, using 5% low-fat milk-TBST, to evaluate N1-phosphorylated histidine proteins (Figure 5.1A) or N3-phosphorylated histidine proteins (Figure 5.1B). Lysates were split into two samples and one sample was heat-treated to 95 °C to confirm whether any proteins detected were heat sensitive (indicative of non-canonical phosphorylation) and not due to non-specific binding of the antibodies. Lysis conditions in a Tris buffer, but differing in types and therefore strength of detergent, were also compared (Section 2.21). One consisted of lysing HeLa or HEK293T cells in SDS sample buffer (2% SDS, 1% Triton X-100), as described by Hunter and colleagues (8, 9). In HeLa cell lysate, two major protein bands were detected at ~ 20 kDa and ~19 kDa, likely to be equivalent to endogenous pHis-containing NME1 and pHis-containing NME2. Upon heat treatment, these signals were no longer be detected. The second lysis condition comprised 2% SDS, but lacked 1% Triton X-100; in the HeLa cell lysate a polypeptide band at ~20 kDa was seen. A similar pattern was also detected under lysis condition three (no SDS, 1% Triton X-100) in a HeLa cell lysate, but the signal detected for N1 pHis was weaker than that seen when the first two lysis conditions were employed.

In HEK293T cell lines, identical lysis conditions were also compared. A signal consistent with NME1 was detected in HEK293T cell lysate using condition 1. This band was also shown in lysis condition two but to a lesser degree, and this signal weakened further for non-heat-treated lysis condition three. Across all lysis conditions in the heat-treated samples, the putative signal for an N1 phosphorylated protein was abolished. This is in broad accordance with data obtained using recombinant purified NME1 controls (Section 3.5). The presence of N3 histidine phosphorylated proteins in HeLa and HEK293T cell lysates was also examined (Figure 5.1B). In both cell lines, no N3 pHis proteins could be detected under any experimental conditions, although the purified recombinant PGAM control was detected.

To compare experimental procedures and conditions, identical cell extracts were processed using a 5% BSA-TBST (Figure 5.2). An additional sample, provided by Dr Christopher Clarke, comprising of HeLa cells lysed in 1% SDS, 1% deoxycholate and 1% NP40, was also analysed to further investigate how the difference in lysis conditions effects pHis detection. Figure 5.2A shows HeLa cell lysates under the different lysis conditions after western blot analysis using anti-N1 phosphohistidine and anti-N3 phosphohistidine antibodies with recombinant NME1 and PGAM in the presence of phosphate donor as a positive control. When probed for N1 phosphohistidine antibodies, the HeLa cell lysate in condition one detected a variety of signals, with the strongest present at ~19 kDa alongside a lower band of ~17 kDa. The ~19 kDa band

is consistent with the cleaved recombinant NME1 control, and likely represents endogenous NME1. As reported previously, NME2 migrates more quickly than NME1 during SDS-PAGE, (Figure 3.3) and appears below endogenous NME1 at ~17 kDa.

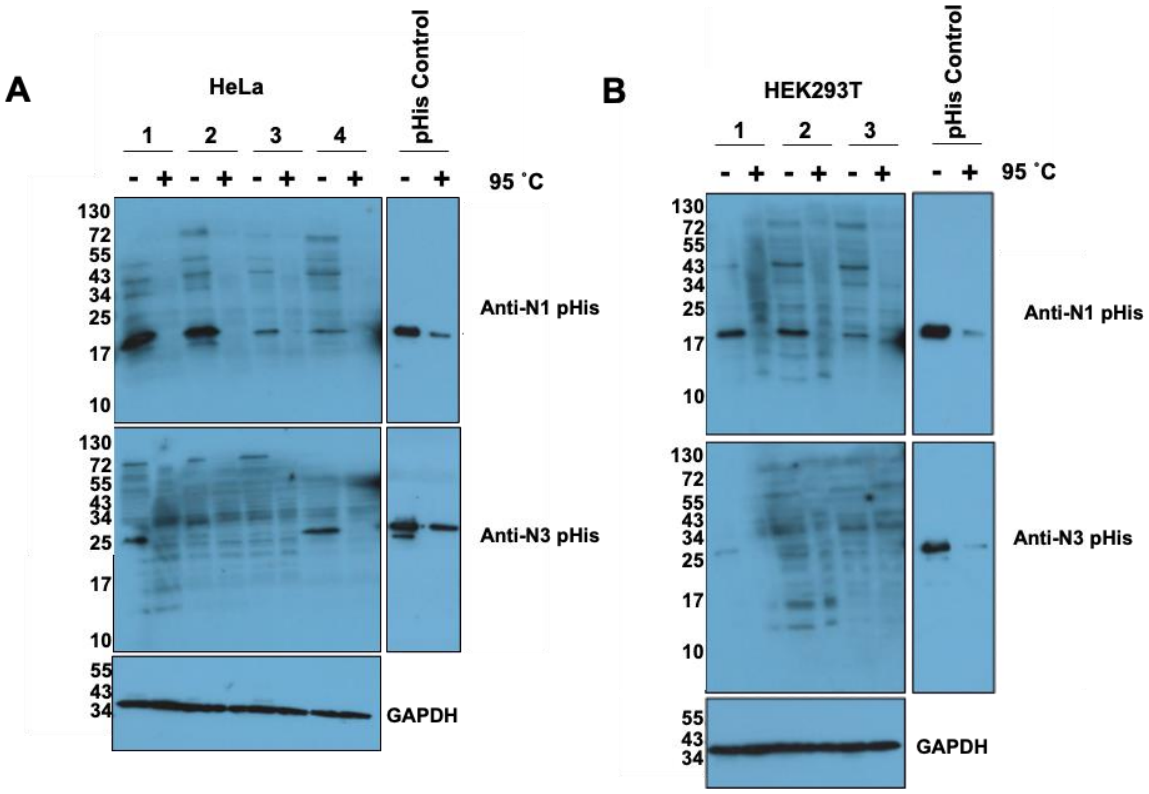

Figure 5.2. Thermal analysis of global pHis levels in human HEK293T and HeLa cells under different lysis conditions and blocked with 5% BSA-TBST solution. HeLa or HEK293T cells were lysed in 2% SDS and 1% Triton X-100 (Condition 1), 2% SDS (Condition 2) or 1% Triton X-100 (Condition 3) and for (A) 1% SDS, 1% deoxycholate and 1% NP40 (Condition 4). Samples were split into two and one was heat-treated to 95 ºC for 30 mins. Recombinant NME1 and PGAM in the presence of phosphate donors ATP and DPG were used as positive controls. 50 µg samples of cell lysate were subjected to electrophoresis on a 15% acrylamide gel and processed for immunoblotting. The nitrocellulose membranes were blocked in 5% BSA-TBST solution before being probed with (A) N1-phosphohistidine antibody or (B) N3-phosphohistidine antibody. Total cell lysate loaded was determined by stripping and reprobing the membrane for anti-GAPDH. A representative immunoblot is shown.

Cell lysates that were processed using western blot analysis were split in two and one sample was heat-treated to 95 °C. When this was done, only a faint band at ~25 kDa is detectable and as N1-phosphohistidine is heat labile, this is likely to be due to either non-specific antibody binding or the presence of a N1 pHis protein that is highly resistant to heat treatment. The identity of the signals at ~48 kDa, ~40 kDa, ~ 34 kDa, ~25 kDa in the non-heat-treated sample under lysis condition one are unknown, although they could be oligomers of NME1 or NME2, for example the band at ~34 kDa band that is detected corresponds to the molecular weight of a NME1 or NME2 dimer (see Section 3.6).

HEK293T mammalian cell lysates were analysed in the same way as HeLa cell lysates and as shown in Figure 5.1 under three different lysis conditions (Figure 5.2B). As before, samples were divided in two, and one half was heated at 95 °C for 30 minutes. In Lane 1, under lysis condition one, the non-heat-treated sample shows a protein band at ~19 kDa, and a weaker protein band signal at ~40 kDa. Under these same conditions, when heat-treated these bands were no longer detected. In the presence of only 2% SDS, the same ~19 kDa and ~40 kDa bands were detected, with the addition of a band at ~34 kDa and ~80 kDa. When lysed in 1% Triton X-100, bands detected in the HEK293T cell lysate was consistent with lysis condition two. In contrast to condition one, in lysis conditions two and three, the signal corresponding to a protein of ~40 kDa possessed a stronger signal, whereas endogenous NME1 at ~19 kDa.

The HEK293T cell lysates were also immunoblotted with commercial monoclonal anti-N3 pHis antibody in order to identify if any N3 pHis proteins are present. When lysed in condition one, a polypeptide band was detected at ~27 kDa which was not present when the sample was heat-treated. For lysis conditions two and three, it was not possible to determine specific binding from non-specific binding, but it was apparent that the ~27 kDa band detected in lysis condition one, was not detectable in these conditions. The pHis control, PGAM prepared in the presence of DPG in order to generate 3-His autophosphorylate protein (Section 3.5), migrated at a similar position to that established in lysis condition one and it is therefore likely to be endogenous N3 pHis PGAM.

NME1 and NME2 play a key role in nucleotide homeostasis and have been reported to employ their intrinsic nucleoside diphosphate kinase machinery to phosphorylate proteins on histidine residues (7, 180, 373). To test whether supplementation of cell lysate with active NME1 or NME2 could alter and/or enhance global pHis levels, a ‘spiking’ experiment was performed. As shown in Figure 5.3, no signal was detected at the position of endogenous NME1 or NME2, although the positive control revealed that the added NME1/2 were phosphorylated. When immunoblotted using N3 pHis antibodies, no bands corresponding to endogenous N3 pHis proteins were detected, with the exception of the recombinant PGAM N3 pHis control.

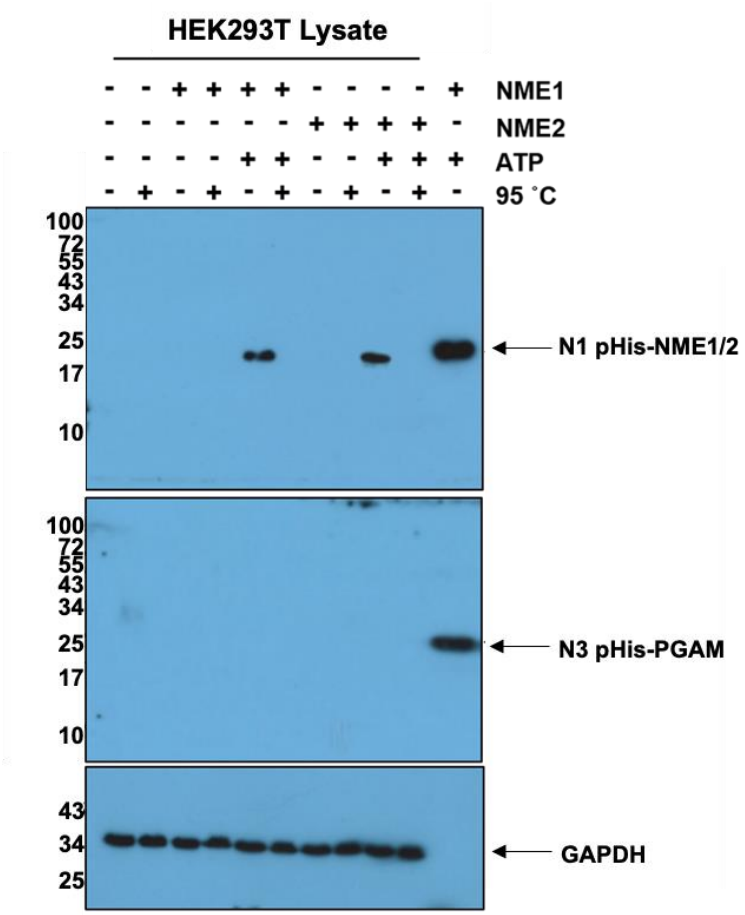

Figure 5.3. Thermal analysis of mammalian cell lysate 'spiked' with recombinant NME1 and NME2 in the presence and absence of ATP. 50 µg of HEK293T cell extract lysed in 1% Triton X-100 were incubated in the presence and absence of purified recombinant NME1, NME2 and 1 mM ATP. Samples were split into two and one was heat-treated to 95 ºC for 30 mins. 1 µg recombinant NME1 or PGAM in the presence of ATP and DPG was used as a ug positive control. Samples were then subjected to electrophoresis on a 15% acrylamide gel and processed for immunoblotting with (A) N1-phosphohistidine antibody or (B) N3-phosphohistidine antibody. Total cell lysate loaded was determined by stripping and reprobing the membrane for anti-GAPDH. A representative immunoblot is shown. Similar results were seen in a repeat experiment.

The next step taken to evaluate whether NME1 and/or NME2 were able to act as protein histidine kinases *in trans* was to determine whether they were capable of transferring a phosphate from their own active site histidine onto a separate NME protein. To this end, trans-phosphorylation on N1 or N3 of His amino acid present in 3C-cleaved untagged NME2 was analysed by western blot (Figure 5.4) (Section 2.23). In order to distinguish between trans-phosphorylation and cis-phosphorylation in this experiment GST-tagged protein was utilised to ensure excess ATP was removed from the histidine kinase being tested, in this case GST-tagged NME1. However, as an additional control, NME2 was also analysed in the presence of GST-tagged H118A NME1 (inactive) to determine whether the ATP was successfully removed. The GST-tagged proteins were incubated with glutathione beads and subsequently

ATP. The protein conjugated beads were then thoroughly washed to remove the excess ATP and to obtain pHis NME1.

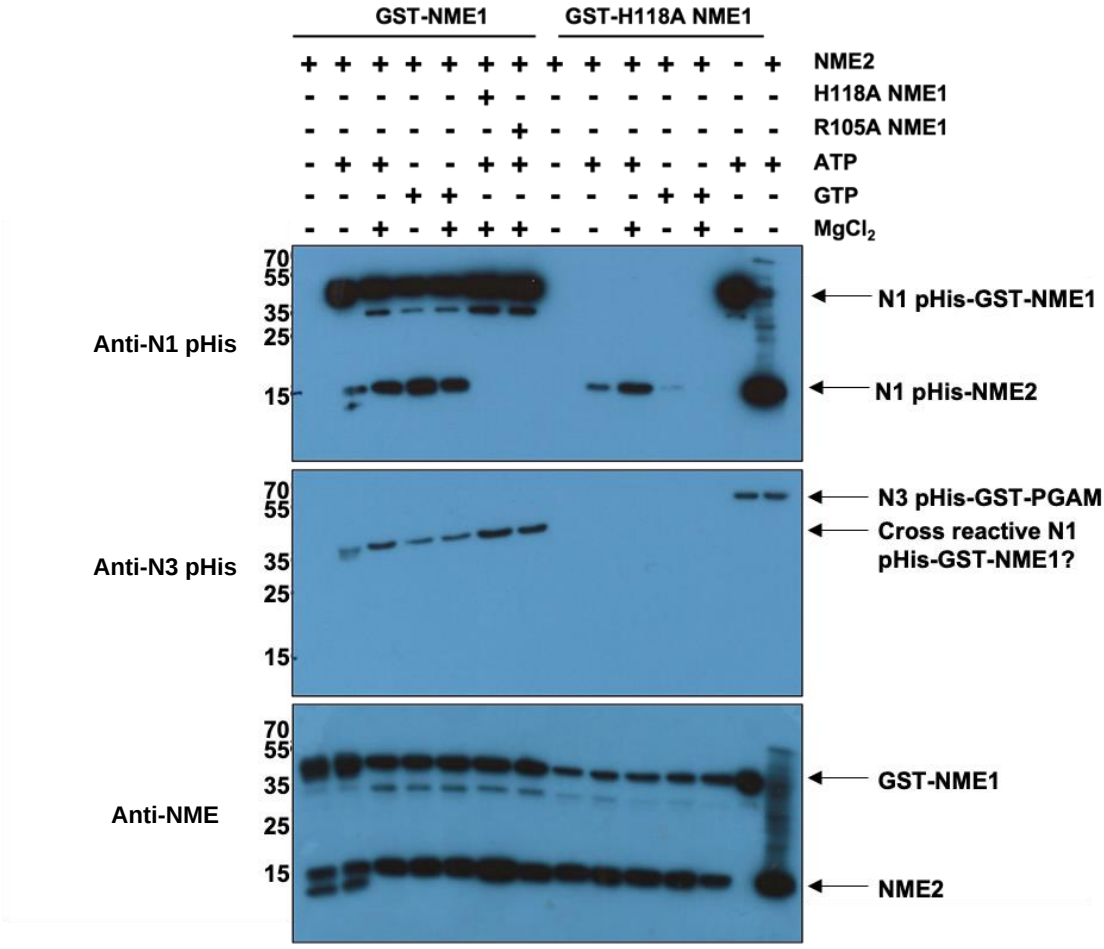

Figure 5.4. Analysis of potential trans-phosphorylation of NME on N1 or N3 pHis. 5 µg of GST-tagged NME1 or GST-tagged H118A NME1 were pre-incubated with glutathione Sepharose beads and 2 mM ATP and/or 10 mM $MgCl_2$. Excess ATP was removed and then 5 µg untagged NME2, H118A NME1 or R105A NME1 was incubated with GST-NME1 or GST-H118A NME1 for 30 mins at 25 ºC. Sample buffer was added to terminate the reaction. Samples were then subjected to western blot analysis by using an N1 pHis antibody or N3 pHis antibody. Samples were split in two and one was heat-treated at 95 ºC. Heat-treated samples were probed with anti-NME1 antibody to determine total protein.

In the absence of any ATP or untagged NME2, no N1 pHis NME1 was detected. When GST-NME1 and GST-H118A NME1 were incubated in the presence of ATP, in all conditions, only wild-type pHis GST-NME1 was detected by the N1 pHis antibody, and due to high levels of N1 pHis NME1 and therefore likely cross reactivity with the N3 pHis antibody, it was also detected when probed for N3 pHis. The GST-H118A NME1 protein was not detected by either antibody as expected. On the other hand, a signal for untagged NME2 appeared in the presence of ATP and GTP, both with and without the addition of $MgCl_2$. The observed signal was lower in the presence of ATP alone, and increased with $MgCl_2$, whereas in the presence

of GTP alone the signal for N1 pHis NME2 was highest, reducing after the addition of $MgCl_2$. No untagged N1 pHis H118A NME1 was evident in this experiment, consistent with a lack of pHis in these proteins. Untagged R105A NME1 was included in this experiment as it displays a reduced ability to autophosphorylate (Figure 3.19), but still possesses the active site His118 and because of this, it was hypothesised that it may be a potential target for trans-phosphorylation. Despite this, no N1 pHis R105A NME1 was revealed.

The presence of pHis-containing NME2 after incubation with GST-H118A NME1, ATP and ATP/$MgCl_2$ demonstrated that the excess ATP may not have been completely removed. This makes it challenging to determine whether or not the pHis NME2 present when incubated with the pHis GST-NME1 was a result of trans-phosphorylation. However, where the pHis NME2 signal was strongest, the level of pHis GST-NME1 was reduced compared to the GST-NME1 controls for example. Furthermore, when GST-H118A NME1 was pre-incubated with GTP and GTP plus $MgCl_2$ no pHis NME2 was observed, or the levels of pHis NME2 were undetectable via this method. This suggests, but does not prove, that trans-phosphorylation might be occurring in the presene of GTP.

5.2 Investigating the histidine kinase ability of recombinant NME1 and NME2 towards artificial substrates

In order to further explore pHis deposition in substrates by the putative histidine kinases NME1 and NME2, GST-fusion peptides containing a histidine amino acid previously shown to undergo phosphate transfer, were generated in bacteria and purified. Each peptide sequence was derived from the putative protein substrates shown in Table 5.1 and GST-peptide sequences are shown in Table 5.2.

Peptide	Sequence
NME1-tide	**QVGRNIIHGSDSVES**
NME2-tide	**QVGRNIIHGSDSVKS**
KCNN4-tide	**FRQVRLKHRKLREQV**
HisH4-tide	**GKGGAKRHRKVLRDN**
TRV5-tide	**LRQNTLGHLNLGLNL**
SUCLG2-tide	**SGLKGGVHLTKDP NV**

Table 5.2. Peptide sequences derived from putative substrates containing pHis site (highlighted in red)

The GST-fusion peptides were expressed in E. Coli and purified using affinity chromatography (Section 2.18). Once the peptides were eluted from the glutathione beads using reduced-glutathione (R-Glutathione), the identity of the proteins were confirmed by proteolytic cleavage with 3C protease. Each GST-peptide contained a 3C cleavage site (Leu-Glu-Val-Leu-Phe-Gln/Gly-Pro) to allow removal of the tag from the peptide in the presence of 3C protease, detected by a change in electrophoretic mobility. Figure 5.5 shows the unbound fraction that was collected prior to elution of each GST-peptides alongside the peptides after purification, both before and after proteolytic cleavage by 3C. Figure 5.5A and B demonstrate the appearance of proteins at the predicted molecular weight of ~25 kDa, corresponding to GST. For all GST-fusion peptides, this band migrates slightly more quickly in the presence of 3C protease, confirming the presence of the substrate peptide.

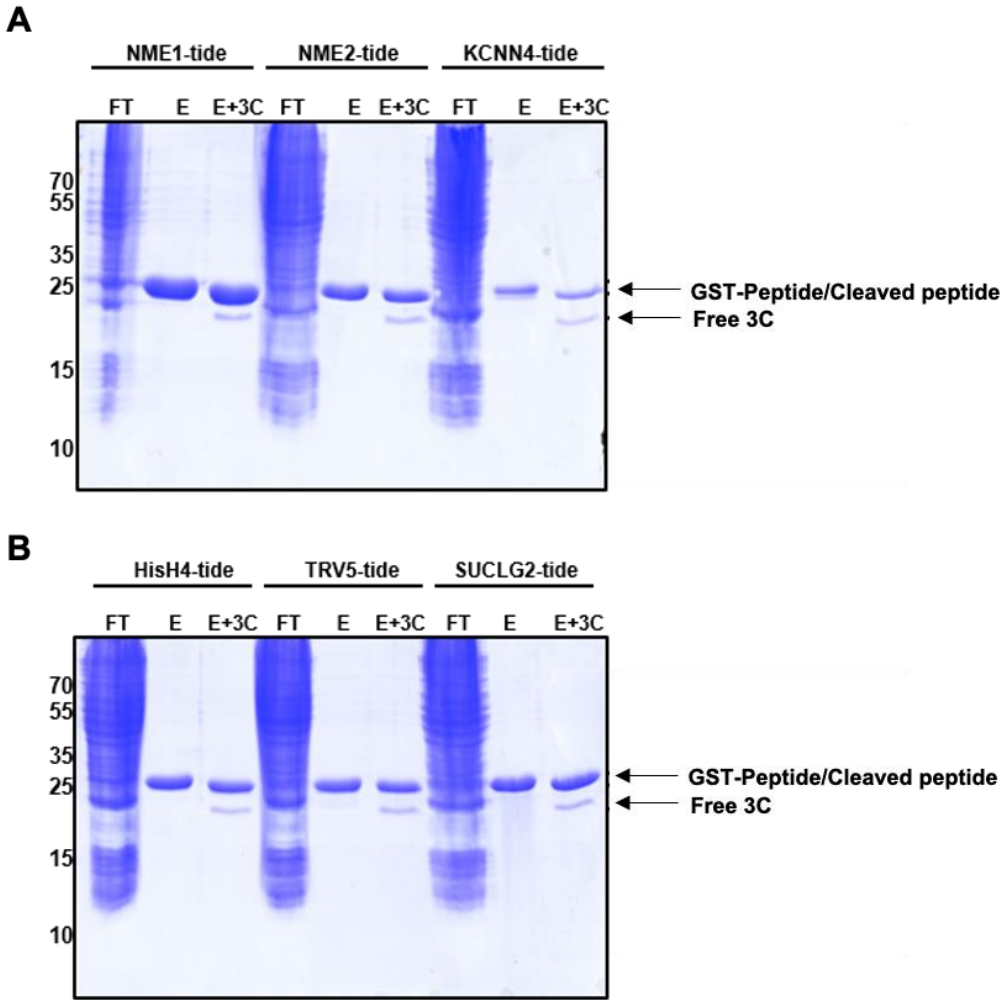

Figure 5.5. Purification and SDS-PAGE analysis of GST-His tagged putative substrate peptides. Lysates containing expressed GST-fused peptides were incubated with Glutathione Sepharose and bound peptides were eluted using competition with soluble Glutathione. The eluate was then incubated with 3C protease at 30 ˚C for 30 minutes. Samples of unbound flow-through (FT), eluate (E) and eluate incubated with 3C (E+3C) were subjected to electrophoresis on a 12% acrylamide gel.

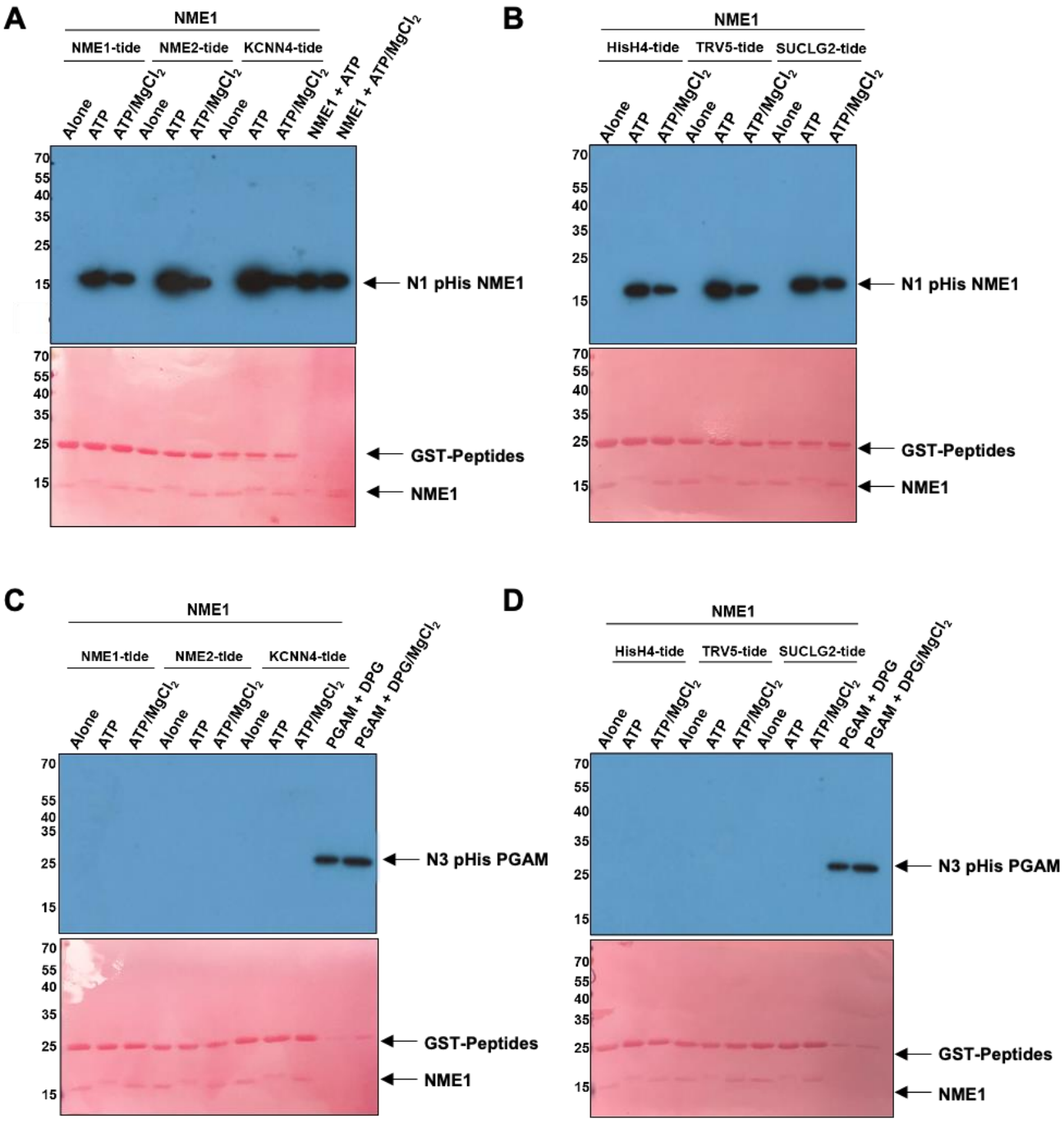

Figure 5.6. Western blot analysis of purified recombinant NME1 incubated with His containing GST-peptides. 1 µg of NME1 was incubated with 1 µg of the indicated GST-peptide for 10 minutes at ambient temperature before adding 500 µM of ATP in the presence and absence of either 10 mM $MgCl_2$ for 1 min before being resolved by SDS PAGE on a 15% acrylamide gel and analysed by western blot. Top panels: Samples were processed for western blot analysis using (A) and (B) N1-pHis or (C) and (D) N3-pHis antibody. Bottom panels: membranes were stained using ponceau to determine total GST-peptide and total NME1 protein levels.

I next used immunoblotting analysis to evaluate His phosphorylation before and after incubation of peptides (Figure 5.5) with enzymatically active NME1 (Figure 5.6) or NME2 (Figure 5.7) in the presence and absence of ATP and $MgCl_2$. Unfortunately, no evidence of peptide phosphorylation was present using N1 pHis antibodies, although the antibodies recognised N1 pHis in both NME1 or NME2.

The TRV5 and KCNN4 (KCa3.1) ion channels are both reported to be phosphorylated at the N3 position of His (273, 468). Therefore, these samples were also immunoblotted with anti N3 pHis antibodies (Figure 5.6C and D). However, no N3 pHis was detected at the appropriate position for the fusion peptide (~25 kDa), although the antibody detected PGAM in the presence of DPG, consistent with the presence of N3 pHis in the control. A similar result was obtained when purified recombinant NME2 was incubated with the indicated GST fused peptides (Figure 5.7) and no N1 pHis or N3 pHis signal was detected in the peptides. This shows that under these experimental conditions, recombinant NME1 and NME2 are unable to phosphorylate these peptides at the proposed site of His phosphorylation reported in the full-length proteins. However, it remained possible that since excess ATP or ADP would occupy the nucleotide binding pocket of NME1 and NME2, this might continuously catalyse the forward and reverse reaction of the nucleoside diphosphate kinase reaction (Figure 1.9), leading to loss of pHis in a protein substrate.

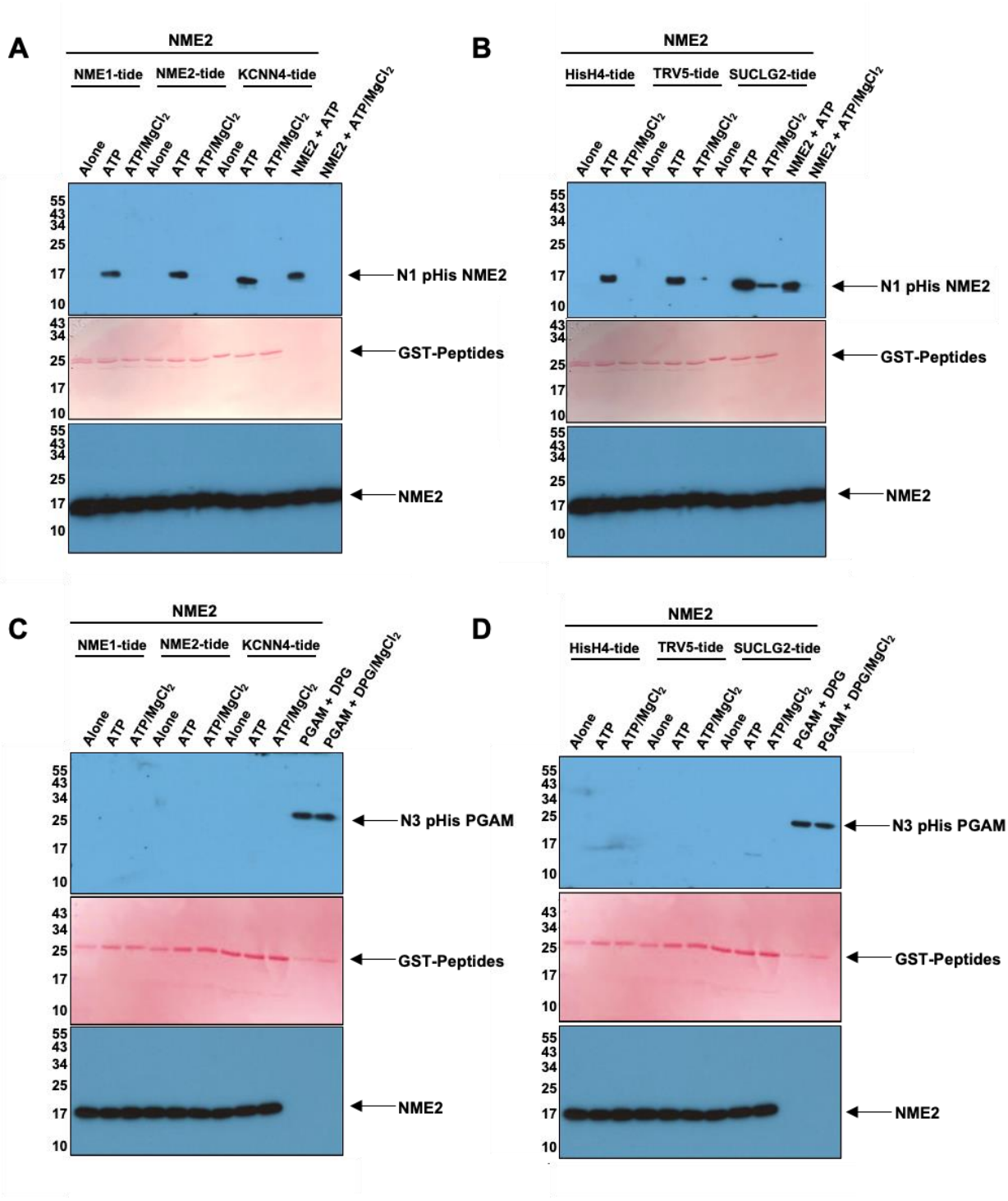

Figure 5.7. Western blot analysis of purified recombinant NME2 incubated with His containing GST-peptides. 1 µg of NME2 was incubated with the indicated 1 µg GST-peptide for 10 minutes at ambient temperature before adding 500 µM of ATP in the presence and absence of either 10 mM $MgCl_2$ for 1 min before being resolved by SDS PAGE on a 15% acrylamide gel. Top panels: Samples were processed for western blot analysis using (A) and (B) N1-pHis or (C) and (D) N3-pHis antibody. Middle panels: Membranes were stained using ponceau to determine total GST-peptide. Bottom panels: Samples generated for the top panel were split into two reactions and one half was heated-treated at 95 ˚C and analysed by western blot using anti-NME1 antibody to determine total NME2 protein.

To investigate this further, excess ATP removed from His-phosphorylated purified recombinant NME (Section 2.15) and an experiment performed with either pNME1 (Figure 5.8) or pNME2 (Figure 5.9) in the presence of GST-peptides was carried out. These proteins were already phosphorylated on His118, and no nucleotide substrate was added to the reaction mixtures, to evaluate if phosphotransfer could occur. The controls in this experiment were GST, to ensure that any phosphate transfer observed was not transferred to GST itself and pNME incubated with ADP. Like that shown in Figure 3.28, pHis signal of pNME reduced in the presence of ADP, indicative of phosphate transfer, and was therefore utilised as a benchmark for histidine protein kinase activity. For both pNME1 and pNME2, no histidine protein kinase activity was observed when analysed by western blot. This was apparent as no band at ~25 kDa was revealed when incubated with the GST-peptides, indicating no phosphate was transferred to a His residue at either the N1 or N3 position on these peptides. Furthermore, the only reduction in N1 pHis NME signal was revealed in the presence of ADP, a substrate of the NDPK reaction.

Once more, the samples were analysed utilising the N3 pHis antibody. However, apart from the PGAM N3 pHis control, no signal was detected. Figure 5.8C shows a control experiment involving the Tyrosine kinase EPHA3 and a substrate peptide, GST-tagged STAT5 (provided by Dr Dominic Byrne). This experiment was carried out in order to verify the ability of GST-fused peptides to become phosphorylated. EPHA3 autophosphorylates on several Tyr residues, including Tyr602 and Tyr770 (469-471) and when immunoblotted with pTyr antibodies, it was apparent that EPHA3 could be detected. When incubated with GST-STA5 alone and ATP, only pTyr EPHA3 was observed, whereas in the presence of ATP and $MgCl_2$, pTyr containing STA5 could also be detected, indicating that the assay was functional for canonical phosphorylation.

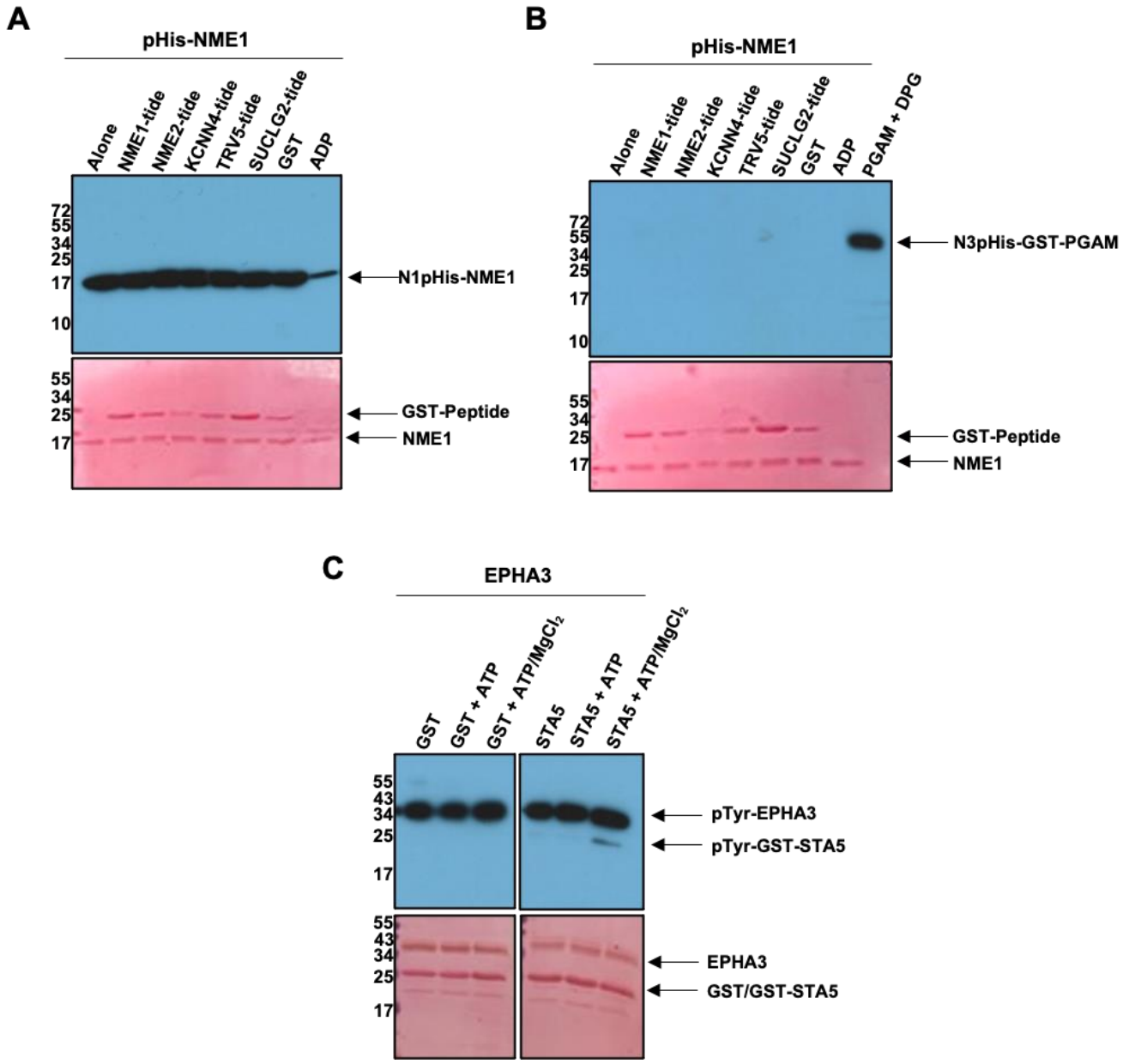

Figure 5.8. His-containing GST-peptides incubated in the presence of pHis NME1 and analysed by western blot. 500 ng of histidine phosphorylated (pHis) NME1 was incubated in the presence of 1 µg indicated GST-peptides and resolved on a 15% acrylamide gel before being subjected to immunoblot analysis with (A) N1-phosphohistidine antibody or (B) N3-phosphohistidine antibody. 1 µg of GST and 2 mM ADP were used as controls. Total GST-peptide and total NME1 protein was determined by ponceau staining. (C) 500 ng of EPHA3 was incubated with 1 µg of GST-fused STA5 peptide and subjected to immunoblot analysis using a phosphotyrosine (pTyr) antibody. Total protein was determined using an antibody against anti-His.

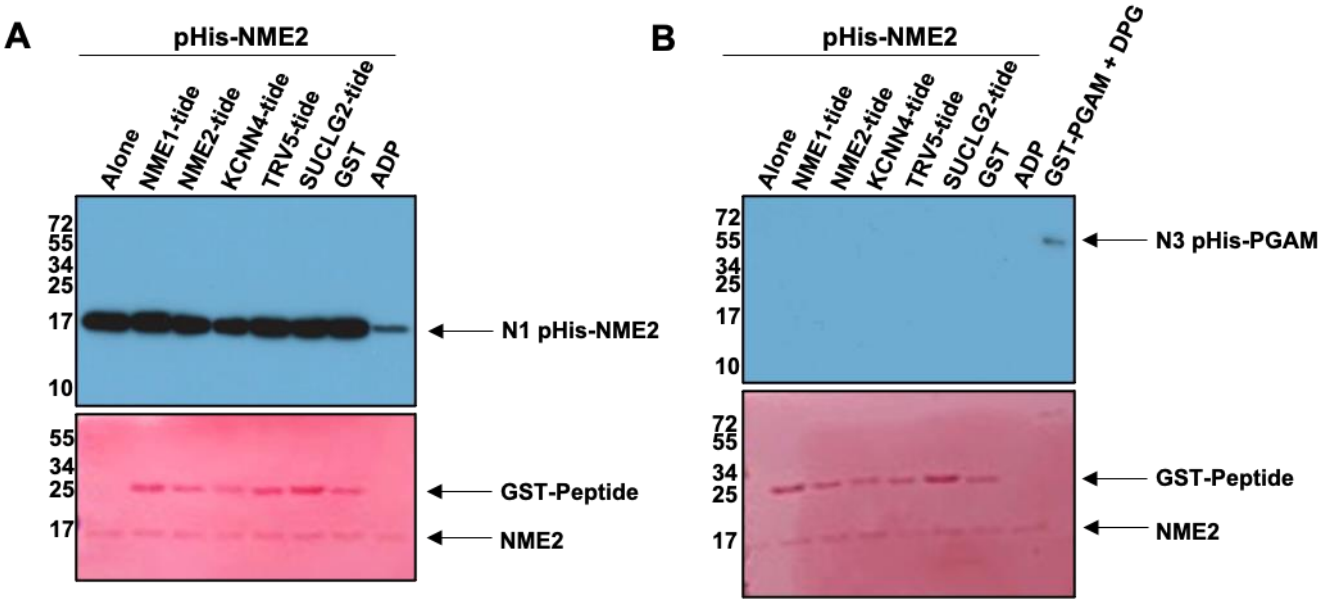

Figure 5.9. His-containing GST-peptides incubated in the presence of pHis NME2 and analysed by western blot. 500 ng of histidine phosphorylated (pHis) NME2 was incubated in the presence of 1 µg indicated GST-peptides and resolved on a 15% acrylamide gel before being subjected to immunoblot analysis with (A) N1-phosphohistidine antibody or (B) N3-phosphohistidine antibody. 1 µg of GST and 2 mM ADP were used as controls. Total GST-peptide and total NME2 protein was determined by ponceau staining.

In Chapter 3, I showed that the R105A NME1 and NME2 mutants were enzymatically active and were able to autophosphorylate on His in the active site (Figure 3.19) despite a marked change in overall protein structure from a hexamer (wild-type) to a dimer. When analysed by intact MS, the percentage of protein that underwent a mass shift consistent with addition of a phosphate group was higher in the presence of $MgCl_2$ (Figure 3.21). Canonical Ser/Thr protein kinases, such as Aurora A, and tyrosine kinases, such as EPHA3 (Figure 5.8C) require ATP *and* Mg^{2+} ions for enzyme activity. In contrast, autophosphorylation of wild-type NME1 and NME2 is partially inhibited by $MgCl_2$ (Figure 3.5 and 3.6), and they do not require this co-factor for the NDPK reaction. I therefore speculated that since the R105A mutant protein bound Mg-ATP, it might now possess a protein kinase-like activity, and evaluated if any histidine kinase activity could therefore be detected towards peptides.

To do this, in a similar way to recombinant wild-type (Figure 5.6 and 5.7), R105A NME1 was incubated with the indicated GST-fused peptides in the presence and absence of ATP and $MgCl_2$ and analysed by western blot (Figure 5.10). In Figure 5.10A and 5.10B, when immunoblotted for N1 pHis, a signal for R105A NME1 was demonstrated in the presence of both ATP alone, and ATP plus $MgCl_2$, with a stronger signal being detected for the latter, which is again, more characteristic of a canonical protein kinase. This was consistent with my

previous MS data (Figure 3.21). However, no N1 or N3 pHis signal was detected in any GST-peptides tested using R105A NME1. This demonstrated that mutating Arg105 to Ala has no effect on protein histidine kinase activity in NME1. This finding is further supported by analysis of R105A NME2, where the absence of any signal for N1 or N3 pHis in GST peptides was again evident (Figure 5.11).

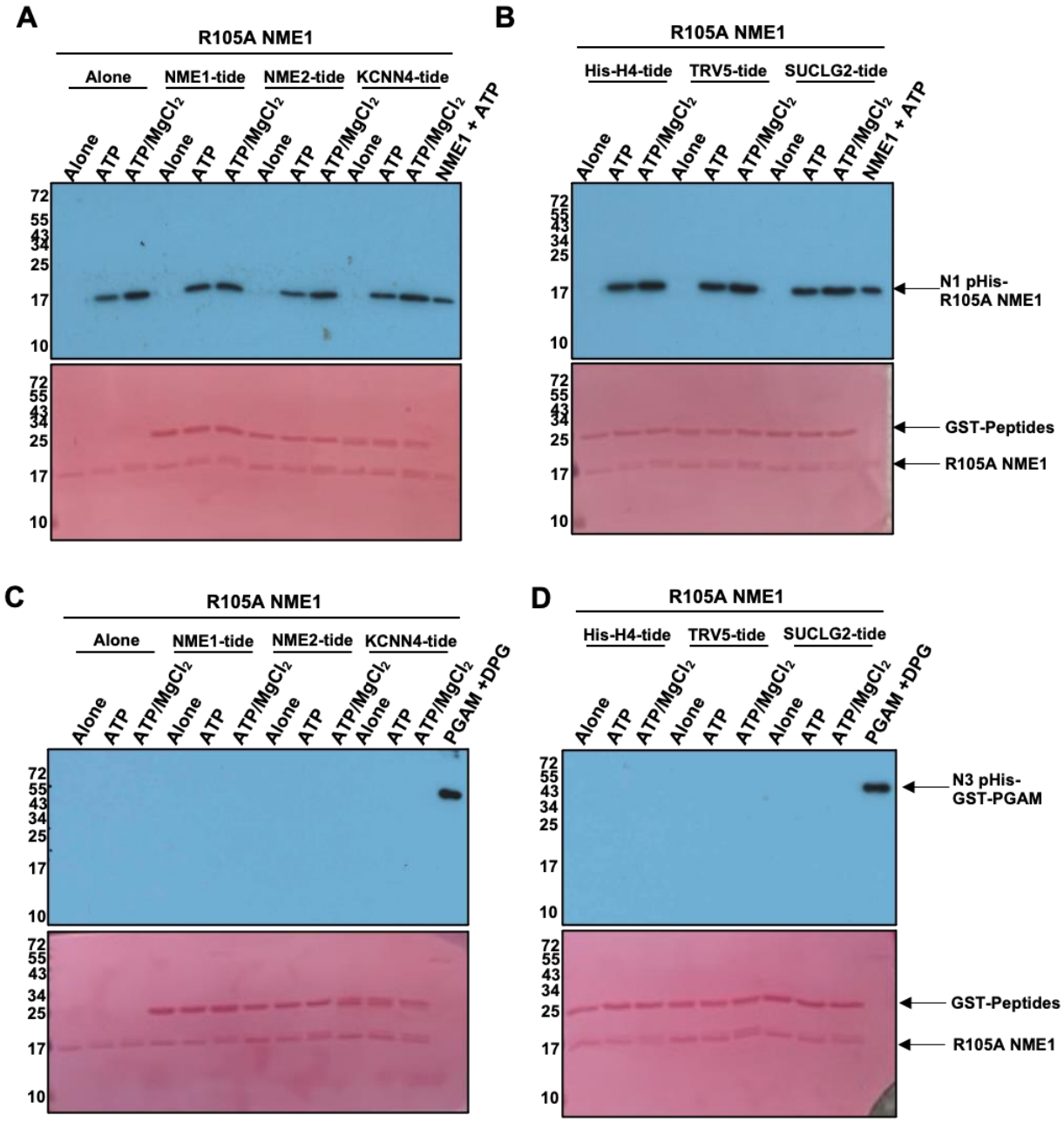

Figure 5.10. Western blot analysis of GST-His containing peptides when incubated with purified recombinant R105A NME1. 500 ng of R105A NME1 was incubated with the indicated 1 µg GST-peptide for 10 minutes at ambient temperature before adding 500 µM of ATP in the presence and absence of either 10 mM $MgCl_2$ for 1 mins before being resolved by SDS PAGE on a 15% acrylamide gel. Top panels: Samples were processed for western blot analysis using (A) and (B) N1-pHis or (C) and (D) N3-pHis antibody. Bottom panels: Membranes were stained using ponceau to determine total GST-peptide and total R105A NME1 protein.

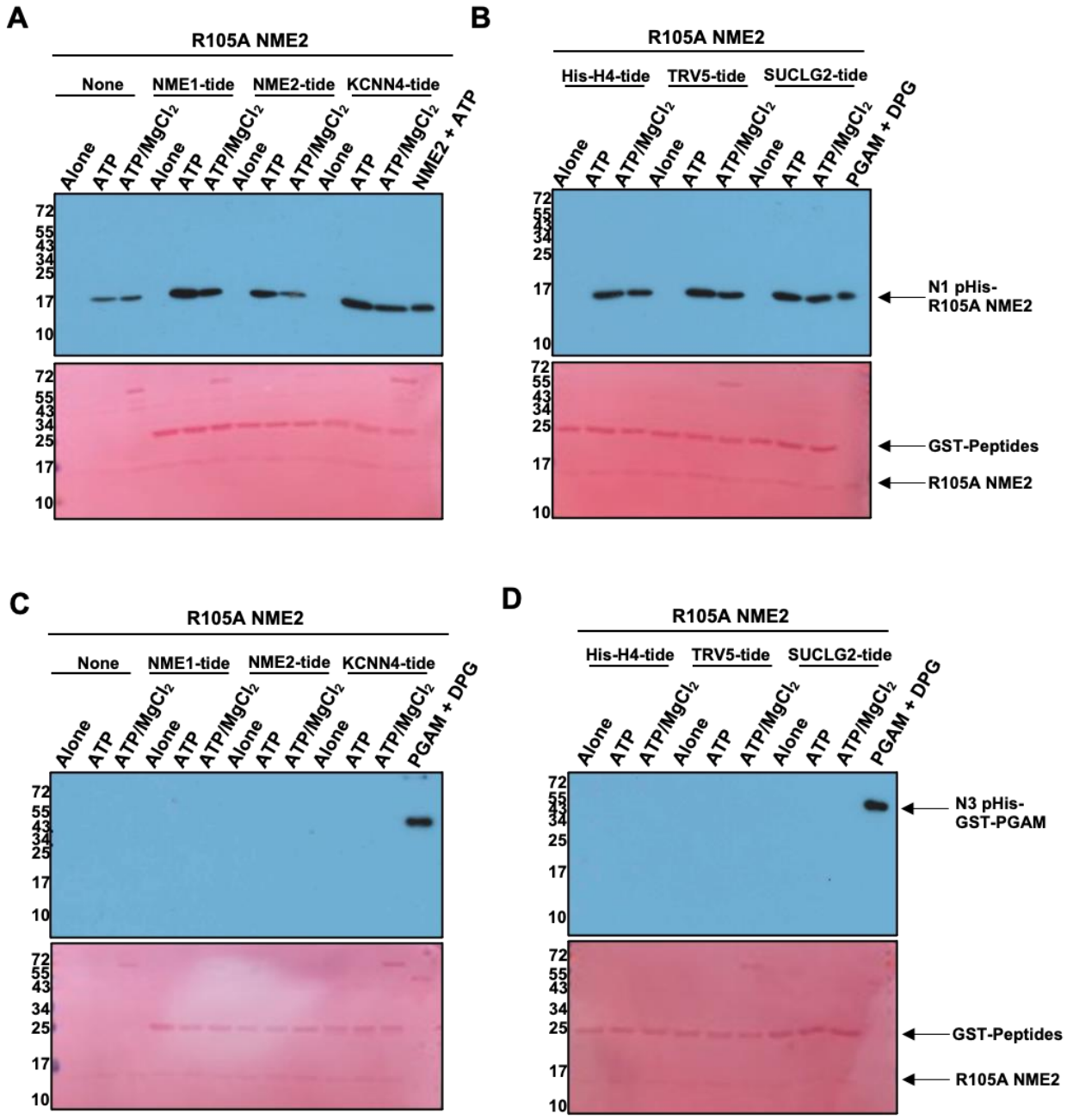

Figure 5.11. Western blot analysis of GST-His containing peptides when incubated with purified recombinant R105A NME2. 500 ng of R105A NME2 was incubated with the indicated 1 µg GST-peptide for 10 minutes at ambient temperature before adding 500 µM of ATP in the presence and absence of either 10 mM $MgCl_2$ for 1 min before being resolved by SDS PAGE on a 15% acrylamide gel. Top panels: Samples were processed for western blot analysis using (A) and (B) N1-pHis or (C) and (D) N3-pHis antibody. Bottom panels: Membranes were stained using ponceau to determine total GST-peptide and total R105A NME2 protein.

Interestingly, when the total protein present in the samples analysed was evaluated by ponceau staining (Figure 5.10 and 5.11; bottom panel), an oligomer at ~65 kDa was observed in the presence of ATP and $MgCl_2$ for all R105A NME2 samples (Figure 5.11) and for R105A NME1 in the presence of the NME1-tide (Figure 5.10C). This molecular mass is likely to be

representative of the tetrameric NME mutant protein. It is deemed unlikely that this oligomeric status is generated due to the presence of GST or the fused peptide sequence, as it was also present in the absence of GST for R105A NME2.

5.3 Investigating the histidine kinase ability of NME1 and NME2 isolated from human cell lines

Bacterial expression systems for protein production can result in improper folding or oligomerisation, though this is deemed unlikely due to experiments described in Chapters 3 and 4). However, a vast number of eukaryotic post-translational modifications do not occur in bacteria, many of which are required to attain the biologically active protein active in cells (472). Therefore, a mammalian expression system was employed to study NME1 and NME2 after processing and isolation from the cellular environment. To achieve this, expression of eptitope-tagged (Myc-tagged NME1 or FLAG-tagged NME2) was optimised in HEK293T human cells (Section 2.22) (Figure 5.12 and 13). eGFP was exploited as a transfection control to monitor transfection efficiency in addition to acting as a negative control for NME1 or NME2 overexpression. Figure 5.12A demonstrates that eGFP transfected cells, do not contain a ~20 kDa protein present when Myc-tagged NME1 transfected cells are immunoblotted using anti-Myc antibody (top panel). The increase in the signal of the ~20 kDa band after 48 hours and addition of valproic acid (VPA, a short chain fatty acid that enhances transient gene expression) (473-475), further suggests that the over expression of Myc-tagged NME1 had been achieved.

To determine whether autophosphorylation of NME1 protein was enhanced upon addition of ATP and $MgCl_2$, purified NME1 or H118A NME1 were analysed using the anti-N1 pHis monoclonal antibody (Figure 5.14C). In the absence of nucleotide, the signal for N1 pHis NME1 was low. When pre-incubated with ATP alone, the signal significantly increased and was then revealed to be slightly decreased by the inclusion of Mg^{2+} ions. Consistently, H118A NME1 showed no evidence of any autophosphorylation activity after analysis by western blot, and had not become phosphorylated *in trans* by endogenous proteins at a different His site.

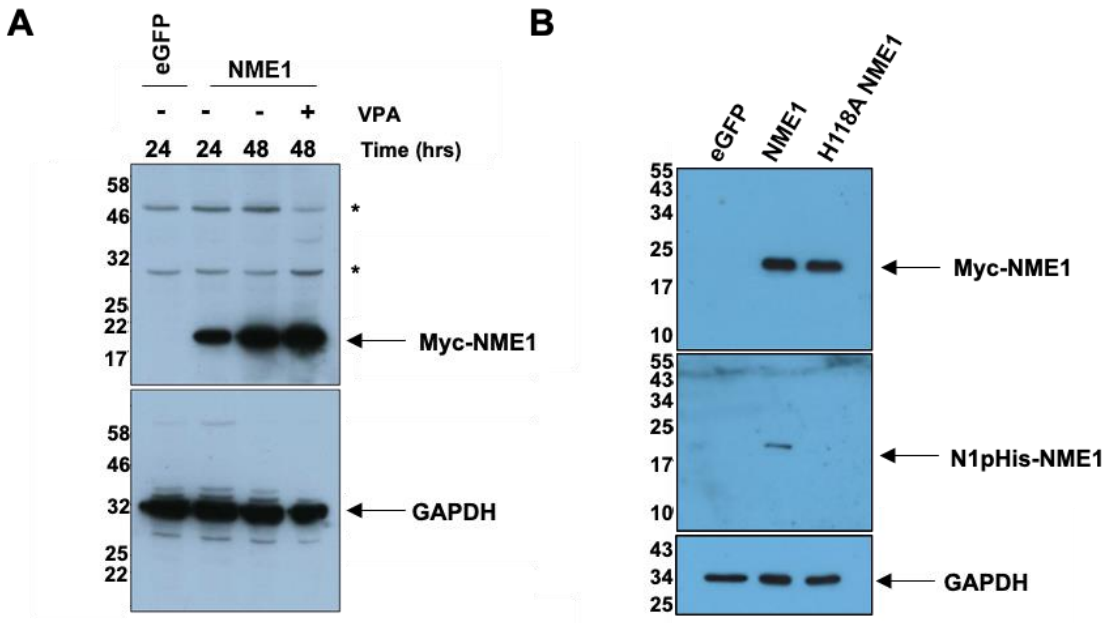

Figure 5.12. Stable expression of NME1 in HEK293T cells and determination of the histidine autophosphorylation activity of the mammalian protein. (A) Optimisation of the expression of Myc-tagged NME1 in HEK293T cells as cell lysis was carried out at indicated time points and/or different conditions post transfection. (B) Myc-tagged NME1 and H118A NME1 were expressed in HEK293T cells as optimised in (A) and Myc-NME1 and Myc-H118A NME1 containing cell extract was analysed by western blot using anti-Myc antibody (top panel) and N1-pHis antibody (middle panel) to assess autophosphorylation activity. Total cell extract loading was compared by immunoblotting with anti-GAPDH antibody (bottom panel).

The catalytic activity of over-expressed Myc-tagged NME1, in the absence of ATP, was evaluated initially. To this end, Myc-H118A NME1 was also generated, and cell extracts were processed for analysis (Figure 5.12B). When analysed with the anti-Myc antibody (top panel), both Myc-NME1 and Myc-H118A NME1 were detected. When probed using anti-N1 pHis antibody (middle panel), a signal was only detected for N1 pHis Myc-NME1. This supports data obtained using bacterially-expressed proteins, in that wild-type NME1 is able to autophosphorylate on His, but H118A NME1 is not. It also demonstrates that in human cells, His118 is the site of phosphate transfer. Interestingly, in contrast to mammalian-expressed NME, NME proteins obtained from bacteria require an exogenous phosphate donor such as ATP or GTP to induce His118 phosphorylation (Figure 3.6), further highlighting the importance of examining NME proteins expressed in a human expression system.

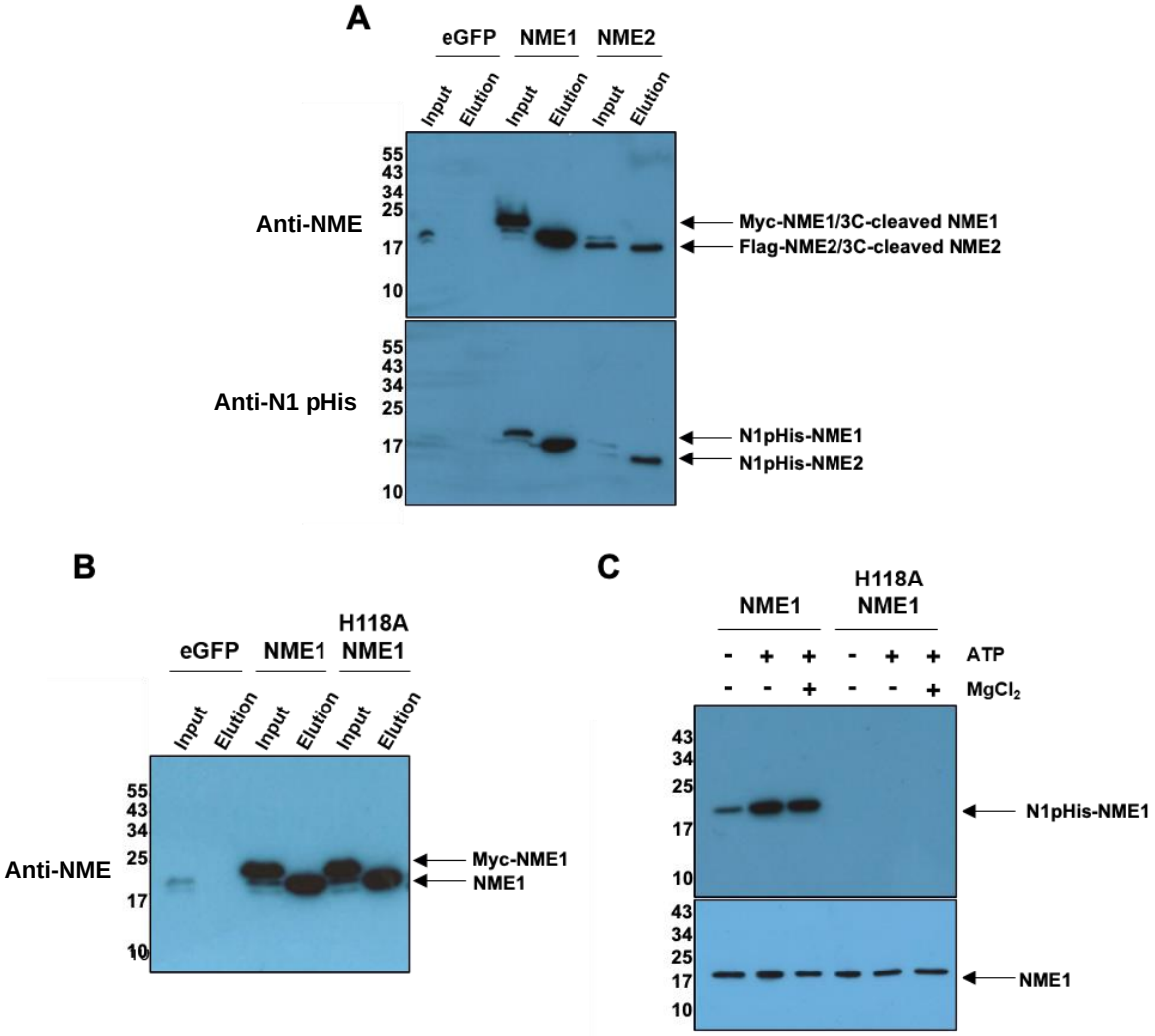

Figure 5.13. Isolation of NME1 and NME2 from HEK293T cells by immunoprecipitation and 3C-proteolytic cleavage. (A) HEK293T cell extract with over-expressed Myc-NME1 and Flag-NME2 (input) were incubated with Myc conjugated (NME1) or Flag conjugated (NME2) agarose beads. The bound proteins were eluted from the beads using 3C protease. Aliquots of the Myc and Flag-tagged input proteins and untagged eluted proteins, including eGFP controls, were resolved on a 15% acrylamide gel and analysed by western blot using anti-NME antibody. These samples were also processed for western blot analysis to with anti-N1 pHis antibody. (B) Myc-tagged NME1 and Myc-tagged H118A NME1 were purified as in (A). (C) Eluates from (B) were incubated in the presence of 1 mM ATP and/or 10 mM $MgCl_2$ and analysed by western blot using N1pHis antibody. Total protein was determine using anti-NME antibody.

To evaluate whether human NME1 and NME2 expressed in HEK293T cells possess the ability to transfer a phosphate group to a His residue in GST-peptides, NME1 and NME2 were isolated from transfected cell extract (Figure 5.13). The Myc and Flag-tags on NME1 and NME2 respectively were exploited to immunoprecipitate Myc-NME1 or Flag-NME2 and activity of these proteins was assessed throughout the immunoprecipitation process. Figure 5.13A demonstrates that cell extract over-expressed either Myc-NME1 or Flag-NME2 (inputs). NME proteins were isolated by incubation with Myc or Flag-conjugated beads (Section 2.22). After

removing non-specific binding proteins by washing, Myc-NME1 and Flag-NME2 were removed from the beads by 3C protease cleavage, leaving NME1 or NME2 in solution (elution). Each protein contained His phosphorylation in the absence of any added nucleoside triphosphate (NTP), since N1 pHis NME1 was detected in both the input and eluted samples, and N1 pHis NME2 was observed in the eluted sample (Figure 5.14A; bottom panel). A similar approach was used to isolate catalytically-inactive NME H118A NME1.

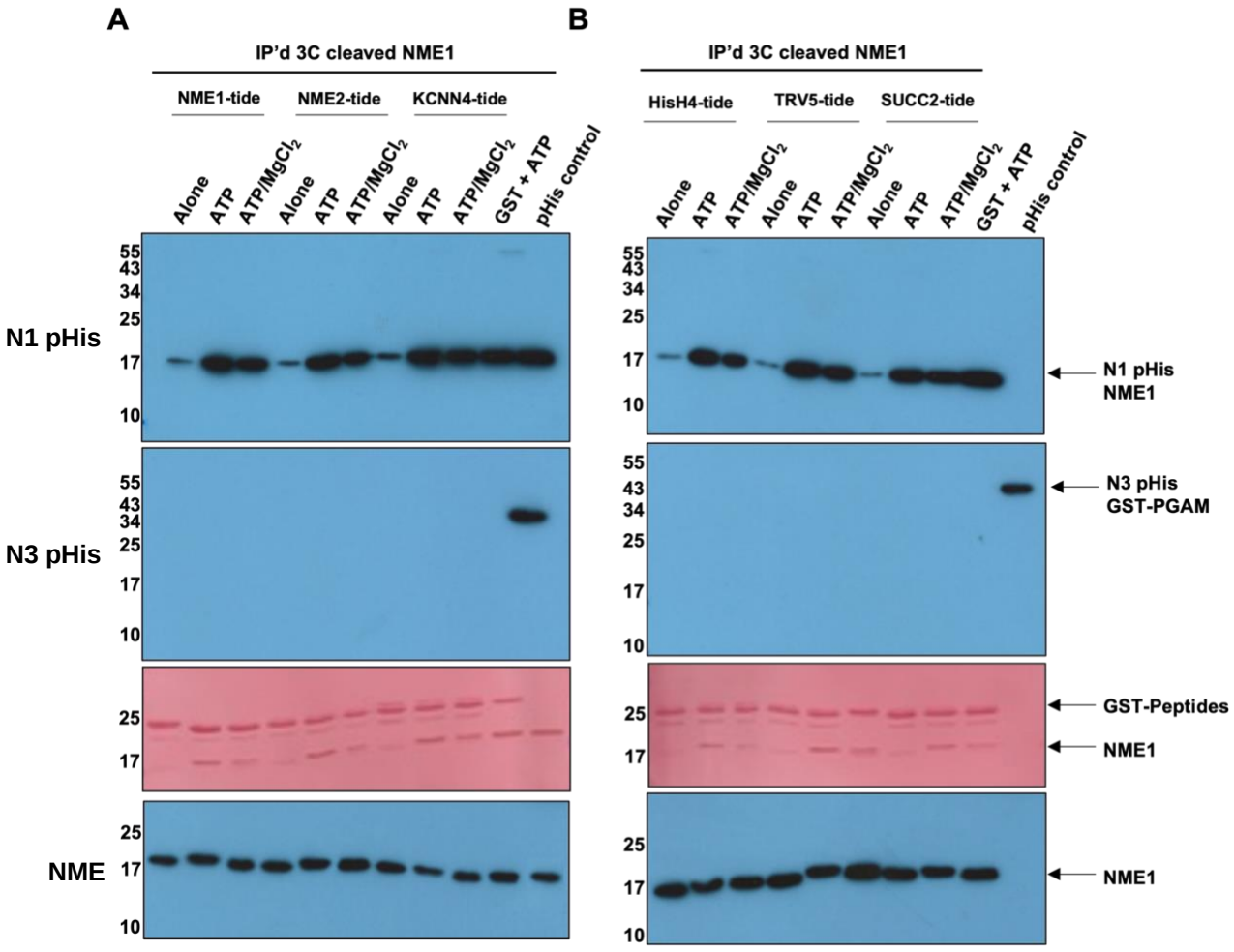

Figure 5.14. Investigating NME1 purified from mammalian HEK293T cells incubated with GST-peptides containing a His site for N1 or N3 histidine phosphorylation by western blot analysis. 500 ng of untagged NME1 purified by immunoprecipitation and eluted by removal of the GST-His tag by 3C protease was incubated with 1 µg of indicated GST-peptides for 10 mins at ambient temperature before adding 500 µM ATP and/or 10 mM $MgCl_2$. Recombinant NME1 and PGAM in the presence of phosphate donors were used as a positive control. Samples were subjected to western blot analysis using the monoclonal anti-N1pHis (top panel) and anti-N3pHis (second panel) antibodies to detect phosphorylated histidine. Total GST-peptide loaded was determined by ponceau staining (third panel) and total NME1 loaded was determined by analysis using the anti-NME1 antibody.

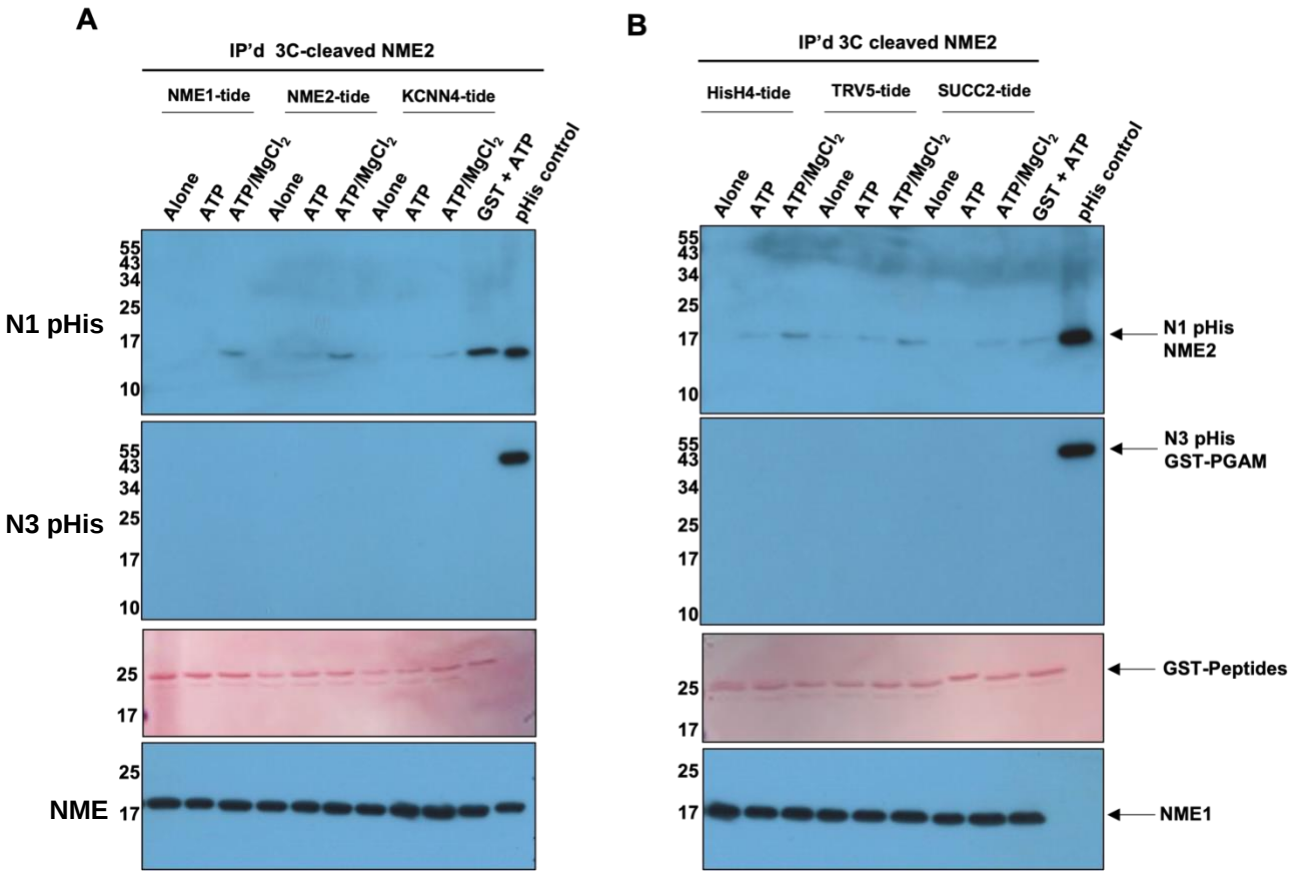

Figure 5.15. Investigating NME2 purified from mammalian HEK293T cells incubated with GST-peptides containing a His site for N1 or N3 histidine phosphorylation by western blot analysis. 500 ng of untagged NME2 purified by immunoprecipitation and eluted by removal of the GST-His tag by 3C protease was incubated with 1 µg of indicated GST-peptides for 10 mins at ambient temperature before adding 500 µM ATP and/or 10 mM $MgCl_2$. Recombinant NME2 and PGAM in the presence of phosphate donors were used as a positive control. Samples were subjected to western blot analysis using the monoclonal anti-N1pHis (top panel) and anti-N3pHis (second panel) antibodies to detect phosphorylated histidine. Total GST-peptide loaded was determined by ponceau staining (third panel) and total NME2 loaded was determined by analysis using the anti-NME1 antibody.

It is possible that purified recombinant NME1 and NME2 from a bacterial expression system do not possess appropriate PTMs or cofactors to promote histidine phosphorylation of GST-peptides assessed above. The indicated GST-peptides were therefore incubated with immunoprecipitated 3C cleaved NME1 (Figure 5.14) or NME2 (Figure 5.15) prior to the addition of either ATP and $MgCl_2$ and then subjected to analysis with N1 pHis and N3 pHis antibodies.

As shown in Figure 5.13C, in the absence of ATP, N1 pHis NME1 was observed and was replicable, as in Figure 5.14, the N1 pHis signal for NME1 also increased in the presence of ATP and ATP/$MgCl_2$. However, no pHis was detected in any of the GST-peptides. This was true when employing both N1 pHis and N3 pHis antibodies. In contrast to NME1,

immunoprecipitated NME2 could not be detected when analysed using the anti-N1 pHis antibody in the absence of ATP (Figure 5.15). However, low levels of N1 pHis NME2 were revealed in the presence of ATP, which increased with the inclusion of $MgCl_2$. However, like mammalian expressed NME1, no signal for N1 or N3 histidine phosphorylated GST-peptides in the presence of mammalian expressed NME2 was detected, including the sequence surrounding His in the putative potassium channel substrate KCNN4 (243, 468).

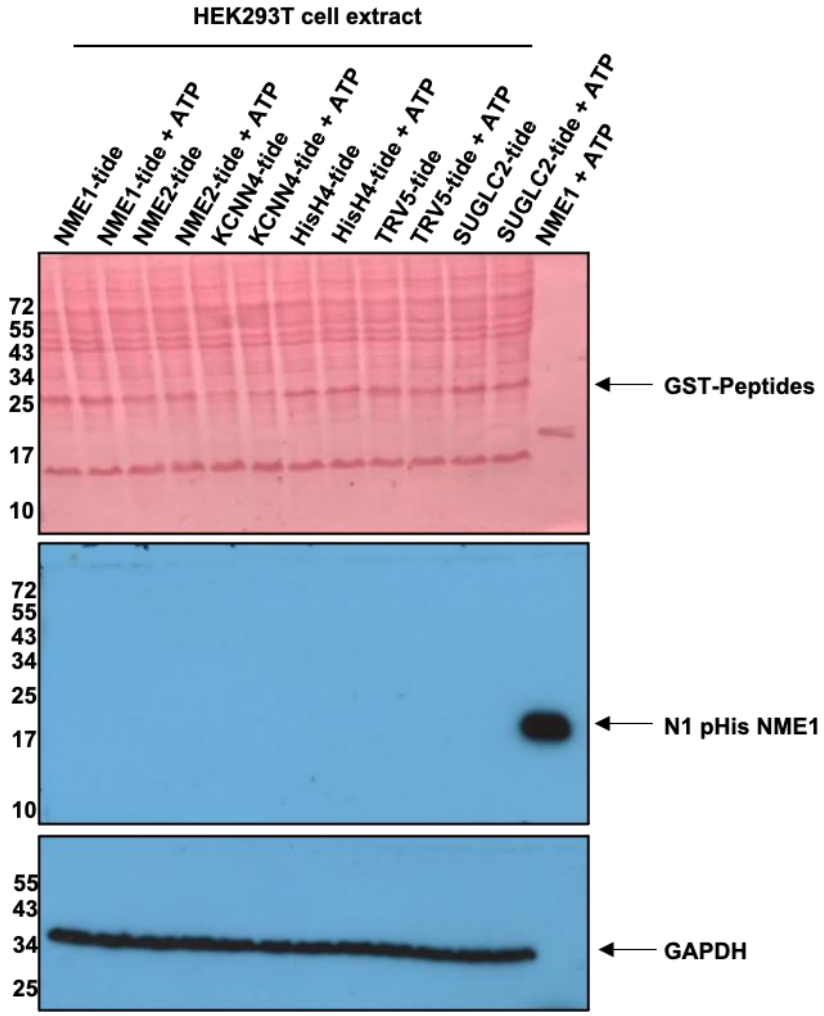

Figure 5.16. Western blot analysis of HEK293T cell lysate incubated with putative substrate, His containing GST-peptides of NME1, NME2, KCNN4, HisH4, TRV5 and SUCLG2 using the monoclonal antibody N1 pHis. HEK293T cells were lysed in 50 mM Tris pH 8.0, 1% Triton-X100, and 70 ug of this lysate was incubated with 1 µg of the indicated GST-peptides incubated in the presence and absence of 1 mM ATP for 20 mins at ambient temperature. These were then subjected to SDS-PAGE at 4 ˚C and transferred to a nitrocellulose membrane at 30V at 4 ˚C. The membranes were then immunoblotted with monoclonal antibody N1-pHis and then reprobed with anti-GAPDH antibody to serve as a loading control. 200 ng recombinant NME1 incubated with 1 mM ATP was used as a positive control for N1 histidine phosphorylation.

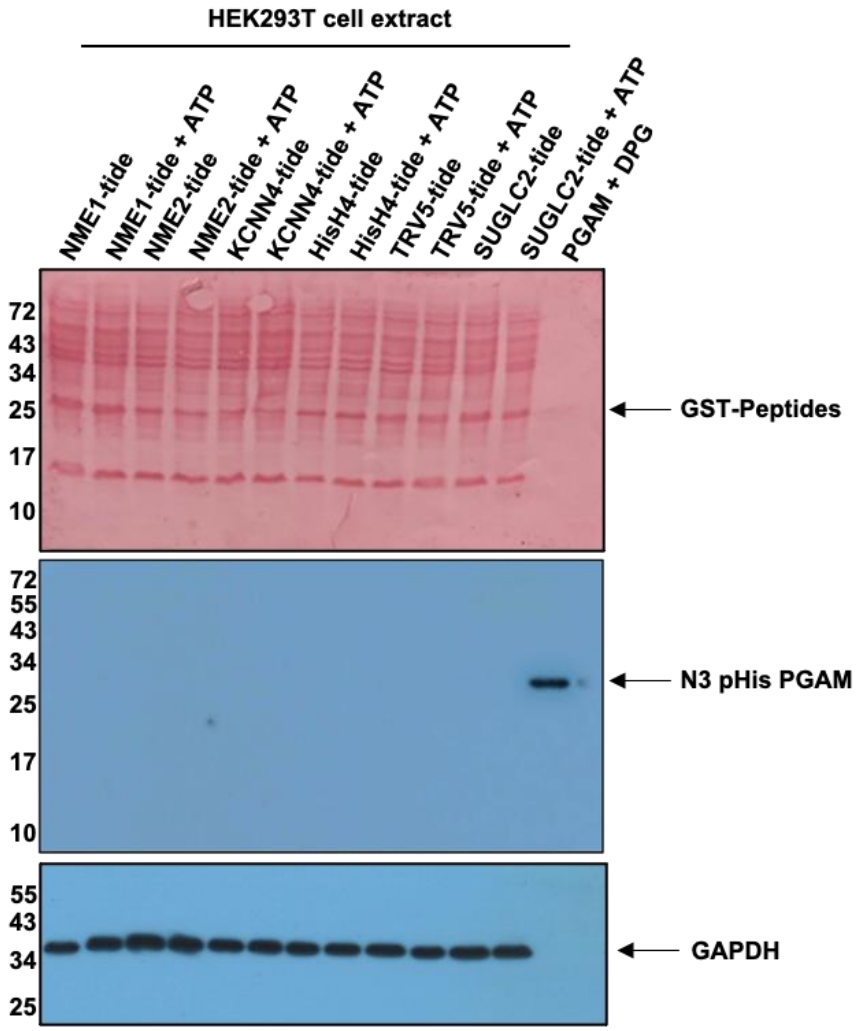

Figure 5.17. Western blot analysis of HEK293T cell lysate incubated with putative substrate, His containing GST-peptides of NME1, NME2, KCNN4, HisH4, TRV5 and SUCLG2 using the monoclonal antibody N3 pHis. HEK293T cells were lysed in 50 mM Tris pH 8.0, 1% Triton-X100, and 70 ug of this lysate was incubated with 1 µg of the indicated GST-peptides incubated in the presence and absence of 1 mM ATP for 20 mins at ambient temperature. These were then subjected to SDS-PAGE at 4 ˚C and transferred to a nitrocellulose membrane at 30V at 4 ˚C. The membranes were then immunoblotted with monoclonal antibody N3-pHis and then reprobed with anti-GAPDH antibody to serve as a loading control. 200 ng recombinant GST-tagged PGAM incubated with 1 mM DPG was used as a positive control for N3 histidine phosphorylation.

From the data presented in this Chapter so far, it is apparent that NME1 and NME2 do not possess the ability to act as histidine protein kinases towards GST-fused peptides *in vitro*. It was next deemed appropriate to evaluate if any proteins in the cell extract (including endogenous NME1/2) were capable of transferring phosphorylating His within these potential peptide substrates. Thus, HEK293T cell extract were spiked with purified GST-peptides, in the presence and absence of ATP, and the levels of N1 pHis or N3 pHis GST-peptides assessed (Figure 5.16 and 5.17). However, no histidine phosphorylation could be detected, including on

endogenous NME1 or NME2, as the levels of pNME1 and pNME2 are often variable, and difficult to detect in cell extract lysed with 1% Triton X-100 (Figure 5.1).

5.4 Analysing the interaction between GST-fused peptides with NME1 and NME2

To extend the experiments discussed above, I tested whether bacterial-expressed NME proteins and NME proteins isolated from mammalian cells show direct binding to any of the GST-peptides, as a lack of pHis phosphorylation may not imply a lack of interaction. The GST-peptides were bound to beads and purified NME1 or NME2 'bait' was added (shown as 'input' in the ponceau stained membrane), washed and evaluated for binding. To elute GST-peptides from the glutathione beads, excess glutathione was added, and the samples analysed for NME1 or NME2 using the anti-NME antibody (Figure 5.18A; top panel). To ensure the pull-down assay had worked, an anti-GST antibody was also employed (Figure 5.18A; bottom panel). However, the GST-peptides containing potential sites of NME1/2 His phosphorylation did not interact with either of the kinases, and only the NME1 and NME2 positive controls were present. To confirm that this assay can detect the interaction of a GST-peptide and a known protein binding partner, PKA and a high affinity GST-PKI peptide were employed (476, 477) (Figure 5.18B). In the presence of a GST control, no PKA (~ 46 kDa) was observed. However, when incubated with an immobilised GST-PKI peptide, PKA was isolated.

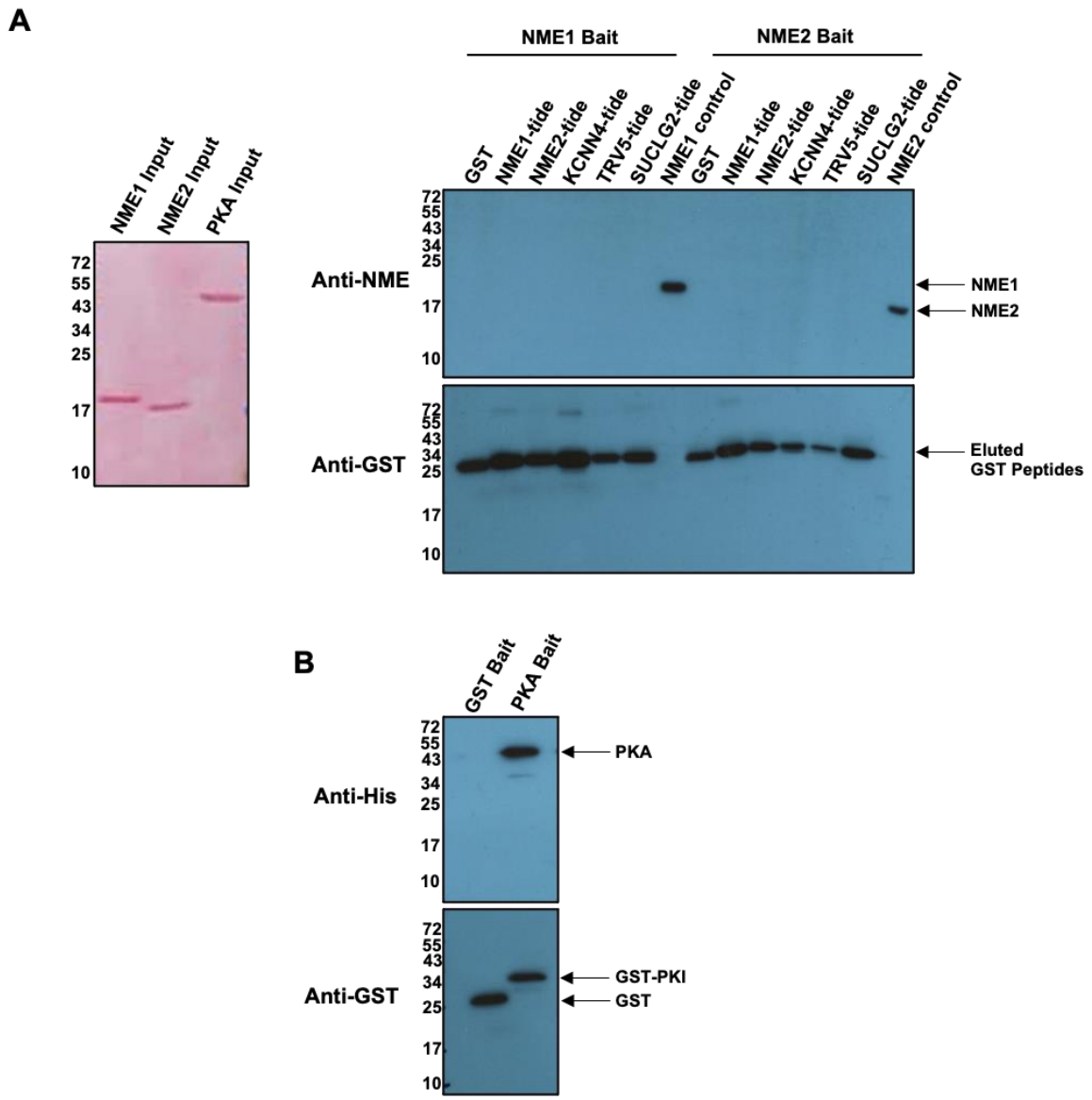

Figure 5.18. GST 'pull-down' interaction assay using GST-peptides and purified recombinant NME1 and NME2. (A) 1 µg of GST or GST-conjugated peptides were incubated with glutathione Sepharose beads. Unbound peptides were removed before 2 µg of purified recombinant NME1 or NME2 was added and incubated at 4 ˚C for 1 hour. The bound fraction was eluted using 10 mM free reduced glutathione and these samples were analysed by western blot using anti-NME1 antibody to identify any NME1 or NME2 pulled down and anti-GST antibody. (B) As a control for the experimental procedure, 1 µg of GST-PKI was incubated with glutathione Sepharose beads and 2 µg of His-PKA was added and processed as in (A) and analysed by western blot to identify PKA pulled down by PKI using the anti-His antibody. To determine the total protein input to the interaction assays ponceau staining was carried out on the membrane.

To further expand these findings, a similar experiment was performed using HEK293T cell extract containing overexpressed Myc-NME1 or Flag-NME2 (Figure 5.19). eGFP transfected extract was used as a control. The input cell extract containing the bait protein is shown in Figure 5.19A and the presence of the bait was demonstrated with either Myc or Flag-tag. Myc-NME1 and Flag-NME2 were detected in the respective transfected cell extracts. The samples

were also analysed with anti-GAPDH to ensure the amount of cell extract added to the GST-peptides immobilised on the glutathione beads was similar. Similar to data presented in Figure 5.18, NME1 and NME2 were not 'pulled down' with any of the GST-peptides.

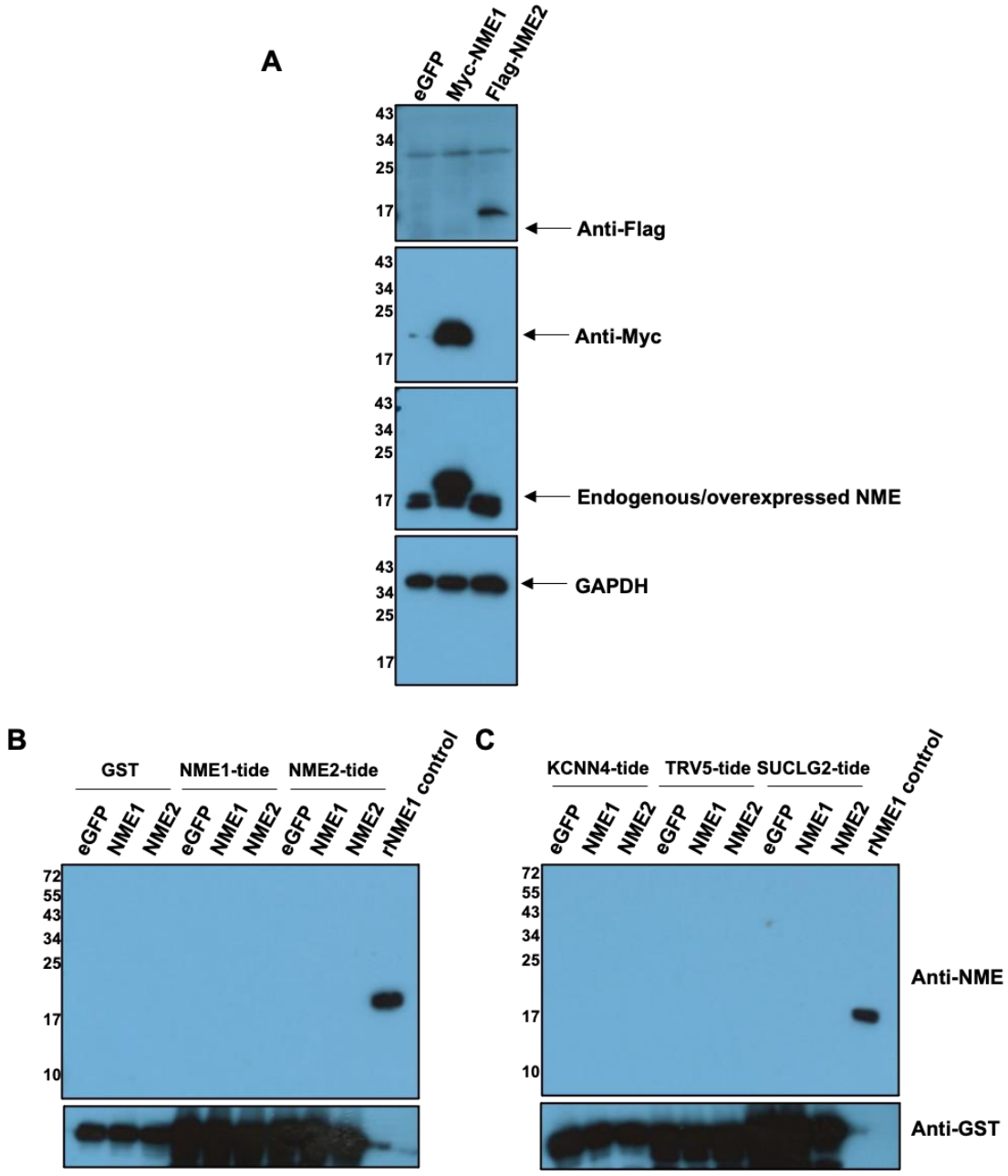

Figure 5.19. GST 'pull-down' interaction assay with GST-peptides and HEK293T cell extract overexpressed with Myc-NME1 and Flag-NME2. (A) Western blot analysis of input cell extract and total protein content of eGFP, Myc-NME1 and Flag-NME2 transfected cell extract. (B) and (C) 1 µg of GST or GST-conjugated peptides were incubated with glutathione Sepharose beads. Unbound peptides were removed before 50 µg of HEK293T cell extract was added and incubated at 4 ˚C for 1 hour. The bound fraction was eluted using 10 mM R-glutathione and these samples were analysed by western blot using anti-NME1 antibody to identify any NME1 or NME2 pulled down, using recombinant NME1 (rNME1) as a control. To assess the efficacy of the pull-down procedure, the membrane was ponceau stained and immunoblotted with anti-GST antibody.

5.5 Discussion

Histidine phosphorylation is crucial for prokaryotic signal transduction and as an enzyme phosphointermediate for human metabolic enzymes, including NME1 and NME2 (8, 12, 132). However, its role in mammalian cells remains largely uncharted. The synthesis of stable pHis analogues enabled the development of pHis specific antibodies (9) and this accelerated pHis research, shedding light onto the importance of this enigmatic post-translational modification. This research has identified several putative pHis-containing substrates and histidine specific phosphatases, such as LHPP and PHPT1 (478-480) being reported. However, it remains unclear how these substrates might access the pHis in the active site of NME1/2 for transfer, or whether NME1/2 might directly transfer phosphate from ATP to a substrate. In particular, none of the reported cellular substrates for NME2 have been shown to be phosphorylated *in vitro* by purified (as opposed to immunoprecipitated) enzymes, which is a standard procedure in the protein kinase field in order to allow site-characterisation and analysis of phosphorylation stoichiometry. In this Chapter, N1 pHis and N3 pHis monoclonal antibodies were utilised to explore conditions under which His kinase activity can be analysed *in vitro* in order to help uncover the functional role of pHis.

In a number of experiments where His protein kinase activity of NME1 and NME2 have been reported, adequate control experiments appear to be lacking. For example, in co-IP assays reporting interaction between overexpressed NME2 and KCa3.1, no control was included to show that the eGFP protein tag on KCa3.1 was either interfering with, or responsible for, the NME2 interaction (243). It was also shown that the activity of the channel increased in the presence of overexpressed NME2, but it is likely that the activity of many other proteins changes alongside NME2, due to the ubiquitous use of ATP by enzymes, in which NME2 plays a role in producing and could therefore be involved either directly in histidine phosphorylation or by aiding complex formation. The same research group reported the histidine phosphorylation of TRPV5 and its activation by NME2 using patch-clamp experiments, however this study that lacked co-IP experiments and adequate controls, such as a broad spectrum small molecule inhibitor approach, or the testing of a range of metal ions to potentially implicate (or rule out) known protein kinases (273).

A lack of reported evidence for HPK activity *in vitro* using highly purified preparations of proteins, also raises the idea that the phosphotransferase activity attributed to NME/NDP kinase activity could be due to contaminating proteins. In addition, other Group I family members, such as NME3 and NME4 possess NDP kinase activity through a pHis118 intermediate, and have strong sequence and structural similarities to NME1/2, but no histidine kinase activity has been reported for them (10). Perhaps most importantly, if NME1 or NME2

were to act as histidine protein kinases (HPK), they do not appear to contain significant structural information in the form of substrate-binding adaptions in order to make this possible. For example, the active site of the 17 kDa proteins forms a small cleft to fit nothing more than a nucleotide (Figure 1.8 and 1.9) (199). As it the case for all the reported protein substrates, it is difficult to conceptualise how a single NTP/NDP binding pocket could also accommodate a positively charged His residue as part of a presented peptide backbone and be properly oriented for transfer of phosphate from pHis118 to the N1 or N3 position of the protein (320). Crystal structures of HPKs in complex with putative substrates might help alleviate this issue and shed light on these unanswered but crucial questions that currently no one has been able to address.

The mechanisms underlying histidine phosphatase substrate selection and the main factors driving their substrate specificity are also unknown. A non-redundant role for histidine phosphatases to regulate different targets in cell signalling pathways has been suggested. To the same degree, the exact mechanisms of histidine kinase activity by the only proposed mammalian histidine kinases to date remain very poorly understood. For these reasons, it is important to continue expanding our understanding of histidine phosphatases in parallel with investigating histidine kinases with the correct and thorough controls, such as NME, which is endeavoured here. The understanding of these understudied enzymes and the role of histidine phosphorylation in eukaryotes might point to new therapeutic targets for diseases.

The challenges associated with the study of chemically unstable post-translational modifications, such as pHis, are demonstrated vividly in Figure 5.1 and 5.2. Conditions under which global pHis levels in HEK293T and HeLa cells could be detected were assessed using a variety of lysis conditions, as well as different immunoblotting procedures. In Figure 5.1, HEK293T and HeLa cell extracts lysed in buffers comprising of a mixture of SDS and/or Triton X-100, and post-processing for western blot analysis, blocked in 5% Milk-TBST. Milk contains a number of proteins (notably phosphorylated casein) that might influence antibody binding to proteins in the blot, whereas BSA does not (Figure 5.2) (481).

Results presented in Figures 5.1 and 5.2 also show that a different level and pattern of pHis signal is observed depending on the lysis buffer components as well as the antibody blocking solution employed. For instance, the presence of SDS in the lysis buffer increased the signal of N1 pHis of the protein migrating at ~19 kDa. This was also the case for N3 pHis, particularly in HeLa cells, for a protein that migrated to a molecular mass of ~25 kDa. It is predicted that the bands at ~19 kDa and ~25 kDa are NME1 or NME2 and PGAM, respectively. Compared to when membranes were blocked with 5% Milk-TBST, more proteins were detected with a

N1 or N3 pHis signal in the presence of a BSA blocking buffer. In fact, only NME1 or NME2 are and no N3 pHis signal is present in any of the lysis conditions or cell types when 'non-specific' antibody epitopes were blocked with milk (Figure 5.1B).

Proteins with a similar molecular mass were observed in Figure 5.2 and the band at ~25 kDa, which is proposed to be PGAM, is observed only in harsh lysis conditions, and more so in HeLa cells, as only a very faint band was visible in lysis condition 1 in HEK293T cell extract. Together, this data demonstrates some of the challenges associated with the study of pHis, as detection is heavily dependent on the conditions used. However, it is clear that the signal at ~19 kDa, which is likely to be endogenous NME1 or NME2, possesses a strong N1 pHis signal in both HEK293T cells and HeLa cell lysates.

To assess whether any N1 pHis signal was detected after addition of recombinant NME1 or NME2, the purified recombinant proteins were spiked into HEK293T cell extract lysed in 1% Triton X-100 to maintain the integrity of the proteins within the extract, and analysed by western blot (Figure 5.3). As established in Figure 5.1, in lysis condition 3 and when blocked with milk, only a very faint band for endogenous NME was detected and endogenous NME could not be observed. Furthermore, no N1 or N3 pHis signal was enhanced by inclusion of NME1. This data did imply that endogenous levels of pHis remain unaffected after incubation with recombinant NME1 or NME2, although this could be caused by competing His phosphatases present in the cells, as is the case for high activity protein Ser/Thr/Tyr phosphatases.

NME1 and NME2 exist in solution as heterohexamers, sometimes containing both NME1 and NME2 (482). This led me to investigate whether NME1 or NME2 could induce histidine phosphorylation of each other; to do this a GST-tagged NME1 and a 3C-cleaved NME2 were exploited in a series of binding assays (Figure 5.4). This study clearly demonstrated lower levels of pHis NME2 when incubated with GST-NME1 (compared to an inactive GST-H118A NME1 control). Nevertheless, due to the presence of pHis NME2 in the GST-H118A NME1 control, this raised the possibility that an excess ATP may still have been present, which would be capable of inducing NME2 autophosphorylation. Therefore, although there are differences in pHis NME2 signals, it is likely that no trans-phosphorylation from NME1 to NME2 had actually occurred. This is further supported by experiments carried out using the NME1 and NME2 GST-fused peptides in Figure 5.6 and 5.7, where no pHis signal was observed for these peptides in the presence of purified recombinant NME1 or NME2. The enzyme activity towards each isoform of NME would be difficult to determine through the PK/LDH enzyme assay

described in Section 2.17 as the 'substrate' NME would interfere. Therefore an NME mutant, that is inactive but still possesses the His residue, would be required using this approach.

GST-peptides derived from sequences surrounding the His residue in putative NME substrates were exploited to try to identify histidine kinase activity exhibited by NME1 and NME2 isolated from both *E. coli* and human cells. However, no evidence for phosphate transfer to a histidine residue was observed beyond the known autophosphorylation on His118 of NME1/2. The data gathered here, under these particular experimental conditions, does not support the literature reporting the identification of several NME1/2 protein substrates that are phosphorylated. This may be due to the assay not actually being able to detect a pHis signal (i.e. the antibodies are not pan-pHis antibodies) or it may be a result of the peptides alone being poor substrates and/or when fused to GST. The finding that human cell extracts possess multiple pHis-responsive proteins, and that MS can be used in conjunction with UPAX to identify pHis-containing proteins in cells, suggests the latter. Indeed, although these pull-down approaches have been used throughout the protein kinase literature, issues can sometimes arise when employing peptides as potential substrates. For example, the absence of critical docking sequences and PTMs surrounding the peptide sequence are absent in synthetic peptides, and although my experiments do not provide any new evidence for phosphorylation of these His sites in these peptides, further work is needed to study the kinases that do deposit pHis in human cell extracts.

The data presented here do, however, build on recent work in the literature evaluating His kinase activity of NME1 and NME2. For example, Levit *et al* found that recombinant NME added to a two-component signalling system led to His kinase protein substrates only becoming phosphorylated in the presence of ADP. This led the authors to propose that histidine phosphorylation, and therefore activation of the bacterial His kinase component, was due to the presence of residual ADP as opposed NME catalysed phosphotransfer to His. This suggests no direct effect of the recombinant human NME proteins tested (483), consistent with my findings.

The high affinity of NME1 and NME2 for both di and tri-phosphorylated nucleotides, which I confirmed by DSF analysis in Chapter 3 (Figure 3.9), was predicted to interfere with enzymatic investigations of NME1 and NME2, since the NME proteins may favour the NDPK reaction instead if excess ATP is present in an attempt to drive protein His phosphorylation. To combat this, previously His phosphorylated pHis-NME1 and pHis-NME2 were utilised. Although every effort was made to remove ATP (Figure 5.8 and Figure 5.9), this issue was somewhat negated due to the ability to compare the pNME signal in the absence and presence of the known

substrate, ADP (199, 335). Indeed, despite the very low levels of ATP likely present, the signal for pNME was markedly reduced. This is indicative of the His active site NME phosphate being transferred to ADP during the NDPK reaction, and this was not seen in the presence of any GST peptide. These experiments were therefore unable to verify protein histidine kinase activity, although they validated NME1 and NME2 as NDP kinases entirely.

R105A NME1 and R105A NME2 were also assessed for their ability to histidine phosphorylate GST-peptides as they are both NDPK active, but dimeric, versions of NME. Indeed, it was hypothesised that a dimer of NME might have a differential ability to phosphorylate presented peptide substrates. However, no pHis signal was detected in any of the GST-peptides after incubation with R105A NME1 or NME2, although it was noted that the level of N1 pHis R105A NME2 was found to be lower in the absence of any peptide. This may not have any significance for the analysis of histidine kinase activity, however it may indicate that the presence of GST-peptide increases the stability of R105A NME2 and as a consequence increase autophosphorylation activity. Interestingly, when compared to R105A NME1, Mg ions increase autophosphorylation activity of R105A NME2. In addition, in the presence of Mg^{2+} ions, NME2 migrated at ~ 60 kDa, which is likely to be a tetramer, but this band was not detected with the N1 pHis antibody and therefore might not be 'active'. Mg may therefore induce a conformation that stabilises two R105A NME2 dimers to form a tetramer, however, due to the lack of Arg105, the Kpn loop may still not be in a favourable conformation for ATP binding, and a reduced interaction with ATP molecule due to the absence of Arg105 may account for the lack of autophosphorylation.

When GST-peptides were analysed for pHis modifications in the presence of HEK293T cell lysate, no pHis signal was revealed (Figure 5.16 and 17). The nucleotide pools within the cell varies considerably, with ATP estimated at ~ 1-5 mM and particularly for Figures 5.16 and 5.17, this may therefore mean that reactions that utilise ATP, such as the NDPK reaction, catalysed by additional NME proteins other than just NME1 and NME2, may outcompete phosphotransfer to the peptide substrates analysed here. However, a similar result was observed when incubated with NME1 and NME2 isolated from HEK293T cells, as only pHis NME1 and NME2 were detected (Figure. 5.14 and 15).

Overall, my work suggests that NME1 and NME2 do not possess histidine kinase activity towards GST-peptides when analysed *in vitro.* Global pHis levels in extracts vary in the experimental data presented here and, in the literature, hence making reliable conclusions and extrapolating from other published data difficult. As stated previously, heterohexamers are predicted to be the most prominent proteoforms of NME1 and NME2 in cells, and

potentially this might also explain discrepancies between histidine kinase activity assessed *in vivo* and *in vitro*. However, it remains unclear how putative kinase substrates such as KCNN4 and TRV5, might bind adjacent to the very small nucleotide binding pocket found in NME proteins.

However, a lack of interaction observed in Figure 5.18 and 5.19 with NME1 and NME2 and the GST-peptides clarifies that proteins do not interact via the His residue, or the residues surrounding them (Table 5.2).

Additional experiments exploring NME1 and NME2 and their putative protein substrates are clearly needed to establish whether NME1 and 2 either work alone, or could co-operate, to regulate His phosphorylation of proteins. By using the recombinant proteins, procedures and assays developed in this Chapter, alongside knowledge garnered from Chapters 3 and 4, including mass spectrometry, this should be possible in the near future. Some of these approaches, and an overview of the work described, are presented in Chapter 6.

Chapter 6: Conclusions and Future investigations

6.1. Conclusions

Phosphohistidine (pHis) is commonly used by prokaryotes and in plants as an intermediate for signal transduction across membranes (12). In higher eukaryotes, pHis is also a known enzyme intermediate, and recent work has revealed that protein His phosphorylation is much more common than previously thought, despite remaining relatively challenging to analyse. However, the kinases and phosphatases that control endogenous His phosphorylation in human cells remain a mystery. It is widely accepted that NME proteins operate as pHis-containing nucleoside diphosphate kinases (NDPK), which modulate the levels of nucleotide di and triphosphates in both prokaryotic and eukaryotic organisms (180). However, in eukaryotic species, evidence is accumulating that the N1 pHis-containing enzyme NME1/2 and the N3 pHis-containing enzyme PGAM, might also possess an additional histidine protein kinase activity, which would permit trans-phosphorylation of distinct intracellular proteins on His residues in order to regulate their function. In order to evaluate the NME and PGAM proteins carefully, I set out to purify and analyse these enzymes using a set of approaches that are standard in the protein kinase field, including the semi-quantitative measurement of nucleotide binding and the potential for small molecule protein kinase inhibitors to target the active site, where phosphotransfer occurs.

Although impacted by the COVID-19 pandemic, the work described in this thesis allowed me to create a large number of useful reagents that will be critical for future studies aimed at studying His phosphorylation in proteins. Alongside this, I developed several novel approaches for evaluating NME1, NME2 and PGAM, all of which contain a phosphorylated His residue when exposed to nucleotides. Intriguingly, none of these enzymes contain pHis when purified from E. *coli*, suggesting either that bacteria lack appropriate nucleotide substrates, or that a bacterial pHis phosphatase was active. In Chapter 3, I purified human recombinant NME1, NME2 and PGAM from *E.coli* and used several approaches to investigate each protein, including evaluation of subunit stoichiometry, nucleotide binding and the formation of a pHis enzyme intermediate. Using differential scanning fluorimetry (DSF), I found that NME1, NME2 and PGAM can bind to a variety of purine and pyrimidine diphosphate and triphosphate nucleotide bases, using thermal stabilization as a proxy for interaction. Much of this data agrees with the published literature, however through the use of DSF alongside temperature ramping, in addition to intact MS and immunoblot analysis, I uncovered an inhibitory effect of Mg^{2+} ions when nucleotide was examined, in marked contrast to protein kinases. For NME proteins, Mg^{2+} ions were also found to have the opposite effect in the presence of nucleoside diphosphates, actually enhancing binding as determined by

comparative thermoanalysis.

After optimizing the conditions in which the acid and heat labile pHis modification could be analysed, I employed two strategies to evaluate NDPK activity, including mutagenesis and the development of an enzyme-linked assay. This was performed alongside immunoblotting with pHis-specific antibodies to evaluate NME and PGAM autophosphorylation at the site of phosphotransfer between nucleotides. I found that autophosphorylation on His occurred only in the presence of triphosphate nucleotides for NME and only in the presence of 2,3-DPG for PGAM, despite PGAM demonstrating thermal stabilization by the majority of nucleotides tested. This data was expanded *via* the analysis of various mutants, including H118A, which is inactive, and R105A NME, which behaved as an enzymatically active dimer, as opposed to the native wild-type hexamer observed *in vitro*. Due to a lack of time, I was unable to develop a highly-sensitive NDPK assay appropriate for measuring the NDPK reaction, which was shown occur almost instantaneously *in vitro*. However, a thermal shift DSF assay was deemed to be suitable for further analysis of ligand binding, including screening of a small molecule libraries.

In Chapter 4, I showed that non ATP/GTP nucleotides also interact with NME proteins, and established that PGAM is a target for a variety of cellular nucleotides and acetyl donors, including PAP, PAPS and Coenzyme A, whose binding was unaffected by the His11 to Ala mutation, which abolishes formation of the 3-pHis intermediate. I next went on to evaluate canonical NDPK phosphotransfer in the presence of several ligands, and discovered that as well as Coenzyme A, which is a known NME1 inhibitor, 3' dephosphorylated Coenzyme A also inhibited NDPK activity. These findings support a model in which NME and PGAM might be CoAlated within the cell. To further explore ligand binding and potential inhibition of NME1, I undertook an unbiased screen of 976 FDA-approved drugs for NME1 binding to NME1 and found that a broad spectrum of drug molecules appear to interact with NME1.

The presence of conserved Cys residues makes NME1 susceptible to hexamer dissociation, potentially as part of a redox mechanism. In the absence of Cys109, the NME1 hexamer was stabilised, particularly under oxidative conditions. Encouraged by this observation, I evaluated requirement for three conserved Cys residues in NME1 using DSF, native PAGE and native MS; in addition several potential NME ligands were analysed by molecular docking. The destabilizing effect of many of these drug-like molecules were further evaluated using purified NME1 Cys mutants, and I found that they destabilise the NME1 oligomer, potentially due to oxidative stress sensing by Cys residues. Given further time, I would also have liked to analyse effects of these molecules on conserved Cys residues in NME2, particularly as Cys4 from NME1 is absent in NME2 (183).

In particular, due to restrictions associated with the COVID-19 pandemic, I was not able to explore the effects of any NME1-binding compounds in cells. For example, I would have liked to assess whether NME1 expression levels were influenced by NME1 destabilising agents discovered in vitro. I predict that reduced stability or changes in subunit architecture might also have a more profound effect on cell viability, and these could be correlated with in cell thermal approaches such as CETSA.

In Chapter 5, I analysed whether purified NME1 or NME2 could phosphorylate a series of fusion peptides corresponding to reported His-phoshorylated literature substrates. This established that the enzymes purified from both human cells and bacterial cells, possessed no histidine protein kinase activity towards the fusion peptides at either the N1 or N3 position. This is not in agreement with the current literature, as several ion channels have been reported to be direct substrates of NME2. My plans to analyse full-length KCa3.1 channel activity under conditions where NME1/2 were repressed or inhibited did not come to fruition. KCa3.1 has reported to be a cellular NME2 substrate, and although conditions for KCa3.1 immunoprecipitated from human cells were established, given further time this would have been a very interesting area to explore.

6.2. Future Plans for Investigation

An important aspect of future studies will be to employ phosphospecific antibodies and liquid chromatography mass spectrometry (LC/MS) to probe pHis occupancy in various putative NME protein substrates, including those proteins that were present in HEK293T/HeLa cell lysates when probed for the N1 and N3 pHis signal. Proteins such as KCa3.1 would be digested under conditions suitable for pHis detection and a peptide map would be obtained displaying different modifications, including sites of histidine phosphorylation, present in the protein. Global phosphoproteomics first requires phosphopeptides to be enriched or simplified as they are at a low abundance and due to this are not detectable by MS. This can be done by fractionation via anion exchange at neutral pH to avoid any pHis hydrolysis. Hardman et al showed that pHis can be readily detected in peptides derived from proteins in human cell lines through the UPAX/MS procedure (116). In order to build on this, identifying pHis containing proteins might help to determine the relevance of pHis in mammalian cell signalling and by analysing the kinases within these cell signalling pathways, help characterise if a specific histidine protein kinase is responsible. When investigating potential histidine protein kinase substrates, it would be interesting to explore the different co-factors that may be necessary for histidine kinase activity, and also to rule in or rule out potential Ser/Thr/Tyr protein kinases and various pseudokinases, which could possess atypical phosphotransferase activities. As NME1 and NME2 do not require Mg^{2+} ions for autophosphorylation, they are distinct from

protein kinases, and *bona fide* protein histidine kinases may also require a unique set of conditions and cofactors to be active.

To expand on the analysis of NME1 and NME2 as potential histidine protein kinases, other catalytically active NME proteins could also be explored. For example, NME3 and NME4 proteins are part of the Group I NME family members (Section 1.8.2), and share 58 to 88% identity and like NME1 and NME2 as well as employing phosphotransfer reactions via a pHis intermediate. Interestingly, NME7 is the only enzymatically active member of Group II reported. These proteins are much less extensively studied than NME1 and NME2, and because of this, may possess unknown enzymology *in vitro* or in the cell. Therefore, the ability of any of these pHis containing enzymes to transfer a phosphate onto a His in a protein substrate, would be an obvious next step for the identification of mammalian histidine protein kinases.

To extend the semi-quantitative work reported in this thesis, future investigations could also define the affinity for small molecules discovered to target NME1 by DSF. Evaluation of dissociation constants for NME1 ligands could be performed using isothermal calorimetry (ITC) a useful tool to measure thermodynamic data as well as kinetic parameters (484). Further studies would also focus on establishing the effects of global pHis levels in human cells in the presence of potential NME1 inhibitors. However, the suitability of these inhibitors being explored within cells would initially have to be explore, for example, cell viability assays in the presence of these compounds would have to be assessed and what's more, whether they are distributed intracellularly. Furthermore, to help build on the docking analysis carried out in this thesis, future studies would focus on solving co-crystal structures of NME1 or NME2 with a panel of compounds found to bind to NME1. Thus, the mode in which NME1 ligands bind could be established in order to help understand the mechanism by which they modulate the oligomeric state of the protein, without greatly effecting the NDPK activity.

Although the NME proteins are not 'standard protein kinases', since they possess different structural elements related to activity and have an active site that functions as a small nucleotide binding pocket, nevertheless, it would also be useful to screen a broad variety of protein kinase inhibitor-focused libraries. For example, the protein kinase inhibitor set 1 (PKIS1) library, which is comprised of 367 ATP-competitive kinase inhibitors, covering ~30 chemotypes. This additional data would be useful in identifying any more NME1 or NME2 ligands and the knowledge gained would be used for the basis of future structure guided design of NME1 and NME2 protein inhibitors for the utilization in therapeutic strategies to treat cancers and disease associated with aberrant NME1 and NME2.

To conclude, it will be interesting to establish NME1, NME2 and PGAM CRISPR-edited cell lines. Knockdown studies on NME1 and NME2 have been carried out. For example, single mutant knockout mice were viable but did possess developmental defects, whereas knockdown of both NME1 and NME2 was lethal (373). CRISPR would allow further investigations of the viability of mammalian cells when NME1 and NME2 are eliminated from the genome, but would also allow other mutant NMEs to be explored, including R105A, in order to better understand down-stream signalling driven by NME1 and NME2. Studies into the CRISPR-Cas9 molecular machinery has rapidly advanced and by generating CRISPR-edited cell lines that no longer express NME1 or NME2, global pHis levels could be investigated. Finally, this would help establish the potential mechanisms by which NME1 and NME2 control central cellular mechanisms, potentially including G-protein activation as a function of nucleotide levels.

Appendix

The following data presents the spectra obtained from native mass spectrometry (MS) analysis of wild-type NME1 and C109A NME1 in the presence of the FDA library drug 'hits'. This data demonstrates the oligomeric state of the proteins, which is summarised in Section 4.5, Table 4.1.

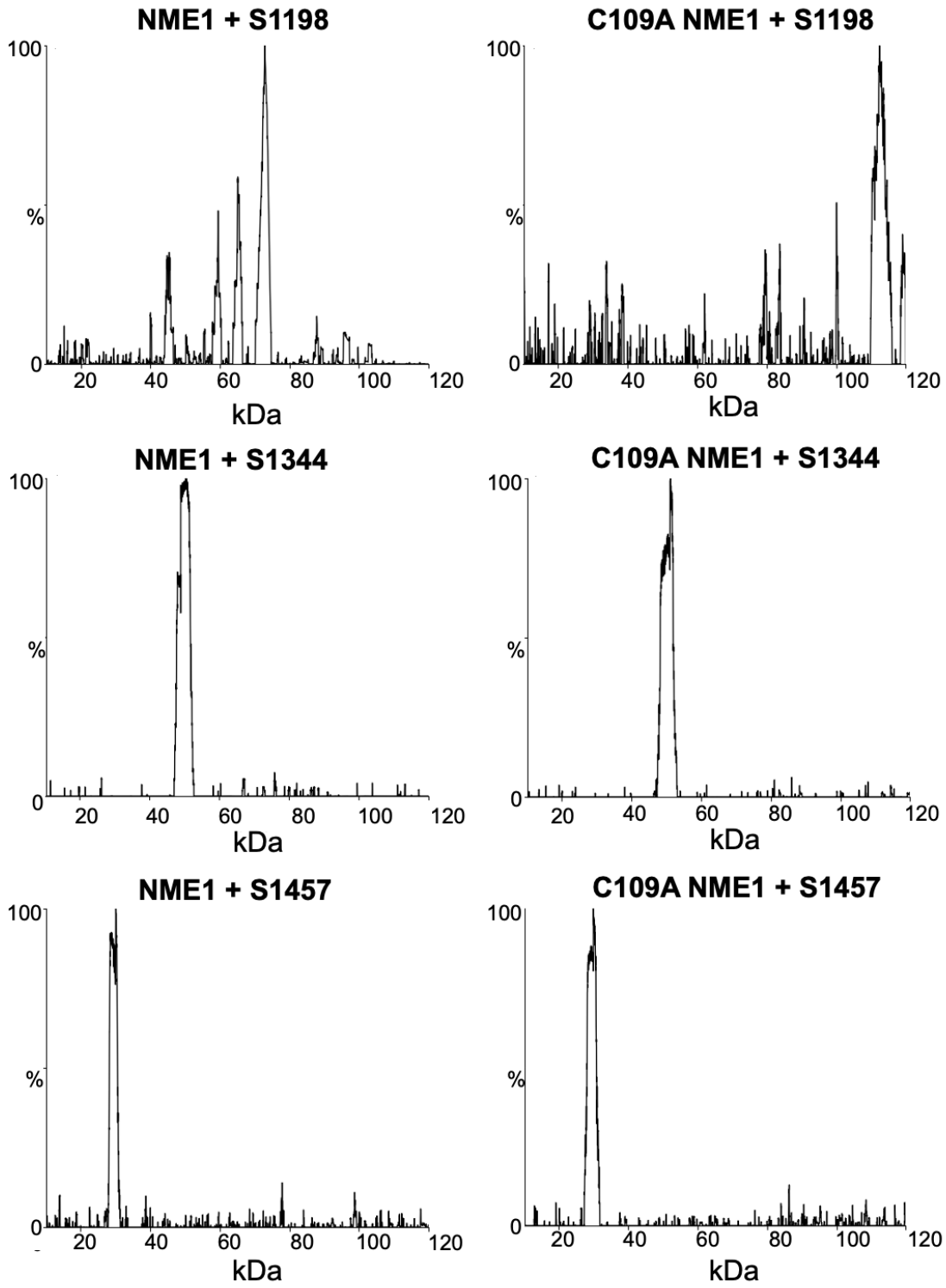

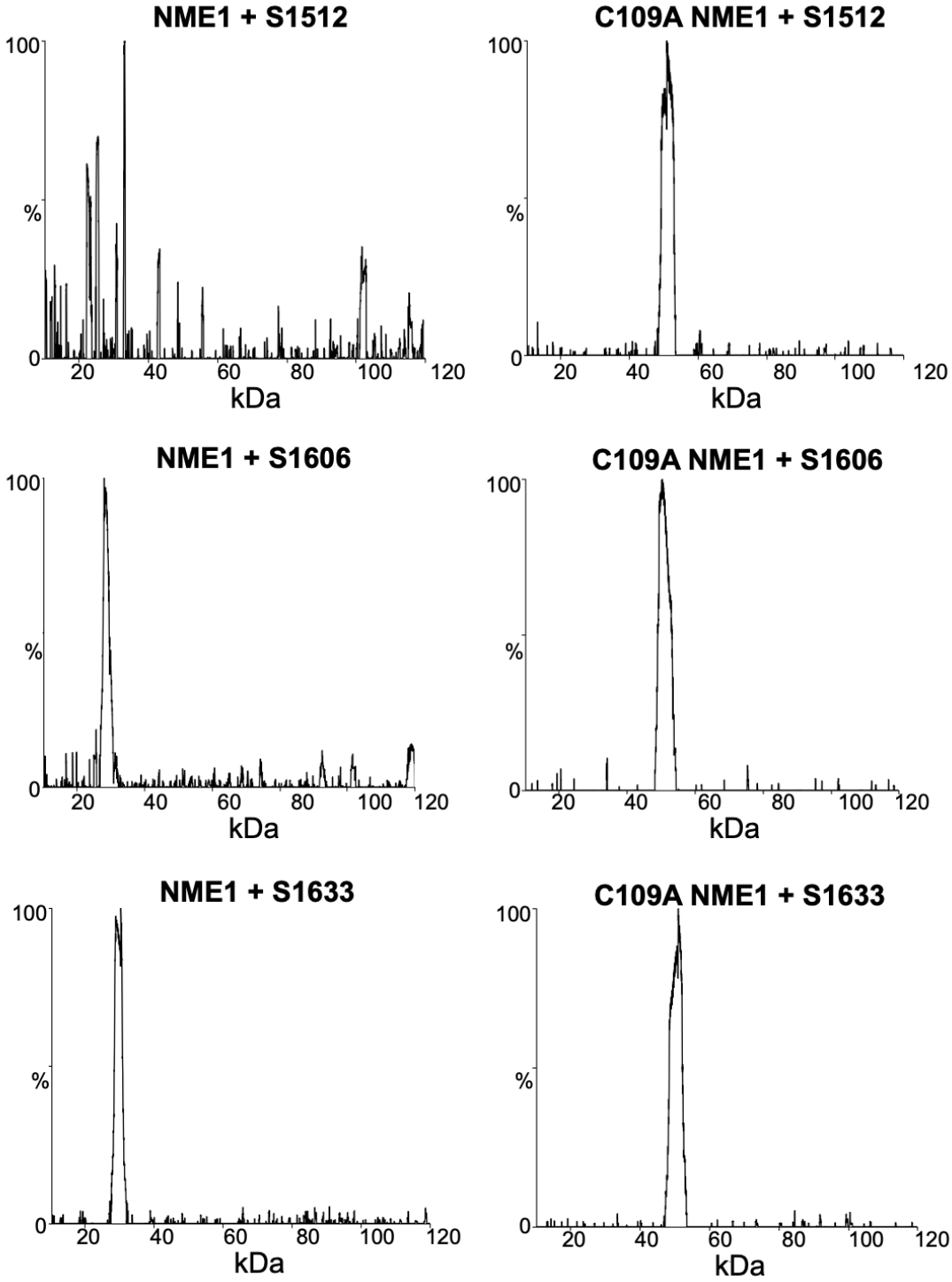
NME1 + S1512
C109A NME1 + S1512
NME1 + S1606
C109A NME1 + S1606
NME1 + S1633
C109A NME1 + S1633
100
%
0
20
40
60
80
100
120
kDa

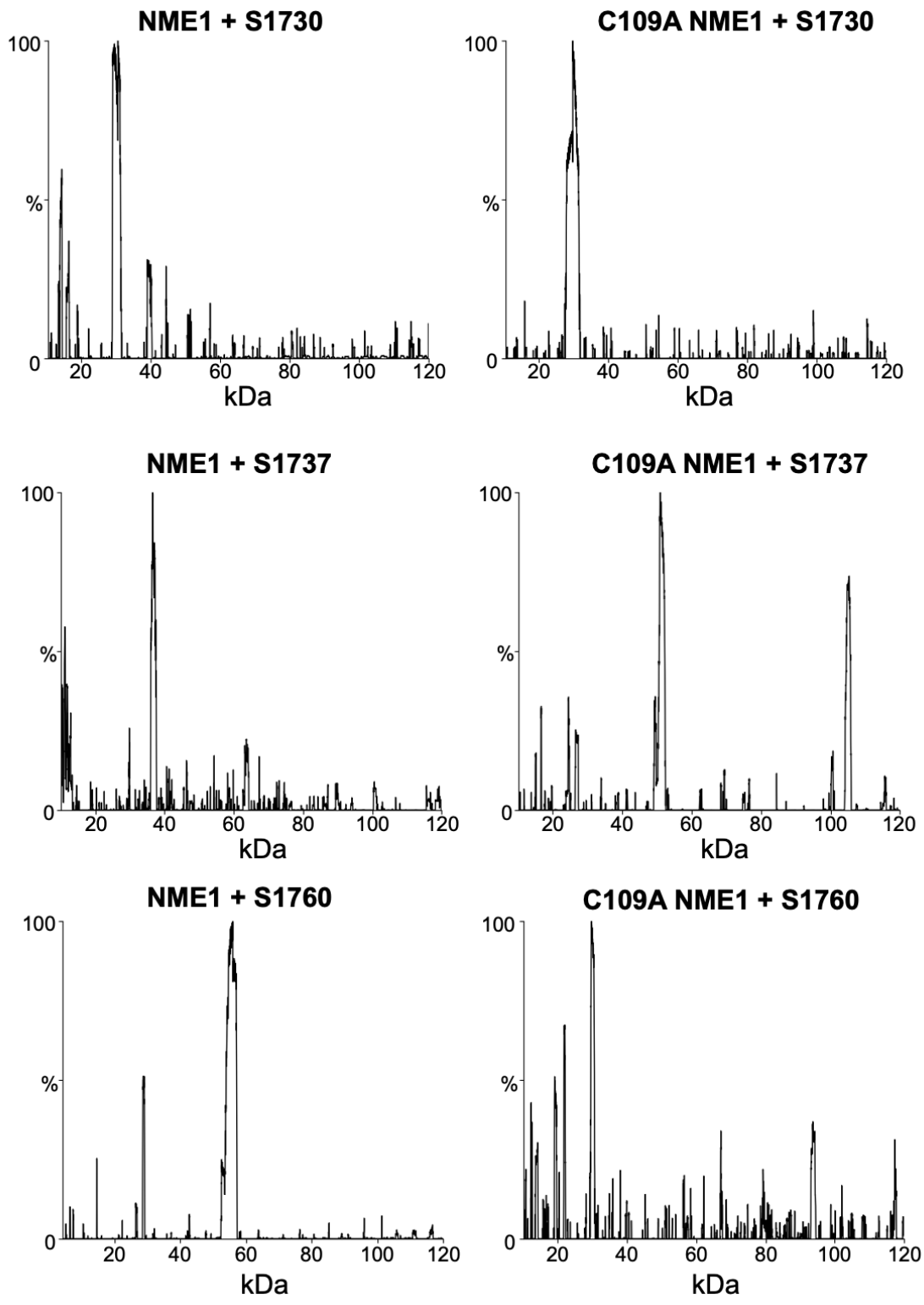
NME1 + S1730
C109A NME1 + S1730
NME1 + S1737
C109A NME1 + S1737
NME1 + S1760
C109A NME1 + S1760
100
%
0
20
40
60
80
100
120
kDa

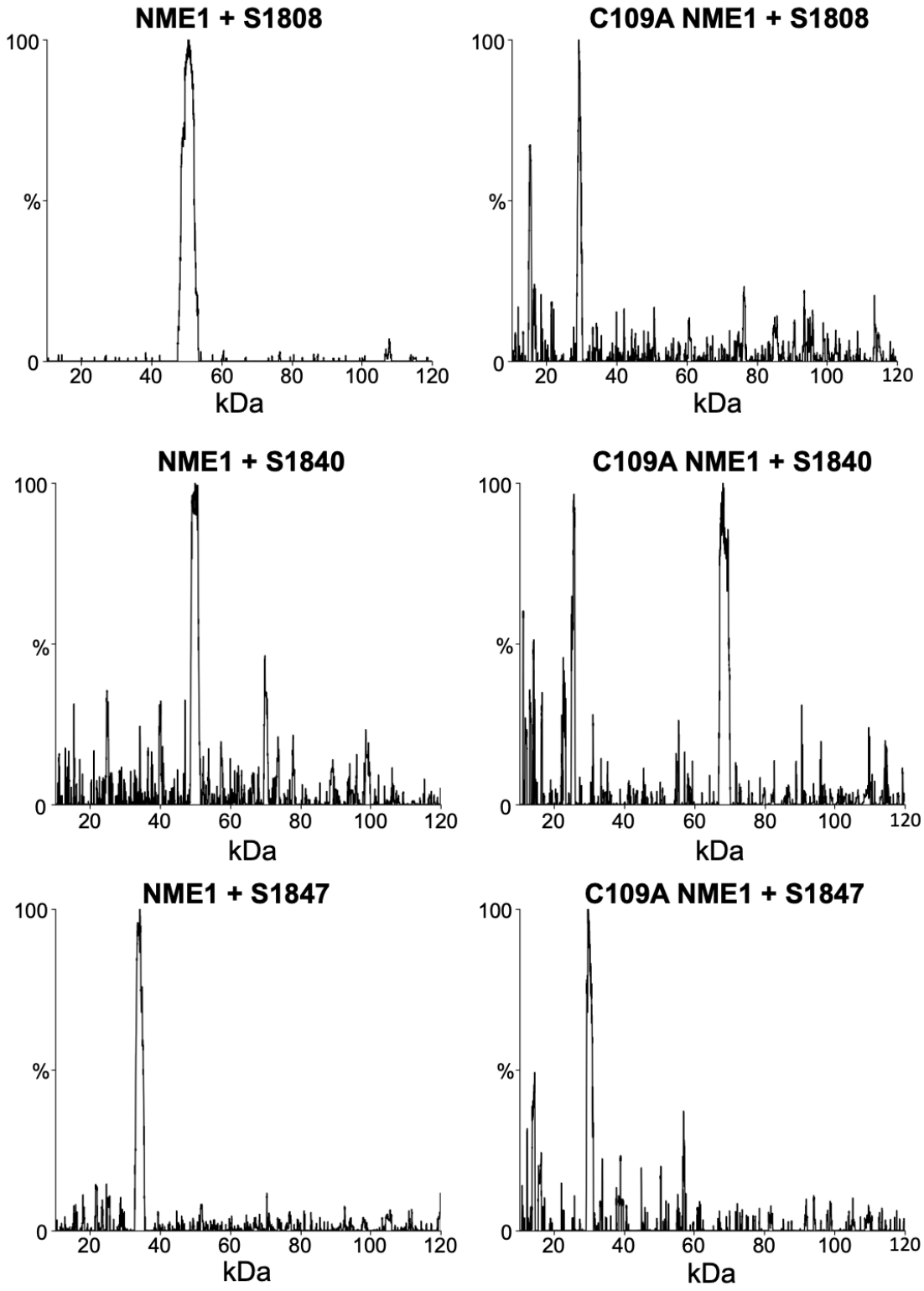
NME1 + S1808
C109A NME1 + S1808
NME1 + S1840
C109A NME1 + S1840
NME1 + S1847
C109A NME1 + S1847
100
%
0
20
40
60
80
100
120
kDa

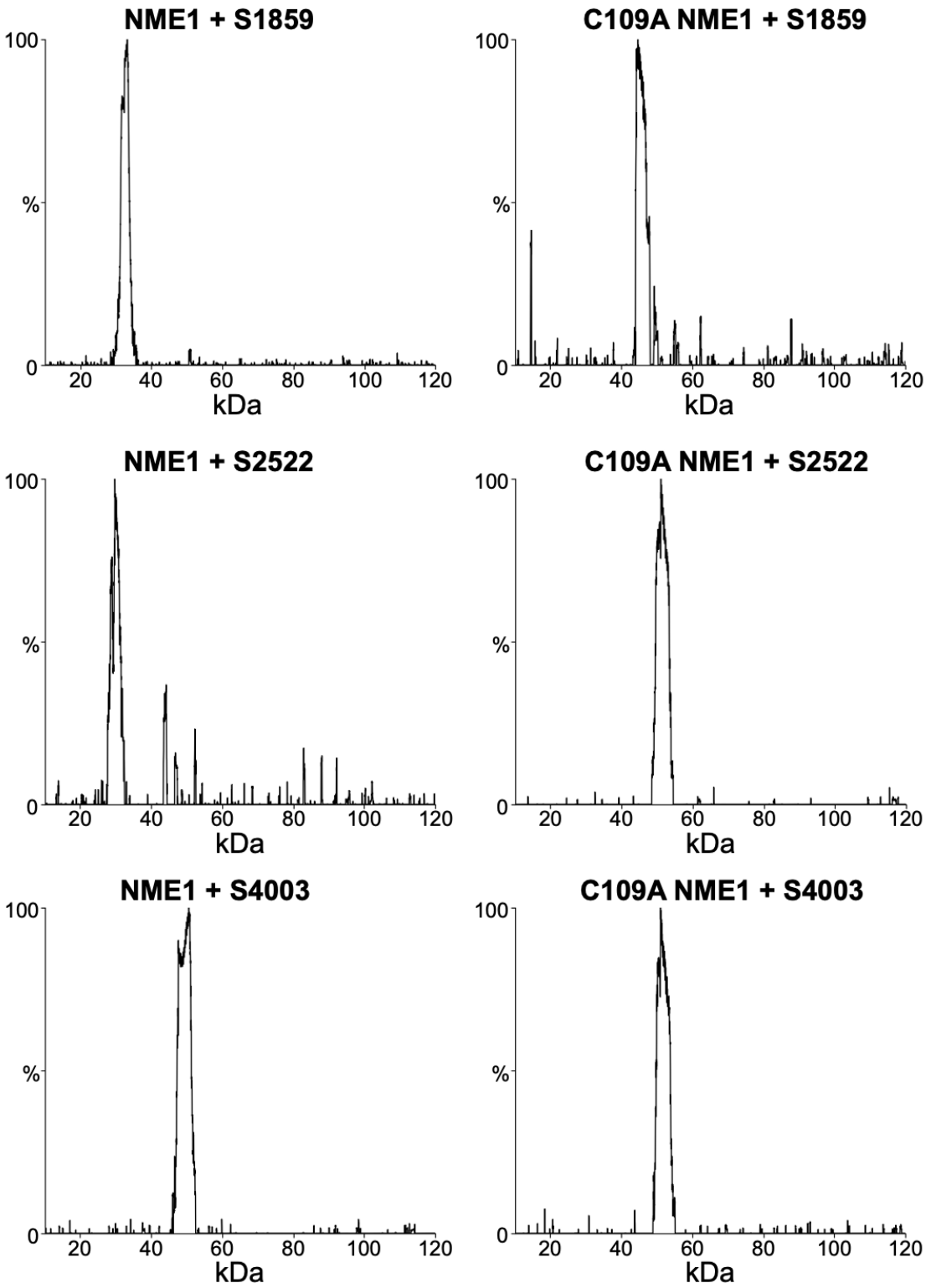
NME1 + S1859
C109A NME1 + S1859
NME1 + S2522
C109A NME1 + S2522
NME1 + S4003
C109A NME1 + S4003
100
%
0
20
40
60
80
100
120
kDa

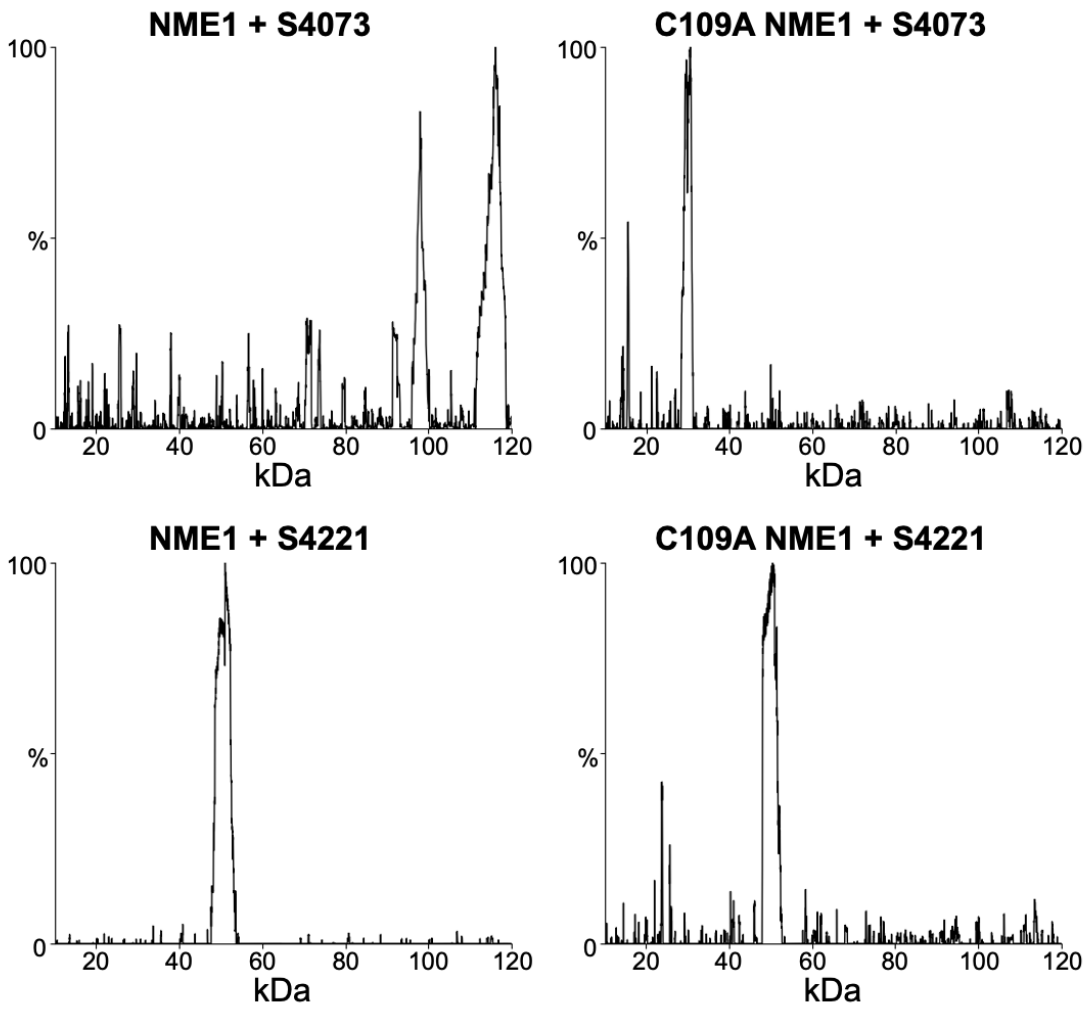

Appendix Figure 1. Native ESI spectrum for NME1 WT (left) and C109A (right) in the presence of FDA compound hits. Data analysis carried out using MassLynx 4.1 and figures created using UniDec. Protein buffer exchanged into 150 mM ammonium acetate using Amicon 10 kDa cut-off spin columns prior to MS analysis.

References

1. Ezkurdia I, Juan D, Rodriguez JM, Frankish A, Diekhans M, Harrow J, et al. Multiple evidence strands suggest that there may be as few as 19,000 human protein-coding genes. Hum Mol Genet. 2014;23(22):5866-78.
2. Manning G, Whyte DB, Martinez R, Hunter T, Sudarsanam S. The Protein Kinase Complement of the Human Genome. Science. 2002;298(5600):1912.
3. Bonora M, Patergnani S, Rimessi A, De Marchi E, Suski JM, Bononi A, et al. ATP synthesis and storage. Purinergic Signal. 2012;8(3):343-57.
4. Bergman JW. ATP: The Perfect Energy Currency for the Cell. Conference Proceedings. 2002.
5. Roskoski R, Jr. A historical overview of protein kinases and their targeted small molecule inhibitors. Pharmacol Res. 2015;100:1-23.
6. Anjian x, Hao J, Zhang Z, Tian T, Jiang S, Hao J, et al. 14-kDa phosphohistidine phosphatase and its role in human lung cancer cell migration and invasion. Lung cancer (Amsterdam, Netherlands). 2009;67:48-56.
7. Besant PG, Attwood PV. Mammalian histidine kinases. Biochim Biophys Acta. 2005;1754(1-2):281-90.
8. Fuhs S, Hunter T. pHisphorylation: the emergence of histidine phosphorylation as a reversible regulatory modification. Current Opinion in Cell Biology. 2017;45:8-16.
9. Fuhs SR, Meisenhelder J, Aslanian A, Ma L, Zagorska A, Stankova M, et al. Monoclonal 1- and 3-Phosphohistidine Antibodies: New Tools to Study Histidine Phosphorylation. Cell. 2015;162(1):198-210.
10. Boissan M, Dabernat S, Peuchant E, Schlattner U, Lascu I, Lacombe ML. The mammalian Nm23/NDPK family: from metastasis control to cilia movement. Mol Cell Biochem. 2009;329(1-2):51-62.
11. Boyer PD, Deluca M, Ebner KE, Hultquist DE, Peter JB. Identification of phosphohistidine in digests from a probable intermediate of oxidative phosphorylation. J Biol Chem. 1962;237:Pc3306-pc8.
12. Stock AM, Robinson VL, Goudreau PN. Two-component signal transduction. Annual review of biochemistry. 2000;69(1):183-215.
13. Attwood PV, Wieland T. Nucleoside diphosphate kinase as protein histidine kinase. Naunyn-Schmiedeberg's Archives of Pharmacology. 2015;388(2):153-60.
14. Steeg PS, Bevilacqua G, Kopper L, Thorgeirsson UP, Talmadge JE, Liotta LA, et al. Evidence for a novel gene associated with low tumor metastatic potential. J Natl Cancer Inst. 1988;80(3):200-4.
15. Lacombe M-LL, Munier A, Mehus JG, Lambeth DO. The Human Nm23/Nucleoside Diphosphate Kinases. Journal of Bioenergetics and Biomembranes. 2000;32(3):247-58.
16. Steeg PS, Zollo M, Wieland T. A critical evaluation of biochemical activities reported for the nucleoside diphosphate kinase/Nm23/Awd family proteins: opportunities and missteps in understanding their biological functions. Naunyn-Schmiedeberg's Archives of Pharmacology. 2011;384(4):331-9.
17. Lee J-J, Kim H, Lee J-S, Park J, Shin S, Song S, et al. Small molecule activator of Nm23/NDPK as an inhibitor of metastasis. Scientific Reports. 2018;8.
18. Hanahan D, Weinberg RA. The Hallmarks of Cancer. Cell. 2000;100(1):57-70.
19. Hanahan D, Weinberg Robert A. Hallmarks of Cancer: The Next Generation. Cell. 2011;144(5):646-74.
20. Warburg O. The metabolism of carcinoma cells. The Journal of Cancer Research. 1925;9(1):148-63.
21. Warburg O, Wind F, Negelein E. Ueber den stoffwechsel von tumoren im körper. Klinische Wochenschrift. 1926;5(19):829-32.
22. Soleymani S, Gravel N, Huang L-C, Yeung W, Bozorgi E, Bendzunas NG, et al. Dark kinase annotation, mining and visualization using the Protein Kinase Ontology. bioRxiv. 2022:2022.02.25.482021.
23. Krebs EG. An accidental biochemist. Annu Rev Biochem. 1998;67:xii-xxxii.
24. Manning G, Plowman GD, Hunter T, Sudarsanam S. Evolution of protein kinase signaling from yeast to man. Trends in Biochemical Sciences. 2002;27(10):514-20.
25. Knighton DR, Zheng JH, Ten Eyck LF, Xuong NH, Taylor SS, Sowadski JM. Structure of a peptide inhibitor bound to the catalytic subunit of cyclic adenosine monophosphate-dependent protein kinase. Science. 1991;253(5018):414-20.
26. Taylor SS, Kornev AP. Protein kinases: evolution of dynamic regulatory proteins. Trends in biochemical sciences. 2011;36(2):65-77.
27. Eyers PA, Murphy JM. Dawn of the dead: protein pseudokinases signal new adventures in cell biology. Biochem Soc Trans. 2013;41(4):969-74.
28. Ramakrishnan C, Dani VS, Ramasarma T. A conformational analysis of Walker motif A [GXXXXGKT (S)] in nucleotide-binding and other proteins. Protein Engineering, Design and Selection. 2002;15(10):783-98.
29. Madhusudan, Akamine P, Xuong NH, Taylor SS. Crystal structure of a transition state mimic of the catalytic subunit of cAMP-dependent protein kinase. Nat Struct Biol. 2002;9(4):273-7.

30. Johnson DA, Akamine P, Radzio-Andzelm E, Madhusudan M, Taylor SS. Dynamics of cAMP-dependent protein kinase. Chem Rev. 2001;101(8):2243-70.
31. Narayana N, Cox S, Shaltiel S, Taylor SS, Xuong N. Crystal structure of a polyhistidine-tagged recombinant catalytic subunit of cAMP-dependent protein kinase complexed with the peptide inhibitor PKI(5-24) and adenosine. Biochemistry. 1997;36(15):4438-48.
32. Yang J, Cron P, Good VM, Thompson V, Hemmings BA, Barford D. Crystal structure of an activated Akt/protein kinase B ternary complex with GSK3-peptide and AMP-PNP. Nat Struct Biol. 2002;9(12):940-4.
33. Mobitz H. The ABC of protein kinase conformations. Biochim Biophys Acta. 2015;1854(10 Pt B):1555-66.
34. Kannan N, Haste N, Taylor SS, Neuwald AF. The hallmark of AGC kinase functional divergence is its C-terminal tail, a cis-acting regulatory module. Proc Natl Acad Sci U S A. 2007;104(4):1272-7.
35. Leroux AE, Schulze JO, Biondi RM. AGC kinases, mechanisms of regulation and innovative drug development. Semin Cancer Biol. 2018;48:1-17.
36. Biondi RM, Komander D, Thomas CC, Lizcano JM, Deak M, Alessi DR, et al. High resolution crystal structure of the human PDK1 catalytic domain defines the regulatory phosphopeptide docking site. Embo j. 2002;21(16):4219-28.
37. Yang J, Cron P, Thompson V, Good VM, Hess D, Hemmings BA, et al. Molecular mechanism for the regulation of protein kinase B/Akt by hydrophobic motif phosphorylation. Mol Cell. 2002;9(6):1227-40.
38. Sicheri F, Moarefi I, Kuriyan J. Crystal structure of the Src family tyrosine kinase Hck. Nature. 1997;385(6617):602-9.
39. Xu W, Harrison SC, Eck MJ. Three-dimensional structure of the tyrosine kinase c-Src. Nature. 1997;385(6617):595-602.
40. De Bondt HL, Rosenblatt J, Jancarik J, Jones HD, Morgan DO, Kim SH. Crystal structure of cyclin-dependent kinase 2. Nature. 1993;363(6430):595-602.
41. Jeffrey PD, Russo AA, Polyak K, Gibbs E, Hurwitz J, Massague J, et al. Mechanism of CDK activation revealed by the structure of a cyclinA-CDK2 complex. Nature. 1995;376(6538):313-20.
42. Kornev AP, Haste NM, Taylor SS, Eyck LF. Surface comparison of active and inactive protein kinases identifies a conserved activation mechanism. Proc Natl Acad Sci U S A. 2006;103(47):17783-8.
43. Hubbard SR, Wei L, Ellis L, Hendrickson WA. Crystal structure of the tyrosine kinase domain of the human insulin receptor. Nature. 1994;372(6508):746-54.
44. Levinson NM, Seeliger MA, Cole PA, Kuriyan J. Structural basis for the recognition of c-Src by its inactivator Csk. Cell. 2008;134(1):124-34.
45. Shan Y, Seeliger MA, Eastwood MP, Frank F, Xu H, Jensen MO, et al. A conserved protonation-dependent switch controls drug binding in the Abl kinase. Proc Natl Acad Sci U S A. 2009;106(1):139-44.
46. Kannan N, Neuwald AF. Did protein kinase regulatory mechanisms evolve through elaboration of a simple structural component? J Mol Biol. 2005;351(5):956-72.
47. Huse M, Kuriyan J. The conformational plasticity of protein kinases. Cell. 2002;109(3):275-82.
48. Bayliss R, Fry A, Haq T, Yeoh S. On the molecular mechanisms of mitotic kinase activation. Open Biol. 2012;2(11):120136.
49. Steichen JM, Iyer GH, Li S, Saldanha SA, Deal MS, Woods VL, Jr., et al. Global consequences of activation loop phosphorylation on protein kinase A. J Biol Chem. 2010;285(6):3825-32.
50. Lemmon MA, Schlessinger J. Cell signaling by receptor tyrosine kinases. Cell. 2010;141(7):1117-34.
51. Nunes QM, Li Y, Sun C, Kinnunen TK, Fernig DG. Fibroblast growth factors as tissue repair and regeneration therapeutics. PeerJ. 2016;4:e1535.
52. Scheeff ED, Bourne PE. Structural evolution of the protein kinase-like superfamily. PLoS Comput Biol. 2005;1(5):e49.
53. Schulze Jörg O, Saladino G, Busschots K, Neimanis S, Süß E, Odadzic D, et al. Bidirectional Allosteric Communication between the ATP-Binding Site and the Regulatory PIF Pocket in PDK1 Protein Kinase. Cell Chemical Biology. 2016;23(10):1193-205.
54. Zhang H, Neimanis S, Lopez-Garcia LA, Arencibia JM, Amon S, Stroba A, et al. Molecular mechanism of regulation of the atypical protein kinase C by N-terminal domains and an allosteric small compound. Chem Biol. 2014;21(6):754-65.
55. Arencibia JM, Pastor-Flores D, Bauer AF, Schulze JO, Biondi RM. AGC protein kinases: from structural mechanism of regulation to allosteric drug development for the treatment of human diseases. Biochim Biophys Acta. 2013;1834(7):1302-21.
56. Manning BD, Toker A. AKT/PKB Signaling: Navigating the Network. Cell. 2017;169(3):381-405.

57. Pearce LR, Komander D, Alessi DR. The nuts and bolts of AGC protein kinases. Nat Rev Mol Cell Biol. 2010;11(1):9-22.
58. Toker A, Marmiroli S. Signaling specificity in the Akt pathway in biology and disease. Adv Biol Regul. 2014;55:28-38.
59. Alessi DR, Andjelkovic M, Caudwell B, Cron P, Morrice N, Cohen P, et al. Mechanism of activation of protein kinase B by insulin and IGF-1. Embo j. 1996;15(23):6541-51.
60. Vanhaesebroeck B, Guillermet-Guibert J, Graupera M, Bilanges B. The emerging mechanisms of isoform-specific PI3K signalling. Nat Rev Mol Cell Biol. 2010;11(5):329-41.
61. Keshwani MM, von Daake S, Newton AC, Harris TK, Taylor SS. Hydrophobic motif phosphorylation is not required for activation loop phosphorylation of p70 ribosomal protein S6 kinase 1 (S6K1). J Biol Chem. 2011;286(26):23552-8.
62. Lachmann S, Jevons A, De Rycker M, Casamassima A, Radtke S, Collazos A, et al. Regulatory domain selectivity in the cell-type specific PKN-dependence of cell migration. PLoS One. 2011;6(7):e21732.
63. O'Sullivan AG, Mulvaney EP, Kinsella BT. Regulation of protein kinase C-related kinase (PRK) signalling by the TPalpha and TPbeta isoforms of the human thromboxane A2 receptor: Implications for thromboxane- and androgen- dependent neoplastic and epigenetic responses in prostate cancer. Biochim Biophys Acta Mol Basis Dis. 2017;1863(4):838-56.
64. Bauer AF, Sonzogni S, Meyer L, Zeuzem S, Piiper A, Biondi RM, et al. Regulation of protein kinase C-related protein kinase 2 (PRK2) by an intermolecular PRK2-PRK2 interaction mediated by Its N-terminal domain. J Biol Chem. 2012;287(24):20590-602.
65. Balendran A, Biondi RM, Cheung PC, Casamayor A, Deak M, Alessi DR. A 3-phosphoinositide-dependent protein kinase-1 (PDK1) docking site is required for the phosphorylation of protein kinase Czeta (PKCzeta) and PKC-related kinase 2 by PDK1. J Biol Chem. 2000;275(27):20806-13.
66. Bayliss R, Sardon T, Vernos I, Conti E. Structural basis of Aurora-A activation by TPX2 at the mitotic spindle. Mol Cell. 2003;12(4):851-62.
67. Elkins JM, Santaguida S, Musacchio A, Knapp S. Crystal structure of human aurora B in complex with INCENP and VX-680. J Med Chem. 2012;55(17):7841-8.
68. Eyers PA, Erikson E, Chen LG, Maller JL. A novel mechanism for activation of the protein kinase Aurora A. Curr Biol. 2003;13(8):691-7.
69. Cheng KY, Lowe ED, Sinclair J, Nigg EA, Johnson LN. The crystal structure of the human polo-like kinase-1 polo box domain and its phospho-peptide complex. Embo j. 2003;22(21):5757-68.
70. Miettinen PJ, Berger JE, Meneses J, Phung Y, Pedersen RA, Werb Z, et al. Epithelial immaturity and multiorgan failure in mice lacking epidermal growth factor receptor. Nature. 1995;376(6538):337-41.
71. Olayioye MA, Neve RM, Lane HA, Hynes NE. The ErbB signaling network: receptor heterodimerization in development and cancer. Embo j. 2000;19(13):3159-67.
72. Sibilia M, Wagner EF. Strain-dependent epithelial defects in mice lacking the EGF receptor. Science. 1995;269(5221):234-8.
73. Threadgill DW, Dlugosz AA, Hansen LA, Tennenbaum T, Lichti U, Yee D, et al. Targeted disruption of mouse EGF receptor: effect of genetic background on mutant phenotype. Science. 1995;269(5221):230-4.
74. Harris RC, Chung E, Coffey RJ. EGF receptor ligands. Exp Cell Res. 2003;284(1):2-13.
75. Hynes NE, Lane HA. ERBB receptors and cancer: the complexity of targeted inhibitors. Nat Rev Cancer. 2005;5(5):341-54.
76. Hynes NE, MacDonald G. ErbB receptors and signaling pathways in cancer. Curr Opin Cell Biol. 2009;21(2):177-84.
77. Maruyama IN. Mechanisms of activation of receptor tyrosine kinases: monomers or dimers. Cells. 2014;3(2):304-30.
78. Ullrich A, Coussens L, Hayflick JS, Dull TJ, Gray A, Tam AW, et al. Human epidermal growth factor receptor cDNA sequence and aberrant expression of the amplified gene in A431 epidermoid carcinoma cells. Nature. 1984;309(5967):418-25.
79. Miloso M, Mazzotti M, Vass WC, Beguinot L. SHC and GRB-2 are constitutively by an epidermal growth factor receptor with a point mutation in the transmembrane domain. J Biol Chem. 1995;270(33):19557-62.
80. Pawson T. Regulation and targets of receptor tyrosine kinases. Eur J Cancer. 2002;38 Suppl 5:S3-10.
81. Jones S, Rappoport JZ. Interdependent epidermal growth factor receptor signalling and trafficking. Int J Biochem Cell Biol. 2014;51:23-8.
82. Mendoza MC, Er EE, Blenis J. The Ras-ERK and PI3K-mTOR pathways: cross-talk and compensation. Trends Biochem Sci. 2011;36(6):320-8.

83. Jura N, Endres NF, Engel K, Deindl S, Das R, Lamers MH, et al. Mechanism for activation of the EGF receptor catalytic domain by the juxtamembrane segment. Cell. 2009;137(7):1293-307.
84. Red Brewer M, Choi SH, Alvarado D, Moravcevic K, Pozzi A, Lemmon MA, et al. The juxtamembrane region of the EGF receptor functions as an activation domain. Mol Cell. 2009;34(6):641-51.
85. Cohen P. Protein kinases--the major drug targets of the twenty-first century? Nat Rev Drug Discov. 2002;1(4):309-15.
86. Witte ON, Dasgupta A, Baltimore D. Abelson murine leukaemia virus protein is phosphorylated in vitro to form phosphotyrosine. Nature. 1980;283(5750):826-31.
87. Veale D, Ashcroft T, Marsh C, Gibson GJ, Harris AL. Epidermal growth factor receptors in non-small cell lung cancer. British journal of cancer. 1987;55(5):513-6.
88. Haeder M, Rotsch M, Bepler G, Hennig C, Havemann K, Heimann B, et al. Epidermal growth factor receptor expression in human lung cancer cell lines. Cancer Res. 1988;48(5):1132-6.
89. Cohen P, Cross D, Jänne PA. Kinase drug discovery 20 years after imatinib: progress and future directions. Nat Rev Drug Discov. 2021;20(7):551-69.
90. Zhang J, Yang PL, Gray NS. Targeting cancer with small molecule kinase inhibitors. Nature Reviews Cancer. 2009;9(1):28-39.
91. Liu Y, Gray NS. Rational design of inhibitors that bind to inactive kinase conformations. Nature chemical biology. 2006;2(7):358-64.
92. André F, Ciruelos E, Rubovszky G, Campone M, Loibl S, Rugo HS, et al. Alpelisib for PIK3CA-mutated, hormone receptor–positive advanced breast cancer. New England Journal of Medicine. 2019;380(20):1929-40.
93. Lindsley CW, Zhao Z, Leister WH, Robinson RG, Barnett SF, Defeo-Jones D, et al. Allosteric Akt (PKB) inhibitors: discovery and SAR of isozyme selective inhibitors. Bioorg Med Chem Lett. 2005;15(3):761-4.
94. Barnett SF, Defeo-Jones D, Fu S, Hancock PJ, Haskell KM, Jones RE, et al. Identification and characterization of pleckstrin-homology-domain-dependent and isoenzyme-specific Akt inhibitors. Biochem J. 2005;385(Pt 2):399-408.
95. Guertin KR, Grimsby J. Small molecule glucokinase activators as glucose lowering agents: a new paradigm for diabetes therapy. Curr Med Chem. 2006;13(15):1839-43.
96. Gehringer M. Covalent Kinase Inhibitors: An Overview. In: Laufer S, editor. Proteinkinase Inhibitors. Cham: Springer International Publishing; 2021. p. 43-94.
97. Sanderson K. Irreversible kinase inhibitors gain traction: the approval of boehringer ingelheim's anticancer drug afatinib highlights the growing enthusiasm for once-shunned irreversible kinase inhibitors. Nature Reviews Drug Discovery. 2013;12(9):649-52.
98. Miklos D, Cutler CS, Arora M, Waller EK, Jagasia M, Pusic I, et al. Ibrutinib for chronic graft-versus-host disease after failure of prior therapy. Blood, The Journal of the American Society of Hematology. 2017;130(21):2243-50.
99. Soria J-C, Ohe Y, Vansteenkiste J, Reungwetwattana T, Chewaskulyong B, Lee KH, et al. Osimertinib in untreated EGFR-mutated advanced non–small-cell lung cancer. New England journal of medicine. 2018;378(2):113-25.
100. Kwak EL, Sordella R, Bell DW, Godin-Heymann N, Okimoto RA, Brannigan BW, et al. Irreversible inhibitors of the EGF receptor may circumvent acquired resistance to gefitinib. Proc Natl Acad Sci U S A. 2005;102(21):7665-70.
101. Cohen MS, Zhang C, Shokat KM, Taunton J. Structural bioinformatics-based design of selective, irreversible kinase inhibitors. Science. 2005;308(5726):1318-21.
102. Wissner A, Fraser HL, Ingalls CL, Dushin RG, Floyd MB, Cheung K, et al. Dual irreversible kinase inhibitors: quinazoline-based inhibitors incorporating two independent reactive centers with each targeting different cysteine residues in the kinase domains of EGFR and VEGFR-2. Bioorg Med Chem. 2007;15(11):3635-48.
103. Fry DW, Kraker AJ, McMichael A, Ambroso LA, Nelson JM, Leopold WR, et al. A specific inhibitor of the epidermal growth factor receptor tyrosine kinase. Science. 1994;265(5175):1093-5.
104. Yun CH, Mengwasser KE, Toms AV, Woo MS, Greulich H, Wong KK, et al. The T790M mutation in EGFR kinase causes drug resistance by increasing the affinity for ATP. Proc Natl Acad Sci U S A. 2008;105(6):2070-5.
105. Yu HA, Arcila ME, Hellmann MD, Kris MG, Ladanyi M, Riely GJ. Poor response to erlotinib in patients with tumors containing baseline EGFR T790M mutations found by routine clinical molecular testing. Ann Oncol. 2014;25(2):423-8.
106. Lovly CM, Shaw AT. Molecular pathways: resistance to kinase inhibitors and implications for therapeutic strategies. Clin Cancer Res. 2014;20(9):2249-56.
107. Robey RW, Pluchino KM, Hall MD, Fojo AT, Bates SE, Gottesman MM. Revisiting the role of ABC transporters in multidrug-resistant cancer. Nature Reviews Cancer. 2018;18(7):452-64.

108. Yamashita H, Yano Y, Kawano K, Matsuzaki K. Oligomerization-function relationship of EGFR on living cells detected by the coiled-coil labeling and FRET microscopy. Biochim Biophys Acta. 2015;1848(6):1359-66.
109. Reiterer V, Eyers PA, Farhan H. Day of the dead: pseudokinases and pseudophosphatases in physiology and disease. Trends in Cell Biology. 2014;24(9):489-505.
110. Valley CC, Arndt-Jovin DJ, Karedla N, Steinkamp MP, Chizhik AI, Hlavacek WS, et al. Enhanced dimerization drives ligand-independent activity of mutant epidermal growth factor receptor in lung cancer. Mol Biol Cell. 2015;26(22):4087-99.
111. Chung I, Akita R, Vandlen R, Toomre D, Schlessinger J, Mellman I. Spatial control of EGF receptor activation by reversible dimerization on living cells. Nature. 2010;464(7289):783-7.
112. Ferguson KM. Structure-based view of epidermal growth factor receptor regulation. Annu Rev Biophys. 2008;37:353-73.
113. Ferguson KM, Berger MB, Mendrola JM, Cho HS, Leahy DJ, Lemmon MA. EGF activates its receptor by removing interactions that autoinhibit ectodomain dimerization. Mol Cell. 2003;11(2):507-17.
114. Needham SR, Roberts SK, Arkhipov A, Mysore VP, Tynan CJ, Zanetti-Domingues LC, et al. EGFR oligomerization organizes kinase-active dimers into competent signalling platforms. Nat Commun. 2016;7:13307.
115. Huang Y, Bharill S, Karandur D, Peterson SM, Marita M, Shi X, et al. Molecular basis for multimerization in the activation of the epidermal growth factor receptor. Elife. 2016;5.
116. Hardman G, Perkins S, Brownridge PJ, Clarke CJ, Byrne DP, Campbell AE, et al. Strong anion exchange-mediated phosphoproteomics reveals extensive human non-canonical phosphorylation. The EMBO journal. 2019;38(21):e100847.
117. Sun F, Ding Y, Ji Q, Liang Z, Deng X, Wong CC, et al. Protein cysteine phosphorylation of SarA/MgrA family transcriptional regulators mediates bacterial virulence and antibiotic resistance. Proc Natl Acad Sci U S A. 2012;109(38):15461-6.
118. Tonks NK. Protein tyrosine phosphatases--from housekeeping enzymes to master regulators of signal transduction. Febs j. 2013;280(2):346-78.
119. Pannifer AD, Flint AJ, Tonks NK, Barford D. Visualization of the cysteinyl-phosphate intermediate of a protein-tyrosine phosphatase by x-ray crystallography. J Biol Chem. 1998;273(17):10454-62.
120. Buchowiecka AK. Puzzling over protein cysteine phosphorylation--assessment of proteomic tools for S-phosphorylation profiling. The Analyst. 2014;139 17:4118-23.
121. Guan KL, Dixon JE. Evidence for protein-tyrosine-phosphatase catalysis proceeding via a cysteine-phosphate intermediate. J Biol Chem. 1991;266(26):17026-30.
122. Matthews HR. Protein kinases and phosphatases that act on histidine, lysine, or arginine residues in eukaryotic proteins: a possible regulator of the mitogen-activated protein kinase cascade. Pharmacol Ther. 1995;67(3):323-50.
123. Fuhrmann J, Schmidt A, Spiess S, Lehner A, Turgay K, Mechtler K, et al. McsB Is a Protein Arginine Kinase That Phosphorylates and Inhibits the Heat-Shock Regulator CtsR. Science. 2009;324(5932):1323.
124. Hecker M, Schumann W, Völker U. Heat-shock and general stress response in Bacillus subtilis. Mol Microbiol. 1996;19(3):417-28.
125. Haldenwang WG, Losick R. A modified RNA polymerase transcribes a cloned gene under sporulation control in Bacillus subtilis. Nature. 1979;282(5736):256-60.
126. Hyyryläinen HL, Bolhuis A, Darmon E, Muukkonen L, Koski P, Vitikainen M, et al. A novel two-component regulatory system in Bacillus subtilis for the survival of severe secretion stress. Mol Microbiol. 2001;41(5):1159-72.
127. Schulz A, Schumann W. hrcA, the first gene of the Bacillus subtilis dnaK operon encodes a negative regulator of class I heat shock genes. Journal of Bacteriology. 1996;178(4):1088.
128. Krüger E, Hecker M. The First Gene of the Bacillus subtilis clpC Operon,ctsR, Encodes a Negative Regulator of Its Own Operon and Other Class III Heat Shock Genes. Journal of Bacteriology. 1998;180(24):6681.
129. Derré I, Rapoport G, Msadek T. CtsR, a novel regulator of stress and heat shock response, controls clp and molecular chaperone gene expression in gram-positive bacteria. Mol Microbiol. 1999;31(1):117-31.
130. Krüger E, Zühlke D, Witt E, Ludwig H, Hecker M. Clp-mediated proteolysis in Gram-positive bacteria is autoregulated by the stability of a repressor. Embo j. 2001;20(4):852-63.
131. Kirstein J, Turgay K. A new tyrosine phosphorylation mechanism involved in signal transduction in Bacillus subtilis. J Mol Microbiol Biotechnol. 2005;9(3-4):182-8.
132. Adam K, Hunter T. Histidine kinases and the missing phosphoproteome from prokaryotes to eukaryotes. Laboratory Investigation. 2018;98(2):233-47.

133. Attwood PV, Piggott MJ, Zu XL, Besant PG. Focus on phosphohistidine. Amino Acids. 2007;32(1):145-56.
134. Witt JJ, Roskoski Jr R. Rapid protein kinase assay using phosphocellulose-paper absorption. Analytical biochemistry. 1975;66(1):253-8.
135. Smith DL, Chen C-C, Bruegger BB, Holtz SL, Halpern RM, Smith RA. Characterization of protein kinases forming acid-labile histone phosphates in Walker-256 carcinosarcoma cell nuclei. Biochemistry. 1974;13(18):3780-5.
136. Wei Y-F, Morgan JE, Matthews HR. Studies of histidine phosphorylation by a nuclear protein histidine kinase show that histidine-75 in histone H4 is masked in nucleosome core particles and in chromatin. Archives of biochemistry and biophysics. 1989;268(2):546-50.
137. Besant PG, Attwood PV. Detection of a mammalian histone H4 kinase that has yeast histidine kinase-like enzymic activity. The international journal of biochemistry & cell biology. 2000;32(2):243-53.
138. Fujitaki JM, Smith RA. Techniques in the detection and characterization of phosphoramidate-containing proteins. Methods Enzymol. 107: Elsevier; 1984. p. 23-36.
139. Wieland T, Nürnberg B, Ulibarri I, Kaldenberg-Stasch S, Schultz G, Jakobs K. Guanine nucleotide-specific phosphate transfer by guanine nucleotide-binding regulatory protein beta-subunits. Characterization of the phosphorylated amino acid. Journal of Biological Chemistry. 1993;268(24):18111-8.
140. WIELAND T, ULIBARRI I, GIERSCHIK P, JAKOBS KH. Activation of signal-transducing guanine-nucleotide-binding regulatory proteins by guanosine 5'-[γ-thio] triphosphate: Information transfer by intermediately thiophosphorylated βγ subunits. European journal of biochemistry. 1991;196(3):707-16.
141. Medzihradszky KF, Phillipps NJ, Senderowicz L, Wang P, Turck CW. Synthesis and characterization of histidine-phosphorylated peptides. Protein science. 1997;6(7):1405-11.
142. Wind M, Wegener A, Kellner R, Lehmann WD. Analysis of CheA histidine phosphorylation and its influence on protein stability by high-resolution element and electrospray mass spectrometry. Analytical chemistry. 2005;77(7):1957-62.
143. Hardman G, Eyers CE. High-Throughput Characterization of Histidine Phosphorylation Sites Using UPAX and Tandem Mass Spectrometry. Methods Mol Biol. 2020;2077:225-35.
144. Zschiedrich CP, Keidel V, Szurmant H. Molecular Mechanisms of Two-Component Signal Transduction. Journal of molecular biology. 2016;428(19):3752-75.
145. Ortet P, Whitworth DE, Santaella C, Achouak W, Barakat M. P2CS: updates of the prokaryotic two-component systems database. Nucleic Acids Res. 2015;43(Database issue):D536-D41.
146. Igo MM, Ninfa AJ, Stock JB, Silhavy TJ. Phosphorylation and dephosphorylation of a bacterial transcriptional activator by a transmembrane receptor. Genes Dev. 1989;3(11):1725-34.
147. Albanesi D, Martín M, Trajtenberg F, Mansilla MC, Haouz A, Alzari PM, et al. Structural plasticity and catalysis regulation of a thermosensor histidine kinase. Proc Natl Acad Sci U S A. 2009;106(38):16185-90.
148. Sevvana M, Vijayan V, Zweckstetter M, Reinelt S, Madden DR, Herbst-Irmer R, et al. A ligand-induced switch in the periplasmic domain of sensor histidine kinase CitA. J Mol Biol. 2008;377(2):512-23.
149. Bader MW, Sanowar S, Daley ME, Schneider AR, Cho U, Xu W, et al. Recognition of antimicrobial peptides by a bacterial sensor kinase. Cell. 2005;122(3):461-72.
150. Unden G, Nilkens S, Singenstreu M. Bacterial sensor kinases using Fe-S cluster binding PAS or GAF domains for O2 sensing. Dalton Trans. 2013;42(9):3082-7.
151. Neiditch MB, Federle MJ, Pompeani AJ, Kelly RC, Swem DL, Jeffrey PD, et al. Ligand-induced asymmetry in histidine sensor kinase complex regulates quorum sensing. Cell. 2006;126(6):1095-108.
152. Meadow ND, Fox DK, Roseman S. THE BACTERIAL PHOSPHOENOL-PYRUVATE: GLYCOSE PHOSPHOTRANSFERASE SYSTEM. Annual Review of Biochemistry. 1990;59(1):497-542.
153. Postma PW, Lengeler JW, Jacobson G. Phosphoenolpyruvate: carbohydrate phosphotransferase systems of bacteria. Microbiological reviews. 1993;57(3):543-94.
154. Puttick J, Baker EN, Delbaere LTJ. Histidine phosphorylation in biological systems. Biochimica et Biophysica Acta (BBA) - Proteins and Proteomics. 2008;1784(1):100-5.
155. Popov K, Zhao Y, Shimomura Y, Kuntz M, Harris R. Branched-chain alpha-ketoacid dehydrogenase kinase. Molecular cloning, expression, and sequence similarity with histidine protein kinases. Journal of Biological Chemistry. 1992;267(19):13127-30.
156. Davie JR, Wynn RM, Meng M, Huang Y-s, Aalund G, Chuang DT, et al. Expression and characterization of branched-chain α-ketoacid dehydrogenase kinase from the rat: is it a histidine-protein kinase? Journal of Biological Chemistry. 1995;270(34):19861-7.
157. Thelen JJ, MIERNYK JA, RANDALL DD. Pyruvate dehydrogenase kinase from Arabidopsis thaliana: a protein histidine kinase that phosphorylates serine residues. Biochemical Journal. 2000;349(1):195-201.

158. Tuganova A, Yoder MD, Popov KM. An essential role of Glu-243 and His-239 in the phosphotransfer reaction catalyzed by pyruvate dehydrogenase kinase. Journal of Biological Chemistry. 2001;276(21):17994-9.
159. Tovar-Mendez A, Miernyk JA, Randall DD. Histidine mutagenesis of Arabidopsis thaliana pyruvate dehydrogenase kinase. European journal of biochemistry. 2002;269(10):2601-6.
160. Morera S, Chiadmi M, LeBras G, Lascu I, Janin J. Mechanism of phosphate transfer by nucleoside diphosphate kinase: X-ray structures of the phosphohistidine intermediate of the enzymes from Drosophila and Dictyostelium. Biochemistry. 1995;34(35):11062-70.
161. Krebs HA, Hems R. Some reactions of adenosine and inosine phosphates in animal tissues. Biochim Biophys Acta. 1953;12(1-2):172-80.
162. Berg P, Joklik WK. Transphosphorylation between nucleoside polyphosphates. Nature. 1953;172(4387):1008-9.
163. Muñoz-Dorado J, Inouye S, Inouye M. Nucleoside diphosphate kinase from Myxococcus xanthus. II. Biochemical characterization. J Biol Chem. 1990;265(5):2707-12.
164. Lacombe ML, Wallet V, Troll H, Véron M. Functional cloning of a nucleoside diphosphate kinase from Dictyostelium discoideum. J Biol Chem. 1990;265(17):10012-8.
165. Kimura N, Shimada N, Nomura K, Watanabe K. Isolation and characterization of a cDNA clone encoding rat nucleoside diphosphate kinase. J Biol Chem. 1990;265(26):15744-9.
166. Biggs J, Tripoulas N, Hersperger E, Dearolf C, Shearn A. Analysis of the lethal interaction between the prune and Killer of prune mutations of Drosophila. Genes Dev. 1988;2(10):1333-43.
167. Hama H, Almaula N, Lerner CG, Inouye S, Inouye M. Nucleoside diphosphate kinase from Escherichia coli; its overproduction and sequence comparison with eukaryotic enzymes. Gene. 1991;105(1):31-6.
168. Rosengard AM, Krutzsch HC, Shearn A, Biggs JR, Barker E, Margulies IM, et al. Reduced Nm23/Awd protein in tumour metastasis and aberrant Drosophila development. Nature. 1989;342(6246):177-80.
169. Ishikawa N, Shimada N, Takagi Y, Ishijima Y, Fukuda M, Kimura N. Molecular evolution of nucleoside diphosphate kinase genes: conserved core structures and multiple-layered regulatory regions. J Bioenerg Biomembr. 2003;35(1):7-18.
170. Yoon JH, Qiu J, Cai S, Chen Y, Cheetham ME, Shen B, et al. The retinitis pigmentosa-mutated RP2 protein exhibits exonuclease activity and translocates to the nucleus in response to DNA damage. Exp Cell Res. 2006;312(8):1323-34.
171. Schwahn U, Lenzner S, Dong J, Feil S, Hinzmann B, van Duijnhoven G, et al. Positional cloning of the gene for X-linked retinitis pigmentosa 2. Nat Genet. 1998;19(4):327-32.
172. Boissan M, Schlattner U, Lacombe M-L. The NDPK/NME superfamily: state of the art. Laboratory Investigation. 2018;98(2):164-74.
173. Schlattner U. The Complex Functions of the NME Family-A Matter of Location and Molecular Activity. International journal of molecular sciences. 2021;22(23):13083.
174. Kaetzel DM, Zhang Q, Yang M, McCorkle JR, Ma D, Craven RJ. Potential roles of 3'-5' exonuclease activity of NM23-H1 in DNA repair and malignant progression. J Bioenerg Biomembr. 2006;38(3-4):163-7.
175. Puts GS, Leonard MK, Pamidimukkala NV, Snyder DE, Kaetzel DM. Nuclear functions of NME proteins. Laboratory Investigation. 2018;98(2):211-8.
176. Sharma S, Sengupta A, Chowdhury S. Emerging Molecular Connections between NM23 Proteins, Telomeres and Telomere-Associated Factors: Implications in Cancer Metastasis and Ageing. International Journal of Molecular Sciences. 2021;22(7):3457.
177. Chen CW, Wang HL, Huang CW, Huang CY, Lim WK, Tu IC, et al. Two separate functions of NME3 critical for cell survival underlie a neurodegenerative disorder. Proc Natl Acad Sci U S A. 2019;116(2):566-74.
178. Tokarska-Schlattner M, Boissan M, Munier A, Borot C, Mailleau C, Speer O, et al. The nucleoside diphosphate kinase D (NM23-H4) binds the inner mitochondrial membrane with high affinity to cardiolipin and couples nucleotide transfer with respiration. J Biol Chem. 2008;283(38):26198-207.
179. Janin J, Dumas C, Moréra S, Xu Y, Meyer P, Chiadmi M, et al. Three-Dimensional Structure of Nucleoside Diphosphate Kinase. Journal of Bioenergetics and Biomembranes. 2000;32(3):215-25.
180. Adam K, Ning J, Reina J, Hunter T. NME/NM23/NDPK and Histidine Phosphorylation. International journal of molecular sciences. 2020;21(16):5848.
181. Webb PA, Perisic O, Mendola CE, Backer JM, Williams RL. The crystal structure of a human nucleoside diphosphate kinase, NM23-H2. J Mol Biol. 1995;251(4):574-87.
182. Lascu I, Giartosio A, Ransac S, Erent M. Quaternary Structure of Nucleoside Diphosphate Kinases. Journal of Bioenergetics and Biomembranes. 2000;32(3):227-36.
183. Georgescauld F, Song Y, Dautant A. Structure, Folding and Stability of Nucleoside Diphosphate Kinases. Int J Mol Sci. 2020;21(18).

184. Milon L, Meyer P, Chiadmi M, Munier A, Johansson M, Karlsson A, et al. The human nm23-H4 gene product is a mitochondrial nucleoside diphosphate kinase. J Biol Chem. 2000;275(19):14264-72.
185. Moynié L, Giraud MF, Georgescauld F, Lascu I, Dautant A. The structure of the Escherichia coli nucleoside diphosphate kinase reveals a new quaternary architecture for this enzyme family. PROTEINS: Structure, Function, and Bioinformatics. 2007;67(3):755-65.
186. Vieira PS, de Giuseppe PO, de Oliveira AHC, Murakami MT. The role of the C-terminus and Kpn loop in the quaternary structure stability of nucleoside diphosphate kinase from Leishmania parasites. Journal of Structural Biology. 2015;192(3):336-41.
187. Georgescauld F, Song Y, Dautant A. Structure, Folding and Stability of Nucleoside Diphosphate Kinases. International journal of molecular sciences. 2020;21(18):6779.
188. Lascu I, Chaffotte A, Limbourg-Bouchon B, Véron M. A Pro/Ser substitution in nucleoside diphosphate kinase of Drosophila melanogaster (mutation killer of prune) affects stability but not catalytic efficiency of the enzyme. Journal of Biological Chemistry. 1992;267(18):12775-81.
189. Abu-Taha IH, Vettel C, Wieland T. Targeting altered Nme heterooligomerization in disease? Oncotarget. 2017;9(2):1492-3.
190. Abu-Taha IH, Heijman J, Hippe HJ, Wolf NM, El-Armouche A, Nikolaev VO, et al. Nucleoside Diphosphate Kinase-C Suppresses cAMP Formation in Human Heart Failure. Circulation. 2017;135(9):881-97.
191. Kim MS, Jeong J, Jeong J, Shin DH, Lee KJ. Structure of Nm23-H1 under oxidative conditions. Acta Crystallogr D Biol Crystallogr. 2013;69(Pt 4):669-80.
192. Song EJ, Kim YS, Chung JY, Kim E, Chae S-K, Lee K-J. Oxidative Modification of Nucleoside Diphosphate Kinase and Its Identification by Matrix-Assisted Laser Desorption/Ionization Time-of-Flight Mass Spectrometry. Biochemistry. 2000;39(33):10090-7.
193. Peuchant E, Bats ML, Moranvillier I, Lepoivre M, Guitton J, Wendum D, et al. Metastasis suppressor NM23 limits oxidative stress in mammals by preventing activation of stress-activated protein kinases/JNKs through its nucleoside diphosphate kinase activity. Faseb j. 2017;31(4):1531-46.
194. Schaertl S, Konrad M, Geeves MA. Substrate specificity of human nucleoside-diphosphate kinase revealed by transient kinetic analysis. Journal of Biological Chemistry. 1998;273(10):5662-9.
195. Garces E, Cleland WW. Kinetic study of yeast nucleosidediphosphate kinase. Biochemistry. 1969;8(2):633-40.
196. Parks RE, Aganwal RP. 9 Nucleoside Diphosphokinases. In: Boyer PD, editor. The Enzymes. 8: Academic Press; 1973. p. 307-33.
197. Moréra S, Lacombe M-L, Yingwu X, Joël Janin GLa. X-ray structure of human nucleoside diphosphate kinase B complexed with GDP at 2 å resolution. Structure. 1995;3(12):1307-14.
198. Dumas C, Lascu I, Moréra S, Glaser P, Fourme R, Wallet V, et al. X-ray structure of nucleoside diphosphate kinase. Embo j. 1992;11(9):3203-8.
199. Chen Y, Gallois-Montbrun S, Schneider B, Véron M, Moréra S, Deville-Bonne D, et al. Nucleotide binding to nucleoside diphosphate kinases: X-ray structure of human NDPK-A in complex with ADP and comparison to protein kinases. J Mol Biol. 2003;332(4):915-26.
200. Xu Y-W, Moréra S, Janin J, Cherfils J. AlF3 mimics the transition state of protein phosphorylation in the crystal structure of nucleoside diphosphate kinase and MgADP. Proceedings of the National Academy of Sciences. 1997;94(8):3579-83.
201. Cherfils J, Moréra S, Lascu I, Véron M, Janin J. X-ray structure of nucleoside diphosphate kinase complexed with thymidine diphosphate and Mg2+ at 2-A resolution. Biochemistry. 1994;33(31):9062-9.
202. Stafford LJ, Vaidya KS, Welch DR. Metastasis suppressors genes in cancer. Int J Biochem Cell Biol. 2008;40(5):874-91.
203. Khan I, Steeg PS. Metastasis suppressors: functional pathways. Lab Invest. 2018;98(2):198-210.
204. Bevilacqua G, Sobel ME, Liotta LA, Steeg PS. Association of low nm23 RNA levels in human primary infiltrating ductal breast carcinomas with lymph node involvement and other histopathological indicators of high metastatic potential. Cancer research. 1989;49(18):5185-90.
205. Flørenes VA, Aamdal S, Myklebost O, Maelandsmo GM, Bruland ØS, Fodstad Ø. Levels of nm23 messenger RNA in metastatic malignant melanomas: inverse correlation to disease progression. Cancer research. 1992;52(21):6088-91.
206. Xerri L, Grob J, Battyani Z, Gouvernet J, Hassoun J, Bonerandi J. NM23 expression in metastasis of malignant melanoma is a predictive prognostic parameter correlated with survival. British journal of cancer. 1994;70(6):1224-8.
207. Boissan M, Lacombe M-L. Nm23/NDP kinases in hepatocellular carcinoma. Journal of bioenergetics and biomembranes. 2006;38(3):169-75.

208. Run A, Jie M, Qi S, Xiao-Xia D, Jing-Hong C, Yan-Jun L, et al. Expressions of nucleoside diphosphate kinase (nm23) in tumor tissues are related with metastasis and length of survival of patients with hepatocellular carcinoma. Biomedical and Environmental Sciences. 2010;23(4):267-73.
209. Hartsough MT, Steeg PS. Nm23/nucleoside diphosphate kinase in human cancers. Journal of bioenergetics and biomembranes. 2000;32(3):301-8.
210. Lacombe M-L, Boissan M. NME1 (NME/NM23 nucleoside diphosphate kinase 1). Atlas of Genetics and Cytogenetics in Oncology and Haematology. 2013.
211. Liu L, Li M, Zhang C, Zhang J, Li G, Zhang Z, et al. Prognostic value and clinicopathologic significance of nm23 in various cancers: A systematic review and meta-analysis. International Journal of Surgery. 2018;60:257-65.
212. Leonard MK, McCorkle JR, Snyder DE, Novak M, Zhang Q, Shetty AC, et al. Identification of a gene expression signature associated with the metastasis suppressor function of NME1: prognostic value in human melanoma. Laboratory Investigation. 2018;98(3):327-38.
213. Howlett AR, Petersen OW, Bissell MJ, Steeg PS. A novel function for the nm23-H1 gene: overexpression in human breast carcinoma cells leads to the formation of basement membrane and growth arrest. JNCI: Journal of the National Cancer Institute. 1994;86(24):1838-44.
214. Andolfo I, De Martino D, Liguori L, Petrosino G, Troncone G, Tata N, et al. Correlation of NM23-H1 cytoplasmic expression with metastatic stage in human prostate cancer tissue. Naunyn Schmiedebergs Arch Pharmacol. 2011;384(4-5):489-98.
215. Harłozińska A, Bar JK, Gerber J. nm23 expression in tissue sections and tumor effusion cells of ovarian neoplasms. Int J Cancer. 1996;69(5):415-9.
216. Garcia I, Mayol G, Ríos J, Domenech G, Cheung NK, Oberthuer A, et al. A three-gene expression signature model for risk stratification of patients with neuroblastoma. Clin Cancer Res. 2012;18(7):2012-23.
217. Chang CL, Zhu XX, Thoraval DH, Ungar D, Rawwas J, Hora N, et al. Nm23-H1 mutation in neuroblastoma. Nature. 1994;370(6488):335-6.
218. Tan CY, Chang CL. NDPKA is not just a metastasis suppressor - be aware of its metastasis-promoting role in neuroblastoma. Lab Invest. 2018;98(2):219-27.
219. Boissan M, De Wever O, Lizarraga F, Wendum D, Poincloux R, Chignard N, et al. Implication of metastasis suppressor NM23-H1 in maintaining adherens junctions and limiting the invasive potential of human cancer cells. Cancer Res. 2010;70(19):7710-22.
220. Farkas Z, Fancsalszky L, Saskői É, Gráf A, Tárnok K, Mehta A, et al. The dosage-dependent effect exerted by the NM23-H1/H2 homolog NDK-1 on distal tip cell migration in C. elegans. Lab Invest. 2018;98(2):182-9.
221. Boissan M, Wendum D, Arnaud-Dabernat S, Munier A, Debray M, Lascu I, et al. Increased lung metastasis in transgenic NM23-Null/SV40 mice with hepatocellular carcinoma. J Natl Cancer Inst. 2005;97(11):836-45.
222. Leone A, Flatow U, VanHoutte K, Steeg PS. Transfection of human nm23-H1 into the human MDA-MB-435 breast carcinoma cell line: effects on tumor metastatic potential, colonization and enzymatic activity. Oncogene. 1993;8(9):2325-33.
223. Parhar RS, Shi Y, Zou M, Farid NR, Ernst P, al-Sedairy ST. Effects of cytokine-mediated modulation of nm23 expression on the invasion and metastatic behavior of B16F10 melanoma cells. Int J Cancer. 1995;60(2):204-10.
224. Baba H, Urano T, Okada K, Furukawa K, Nakayama E, Tanaka H, et al. Two isotypes of murine nm23/nucleoside diphosphate kinase, nm23-M1 and nm23-M2, are involved in metastatic suppression of a murine melanoma line. Cancer Res. 1995;55(9):1977-81.
225. Ory S, Zhou M, Conrads TP, Veenstra TD, Morrison DK. Protein phosphatase 2A positively regulates Ras signaling by dephosphorylating KSR1 and Raf-1 on critical 14-3-3 binding sites. Curr Biol. 2003;13(16):1356-64.
226. Hartsough MT, Morrison DK, Salerno M, Palmieri D, Ouatas T, Mair M, et al. Nm23-H1 metastasis suppressor phosphorylation of kinase suppressor of Ras via a histidine protein kinase pathway. J Biol Chem. 2002;277(35):32389-99.
227. Alexa A, Varga J, Reményi A. Scaffolds are 'active' regulators of signaling modules. Febs j. 2010;277(21):4376-82.
228. Morrison DK. KSR: a MAPK scaffold of the Ras pathway? J Cell Sci. 2001;114(Pt 9):1609-12.
229. Karnoub AE, Weinberg RA. Ras oncogenes: split personalities. Nat Rev Mol Cell Biol. 2008;9(7):517-31.
230. Lowe SW, Cepero E, Evan G. Intrinsic tumour suppression. Nature. 2004;432(7015):307-15.
231. Hanahan D, Weinberg RA. Hallmarks of cancer: the next generation. Cell. 2011;144(5):646-74.

232. Wu Z, Guo L, Ge J, Zhang Z, Wei H, Zhou Q. Two serine residues of non-metastasis protein 23-H1 are critical in inhibiting signal transducer and activator of transcription 3 activity in human lung cancer cells. Oncol Lett. 2017;14(2):2475-82.
233. Sturtevant AH. A Highly Specific Complementary Lethal System in Drosophila Melanogaster. Genetics. 1956;41(1):118-23.
234. Xu J, Liu LZ, Deng XF, Timmons L, Hersperger E, Steeg PS, et al. The enzymatic activity of Drosophila AWD/NDP kinase is necessary but not sufficient for its biological function. Dev Biol. 1996;177(2):544-57.
235. Krishnan KS, Rikhy R, Rao S, Shivalkar M, Mosko M, Narayanan R, et al. Nucleoside diphosphate kinase, a source of GTP, is required for dynamin-dependent synaptic vesicle recycling. Neuron. 2001;30(1):197-210.
236. Ferguson SM, De Camilli P. Dynamin, a membrane-remodelling GTPase. Nat Rev Mol Cell Biol. 2012;13(2):75-88.
237. Khan I, Gril B, Steeg PS. Metastasis Suppressors NME1 and NME2 Promote Dynamin 2 Oligomerization and Regulate Tumor Cell Endocytosis, Motility, and Metastasis. Cancer Res. 2019;79(18):4689-702.
238. Boissan M, Montagnac G, Shen Q, Griparic L, Guitton J, Romao M, et al. Membrane trafficking. Nucleoside diphosphate kinases fuel dynamin superfamily proteins with GTP for membrane remodeling. Science. 2014;344(6191):1510-5.
239. Massé K, Dabernat S, Bourbon PM, Larou M, Amrein L, Barraud P, et al. Characterization of the nm23-M2, nm23-M3 and nm23-M4 mouse genes: comparison with their human orthologs. Gene. 2002;296(1-2):87-97.
240. Arnaud-Dabernat S, Bourbon PM, Dierich A, Le Meur M, Daniel JY. Knockout mice as model systems for studying nm23/NDP kinase gene functions. Application to the nm23-M1 gene. J Bioenerg Biomembr. 2003;35(1):19-30.
241. Deplagne C, Peuchant E, Moranvillier I, Dubus P, Dabernat S. The anti-metastatic nm23-1 gene is needed for the final step of mammary duct maturation of the mouse nipple. PLoS One. 2011;6(4):e18645.
242. Di L, Srivastava S, Zhdanova O, Sun Y, Li Z, Skolnik EY. Nucleoside diphosphate kinase B knock-out mice have impaired activation of the K+ channel KCa3.1, resulting in defective T cell activation. J Biol Chem. 2010;285(50):38765-71.
243. Srivastava S, Li Z, Ko K, Choudhury P, Albaqumi M, Johnson AK, et al. Histidine phosphorylation of the potassium channel KCa3.1 by nucleoside diphosphate kinase B is required for activation of KCa3.1 and CD4 T cells. Mol Cell. 2006;24(5):665-75.
244. Postel EH, Wohlman I, Zou X, Juan T, Sun N, D'Agostin D, et al. Targeted deletion of Nm23/nucleoside diphosphate kinase A and B reveals their requirement for definitive erythropoiesis in the mouse embryo. Dev Dyn. 2009;238(3):775-87.
245. Gold ES, Underhill DM, Morrissette NS, Guo J, McNiven MA, Aderem A. Dynamin 2 is required for phagocytosis in macrophages. J Exp Med. 1999;190(12):1849-56.
246. Farkas Z, Petric M, Liu X, Herit F, Rajnavölgyi É, Szondy Z, et al. The nucleoside diphosphate kinase NDK-1/NME1 promotes phagocytosis in concert with DYN-1/Dynamin. Faseb j. 2019;33(10):11606-14.
247. Murakami M, Meneses PI, Knight JS, Lan K, Kaul R, Verma SC, et al. Nm23-H1 modulates the activity of the guanine exchange factor Dbl-1. Int J Cancer. 2008;123(3):500-10.
248. Marino N, Marshall JC, Collins JW, Zhou M, Qian Y, Veenstra T, et al. Nm23-h1 binds to gelsolin and inactivates its actin-severing capacity to promote tumor cell motility and metastasis. Cancer Res. 2013;73(19):5949-62.
249. Garzia L, D'Angelo A, Amoresano A, Knauer SK, Cirulli C, Campanella C, et al. Phosphorylation of nm23-H1 by CKI induces its complex formation with h-prune and promotes cell motility. Oncogene. 2008;27(13):1853-64.
250. D'Angelo A, Garzia L, André A, Carotenuto P, Aglio V, Guardiola O, et al. Prune cAMP phosphodiesterase binds nm23-H1 and promotes cancer metastasis. Cancer Cell. 2004;5(2):137-49.
251. Tran AT, Chapman EM, Flamand MN, Yu B, Krempel SJ, Duchaine TF, et al. MiR-35 buffers apoptosis thresholds in the C. elegans germline by antagonizing both MAPK and core apoptosis pathways. Cell Death Differ. 2019;26(12):2637-51.
252. Chowdhury D, Beresford PJ, Zhu P, Zhang D, Sung JS, Demple B, et al. The exonuclease TREX1 is in the SET complex and acts in concert with NM23-H1 to degrade DNA during granzyme A-mediated cell death. Mol Cell. 2006;23(1):133-42.
253. Fan Z, Beresford PJ, Oh DY, Zhang D, Lieberman J. Tumor suppressor NM23-H1 is a granzyme A-activated DNase during CTL-mediated apoptosis, and the nucleosome assembly protein SET is its inhibitor. Cell. 2003;112(5):659-72.

254. Schlattner U, Tokarska-Schlattner M, Ramirez S, Tyurina YY, Amoscato AA, Mohammadyani D, et al. Dual Function of Mitochondrial Nm23-H4 Protein in Phosphotransfer and Intermembrane Lipid Transfer: A CARDIOLIPIN-DEPENDENT SWITCH *[♦]. Journal of Biological Chemistry. 2013;288(1):111-21.
255. Kagan VE, Jiang J, Huang Z, Tyurina YY, Desbourdes C, Cottet-Rousselle C, et al. NDPK-D (NM23-H4)-mediated externalization of cardiolipin enables elimination of depolarized mitochondria by mitophagy. Cell Death Differ. 2016;23(7):1140-51.
256. Iyer Shankar S, He Q, Janczy John R, Elliott Eric I, Zhong Z, Olivier Alicia K, et al. Mitochondrial Cardiolipin Is Required for Nlrp3 Inflammasome Activation. Immunity. 2013;39(2):311-23.
257. Ernst O, Sun J, Lin B, Banoth B, Dorrington MG, Liang J, et al. A genome-wide screen uncovers multiple roles for mitochondrial nucleoside diphosphate kinase D in inflammasome activation. Sci Signal. 2021;14(694).
258. Anderegg L, Im Hof Gut M, Hetzel U, Howerth EW, Leuthard F, Kyöstilä K, et al. NME5 frameshift variant in Alaskan Malamutes with primary ciliary dyskinesia. PLOS Genetics. 2019;15(9):e1008378.
259. Sahabian A, von Schlehdorn L, Drick N, Pink I, Dahlmann J, Haase A, et al. Generation of two hiPSC clones (MHHi019-A, MHHi019-B) from a primary ciliary dyskinesia patient carrying a homozygous deletion in the NME5 gene (c.415delA (p.Ile139Tyrfs*8)). Stem Cell Research. 2020;48:101988.
260. Cho EH, Huh HJ, Jeong I, Lee NY, Koh W-J, Park H-C, et al. A nonsense variant in NME5 causes human primary ciliary dyskinesia with radial spoke defects. Clinical Genetics. 2020;98(1):64-8.
261. Šedová L, Buková I, Bažantová P, Petrezsélyová S, Prochazka J, Školníková E, et al. Semi-Lethal Primary Ciliary Dyskinesia in Rats Lacking the Nme7 Gene. Int J Mol Sci. 2021;22(8).
262. Šedová L, Prochazka J, Zudová D, Bendlová B, Včelák J, Sedlacek R, et al. Heterozygous Nme7 Mutation Affects Glucose Tolerance in Male Rats. Genes (Basel). 2021;12(7).
263. Šedová L, Školníková E, Hodúlová M, Včelák J, Šeda O, Bendlová B. Expression profiling of Nme7 interactome in experimental models of metabolic syndrome. Physiol Res. 2018;67(Suppl 3):S543-s50.
264. Freije JM, Blay P, MacDonald NJ, Manrow RE, Steeg PS. Site-directed mutation of Nm23-H1. Mutations lacking motility suppressive capacity upon transfection are deficient in histidine-dependent protein phosphotransferase pathways in vitro. J Biol Chem. 1997;272(9):5525-32.
265. Penhoet EE, Kochman M, Rutter WJ. Molecular and catalytic properties of aldolase C. Biochemistry. 1969;8(11):4396-402.
266. Ma D, McCorkle JR, Kaetzel DM. The metastasis suppressor NM23-H1 possesses 3'-5' exonuclease activity. J Biol Chem. 2004;279(17):18073-84.
267. Kalagiri R, Stanfield RL, Meisenhelder J, Clair JJL, Fuhs SR, Wilson IA, et al. Structural basis for differential recognition of phosphohistidine-containing peptides by 1-pHis and 3-pHis monoclonal antibodies. Proceedings of the National Academy of Sciences. 2021;118(6):e2010644118.
268. Crabtree GR, Olson EN. NFAT signaling: choreographing the social lives of cells. Cell. 2002;109 Suppl:S67-79.
269. Ghanshani S, Wulff H, Miller MJ, Rohm H, Neben A, Gutman GA, et al. Up-regulation of the IKCa1 potassium channel during T-cell activation. Molecular mechanism and functional consequences. J Biol Chem. 2000;275(47):37137-49.
270. Srivastava S, Ko K, Choudhury P, Li Z, Johnson AK, Nadkarni V, et al. Phosphatidylinositol-3 phosphatase myotubularin-related protein 6 negatively regulates CD4 T cells. Mol Cell Biol. 2006;26(15):5595-602.
271. Srivastava S, Choudhury P, Li Z, Liu G, Nadkarni V, Ko K, et al. Phosphatidylinositol 3-phosphate indirectly activates KCa3.1 via 14 amino acids in the carboxy terminus of KCa3.1. Molecular biology of the cell. 2006;17(1):146-54.
272. Boros S, Bindels RJ, Hoenderop JG. Active Ca(2+) reabsorption in the connecting tubule. Pflugers Arch. 2009;458(1):99-109.
273. Cai X, Srivastava S, Surindran S, Li Z, Skolnik EY. Regulation of the epithelial Ca^{2+} channel TRPV5 by reversible histidine phosphorylation mediated by NDPK-B and PHPT1. Mol Biol Cell. 2014;25(8):1244-50.
274. Maylie J, Bond CT, Herson PS, Lee WS, Adelman JP. Small conductance Ca2+-activated K+ channels and calmodulin. J Physiol. 2004;554(Pt 2):255-61.
275. de Groot T, Kovalevskaya NV, Verkaart S, Schilderink N, Felici M, van der Hagen EA, et al. Molecular mechanisms of calmodulin action on TRPV5 and modulation by parathyroid hormone. Mol Cell Biol. 2011;31(14):2845-53.
276. de Groot T, Verkaart S, Xi Q, Bindels RJ, Hoenderop JG. The identification of Histidine 712 as a critical residue for constitutive TRPV5 internalization. J Biol Chem. 2010;285(37):28481-7.

277. Wei Y-F, Matthews HR. A filter-based protein kinase assay selective for alkali-stable protein phosphorylation and suitable for acid-labile protein phosphorylation. Analytical biochemistry. 1990;190(2):188-92.
278. Smith DL, Bruegger BB, Halpern RM, Smith RA. New Histone Kinases in Nuclei of Rat Tissues. Nature. 1973;246(5428):103-4.
279. Chen C-C, Smith DL, Bruegger BB, Halpern RM, Smith RA. Occurrence and distribution of acid-labile histone phosphates in regenerating rat liver. Biochemistry. 1974;13(18):3785-9.
280. Chen CC, Bruegger BB, Kern C, Lin Y, Halpern R, Smith RA. Phosphorylation of nuclear proteins in rat regenerating liver. Biochemistry. 1977;16(22):4852-5.
281. Tan E, Besant PG, Zu XL, Turck CW, Bogoyevitch MA, Lim SG, et al. Histone H4 histidine kinase displays the expression pattern of a liver oncodevelopmental marker. Carcinogenesis. 2004;25(11):2083-8.
282. Huebner VD, Matthews H. Phosphorylation of histidine in proteins by a nuclear extract of Physarum polycephalum plasmodia. Journal of Biological Chemistry. 1985;260(30):16106-13.
283. He H, Lehming N. Global effects of histone modifications. Briefings in Functional Genomics. 2003;2(3):234-43.
284. Pascreau G, Arlot-Bonnemains Y, Prigent C. Phosphorylation of histone and histone-like proteins by aurora kinases during mitosis. PROGRESS IN CELL CYCLE RESEARCH. 2003;5:369-74.
285. Iizuka M, Smith MM. Functional consequences of histone modifications. Current opinion in genetics & development. 2003;13(2):154-60.
286. Hake S, Xiao A, Allis C. Linking the epigenetic 'language'of covalent histone modifications to cancer. British journal of cancer. 2004;90(4):761-9.
287. Luger K, Richmond TJ. The histone tails of the nucleosome. Current opinion in genetics & development. 1998;8(2):140-6.
288. Wakim BT, Aswad GD. Ca(2+)-calmodulin-dependent phosphorylation of arginine in histone 3 by a nuclear kinase from mouse leukemia cells. Journal of Biological Chemistry. 1994;269(4):2722-7.
289. Kowluru A. Identification and characterization of a novel protein histidine kinase in the islet β cell: evidence for its regulation by mastoparan, an activator of G-proteins and insulin secretion. Biochemical pharmacology. 2002;63(12):2091-100.
290. Wieland T, Nürnberg B, Ulibarri I, Kaldenberg-Stasch S, Schultz G, Jakobs KH. Guanine nucleotide-specific phosphate transfer by guanine nucleotide-binding regulatory protein beta-subunits. Characterization of the phosphorylated amino acid. J Biol Chem. 1993;268(24):18111-8.
291. Wieland T, Ulibarri I, Gierschik P, Jakobs KH. Activation of signal-transducing guanine-nucleotide-binding regulatory proteins by guanosine 5'-[gamma-thio]triphosphate. Information transfer by intermediately thiophosphorylated beta gamma subunits. Eur J Biochem. 1991;196(3):707-16.
292. Hohenegger M, Mitterauer T, Voss T, Nanoff C, Freissmuth M. Thiophosphorylation of the G protein beta subunit in human platelet membranes: evidence against a direct phosphate transfer reaction to G alpha subunits. Mol Pharmacol. 1996;49(1):73-80.
293. Nürnberg B, Harhammer R, Exner T, Schulze RA, Wieland T. Species- and tissue-dependent diversity of G-protein beta subunit phosphorylation: evidence for a cofactor. Biochem J. 1996;318 (Pt 2)(Pt 2):717-22.
294. Kowluru A, Seavey SE, Rhodes CJ, Metz SA. A novel regulatory mechanism for trimeric GTP-binding proteins in the membrane and secretory granule fractions of human and rodent beta cells. Biochem J. 1996;313 (Pt 1)(Pt 1):97-107.
295. Wieland T, Ronzani M, Jakobs KH. Stimulation and inhibition of human platelet adenylylcyclase by thiophosphorylated transducin beta gamma-subunits. J Biol Chem. 1992;267(29):20791-7.
296. Cuello F, Schulze RA, Heemeyer F, Meyer HE, Lutz S, Jakobs KH, et al. Activation of heterotrimeric G proteins by a high energy phosphate transfer via nucleoside diphosphate kinase (NDPK) B and Gbeta subunits. Complex formation of NDPK B with Gbeta gamma dimers and phosphorylation of His-266 IN Gbeta. J Biol Chem. 2003;278(9):7220-6.
297. Cuello F, Schulze RA, Heemeyer F, Meyer HE, Lutz S, Jakobs KH, et al. Activation of Heterotrimeric G Proteins by a High Energy Phosphate Transfer via Nucleoside Diphosphate Kinase (NDPK) B and Gβ Subunits: COMPLEX FORMATION OF NDPK B WITH Gβγ DIMERS AND PHOSPHORYLATION OF His-266 IN Gβ *. Journal of Biological Chemistry. 2003;278(9):7220-6.
298. Orlov NY, Orlova TG, Nomura K, Hanai N, Kimura N. Transducin-mediated, isoform-specific interaction of recombinant rat nucleoside diphosphate kinases with bleached bovine retinal rod outer segment membranes. FEBS Lett. 1996;389(2):186-90.

299. Klinker JF, Seifert R. Nucleoside diphosphate kinase activity in soluble transducin preparations biochemical properties and possible role of transducin-beta as phosphorylated enzyme intermediate. Eur J Biochem. 1999;261(1):72-80.
300. Wieland T, Jakobs KH. Evidence for nucleoside diphosphokinase-dependent channeling of guanosine 5'-(gamma-thio)triphosphate to guanine nucleotide-binding proteins. Mol Pharmacol. 1992;42(5):731-5.
301. Wall MA, Coleman DE, Lee E, Iñiguez-Lluhi JA, Posner BA, Gilman AG, et al. The structure of the G protein heterotrimer Gi alpha 1 beta 1 gamma 2. Cell. 1995;83(6):1047-58.
302. Wagner PD, Vu N-D. Phosphorylation of ATP-Citrate Lyase by Nucleoside Diphosphate Kinase (∗). Journal of Biological Chemistry. 1995;270(37):21758-64.
303. Fraser ME, Joyce MA, Ryan DG, Wolodko WT. Two Glutamate Residues, Glu 208α and Glu 197β, Are Crucial for Phosphorylation and Dephosphorylation of the Active-Site Histidine Residue in Succinyl-CoA Synthetase. Biochemistry. 2002;41(2):537-46.
304. Kowluru A, Tannous M, Chen HQ. Localization and characterization of the mitochondrial isoform of the nucleoside diphosphate kinase in the pancreatic beta cell: evidence for its complexation with mitochondrial succinyl-CoA synthetase. Arch Biochem Biophys. 2002;398(2):160-9.
305. Wells TN. ATP-citrate lyase from rat liver. Characterisation of the citryl-enzyme complexes. Eur J Biochem. 1991;199(1):163-8.
306. Panda S, Srivastava S, Li Z, Vaeth M, Fuhs SR, Hunter T, et al. Identification of PGAM5 as a Mammalian Protein Histidine Phosphatase that Plays a Central Role to Negatively Regulate CD4(+) T Cells. Mol Cell. 2016;63(3):457-69.
307. Seal US, Binkley F. An inorganic pyrophosphatase of swine brain. J Biol Chem. 1957;228(1):193-9.
308. Hindupur SK, Colombi M, Fuhs SR, Matter MS, Guri Y, Adam K, et al. The protein histidine phosphatase LHPP is a tumour suppressor. Nature. 2018;555(7698):678-82.
309. Hou B, Li W, Li J, Ma J, Xia P, Liu Z, et al. Tumor suppressor LHPP regulates the proliferation of colorectal cancer cells via the PI3K/AKT pathway. Oncol Rep. 2020;43(2):536-48.
310. Wu F, Chen Y, Zhu J. LHPP suppresses proliferation, migration, and invasion and promotes apoptosis in pancreatic cancer. Biosci Rep. 2020;40(3).
311. Sun W, Qian K, Guo K, Chen L, Xiang J, Li D, et al. LHPP inhibits cell growth and migration and triggers autophagy in papillary thyroid cancer by regulating the AKT/AMPK/mTOR signaling pathway. Acta Biochim Biophys Sin (Shanghai). 2020;52(4):382-9.
312. Zheng J, Dai X, Chen H, Fang C, Chen J, Sun L. Down-regulation of LHPP in cervical cancer influences cell proliferation, metastasis and apoptosis by modulating AKT. Biochem Biophys Res Commun. 2018;503(2):1108-14.
313. Gohla A. Do metabolic HAD phosphatases moonlight as protein phosphatases? Biochim Biophys Acta Mol Cell Res. 2019;1866(1):153-66.
314. Back SH, Adapala NS, Barbe MF, Carpino NC, Tsygankov AY, Sanjay A. TULA-2, a novel histidine phosphatase, regulates bone remodeling by modulating osteoclast function. Cell Mol Life Sci. 2013;70(7):1269-84.
315. Völler J-S. A truly active pseudokinase. Nature Catalysis. 2018;1(11):813-.
316. Sreelatha A, Yee SS, Lopez VA, Park BC, Kinch LN, Pilch S, et al. Protein AMPylation by an Evolutionarily Conserved Pseudokinase. Cell. 2018;175(3):809-21.e19.
317. Akamine P, Xuong N-H, Taylor SS. Crystal structure of a transition state mimic of the catalytic subunit of cAMP-dependent protein kinase. Nature structural biology. 2002;9(4):273-7.
318. Saraste M, Sibbald PR, Wittinghofer A. The P-loop—a common motif in ATP-and GTP-binding proteins. Trends in biochemical sciences. 1990;15(11):430-4.
319. Saenger W. Principles of Nucleic Acid Structure. Springer. New York, Berlin, Heidelberg. 1984.
320. Steeg PS, Zollo M, Wieland T. A critical evaluation of biochemical activities reported for the nucleoside diphosphate kinase/Nm23/Awd family proteins: opportunities and missteps in understanding their biological functions. Naunyn Schmiedebergs Arch Pharmacol. 2011;384(4-5):331-9.
321. Randazzo PA, Northup JK, Kahn RA. Activation of a small GTP-binding protein by nucleoside diphosphate kinase. Science. 1991;254(5033):850-3.
322. Hippe HJ, Abu-Taha I, Wolf NM, Katus HA, Wieland T. Through scaffolding and catalytic actions nucleoside diphosphate kinase B differentially regulates basal and β-adrenoceptor-stimulated cAMP synthesis. Cell Signal. 2011;23(3):579-85.
323. Kowluru A. Emerging roles for protein histidine phosphorylation in cellular signal transduction: lessons from the islet beta-cell. J Cell Mol Med. 2008;12(5b):1885-908.

324. Randazzo PA, Northup JK, Kahn RA. Regulatory GTP-binding proteins (ADP-ribosylation factor, Gt, and RAS) are not activated directly by nucleoside diphosphate kinase. J Biol Chem. 1992;267(25):18182-9.
325. Studier FW, Moffatt BA. Use of bacteriophage T7 RNA polymerase to direct selective high-level expression of cloned genes. J Mol Biol. 1986;189(1):113-30.
326. Byrne DP, Li Y, Ngamlert P, Ramakrishnan K, Eyers CE, Wells C, et al. New tools for evaluating protein tyrosine sulfation: tyrosylprotein sulfotransferases (TPSTs) are novel targets for RAF protein kinase inhibitors. Biochem J. 2018;475(15):2435-55.
327. Byrne DP, Vonderach M, Ferries S, Brownridge PJ, Eyers CE, Eyers PA. cAMP-dependent protein kinase (PKA) complexes probed by complementary differential scanning fluorimetry and ion mobility-mass spectrometry. Biochem J. 2016;473(19):3159-75.
328. Moyer JD, Henderson JF. Nucleoside triphosphate specificity of firefly luciferase. Analytical Biochemistry. 1983;131(1):187-9.
329. Longo PA, Kavran JM, Kim M-S, Leahy DJ. Transient mammalian cell transfection with polyethylenimine (PEI). Methods Enzymol. 2013;529:227-40.
330. Steeg PS. Tumor metastasis: mechanistic insights and clinical challenges. Nat Med. 2006;12(8):895-904.
331. Kapetanovich L, Baughman C, Lee TH. Nm23H2 facilitates coat protein complex II assembly and endoplasmic reticulum export in mammalian cells. Mol Biol Cell. 2005;16(2):835-48.
332. Cleland WW. The kinetics of enzyme-catalyzed reactions with two or more substrates or products: I. Nomenclature and rate equations. Biochimica et Biophysica Acta (BBA) - Specialized Section on Enzymological Subjects. 1963;67:104-37.
333. Norman AW, Wedding RT, Black MK. Detection of phosphohistidine in nucleoside diphosphokinase isolated from Jerusalem artichoke mitochondria. Biochemical and Biophysical Research Communications. 1965;20(6):703-9.
334. Hutter MC, Helms V. The Mechanism of Phosphorylation of Natural Nucleosides and Anti-HIV Analogues by Nucleoside Diphosphate Kinase Is Independent of Their Sugar Substituents. ChemBioChem. 2002;3(7):643-51.
335. Lascu I, Gonin P. The Catalytic Mechanism of Nucleoside Diphosphate Kinases. Journal of Bioenergetics and Biomembranes. 2000;32(3):237-46.
336. Plimmer R. Esters of phosphoric acid: Phosphoryl hydroxyamino-acids. Biochemical Journal. 1941;35(4):461.
337. Eckhart W, Hutchinson MA, Hunter T. An activity phosphorylating tyrosine in polyoma T antigen immunoprecipitates. Cell. 1979;18(4):925-33.
338. Blackshear PJ, Nairn AC, Kuo JF. Protein kinases 1988: a current perspective. The FASEB Journal. 1988;2(14):2957-69.
339. Lipmann FA, Levene PA. SERINEPHOSPHORIC ACID OBTAINED ON HYDROLYSIS OF VITELLINIC ACID. Journal of Biological Chemistry. 1932;98(1):109-14.
340. Schwartz PA, Murray BW. Protein kinase biochemistry and drug discovery. Bioorganic Chemistry. 2011;39(5):192-210.
341. Westheimer FH. Why nature chose phosphates. Science. 1987;235(4793):1173-8.
342. Chen CC, Smith DL, Bruegger BB, Halpern RM, Smith RA. Occurrence and distribution of acid-labile histone phosphates in regenerating rat liver. Biochemistry. 1974;13(18):3785-9.
343. Hou Y, Zhao L, Zhang M, He L, Bian L, Zhang L, et al. Study on high-level expression and purification of Nm23-H1/NDPK-A in Escherichia coli. Zhongguo Sheng Wu Hua Xue Yu Fen Zi Sheng Wu Xue Bao. 1998;14(6):655-60.
344. Williams RL, Oren DA, Muñoz-Dorado J, Inouye S, Inouye M, Arnold E. Crystal structure of Myxococcus xanthus nucleoside diphosphate kinase and its interaction with a nucleotide substrate at 2.0 A resolution. J Mol Biol. 1993;234(4):1230-47.
345. Moréra S, Lacombe M-L, Yingwu X, Joël Janin GLa. X-ray structure of human nucleoside diphosphate kinase B complexed with GDP at 2 å resolution. Structure. 1995;3(12):1307-14.
346. Lascu I, Chaffotte A, Limbourg-Bouchon B, Véron M. A Pro/Ser substitution in nucleoside diphosphate kinase of Drosophila melanogaster (mutation killer of prune) affects stability but not catalytic efficiency of the enzyme. J Biol Chem. 1992;267(18):12775-81.
347. Karlsson A, Mesnildrey S, Xu YW, Moréra S, Janin J, Véron M. Nucleoside diphosphate kinase: Investigation of the intersubunit contacts by site-directed mutagenesis and crystallography. The Journal of biological chemistry. 1996;271:19928-34.
348. Fothergill-Gilmore LA, Watson HC. The phosphoglycerate mutases. Adv Enzymol Relat Areas Mol Biol. 1989;62:227-313.

349. Rigden Daniel J. The histidine phosphatase superfamily: structure and function. Biochemical Journal. 2007;409(2):333-48.
350. Stankiewicz PJ, Hass LF. The catalytic bimodality of mammalian phosphoglycerate mutase. J Biol Chem. 1986;261(27):12715-21.
351. Li N, Liu X. Phosphoglycerate Mutase 1: Its Glycolytic and Non-Glycolytic Roles in Tumor Malignant Behaviors and Potential Therapeutic Significance. Onco Targets Ther. 2020;13:1787-95.
352. Lascu I, Gonin P. The catalytic mechanism of nucleoside diphosphate kinases. J Bioenerg Biomembr. 2000;32(3):237-46.
353. Clubbs Coldron AKM, Byrne DP, Eyers PA. Analysis of 1- and 3-Phosphohistidine (pHis) Protein Modification Using Model Enzymes Expressed in Bacteria. Methods Mol Biol. 2020;2077:63-81.
354. Coscia F, Taler-Verčič A, Chang VT, Sinn L, O'Reilly FJ, Izoré T, et al. The structure of human thyroglobulin. Nature. 2020;578(7796):627-30.
355. Fish WW, Bjork I. Native and subunit molecular weights of apoferritin. Biochemistry. 1971;10(15):2844-8.
356. Zucchi T, Rossi G, Cônsoli F. Characterization of a β-amylase from Propionicimonas sp. ENT-18 ectosymbiont of Acromyrmex subterraneus brunneus. Annals of Microbiology - ANN MICROBIOLOG. 2011;61.
357. Hayes JE, Jr., Velick SF. Yeast alcohol dehydrogenase: molecular weight, coenzyme binding, and reaction equilibria. J Biol Chem. 1954;207(1):225-44.
358. Majorek KA, Porebski PJ, Dayal A, Zimmerman MD, Jablonska K, Stewart AJ, et al. Structural and immunologic characterization of bovine, horse, and rabbit serum albumins. Mol Immunol. 2012;52(3-4):174-82.
359. Sapirstein VS, Strocchi P, Wesolowski M, Gilbert JM. Characterization and biosynthesis of soluble and membrane-bound carbonic anhydrase in brain. J Neurochem. 1983;40(5):1251-61.
360. Whitaker JR. Determination of Molecular Weights of Proteins by Gel Filtration of Sephadex. Analytical Chemistry. 1963;35(12):1950-3.
361. Bell MR, Engleka MJ, Malik A, Strickler JE. To fuse or not to fuse: what is your purpose? Protein Sci. 2013;22(11):1466-77.
362. Maru Y, Afar DE, Witte ON, Shibuya M. The dimerization property of glutathione S-transferase partially reactivates Bcr-Abl lacking the oligomerization domain. J Biol Chem. 1996;271(26):15353-7.
363. Kim M-S, Zhong J, Pandey A. Common errors in mass spectrometry-based analysis of post-translational modifications. Proteomics. 2016;16(5):700-14.
364. Savage SR, Zhang B. Using phosphoproteomics data to understand cellular signaling: a comprehensive guide to bioinformatics resources. Clinical Proteomics. 2020;17(1):27.
365. Haydon CE, Eyers PA, Aveline-Wolf LD, Resing KA, Maller JL, Ahn NG. Identification of Novel Phosphorylation Sites on Xenopus laevis Aurora A and Analysis of Phosphopeptide Enrichment by Immobilized Metal-affinity Chromatography *. Molecular & Cellular Proteomics. 2003;2(10):1055-67.
366. Foulkes Daniel M, Byrne Dominic P, Bailey Fiona P, Eyers Patrick A. Tribbles pseudokinases: novel targets for chemical biology and drug discovery? Biochemical Society Transactions. 2015;43(5):1095-103.
367. Fedorov O, Niesen FH, Knapp S. Kinase inhibitor selectivity profiling using differential scanning fluorimetry. Methods Mol Biol. 2012;795:109-18.
368. Vedadi M, Niesen FH, Allali-Hassani A, Fedorov OY, Finerty PJ, Jr., Wasney GA, et al. Chemical screening methods to identify ligands that promote protein stability, protein crystallization, and structure determination. Proc Natl Acad Sci U S A. 2006;103(43):15835-40.
369. Byrne DP, Vonderach M, Ferries S, Brownridge PJ, Eyers CE, Eyers PA. cAMP-dependent protein kinase (PKA) complexes probed by complementary differential scanning fluorimetry and ion mobility–mass spectrometry. Biochemical Journal. 2016;473(19):3159-75.
370. Reineke K, Mathys A, Knorr D. Shift of pH-Value During Thermal Treatments in Buffer Solutions and Selected Foods. International Journal of Food Properties. 2011;14(4):870-81.
371. Niesen FH, Berglund H, Vedadi M. The use of differential scanning fluorimetry to detect ligand interactions that promote protein stability. Nat Protoc. 2007;2(9):2212-21.
372. Norman AW, Wedding RT, Black MK. Detection of phosphohistidine in nucleoside diphosphokinase isolated from Jerusalem artichoke mitochondria. Biochem Biophys Res Commun. 1965;20(6):703-9.
373. Attwood PV, Muimo R. The actions of NME1/NDPK-A and NME2/NDPK-B as protein kinases. Laboratory Investigation. 2018;98(3):283-90.
374. Some D, Amartely H, Tsadok A, Lebendiker M. Characterization of Proteins by Size-Exclusion Chromatography Coupled to Multi-Angle Light Scattering (SEC-MALLS). J Vis Exp. 2019(148).
375. Mogridge J. Using light scattering to determine the stoichiometry of protein complexes. Methods Mol Biol. 2004;261:113-8.

376. Free T. Native mass spectrometry: a powerful tool for structural biology? BioTechniques. 2019;67(5):204-6.
377. Tamara S, den Boer MA, Heck AJR. High-Resolution Native Mass Spectrometry. Chemical Reviews. 2021.
378. Leney AC, Heck AJR. Native Mass Spectrometry: What is in the Name? J Am Soc Mass Spectrom. 2017;28(1):5-13.
379. Hitosugi T, Zhou L, Fan J, Elf S, Zhang L, Xie J, et al. Tyr26 phosphorylation of PGAM1 provides a metabolic advantage to tumours by stabilizing the active conformation. Nature communications. 2013;4:1790-.
380. Wang Y, Liu L, Wei Z, Cheng Z, Lin Y, Gong W. Seeing the process of histidine phosphorylation in human bisphosphoglycerate mutase. J Biol Chem. 2006;281(51):39642-8.
381. Bond CS, White MF, Hunter WN. Mechanistic implications for Escherichia coli cofactor-dependent phosphoglycerate mutase based on the high-resolution crystal structure of a vanadate complex. J Mol Biol. 2002;316(5):1071-81.
382. Lecroisey A, Lascu I, Bominaar A, Véron M, Delepierre M. Phosphorylation mechanism of nucleoside diphosphate kinase: 31P-nuclear magnetic resonance studies. Biochemistry. 1995;34(38):12445-50.
383. Lapek JD, Jr., Tombline G, Friedman AE. Mass spectrometry detection of histidine phosphorylation on NM23-H1. J Proteome Res. 2011;10(2):751-5.
384. Rose ZB. Evidence for a phosphohistidine protein intermediate in the phosphoglycerate mutase reaction. Arch Biochem Biophys. 1970;140(2):508-13.
385. A DATABASE OF PROTEIN POST
TRANSLATIONAL MODIFICATIONS: Association of Biomolecular Research Facilities; [Available from: https://www.abrf.org/delta-mass.
386. Postel EH, Ferrone CA. Nucleoside diphosphate kinase enzyme activity of NM23-H2/PuF is not required for its DNA binding and in vitro transcriptional functions. J Biol Chem. 1994;269(12):8627-30.
387. Postel EH, Weiss VH, Beneken J, Kirtane A. Mutational analysis of NM23-H2/NDP kinase identifies the structural domains critical to recognition of a c-myc regulatory element. Proceedings of the National Academy of Sciences of the United States of America. 1996;93(14):6892-7.
388. Schneider B, Xu YW, Janin J, Véron M, Deville-Bonne D. 3′-Phosphorylated Nucleotides Are Tight Binding Inhibitors of Nucleoside Diphosphate Kinase Activity *. Journal of Biological Chemistry. 1998;273(44):28773-8.
389. Jacobsen DM, Bao ZQ, O'Brien P, Brooks CL, 3rd, Young MA. Price to be paid for two-metal catalysis: magnesium ions that accelerate chemistry unavoidably limit product release from a protein kinase. J Am Chem Soc. 2012;134(37):15357-70.
390. Sugden PH, Holladay LA, Reimann EM, Corbin JD. Purification and characterization of the catalytic subunit of adenosine 3':5'-cyclic monophosphate-dependent protein kinase from bovine liver. The Biochemical journal. 1976;159(2):409-22.
391. Granot J, Mildvan AS, Hiyama K, Kondo H, Kaiser ET. Magnetic resonance studies of the effect of the regulatory subunit on metal and substrate binding to the catalytic subunit of bovine heart protein kinase. J Biol Chem. 1980;255(10):4569-73.
392. Priyakumar UD, Punnagai M, Mohan GK, Sastry GN. A computational study of cation–π interactions in polycyclic systems: exploring the dependence on the curvature and electronic factors. Tetrahedron. 2004;60(13):3037-43.
393. Reddy AS, Sastry GN. Cation [M= H+, Li+, Na+, K+, Ca2+, Mg2+, NH4+, and NMe4+] interactions with the aromatic motifs of naturally occurring amino acids: a theoretical study. The Journal of Physical Chemistry A. 2005;109(39):8893-903.
394. Engerer LK, Hanusa TP. Geometric effects in olefinic cation-π interactions with alkali metals: a computational study. J Org Chem. 2011;76(1):42-9.
395. Crowley PB, Golovin A. Cation-pi interactions in protein-protein interfaces. Proteins. 2005;59(2):231-9.
396. Schottel BL, Chifotides HT, Dunbar KR. Anion-pi interactions. Chem Soc Rev. 2008;37(1):68-83.
397. Burley SK, Petsko GA. Amino-aromatic interactions in proteins. FEBS Lett. 1986;203(2):139-43.
398. Vijay D, Sastry GN. Exploring the size dependence of cyclic and acyclic pi-systems on cation-pi binding. Phys Chem Chem Phys. 2008;10(4):582-90.
399. Zhang L, Wang J-C, Hou L, Cao P-R, Wu L, Zhang Q-S, et al. Functional Role of Histidine in the Conserved His-x-Asp Motif in the Catalytic Core of Protein Kinases. Scientific Reports. 2015;5(1):10115.
400. Giraud MF, Georgescauld F, Lascu I, Dautant A. Crystal structures of S120G mutant and wild type of human nucleoside diphosphate kinase A in complex with ADP. J Bioenerg Biomembr. 2006;38(3-4):261-4.

401. Williams RL, Oren DA, Muñoz-Dorado J, Inouye S, Inouye M, Arnold E. Crystal Structure of Myxococcus xanthus Nucleoside Diphosphate Kinase and its Interaction with a Nucleotide Substrate at 2·0 Å Resolution. Journal of Molecular Biology. 1993;234(4):1230-47.
402. Mårdh S, Ljungström O, Högstedt S, Zetterqvist O. Studies on a rat-liver cell-sap protein yielding 3-[32P]-phosphohistidine after incubation with [32P]ATP and alkaline hydrolysis. Identification of the protein as ATP citrate lyase. Biochim Biophys Acta. 1971;251(3):419-26.
403. Fan F, Williams HJ, Boyer JG, Graham TL, Zhao H, Lehr R, et al. On the catalytic mechanism of human ATP citrate lyase. Biochemistry. 2012;51(25):5198-211.
404. Rochdi MD, Laroche G, Dupré É, Giguère P, Lebel A, Watier V, et al. Nm23-H2 Interacts with a G Protein-coupled Receptor to Regulate Its Endocytosis through an Rac1-dependent Mechanism*. Journal of Biological Chemistry. 2004;279(18):18981-9.
405. Carotenuto M, Pedone E, Diana D, de Antonellis P, Džeroski S, Marino N, et al. Neuroblastoma tumorigenesis is regulated through the Nm23-H1/h-Prune C-terminal interaction. Scientific Reports. 2013;3(1):1351.
406. D'Angelo A, Garzia L, André A, Carotenuto P, Aglio V, Guardiola O, et al. Prune cAMP phosphodiesterase binds nm23-H1 and promotes cancer metastasis. Cancer Cell. 2004;5(2):137-49.
407. Tepper AD, Dammann H, Bominaar AA, Véron M. Investigation of the active site and the conformational stability of nucleoside diphosphate kinase by site-directed mutagenesis. Journal of Biological Chemistry. 1994;269(51):32175-80.
408. Lee E, Jeong J, Kim SE, Song EJ, Kang SW, Lee KJ. Multiple functions of Nm23-H1 are regulated by oxido-reduction system. PLoS One. 2009;4(11):e7949.
409. Chance B. Rapid and Sensitive Spectrophotometry. I. The Accelerated and Stopped-Flow Methods for the Measurement of the Reaction Kinetics and Spectra of Unstable Compounds in the Visible Region of the Spectrum. Review of Scientific Instruments. 1951;22(8):619-27.
410. Schneider B, Xu YW, Janin J, Véron M, Deville-Bonne D. 3'-Phosphorylated Nucleotides Are Tight Binding Inhibitors of Nucleoside Diphosphate Kinase Activity*. Journal of Biological Chemistry. 1998;273(44):28773-8.
411. Reddie KG, Carroll KS. Expanding the functional diversity of proteins through cysteine oxidation. Curr Opin Chem Biol. 2008;12(6):746-54.
412. Gallogly MM, Mieyal JJ. Mechanisms of reversible protein glutathionylation in redox signaling and oxidative stress. Curr Opin Pharmacol. 2007;7(4):381-91.
413. Wang J, Boja ES, Tan W, Tekle E, Fales HM, English S, et al. Reversible glutathionylation regulates actin polymerization in A431 cells. J Biol Chem. 2001;276(51):47763-6.
414. Pineda-Molina E, Klatt P, Vázquez J, Marina A, García de Lacoba M, Pérez-Sala D, et al. Glutathionylation of the p50 subunit of NF-kappaB: a mechanism for redox-induced inhibition of DNA binding. Biochemistry. 2001;40(47):14134-42.
415. Adachi T, Pimentel DR, Heibeck T, Hou X, Lee YJ, Jiang B, et al. S-glutathiolation of Ras mediates redox-sensitive signaling by angiotensin II in vascular smooth muscle cells. J Biol Chem. 2004;279(28):29857-62.
416. Kim MS, Jeong J, Lee KJ, Shin DH. A preliminary X-ray study of human nucleoside diphosphate kinase A under oxidative conditions. Acta Crystallogr Sect F Struct Biol Cryst Commun. 2010;66(Pt 11):1490-2.
417. Yu BYK, Tossounian M-A, Hristov SD, Lawrence R, Arora P, Tsuchiya Y, et al. Regulation of metastasis suppressor NME1 by a key metabolic cofactor coenzyme A. Redox Biology. 2021;44:101978.
418. Leonardi R, Zhang Y-M, Rock CO, Jackowski S. Coenzyme A: Back in action. Progress in Lipid Research. 2005;44(2):125-53.
419. Theodoulou Frederica L, Sibon Ody CM, Jackowski S, Gout I. Coenzyme A and its derivatives: renaissance of a textbook classic. Biochemical Society Transactions. 2014;42(4):1025-32.
420. Shi L, Tu BP. Acetyl-CoA and the regulation of metabolism: mechanisms and consequences. Current opinion in cell biology. 2015;33:125-31.
421. Baković J, Yu BYK, Silva D, Chew SP, Kim S, Ahn S-H, et al. A key metabolic integrator, coenzyme A, modulates the activity of peroxiredoxin 5 via covalent modification. Molecular and Cellular Biochemistry. 2019;461(1):91-102.
422. Gout I. Coenzyme A, protein CoAlation and redox regulation in mammalian cells. Biochemical Society transactions. 2018;46(3):721-8.
423. Tsuchiya Y, Peak-Chew SY, Newell C, Miller-Aidoo S, Mangal S, Zhyvoloup A, et al. Protein CoAlation: a redox-regulated protein modification by coenzyme A in mammalian cells. Biochemical Journal. 2017;474(14):2489-508.
424. Tsuchiya Y, Byrne DP, Burgess SG, Bormann J, Baković J, Huang Y, et al. Covalent Aurora A regulation by the metabolic integrator coenzyme A. Redox biology. 2020;28:101318.

425. Byrne DP, Shrestha S, Galler M, Cao M, Daly LA, Campbell AE, et al. Aurora A regulation by reversible cysteine oxidation reveals evolutionarily conserved redox control of Ser/Thr protein kinase activity. Science Signaling. 2020;13(639):eaax2713.
426. Shrestha S, Katiyar S, Sanz-Rodriguez CE, Kemppinen NR, Kim HW, Kadirvelraj R, et al. A redox-active switch in fructosamine-3-kinases expands the regulatory repertoire of the protein kinase superfamily. Science Signaling. 2020;13(639):eaax6313.
427. Gout I. Coenzyme A: a protective thiol in bacterial antioxidant defence. Biochemical Society Transactions. 2019;47(1):469-76.
428. Sies H. Glutathione and its role in cellular functions. Free Radical Biology and Medicine. 1999;27(9-10):916-21.
429. Kosower NS, Kosower EM. Formation of disulfides with diamide. Methods Enzymol. 143: Elsevier; 1987. p. 264-70.
430. Lu Z, Hunter T. Metabolic Kinases Moonlighting as Protein Kinases. Trends in Biochemical Sciences. 2018;43(4):301-10.
431. Steins M, Thomas M, Geißler M. Erlotinib. Recent Results Cancer Res. 2018;211:1-17.
432. Kim YJ, Shin YK, Sohn DS, Lee CS. Menadione induces the formation of reactive oxygen species and depletion of GSH-mediated apoptosis and inhibits the FAK-mediated cell invasion. Naunyn-Schmiedeberg's Archives of Pharmacology. 2014;387(9):799-809.
433. Moon H, Lee B, Choi G, Shin D, Prasad DT, Lee O, et al. NDP kinase 2 interacts with two oxidative stress-activated MAPKs to regulate cellular redox state and enhances multiple stress tolerance in transgenic plants. Proceedings of the National Academy of Sciences. 2003;100(1):358.
434. Climent F, Bartrons R, Pons G. Effect of vanadate on the formation and stability of the phosphoenzyme forms of 2, 3-bisphosphoglycerate-dependent phosphoglycerate mutase and of phosphoglucomutase. Biochimica et Biophysica Acta (BBA)-Protein Structure and Molecular Enzymology. 1982;705(2):238-42.
435. Bond CS, White MF, Hunter WN. Mechanistic implications for Escherichia coli cofactor-dependent phosphoglycerate mutase based on the high-resolution crystal structure of a vanadate complex1 1Edited by R. Huber. Journal of Molecular Biology. 2002;316(5):1071-81.
436. Wang Y, Wei Z, Liu L, Cheng Z, Lin Y, Ji F, et al. Crystal structure of human B-type phosphoglycerate mutase bound with citrate. Biochemical and Biophysical Research Communications. 2005;331(4):1207-15.
437. Kakuta Y, Petrotchenko EV, Pedersen LC, Negishi M. The sulfuryl transfer mechanism: crystal structure of a vanadate complex of estrogen sulfotransferase and mutational analysis. Journal of Biological Chemistry. 1998;273(42):27325-30.
438. Stankiewicz PJ, Gresser MJ. Inhibition of phosphatase and sulfatase by transition-state analogs. Biochemistry. 1988;27(1):206-12.
439. Niehrs C, Huttner WB. Purification and characterization of tyrosylprotein sulfotransferase. The EMBO journal. 1990;9(1):35-42.
440. Hall A, Karplus PA, Poole LB. Typical 2-Cys peroxiredoxins--structures, mechanisms and functions. Febs j. 2009;276(9):2469-77.
441. van Montfort RL, Congreve M, Tisi D, Carr R, Jhoti H. Oxidation state of the active-site cysteine in protein tyrosine phosphatase 1B. Nature. 2003;423(6941):773-7.
442. Fu X, Kassim SY, Parks WC, Heinecke JW. Hypochlorous acid oxygenates the cysteine switch domain of pro-matrilysin (MMP-7). A mechanism for matrix metalloproteinase activation and atherosclerotic plaque rupture by myeloperoxidase. J Biol Chem. 2001;276(44):41279-87.
443. Nagashima S, Nakasako M, Dohmae N, Tsujimura M, Takio K, Odaka M, et al. Novel non-heme iron center of nitrile hydratase with a claw setting of oxygen atoms. Nat Struct Biol. 1998;5(5):347-51.
444. Ermolayeva E, Sanders D. Mechanism of pyrithione-induced membrane depolarization in Neurospora crassa. Applied and environmental microbiology. 1995;61(9):3385-90.
445. Albert A, Rees C, Tomlinson A. The Influence of Chemical Constitution on Anti-bacterial Activity. Part VIII. 2-Mercaptopyridine-N-Oxide, and Some General Observations on Metal-binding Agents. British Journal of Experimental Pathology. 1956;37(5):500.
446. Gazaryan IG, Krasnikov BF, Ashby GA, Thorneley RN, Kristal BS, Brown AM. Zinc is a potent inhibitor of thiol oxidoreductase activity and stimulates reactive oxygen species production by lipoamide dehydrogenase. Journal of Biological Chemistry. 2002;277(12):10064-72.
447. Dineley KE, Votyakova TV, Reynolds IJ. Zinc inhibition of cellular energy production: implications for mitochondria and neurodegeneration. Journal of neurochemistry. 2003;85(3):563-70.
448. Lemire J, Mailloux R, Appanna VD. Zinc toxicity alters mitochondrial metabolism and leads to decreased ATP production in hepatocytes. Journal of Applied Toxicology: An International Journal. 2008;28(2):175-82.

449. Nixon BT, Ronson CW, Ausubel FM. Two-component regulatory systems responsive to environmental stimuli share strongly conserved domains with the nitrogen assimilation regulatory genes ntrB and ntrC. Proceedings of the National Academy of Sciences of the United States of America. 1986;83(20):7850-4.
450. Ninfa AJ, Ninfa EG, Lupas AN, Stock A, Magasanik B, Stock J. Crosstalk between bacterial chemotaxis signal transduction proteins and regulators of transcription of the Ntr regulon: evidence that nitrogen assimilation and chemotaxis are controlled by a common phosphotransfer mechanism. Proceedings of the National Academy of Sciences. 1988;85(15):5492-6.
451. Hess JF, Oosawa K, Kaplan N, Simon MI. Phosphorylation of three proteins in the signaling pathway of bacterial chemotaxis. Cell. 1988;53(1):79-87.
452. Wurgler-Murphy SM, Saito H. Two-component signal transducers and MAPK cascades. Trends in biochemical sciences. 1997;22(5):172-6.
453. Chang C, Stewart RC. The two-component system. Regulation of diverse signaling pathways in prokaryotes and eukaryotes. Plant Physiol. 1998;117(3):723-31.
454. Loomis WF, Shaulsky G, Wang N. Histidine kinases in signal transduction pathways of eukaryotes. Journal of Cell Science. 1997;110(10):1141-5.
455. Lukat GS, McCleary WR, Stock AM, Stock JB. Phosphorylation of bacterial response regulator proteins by low molecular weight phospho-donors. Proceedings of the National Academy of Sciences of the United States of America. 1992;89(2):718-22.
456. Potel CM, Lin M-H, Heck AJR, Lemeer S. Widespread bacterial protein histidine phosphorylation revealed by mass spectrometry-based proteomics. Nature Methods. 2018;15(3):187-90.
457. Wang F-F, Qian W. The roles of histidine kinases in sensing host plant and cell–cell communication signal in a phytopathogenic bacterium. Philosophical Transactions of the Royal Society B: Biological Sciences. 2019;374(1767):20180311.
458. Nongpiur R, Soni P, Karan R, Singla-Pareek SL, Pareek A. Histidine kinases in plants: cross talk between hormone and stress responses. Plant Signal Behav. 2012;7(10):1230-7.
459. Saito H. Histidine phosphorylation and two-component signaling in eukaryotic cells. Chemical reviews. 2001;101(8):2497-510.
460. Koshland DE. Effect of Catalysts on the Hydrolysis of Acetyl Phosphate. Nucleophilic Displacement Mechanisms in Enzymatic Reactions1. Journal of the American Chemical Society. 1952;74(9):2286-92.
461. Fujimori T, Jencks WP. The kinetics for the phosphoryl transfer steps of the sarcoplasmic reticulum calcium ATPase are the same with strontium and with calcium bound to the transport sites. J Biol Chem. 1992;267(26):18466-74.
462. Smtih DL, Bruegger BB, Halpern RM, Smith RA. New histone kinases in nuclei of rat tissues. Nature. 1973;246(5428):103-4.
463. Desvignes T, Pontarotti P, Fauvel C, Bobe J. Nme protein family evolutionary history, a vertebrate perspective. BMC Evol Biol. 2009;9:256-.
464. Wagner PD, Steeg PS, Vu ND. Two-component kinase-like activity of nm23 correlates with its motility-suppressing activity. Proc Natl Acad Sci U S A. 1997;94(17):9000-5.
465. Bridger WA. Contribution of subunit interactions to the effectiveness of catalysis by succinyl coenzyme A synthetase. Curr Top Cell Regul. 1984;24:345-55.
466. Wagner PD, Vu ND. Phosphorylation of ATP-citrate lyase by nucleoside diphosphate kinase. J Biol Chem. 1995;270(37):21758-64.
467. Wieland T, Attwood PV. Alterations in reversible protein histidine phosphorylation as intracellular signals in cardiovascular disease. Front Pharmacol. 2015;6:173.
468. Srivastava S, Panda S, Li Z, Fuhs SR, Hunter T, Thiele DJ, et al. Histidine phosphorylation relieves copper inhibition in the mammalian potassium channel KCa3.1. Elife. 2016;5.
469. Shi G, Yue G, Zhou R. EphA3 functions are regulated by collaborating phosphotyrosine residues. Cell Research. 2010;20(11):1263-75.
470. Binns KL, Taylor PP, Sicheri F, Pawson T, Holland SJ. Phosphorylation of tyrosine residues in the kinase domain and juxtamembrane region regulates the biological and catalytic activities of Eph receptors. Mol Cell Biol. 2000;20(13):4791-805.
471. Wybenga-Groot LE, Baskin B, Ong SH, Tong J, Pawson T, Sicheri F. Structural basis for autoinhibition of the Ephb2 receptor tyrosine kinase by the unphosphorylated juxtamembrane region. Cell. 2001;106(6):745-57.
472. Chu L, Robinson DK. Industrial choices for protein production by large-scale cell culture. Current opinion in biotechnology. 2001;12(2):180-7.

473. Chen PS, Wang CC, Bortner CD, Peng GS, Wu X, Pang H, et al. Valproic acid and other histone deacetylase inhibitors induce microglial apoptosis and attenuate lipopolysaccharide-induced dopaminergic neurotoxicity. Neuroscience. 2007;149(1):203-12.
474. Kiszel P, Fiesel S, Voit S, Waechtler B, Meier T, Oelschlaegel T, et al. Transient gene expression using valproic acid in combination with co-transfection of SV40 large T antigen and human p21(CIP) /p27(KIP). Biotechnol Prog. 2019;35(3):e2786.
475. Wulhfard S, Baldi L, Hacker DL, Wurm F. Valproic acid enhances recombinant mRNA and protein levels in transiently transfected Chinese hamster ovary cells. J Biotechnol. 2010;148(2-3):128-32.
476. Liu C, Ke P, Zhang J, Zhang X, Chen X. Protein Kinase Inhibitor Peptide as a Tool to Specifically Inhibit Protein Kinase A. Front Physiol. 2020;11:574030-.
477. Cheng HC, Kemp BE, Pearson RB, Smith AJ, Misconi L, Van Patten SM, et al. A potent synthetic peptide inhibitor of the cAMP-dependent protein kinase. J Biol Chem. 1986;261(3):989-92.
478. Hiraishi H, Yokoi F, Kumon A. Bovine liver phosphoamidase as a protein histidine/lysine phosphatase. The Journal of Biochemistry. 1999;126(2):368-74.
479. Hiraishi H, Yokoi F, Kumon A. 3-phosphohistidine and 6-phospholysine are substrates of a 56-kDa inorganic pyrophosphatase from bovine liver. Archives of biochemistry and biophysics. 1998;349(2):381-7.
480. Mäurer A, Wieland T, Meissl F, Niroomand F, Mehringer R, Krieglstein J, et al. The beta-subunit of G proteins is a substrate of protein histidine phosphatase. Biochem Biophys Res Commun. 2005;334(4):1115-20.
481. Mahmood T, Yang P-C. Western blot: technique, theory, and trouble shooting. N Am J Med Sci. 2012;4(9):429-34.
482. Potel CM, Fasci D, Heck AJR. Mix and match of the tumor metastasis suppressor Nm23 protein isoforms in vitro and in vivo. The FEBS Journal. 2018;285(15):2856-68.
483. Levit MN, Abramczyk BM, Stock JB, Postel EH. Interactions between Escherichia coli nucleoside-diphosphate kinase and DNA. J Biol Chem. 2002;277(7):5163-7.
484. Su H, Xu Y. Application of ITC-Based Characterization of Thermodynamic and Kinetic Association of Ligands With Proteins in Drug Design. Front Pharmacol. 2018;9:1133.